Constraining the Ross Embayment glacial history from raised shorelines in the Ross Sea, Antarctica

J. M. Quinn

Research School of Earth Sciences
Australian National University

A thesis submitted for the degree of
Doctor of Philosophy of The Australian National University.

March 2, 2003

Statement

This thesis is an account of my research undertaken during the period November 1996 to March 2003 while I was a student in the Research School of Earth Sciences at the Australian National University. Except as otherwise indicated in the text, the work described is my own. This thesis has never been submitted to another university or similar institution.

Julie Quinn
Canberra
March 2, 2003

Acknowledgments

At the risk of being long winded I have worked with quite a number of people in association with this thesis and I believe their contribution should be noted. Initially the idea for this thesis came up in a conversation with Peter Barrett at Victoria University of Wellington and it was him who really set the ball rolling. Also at Victoria University are Alex Pyne (Antarctic Research Centre) and Jamie Shulmeister who were invaluable in association with field work. My two field assistants, Peter Webb and Alexis Lambeck, both undergraduates at the time at Victoria University provided me with help, advice and friendship. And Ed Butler ran his PhD fieldwork in association with me and was good company for two seasons.

My field work in the Ross Sea area of Antarctica was in association with Antarctica New Zealand and I am indebted to them for the smooth running of the field program, the effort they went to in organising access to Cape Hallett (on the US Coastguard icebreaker Polar Star), the superb teams at Scott Base, and helo crews (both NZ and US) who flew us around. Nothing is too much for anyone in Antarctica when approached with a smile!

In terms of laboratory work I have had the pleasure of working in a vast majority of the labs in the school (and being nosy in others — GFD!). The technicians and academics who run these labs are extraordinarily helpful and have put up with endless dumb questions. Briefly (and I hope I don't leave anyone out): Shane Paxton and John Mya for rock crushing and separation, Robin Maier for K-feldspar measurements, Lois Taylor for trace elements, Joan Cowley, Heather Lynch, Joe Cali (especially for changing that light bulb and locking the door without a key!) for help with the chlorine lab (and Jodie Evans and Tim Barrows). The workshop has been great in preparing bits and pieces. John Head and Yusuke Yokoyama kindly lent me their radiocarbon lines and helped me use them. Nigel Spooner, Norman Hill and Danielle Questiaux spent a lot of time on my OSL samples. Keith Fifield and Richard Cresswell (Nuclear Physics) have both been wonderful with my questions and running my samples on the AMS and letting me help (and the view from the top of the AMS tower at night is great!).

The geodynamics group qualifies you, not only as a scientist, but also as a cake connoisseur - long may this group tradition last! Seriously though, it is a good group to work in: Paul J has helped me endlessly and it has been great sharing an office with him. The other students I have come through with; Jonathan, David, Yusuke and Kevin have always been there for me to moan at! And of course Emma-Kate for all the friendly female chats! Herb and Tony are valuable for their advice but possibly more so for knowing all those trival bits of information when you say "I wonder...". Herb also helped a great deal straightening out the writing. All the others are always willing to help - Georg, Jean, Paul T, Clementine, Janine, Derek, Richard, and Frédéric.

Which brings me to my supervisor, Kurt Lambeck. At times it seemed like he was

To establish whether these ice models contain sufficient ice in the late-Pleistocene the sea-level predictions are, therefore, also compared with observations from Barbados.

The glacio-hydro-isostatic contributions from a standard Northern Hemisphere ice sheet model and several different models for the distal Antarctic Ice Sheet (outside the Ross Embayment area) predict a maximum relative sea level range of +2 to −4 m at 6,000 years before the present, requiring a +18 to +24 m relative sea level contribution (or crustal rebound) from local ice to produce the observed elevated shorelines of about 20 m at this time.

The Ross Embayment ice sheet reconstruction that is in good agreement with both the relative sea level observations and the field evidence for ice movement across the region contains more ice than present-day ice sheet, yet is substantially smaller than maximum models in which the grounding line is at the shelf edge and there are no ice streams. It contains a Last Glacial Maximum grounding line close to Coulman Island in the western Ross Sea and uses trimlines and drift sheet heights to constrain ice location. The total volume of this additional ice in the Ross Embayment at the Last Glacial Maximum is 8.4 m equivalent sea level. This best fit model predicts a present-day relative sea level change (and similar crustal rebound rates) of 1.3 mm/year in McMurdo Sound and higher in other parts of the Ross Embayment. These values are on the lower limit of GPS measurement range but with further development in this area measurements of crustal rebound rates may also help to constrain the former ice sheet in the Ross Embayment.

Ross Ice Shelf

Contents

List of Figures

List of Tables

Chapter 1

Introduction

How big was the Antarctic Ice Sheet at the Last Glacial Maximum? Where was the ice located? How much ice was there? These are questions of immediate relevance to our understanding of recent climate changes on Earth and current debates on how climate may change in the future. To understand the ice sheets, how they effect and are effected by the climate, and what influence the ice sheets have on sea-level is important for modelling the climate system. Yet the answers, the fundamental data which must underpin the debate, are not easily obtained. This thesis addresses some of these issues concentrating on the change in ice volume from the Ross Embayment sector of the Antarctic Ice Sheet since the time of the Last Glacial Maximum. This sector is an important part of the Antarctic Ice Sheet extensively draining both the West Antarctic Ice Sheet and the East Antarctic Ice Sheet. It may also have had the largest retreat area of the Antarctic Ice Sheet since the Last Glacial Maximum and possibly the largest ice volume change as well, of any part of Antarctica.

1.1 Why the Antarctic Ice Sheet

Antarctica, and the Antarctic Ice Sheet, plays an important role in influencing the global climate. The ice sheet stores a vast quantity of water that can be released through global warming. With much coastal development occurring within a few metres of sea level a loss of only a small fraction of this ice volume has the potential to greatly alter coastal areas globally and to impact on large populations. By knowing how the Antarctic Ice Sheet behaved over the last glacial cycle we provide the basis for making informed predictions of how it may behave in the future.

A key element in Antarctica's direct effect on the world climate is the global ocean circulation. Sea-ice formation around the edge of the continent leads to the production of cold, relatively saline water that sinks off the edge of the continent and circulates northwards to modulate the flow of the warmer surface currents that in turn influence the global climate. Thus, any changes in the rate of deep-water formation around the

Antarctic margin impacts directly on global climate.

Sea levels have been measured to be around 120 to 130 m lower at the Last Glacial Maximum (Fairbanks 1989; Chappell and Polach 1991; Yokoyama 1999; Nakada and Lambeck 1987). A large part of this sea level change is due to water released from the Northern Hemisphere ice sheets which are relatively well defined compared to the Antarctic Ice Sheet. The last Northern Hemisphere Ice Sheets consisted of the Laurentian, Inuitian, and Cordillerian ice sheets over North America; Fenoscandinavian and Barents-Kara ice sheets over northern Europe; the Greenland Ice Sheet, and smaller ice caps on the British Isles, Greenland and Iceland. Evidence obtained from palaeoglaciology of large-scale flow-generated lineations (Boulton et al. 2001), relative-sea-level curves from beneath the former ice sheet (Dyke and Peltier 2000), continental shelf deposits (Sejrup et al. 2000), marine limits from beneath the former ice sheet (Cofaigh 1999), stratigraphy and dating (Forman et al. 1999) etc. has made it clear that the history of these ice sheets is complex. However much more is known about the history of ice locations and volumes for the long vanished Northern Hemisphere ice sheets than for Antarctica.

Most estimates for the Northern Hemisphere ice sheet component of sea level rise since the Last Glacial Maximum are around 80 to 90 m equivalent sea level (Nakada and Lambeck 1988; Tushingham and Peltier 1991), leaving 30 to 40 m equivalent sea level to be sourced elsewhere on Earth. Limits have been placed on ice in the other possible locations such as Tibet (Kaufmann and Lambeck 1997). These sources are minor on a global scale with a maximum model for an ice sheet over the Tibetan plateau containing 6 m equivalent sea level. This leaves a substantial amount to be attributed to the Antarctic Ice Sheet (25 to 30 m). Because of this discrepancy and field evidence in Antarctica itself, there is general agreement that the Antarctic Ice Sheet was greater at the Last Glacial Maximum than at the present day (Stuiver et al. 1981, Bentley 1999, Berkman et al. 1998, and Anderson et al. 2002). The present-day ice volume in the Antarctic Ice Sheet is equivalent to about 70 m of global sea level rise so the Last Glacial Maximum volumes may have been as much as 45% larger than the present ice sheet.

Where, then, was the extra ice located in Antarctica? The ice sheet itself can give us some information through ice cores which, depending on where they are located, can provide a record back more than 400,000 years (Petit et al. 1999). Ice core records from the interior of the ice sheet indicate that little change in elevation has occurred at the ice domes, and possibly a reduction in altitude by about 100 m in central East Antarctica (Jouzel et al. 1989). During the Last Glacial Maximum sea ice extended further out from the continent and this would have led to a deprivation of moist air to the interior, shown by a lower level of snow accumulation in the ice cores (Jouzel et al. 1989). However, the coastal areas would have grown outwards without significant increases in the thickness in the interior. Evidence to support this thickening of ice at

the coast is provided by exposure ages of bedrock and erratics (e.g. Brook et al. 1995). Evidence for the ice extending further onto the shelf than today, and in some cases out to the edge of the shelf, is provided by high resolution surveys of the shelf floor (e.g. Anderson et al. 2002).

Records of Antarctic Ice Sheet retreats and advances can also be found on ice free areas. Many mountains and valley walls have records of former ice levels in the form of trimlines and lateral moraines (Bentley and Anderson 1998, Denton et al. 1989, Stone et al. 2003). Coastal areas provide moraines, ice scoured bedrock and erratics recording advances (Sawagaki and Hirakawa 1999). In areas around the edge of the continent where crustal rebound has exposed formerly glaciated surfaces that were below sea level immediately after melting, relative sea level changes can be documented from lake cores. The cores contain sediments that record the transition from marine to freshwater conditions. These lakes are found in the Vestfold Hills and Larsemann Hills (Zwartz 1995) (Figure 1.1).

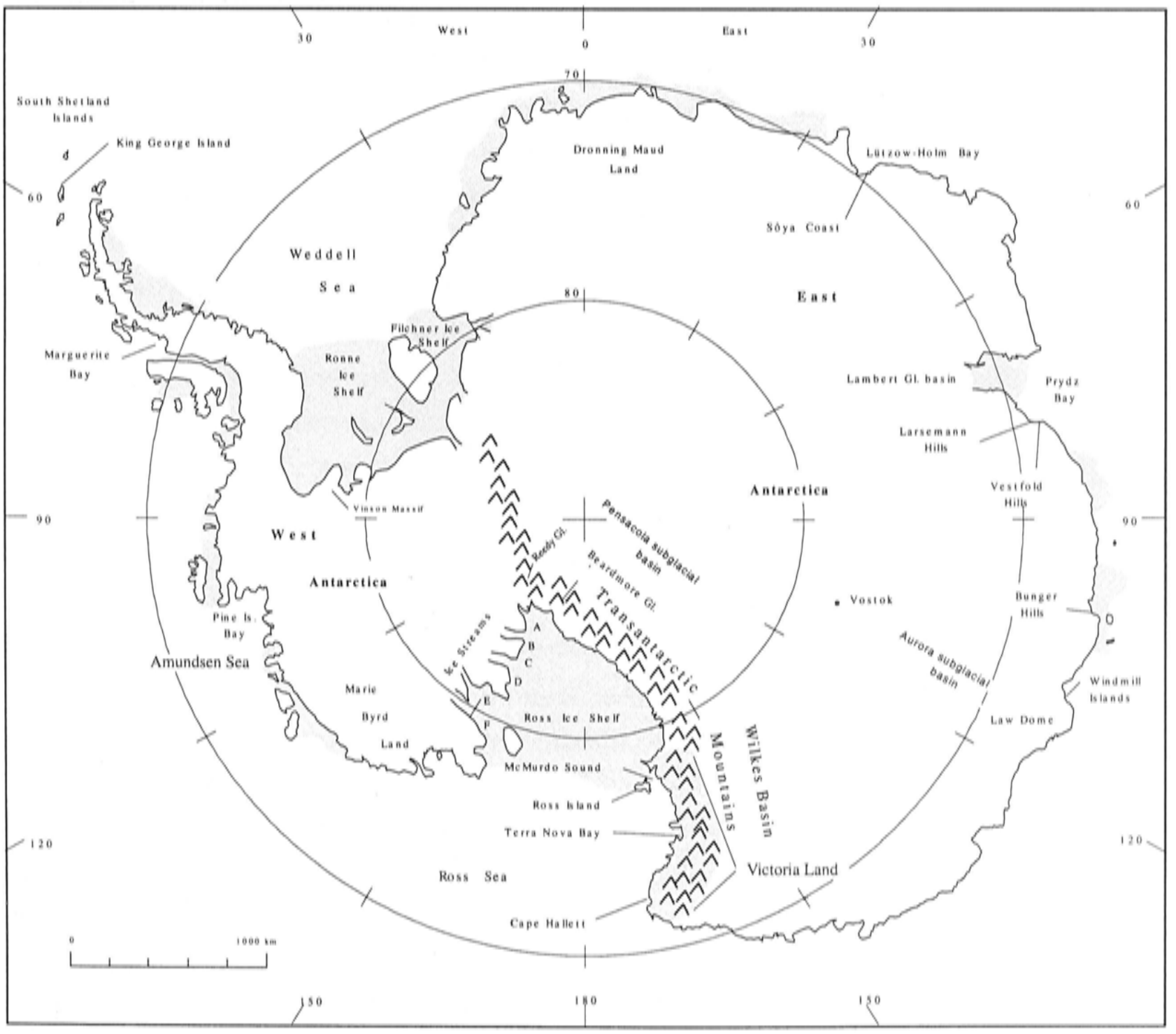

Figure 1.1: Location map of the Antarctic continent

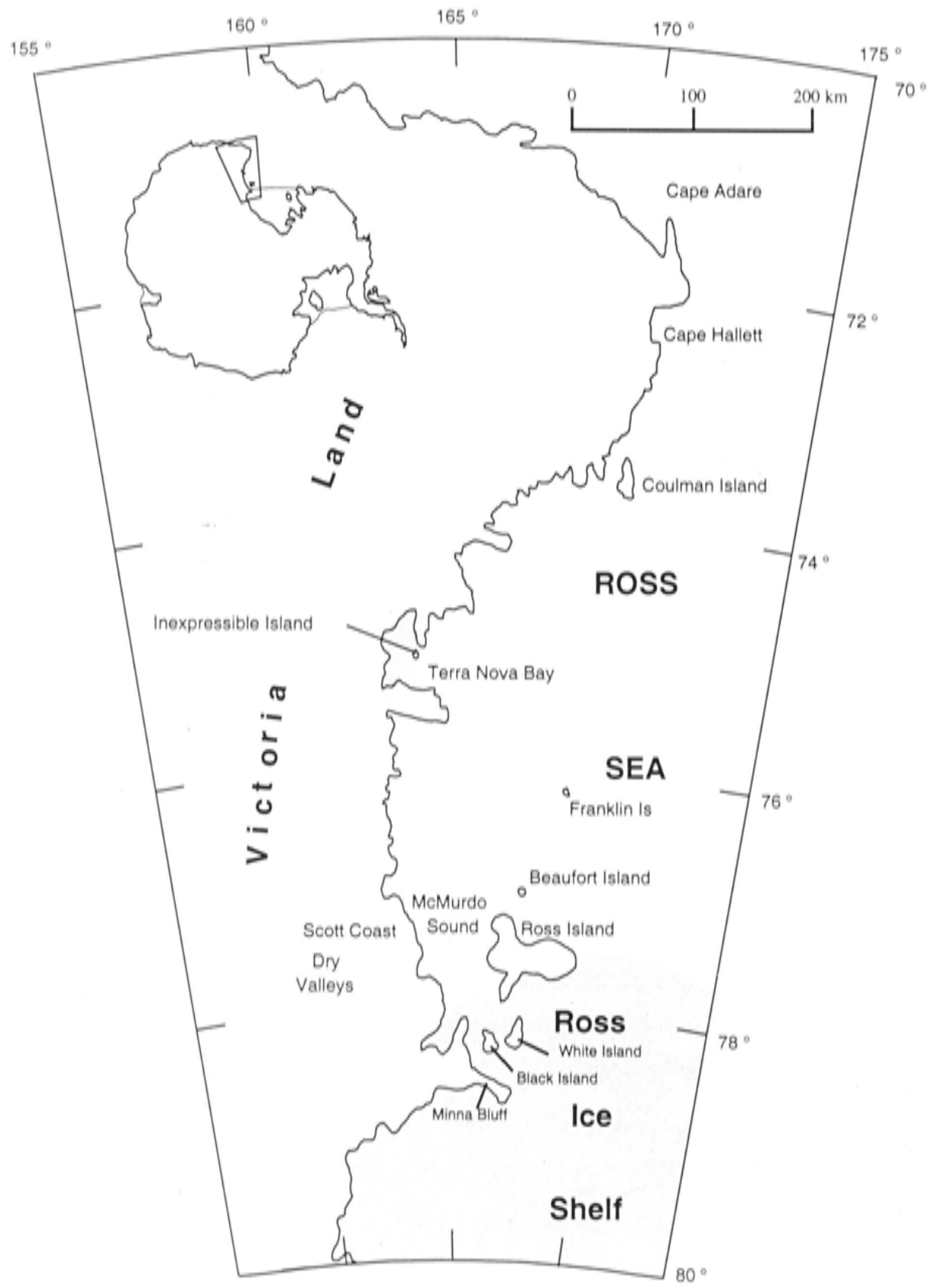

Figure 1.2: Location map of the Ross Sea.

Offshore, core samples and seismic work can differentiate between formerly ice covered land, ice shelf or open water conditions to tell where the ice sheet was located at different times (Licht et al. 1996; Anderson et al. 1992). Through studying these sediment packages an indication of the location of the ice margin and the timing (where true or relative dating is possible) of the fluctuations of the ice margin through time can be obtained. Knowing the ice margin is valuable in estimating the volume of ice in the ice sheet.

This thesis focuses on the Ross Embayment area, specifically field locations south of Terra Nova Bay (Figure 1.1). The drainage basin comprises a grounded ice sheet over East Antarctica, part of which drains through the north-south trending Transantarctic Mountains and feeds into a major ice shelf covering the inner Ross Embayment. A por-

tion of the ice sheet over West Antarctica also drains into the ice shelf and contributes to the ice loading in the Ross Embayment. The Ross Ice Shelf calves over a wide front in the Ross Embayment (see Figure 1.1). Part of the Ross Ice Shelf (the McMurdo Ice Shelf) presently calves at the southern end of McMurdo Sound, close to the field locations.

The main field sites in this thesis are along the coast of McMurdo Sound with an additional location further north at Cape Hallett. In the Ross Embayment there are trimlines of former ice levels in the mountains which provide ice sheet height constraints (Denton et al. 1989), sediments on the continental shelf which provide grounding line constraints (Licht et al. 1996, Anderson et al. 1992), ice-shelf debris which provide timing constraints (Kellogg et al. 1990), drift sheets providing constraints on ice sheet extents and timing (Stuiver et al. 1981; Brook et al. 1995) and raised shorelines which indirectly constrain crustal rebound amount and timing. Together, these different pieces of evidence provide direct and indirect constraints on the history of ice volumes and a starting point to establish ice locations within the Ross Embayment.

1.2 Outline of thesis

The observational evidence for the limits and thickness of the past ice sheet over the Ross Sea Embayment is fragmentary in time and space, and some of the observational material provides only indirect measures of the ice extent. In the absence of a comprehensive data set we therefore use mathematical models to relate the observed quantities to parameters that define the ice sheet and which can be used to interpolate between the fragmentary evidence. In this thesis it is mainly the shoreline height-age relationships that are used to constrain the ice sheet. The position of past sea-level relative to its present position is a function of changes in ocean volume and of land movements. Both, in the absence of tectonic processes, relate to the ice history through the eustatic change and through the isostatic rebound of the Earth to the changing ice-water load. In this case the model links the relative sea level change to ice history through the equations governing the response of the planet to loading and the equations governing the redistribution of the ice and water load as ice sheets grow or decay. In a complete model the ice sheet evolution is expressed by the equations of ice flow and ice accumulation drawn by a particular climate scenario. Ideally the ice-earth models should be coupled: the ice thickness that can accumulate in a function of the amount of deformation beneath the growing ice load, but to date fully coupled models have not yet been developed and the two aspects of the modelling are usually carried out in an iterative manner.

In some instances full inverse solutions can be developed where, sea-level observations within and adjacent to the area of glaciation can be inverted to give estimates of ice thickness. But these solutions are restricted to ice sheets for which there is a good

spatial and temporal distribution of field evidence, as for the British Isles (Johnston and Lambeck 1999). In many other situations unique solutions are not possible. For example, a particular sea level curve showing a falling sea level for the past 6,000 years could mean that a considerable amount of ice was removed over a large area at some remote place or that a small nearby ice load was removed in more recent time.

This is the case for the Ross Sea Embayment and instead of using inverse methods we use forward modelling methods to test glaciological models based on different field-data sets and on different assumptions about the mechanics of ice sheet formation. From discrepancies or agreements between the observed and predicted sea level change inferences are then drawn about the past ice cover over the area.

The success of this approach depends on the availability of good quality sea level curves from locations for which different isostatic responses are anticipated: for example from sites well within the former ice margin and from near the ice margin. Secondly, it requires observational data that extends as far back in time as possible in order to constrain the early part of the deglaciation history. But in the case of Antarctica the observational evidence is very limited and is difficult to access. At the time of starting the thesis work the principal evidence was that for Terra Nova Bay (Baroni and Orombelli 1991) where the record extends back to 7,500 ^{14}C years BP. Later the results of ^{14}C dating of shells and seal fur by Hall and Denton (1999) became available. In between I had started a fieldwork program collecting relative sea level observations in an area to the south of Terra Nova Bay and I used three different dating methods - ^{14}C of mollusc shells and penguin eggshell, optically stimulated luminescence (OSL) of beach sands, and cosmogenic exposure age dating of rock platforms and beach boulders. Both the OSL and cosmogenic exposure age dating methods were essentially exploratory methods at the time. The rationale for this was that each of the methods have limitations when applied to Antarctic materials and that the cosmogenic exposure age dating has the potential of extending the observational record further back in time.

1.2.1 Thesis layout

In this thesis the field work and dating that contributes to the observed relative sea level curve is presented first. This allows my field observations, and other workers observations, to be described and used as constraints in making the ice sheets that are used as input to the glacio-hydro-isostatic modelling process presented in the second half of the thesis. The observed relative sea level curve is also critical for evaluating the validity of the ice-sheet models.

The role of isostasy in ice sheet evolution and sea level change is discussed from both a spatial and a temporal perspective in Chapter 4. Understanding these concepts is necessary for the detailed description of the glacio-hydro-isostatic modelling program. It also helps in understanding the representations of the ice sheet for Antarctica, the parameterization of the Earth and modelling situations that require special treatment

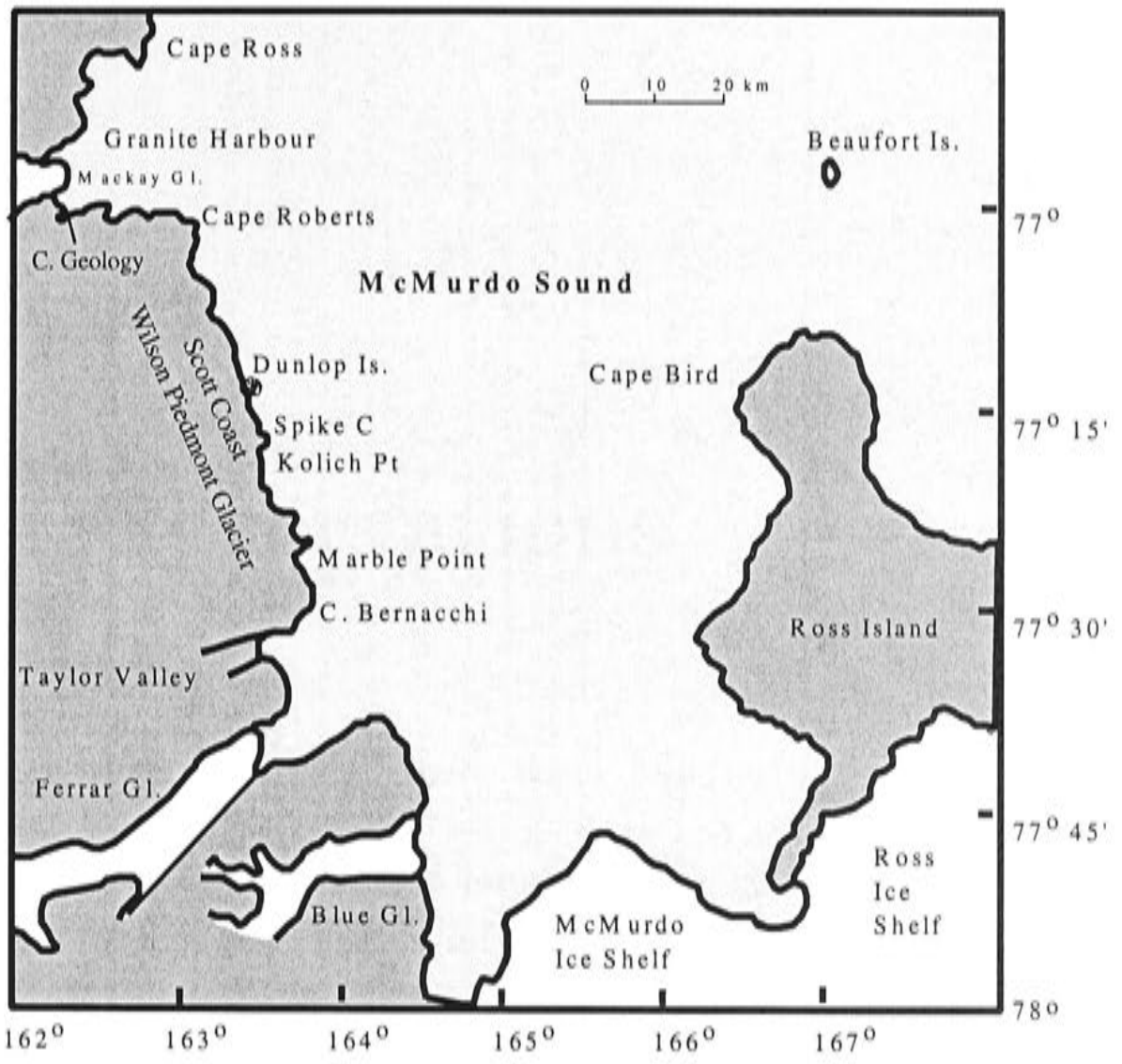

Figure 1.3: Location map for McMurdo Sound and the Scott Coast.

such as the ice and water loading of continental shelves.

As mentioned earlier in this introduction, the ice sheets of the Northern Hemisphere impact on Antarctica in terms of sea level changes, so the possible effects of varying the models of the Northern Hemisphere ice sheets are examined. That part of the Antarctic Ice Sheet outside of the Ross Embayment area will also impact on the Ross Embayment, not only through changing the sea-level, but also by direct loading of the Earth's surface. Possible variations of the Antarctic Ice Sheet are examined to determine the scale of errors which result from using different models.

The final chapter of the thesis examines the ice sheet reconstructions for the Ross Embayment. The local contribution is isolated and other limitations established such as the rate at which the ice sheet melts. The geological constraints from the field are added to define an ice sheet which is possible for the Ross Embayment from the Last Glacial Maximum to the present day. This model is then refined using the comparison between the predicted and observed relative sea levels.

Chapter 2

Field Observations

2.1 Victoria Land Coast and Islands

The coastal area along the Victoria Land Coast is ice free in only a few places (Mabin 1986). These ice-free areas consist of low rocky coasts, beaches and high rocky cliffs (Gregory et al. 1984).

Raised beaches were first recorded by David and Priestley (1914) in the McMurdo Sound area and these were first examined in detail by Nichols (1968) and Kirk (1990). A summary of the early work and radiocarbon dating can be found in Stuiver et al. (1981). Further north, in Terra Nova Bay, Baroni and Orombelli (1991) examined and extensively dated these raised beaches.

This chapter describes and interprets the characteristics of the coastal areas with emphasis on the features and regions examined for this thesis. A description of the sediment sources, morphology and preservation of the beaches is given with examples from the Scott Coast (western side of McMurdo Sound). The boulder pavements, the rock platforms and the glacial moraine above the marine-influenced area are described with relevant details for the dated sites. Further descriptions of each site visited (Cape Bernacchi, South Stream, Marble Point, Kolich Point, Spike Cape, Dunlop Island, and Cape Roberts (all in McMurdo Sound); Cape Geology and Cape Ross in Granite Harbour (to the north of McMurdo Sound); Cape Bird on Ross Island and Cape Hallett in Northern Victoria Land) can be found in Appendix A.

2.2 Marine Limit

The marine limit is the highest altitude at which the sea has had some recorded influence on a coast. This elevation is a function of the amount of uplift of the coastline that has occurred since the coast became ice free (from both sea-ice and any land-based ice). The marine limit therefore, is dependent on both the amount of relative-sea-level change and on ice conditions at any particular location. The marine limit is very clearly defined

in some places (e.g. Kolich Point — Figure 2.1.) where there is an abrupt change from rounded beach boulders of only a few of lithologies (below the marine limit), to poorly sorted, angular clasts of many sizes and lithologies (above the marine limit). At Kolich Point, even cusp features (wave-scalloped areas) are preserved at the marine limit. The majority of marine limits, however, show more subtle changes, with a change in slope or the angularity of the material being the best indicators of the marine limit. The marine limit is often easier to pick from a distance or on aerial photographs (Figure 2.2) than up close. To the south between Cape Bernacchi and Explorers Cove, and also on Cape Bird and Cape Hallett, the marine limit is unclear because of a talus slope or a steep hill of moraine that has subsequently covered the landward edge of the marine influenced area. At these sites the limit of marine influence is defined as the area up to the edge of the talus slopes. Table 2.1 shows the marine limit at each site and how the marine limit is defined there.

Location	**Marine Limit**	**Reference**	**Defining characteristic**
C. Bernacchi	approx. 11 m	3	Talus slope.
Marble Point	approx. 20 m	3	Edge of moraine.
Kolich Point	approx. 17 m	3	Wave cusps into moraine.
Spike Cape	approx. 17 m	1	Change in colour into moraine.
Dunlop Island	>20 m	1	No limit identified.
Cape Roberts	>20 m	1	Limit under ice. (recent ice advance)
Cape Geology	approx. 19 m	1	Change in colour and increase in roundness of boulders below limit.
Cape Ross	approx. 33 m	3	Under snow.
Cape Bird	approx. 9 m	3	Talus slope.
Cape Hallett	>6.5 m	2	Talus slope.
Inexpressible Island (near Terra Nova Bay)	<43 m	4	Degree of weathering.

Table 2.1: Marine limits on the Scott Coast, Cape Ross, Cape Bird, and Cape Hallett. References: 1. Nichols (1968); 2. Kirk (1990); 3. This thesis; 4. Claridge and Campbell (1966).

2.3 Beaches

Beaches are discussed here in some detail because they provide the more obvious evidence of former high sea levels as well as datable material. A typical profile across an

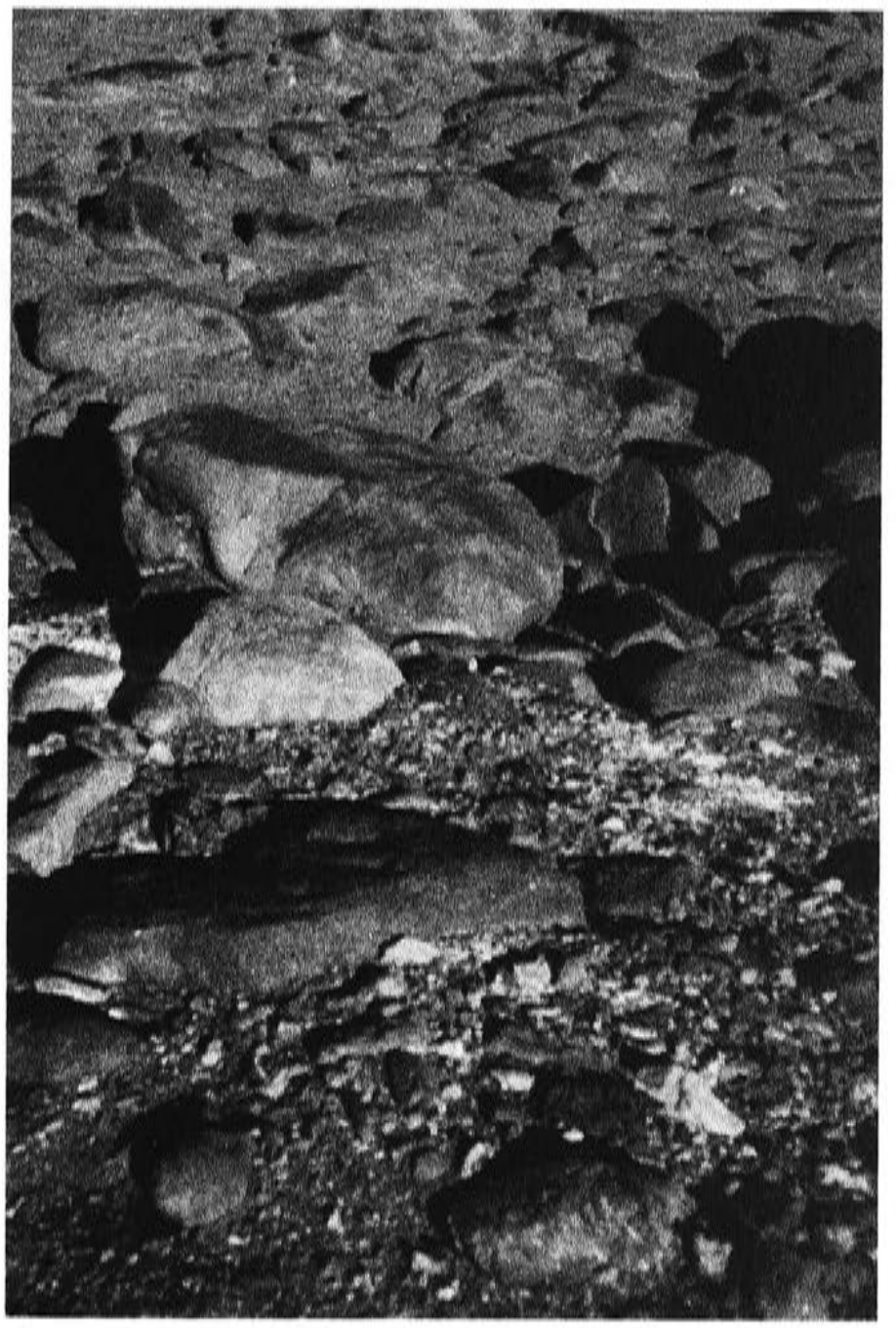

Figure 2.1: The marine limit at Kolich Point. The marine limit here is defined by the change from multiple lithologies, angular clasts and greater weathering above the marine limit to brown, rounded clasts with sand interspersed below the marine limit. The view is from above the marine limit looking down the slope such that the foreground shows the region above the marine limit and the background shows the region below. The size of the larger boulders in the photo are approximately 0.5 m in diameter.

active Antarctic beach is not dissimilar to that of a temperate beach (Figure 2.3) and is predominantly composed of a sand and gravel mix, with small boulders. Generally, the beaches are clast supported (boulders with interstitial sand) with clast sizes up to about 30 to 40 cm in the more active areas. In the front of the beach there is a swash zone made of finer material, sand or gravel — often with some cusp development. Cusps are formed by wave action on the beach berm eroding out small areas to form a scalloped pattern. A typical cusp size is only a few metres wide. Above the swash zone there is a change in slope to a steeper angle and this slope often contains seaward imbricated clasts (orientated towards the sea). The berm at the crest of the beach appears to be formed during major storms with the average clast size being greater

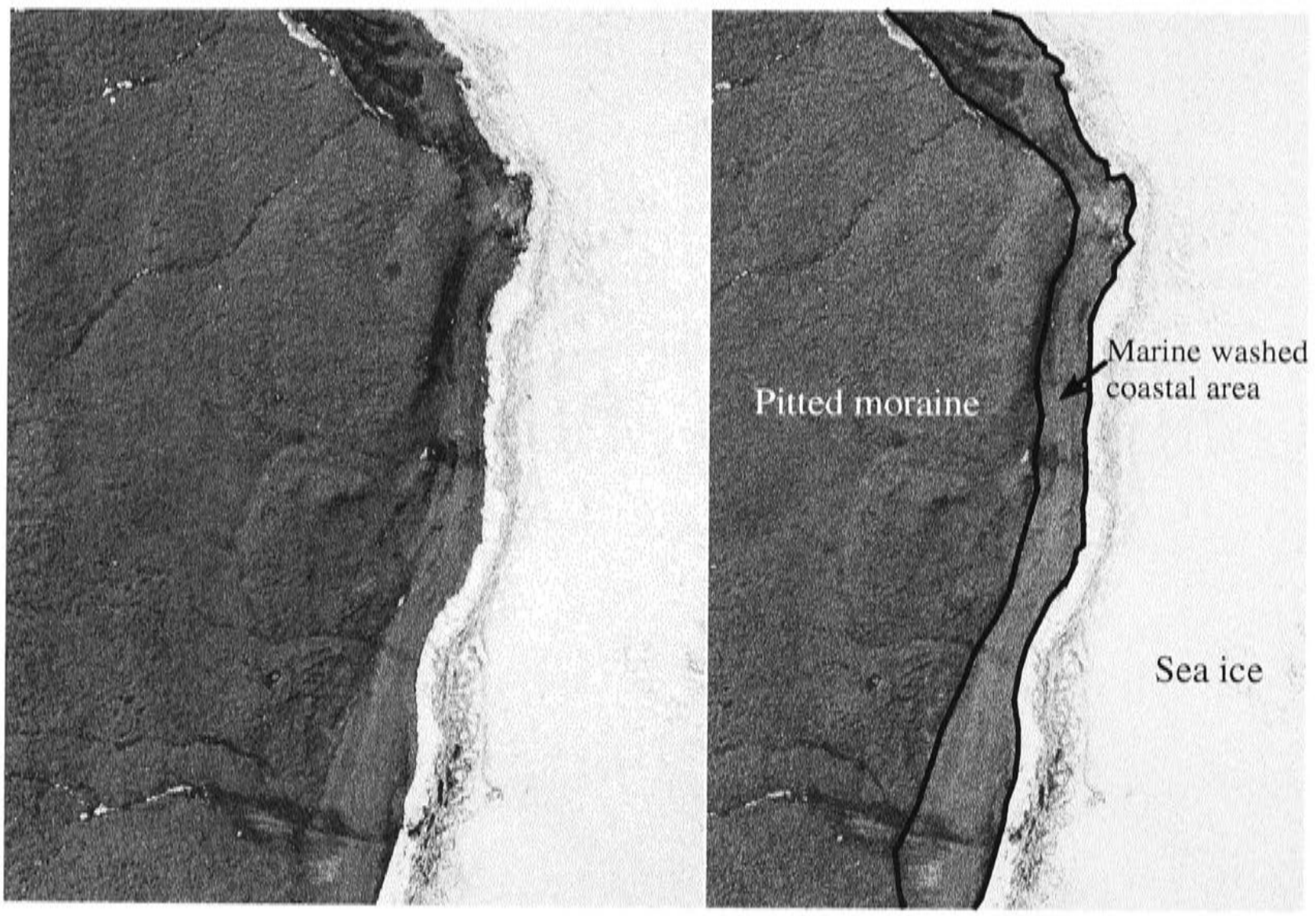

Figure 2.2: Aerial photo showing the raised beaches and marine limit at and to the South of Cape Bernacchi. On the right shows the sea ice, raised beaches up to the marine limit and the pitted moraine above the marine limit.

than it is lower down on the beach. The top of the beach is typically quite flat, with a gentle slope back towards the swale behind the berm. This swale is made up of finer overwash material.

This sequence of features is repeated several times on the Scott Coast of McMurdo Sound, with each successive sequence occurring at increasing elevation with increasing distance from the present shoreline (see Figure 2.4). Rockier beaches are less easily subdivided into wave action areas (e.g. swash or overwash zones) than the sandier beaches. The surface of the swales between the ridges (the overwash zone) is made of finer material than the berms because of a surface accumulation of fines (about 30 cm deep at Marble Point) that have been washed out after beach formation from the ridge or moraine above. Due to a greater degree of weathering of the older ridges the higher swales are more filled in than the lower swales. The beach berms are rocky, and clast supported, with an average boulder size of 10 to 20 cm. Internally, the beaches are

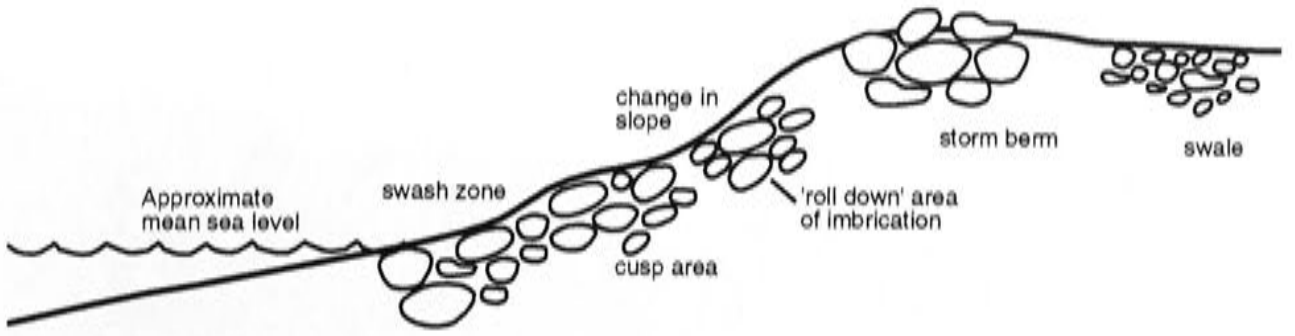

Figure 2.3: Sketch of a profile through a typical Antarctic beach. The scale is vertically exaggerated but shows the area where sea level is normally on the beaches and the high berm formed during storms. The height of the storm berm varies between about 0.5 m in low energy areas to about 4 m in exposed sites. The distance between the berms is dependent on the overall slope of the shore and the wave energy. Cusps form from wave action.

layered, although the characteristics of the layers are usually similar between different layers in a beach, such as the roundness of the pebbles.

Successions of beaches along the shores of McMurdo Sound occur commonly on short stretches of coastline between rocky headlands where the sediment supply is sufficient. The raised beaches consist of a series of 3 to 5 ridge and swale systems up to the marine limit (Figure 2.4). The source of the material that forms Antarctic beaches is likely to be a local reworking of moraine and littoral sediments (Kirk 1970). However, longshore currents supply sediments to a few beaches such as at Kolich Point and Cape Hallett, and sea-ice transports material from gravel size to boulders. The largest boulders on the beaches are erratic boulders up to several metres in size.

In the case of the Scott Coast on the western side of McMurdo Sound the local rock types found in the beaches are granite, granodiorite, dolerite, marble, schist, gneiss, quartzite and the occasional piece of volcanic rock — some of which is sea-ice rafted in from Ross Island. At Cape Bird and Cape Hallett the local rock type is volcanic (olivine basalt to trachytes at Cape Bird and basanite to basalt to hawaiite at Cape Hallett (Le Masurier 1990)).

The dominant beach-forming process is water and wave action, although ice is a feature of Antarctic beaches and ice push features can sometimes be recognised. Ice push features are formed on the active beach, and occasionally are preserved on the raised beaches, such as at Cape Ross. These ice push features occur when a large piece of shore-attached ice is bulldozed up the beach from the breaking-up sea ice. The ice and gravel mix forms an ice-cored mound at the end of the bulldozed area with a flat area seawards of where the ice was. Large pieces of stranded ice can also be incorporated into the beaches which, when they melt, form melt-out pits in the beaches.

Sea ice can also be a major factor in determining whether beaches form or not. If the sea ice does not break out during the summer, the beach will not receive any significant wave action and thus not form a true beach. Poorly formed ridges (such as at Cape

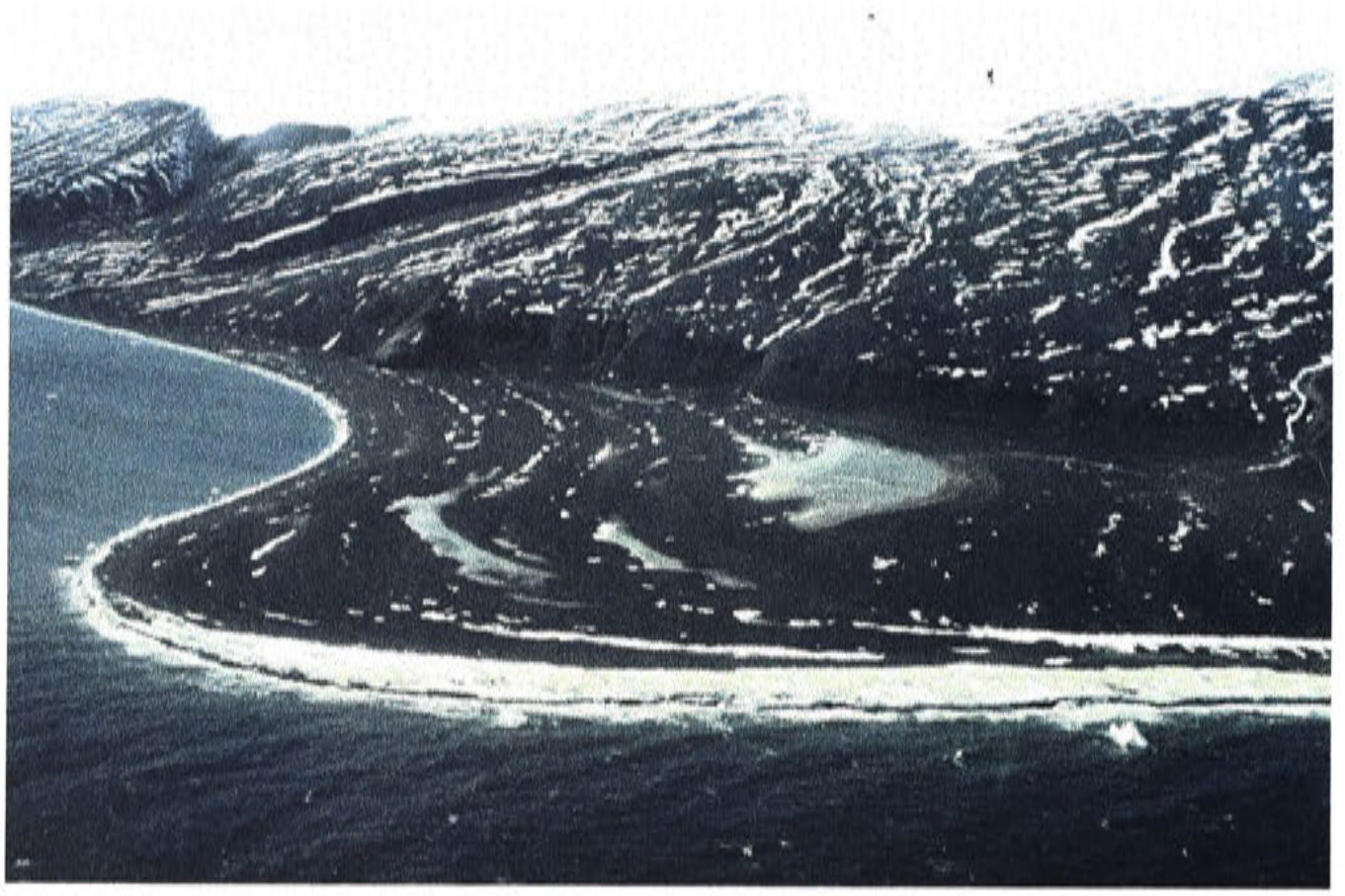

Figure 2.4: Photo looking at the southern point at Cape Bird, Ross Island. A series of raised beaches extend out and around the cape to a height of about 9 metres above present day sea level. The small patches of snow or ponds pick out the swales behind each ridge. The marine limit is at the base of the small cliffs. For scale the distance from the cliffs to the point is approximately 500 m.

Geology. Figure 2.5) are examples of a lack of development due to fewer open water seasons. At present the beaches in McMurdo Sound become ice free in mid-January and the sea ice re-freezes between late-February and early-March. When (if at all) an area of sea ice breaks out depends somewhat on whether it is a whole bay or only a section of an exposed straight coastline that needs to break out. The true break-out times of the sea ice at the head of McMurdo Sound are difficult to estimate in the modern era due to ice-breaking activities by ships that loosen ice earlier in the season than would otherwise occur. Extrapolating break-out times into the past, therefore, becomes even more difficult.

To form discrete beaches either the land has been rebounding sporadically or the conditions that lead to a preservation of a particular beach occur episodically. The latter may be caused by a large storm event as is seen in the creation of the top of the berms or it may be a result of a small change in climate such that the shore is not ice free for a thousand years or so, allowing a beach to be uplifted beyond wave action. With a retreating ice sheet and global climate change, it is surprising to find the higher beaches as well formed as the present day beach, indicating that the past condition of formation must have been similar to that of today. In some places, such as at Marble Point, there is minor development of secondary beach ridges in the swales between two

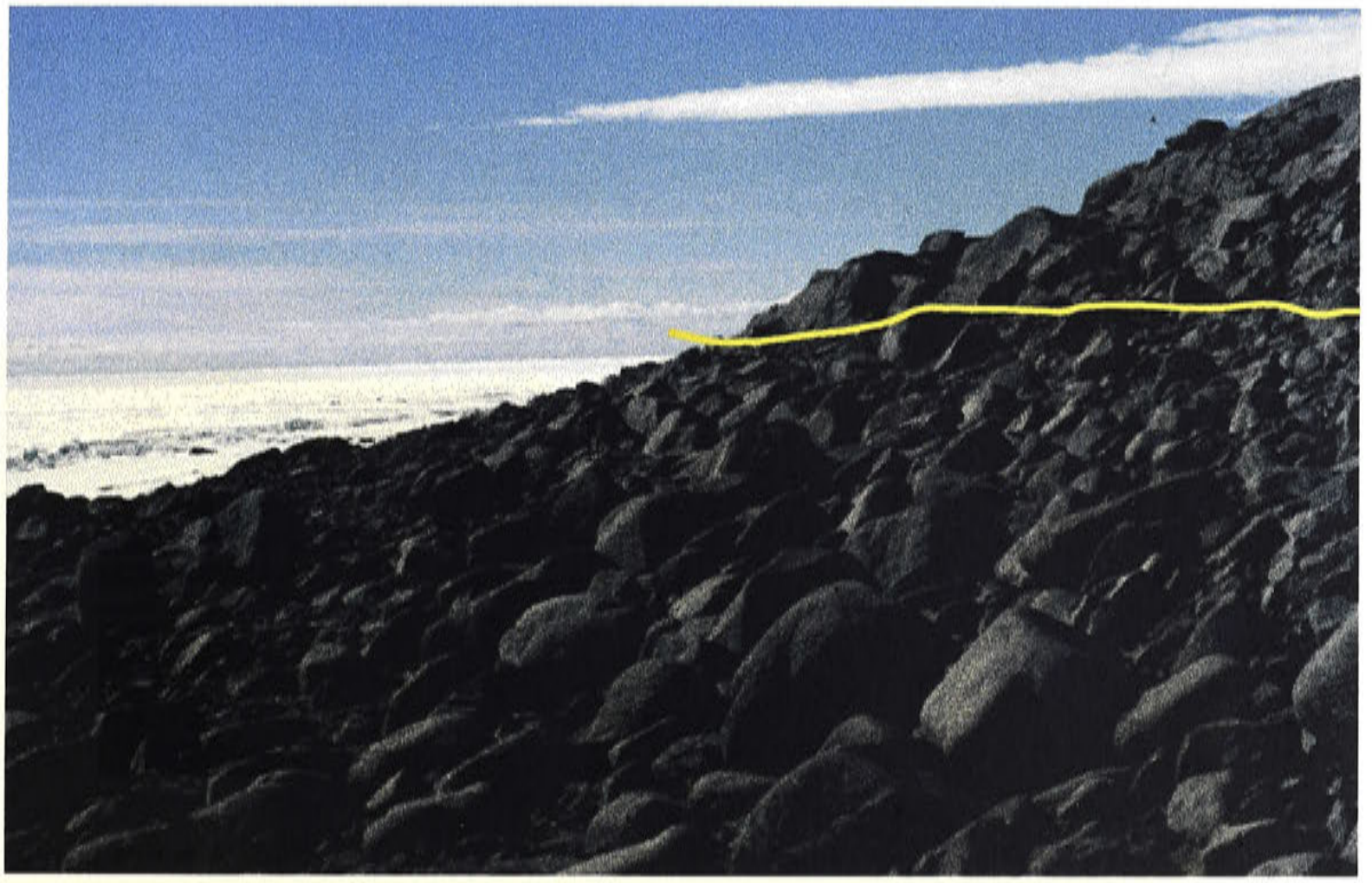

Figure 2.5: Photo of poorly formed ridges at Cape Geology. The marine limit is marked by the yellow line on the right-hand-side of the photo. The marine limit is also visible from the roundness of boulders below the marine limit.

major ridges. These have probably formed in events smaller than those that caused the larger ridges, but not large enough to form a true ridge.

The beaches along the Scott Coast range from very low energy environments (very sandy with little other material) to very high energy environments (large boulder banks). In general, the main fetch (wave generation area) direction is from the north east in McMurdo Sound and this is reflected in the higher energy levels of the north-east facing beaches. The wave energy is also reflected in the morphology of the beach ridge (Figure 2.6). Lower energy beaches are flatter and wider. In the case of Spike Cape the height of the beach ridges reduces significantly where the former-islands (now peninsulas) stopped waves originating from the dominant fetch direction. On the southern side of all the capes there is only the short fetch of McMurdo Sound (in most cases less than 80 km) and often the sea ice does not break out of the southern side of the point so the beaches there tend to be sandier. The same sandy tendency is seen in bays where the sea ice rarely breaks out (such as in Explorers Cove). Low energy beaches and shore deposits still form in these locations from the little wave energy propagated through the sea ice into the small ice-free stretch at the waters edge that develops in the summer.

In order to establish a relative sea level curve for a site it is important to measure the formation height of the raised beach with respect to the height of the modern beach.

Figure 2.6: Top: High rocky berms found at Kolich Point. These berms are up to 5 m in height and show the high wave energy reaching this point. These beaches have well defined cusp areas, storm berms (A), and large, deep swales (B) behind the berms. Bottom: A lower energy sandy beach in the bay near Kolich Point. Cross-section cut through the beach showing a pebbly wind-scoured surface on top with an internal structure of sandy cross-bedding. The height of the section is about 1 m.

The height of the berm above the relict beaches can vary from half a metre to several metres, depending on the wave energy that formed the beach. Because of this height variation, the berm tops are not reliable measures of beach height and a feature such as the break in slope in front of the berm that occurs on both the modern and relict beaches is a more reliable indicator of the relative sea level on the relict beach.

The extent of weathering on the raised beaches must also be accounted for. The wearing down of boulders and filling of the swales can give a false impression of the beach berm height and provides another reason not to use the berm for a measure of beach height. The amount of weathering of the beach boulders is also an important consideration for surface exposure dating because an incorrect estimate of the erosion depth will lead to an incorrect age (see chapter3). Weathering of the beaches increases with height above sea level and the boulders on the top beaches are heavily weathered in places with 'tails' of crystals downwind of the predominant southerly wind direction in the area ('tail' size depends somewhat on boulder material — marble weathers fastest). In many cases the boulders have weathered into a well rounded form. Coarser grained rocks, such as granite, weather by individual crystals breaking off but the marbles also weather by a process of losing flakes. Endolithic algae grow at a depth of 1 to 2 cm within the marble rocks, providing a weak layer at which the rock will flake. Phonolithic (wind sculpting) weathering, common in many places in Antarctica, does not occur below the marine limit because this type of weathering requires a long time of exposure. Chemical weathering is active on the beaches as well, but the physical weathering is dominant. Iron staining is an obvious feature here and appears to be most extensive on the southern facing beaches. All the beaches have a deflation surface of small pebbles less than 30 mm and individual crystals weathered from the surrounding cobbles and boulders (Figure 2.7). The deflation surface is formed by the wind scouring of the finer material, similar in appearance to pebbled concrete.

2.3.1 Sandy beaches

Sand is not common in the McMurdo Sound beaches except as part of the matrix of a boulder beach. Only in the most sheltered areas behind rocky capes or in bays where the sea ice does not break out fully during the summer months will a beach deposit consist solely of sand. Explorers Cove, close to Kolich Point, high on Marble Point and some of the ridges at Cape Bernacchi were the only places visited where sandy deposits occur. Occasionally gravel and cobbles are found within these deposits, indicating the occurrence of a storm event that moved the larger material. More generally, the sands are well stratified and show specific beach deposit bedding such as dipping bedding of an overwash deposit on the rear of a beach dune. Ice can be incorporated into these beaches as very small stranded icebergs on the beaches. These can be seen in the raised beaches, either still as ice or as disturbed slumped sediments where the ice has subsequently melted out. At no site is there a progression from sandier beach deposits to

Figure 2.7: Deflation surface on the beaches at Marble Point with a gravel surface and small scattered boulders. The view is along one of the raised beaches on the south side of Marble Point. Snow to the left-hand-side fills the swale from the seaward beach and the leading edge of the beach berm. The length of beach shown in the photo (to the edge of the hill) is approximately 800 m and a day-pack is in the foreground for scale.

more boulder-rich deposits down a succession of relict beaches (progressively younger). This indicates that it is likely that the sea ice did not break out progressively more over time but rather that seasonally open-water conditions have existed for the entire time of beach formation.

Examples of a sandy beaches are found on the two highest ridges at Marble Point. These ridges contain medium grain size sands that are finely bedded with no larger material. The height of sea level at the time of the highest beach formation indicates that at this time Marble Point would have been an isolated island about 300 m from the main coast with a shallow isthmus in formation. The island would have created a sheltered environment with the shallow water preventing much wave action in the area. Sands would have been the largest particles that the low water energy was capable of shifting, allowing beds of finely layered sands to form. The probable shallow water and thin bedding make this site an ideal target for optically stimulated luminescence dating.

2.3.2 Boulder beaches

Boulder beaches are at an extreme end of the beach types seen along the Scott Coast. They retain all the features of a sand and gravel beach but have a larger typical clast size which can be up to a metre in diameter. On one site where the boulders have been used for surface exposure dating (Cape Bernacchi) the beach faces north-east and is seasonally open to the Ross Sea. Cape Bernacchi appears to become ice-free regularly (on its north-east side) so will be exposed to large storm events capable of building the large rocky berms. There are three wide relict beach ridges above the present-day beach. Any potential higher beaches than this are unformed or covered by the edge of a very steep moraine-covered hill on the back of the beaches with a minor talus slope. Cape Ross is the other sampled location with boulders of a sufficient size for surface exposure dating. This is on the northern side of Granite Harbour and is ice free much earlier in the season than the rest of McMurdo Sound.

2.4 Boulder pavement

Raised shorelines feature boulder pavements in varying stages of development. As their name suggests, they are very flat surfaces formed by the planing action of sea ice which removes the tops off the boulders. In the case of Cape Roberts, where the boulder pavements are superbly developed (Figure 2.8), the boulder pavements consist of former beach ridges made of interlocking boulders . The underside and sides of these boulders are rounded in the usual way of beach boulders but the tops are smoothed flat. There are no ice scours on the top of the boulders but a polished surface is also not developed. There is very little sand on these ridges, only gravel between the boulders and in the swales. The boulder pavements are developed on both the northern and southern sides of the cape whereas the present day beach is well formed only on the northern side. At Cape Roberts the present beach on the northern side is also a boulder ridge but rather than showing evidence of erosion it is a depositional feature, suggesting a change in sea ice and erosion conditions. Each boulder pavement at Cape Roberts was sampled for surface exposure dating.

2.5 Rock Platforms

The rock platforms in Victoria Land are formed in association with the raised beaches along the coastal areas where the bedrock outcrops at elevations higher than elsewhere, typically on headlands but also within the bays. A series of steps that can be correlated to each beach are formed in the rock (Fig. 2.9). Field observations suggest that the rock platforms are formed from ice abrasion rather than wave action. The tide crack between the shore-attached ice and the sea ice works with waves and swell. The working of the crack forces the sea ice up and down in an elliptical motion that scours the bottom.

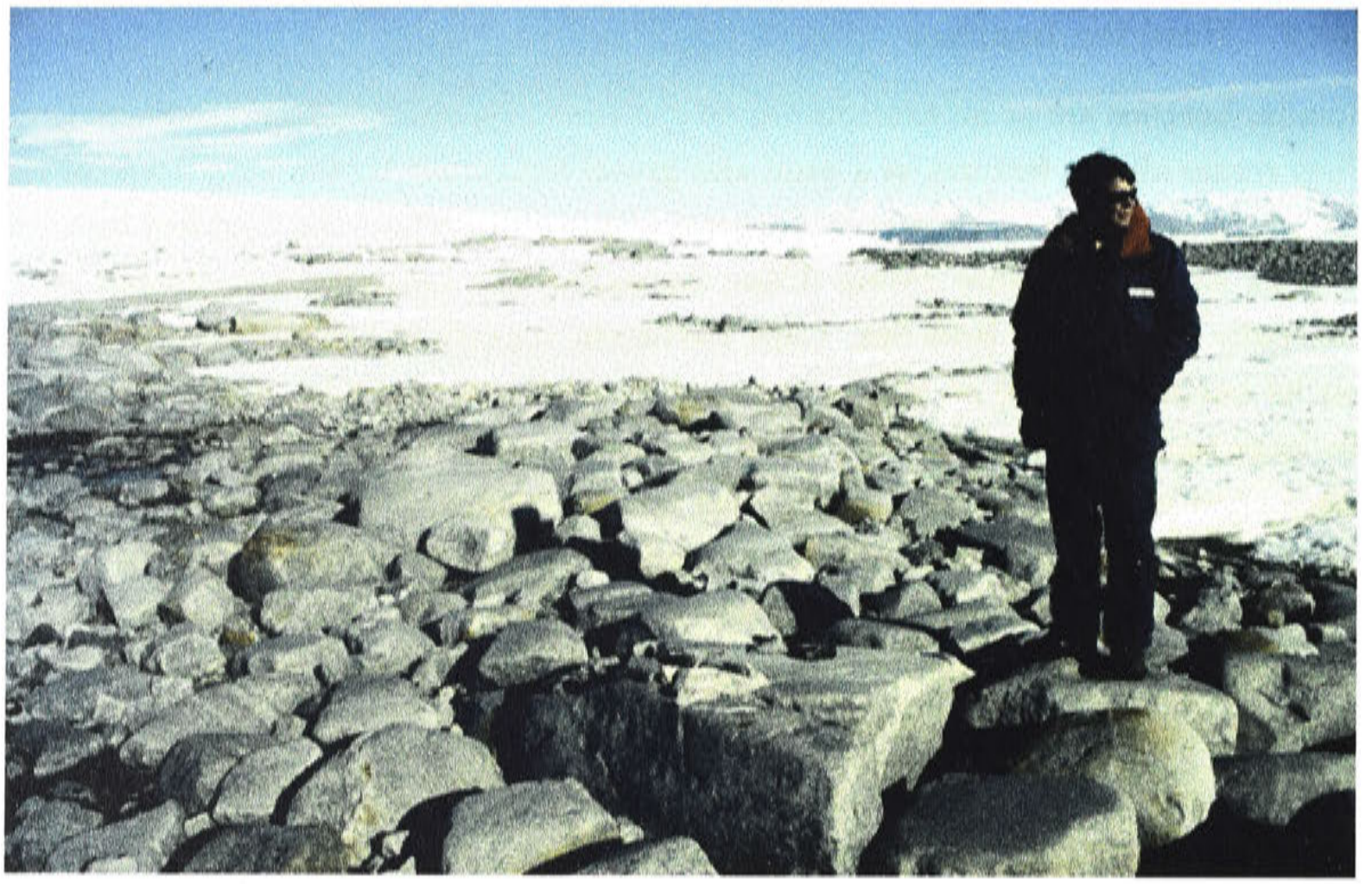

Figure 2.8: Boulder pavement at Cape Roberts. View along one of the raised beaches on the northern side. Note the very flat tops on the boulders with rounded sides. Beaches extend for several hundred metres. The rocky berm on the right-hand-side in the middle ground is the active beach.

If the bottom is rock the ice cuts and polishes the rock into a step. At a later stage some wave action may modify the ice cutting, but the polish retained suggests this is minimal. Because the scouring occurs at the base of the sea ice approximately 2 m below sea level, the platform that correlates to a beach ridge is actually below the beach ridge in true height by about 2 to 3 m, depending on the wave energy that formed the beach. The sampling of wave/ice cut rock platforms for dating purposes has not been attempted in the Antarctic before, although has been successfully used elsewhere — such as on the main rock platform in Scotland (Stone et al. 1996).

2.5.1 Deltas

In the deepest part of the bay between Marble Point and Cape Bernacchi a small delta was formed at the mouth of a stream (Figures 2.10; 2.11) at a time of higher sea levels. The source for this delta, now about 400 m inland from present sea level, is a stream (South Stream) draining from the Wilson Piedmont Glacier. Beach ridges are located to the north and south of the deposit up to about 12 m above sea level. The beach ridges from the north are flat in profile and consist of a wide (10 m) boulder zone of slightly rounded stones, pebbles and sand with a narrow swale in behind. There is pitting,

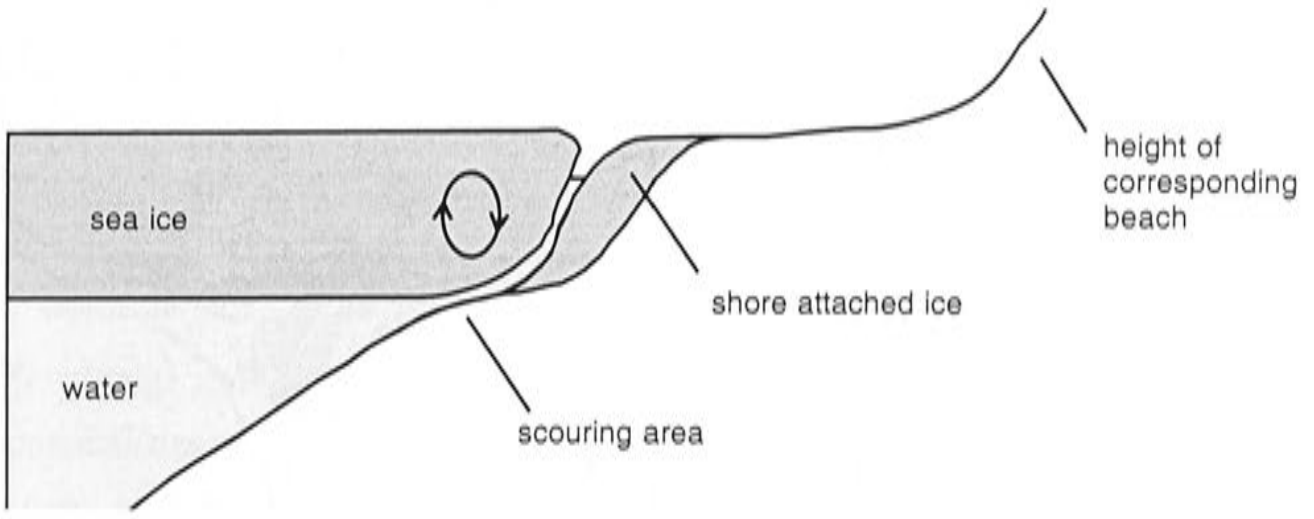

Figure 2.9: Formation of rock platforms by ice scouring. Wave action moves the loose sea ice in an elliptical motion over the scouring area, eroding the bedrock.

from ice melting, of the surfaces in the swales. The beaches are wide (approximately 40 m), composed of well-rounded clasts, with a rise of approximately 2.5 m. The beaches become less distinct towards the delta as they decrease in height and grain size until the ground becomes hummocky with ice-melt pits up to 30 cm deep. On the south side of the stream the beaches are slightly more confused due to multiple streams from the hill slope behind. The ground is well sorted, but pitted, and appears to merge into the highest beach ridge.

The flattening of the beaches and the reduction in grain size suggests a lowering of energy towards the delta. A low wave energy environment with little movement of material would be required to ensure the preservation of the deltas as the sea-level dropped. This could be achieved by a reduction of wave energy levels as waves refract around the Marble Point headland (the dominant wave-front direction is from the north-east). In such a scenario waves arriving in the area of the delta would have very little energy for reworking the deposit.

Aerial photos of the beaches on the northern and southern sides of the delta show that they are at approximately the same altitude. Slightly further up the valley, skirting the top end of the delta, the marine limit probably lies close to but above the delta because it contains marine shells. This would put the marine limit around 15 m asl which is between the limit seen at Marble Point (around 20 m asl) and the 12 m seen at Cape Bernacchi. The surface of the delta is almost as high as the surrounding beach ridges, indicating that it must be younger than the top-most ridges. Steps lower in the delta (closer to present day sea level) that could be interpreted from the aerial photo as a marine limit may actually be lower beaches.

A 5 metre section through the delta was cleared and the stratigraphy and sedimentology examined by Webb (1997) in conjunction with sampling for the shells dated in this thesis (Figure 2.12). The strata in the delta dip 6 to 30° seaward. Webb (1997) also made a detailed analysis of sediment grainsize and diatoms from this section. Grain

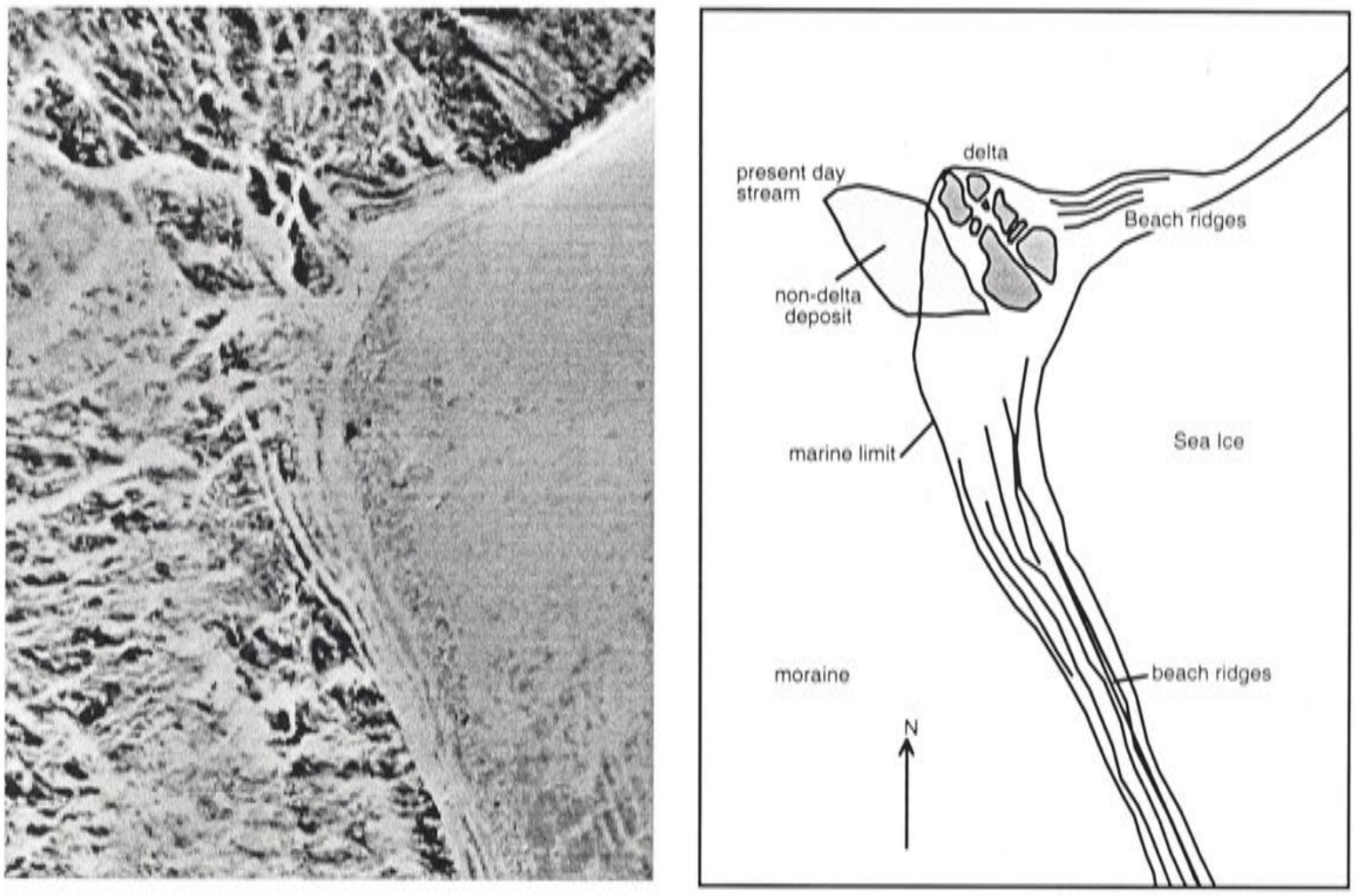

Figure 2.10: Aerial photo of the delta at South Stream, Scott Coast and the surrounding beach ridges. The delta edges are clearer on the ground (see the next figure) but this view shows the marine limit and the beach ridge height lessening towards the head of the bay. The ridge-like appearance across the delta are stream cuts in-filled by snow in this image. Width of the photo is approx. 4 km.

size analysis shows an overall upwards coarsening trend but with a shift to a fining sequence in the middle part of the section. A coarsening trend suggests shallower water or a higher water inflow (it can carry larger grains). A shallowing of water depth would correlate well with relatively rapid delta formation. Fluctuations in the grain size can be interpreted as a function of changing environmental conditions supplying sediment.

Diatom analysis shows a large percentage (average 60%) of fresh water species with the remainder being of brackish or marine origin. There is a larger percentage of marine species at the base of the section. Deposition of the delta would occur in summer when the melt-water streams are flowing and this is when the diatoms would be growing as well. The large influx of fresh water into the near-shore area could provide conditions for the fresh-water and brackish-water diatoms to be deposited in a marine environment. This interpretation fits with the fresh-water algae found in the delta. Stuiver et al. (1981) have described this algae and have used it as part of their dating of the delta (later it will be shown that the ages are consistent with the shell dates).

Some layers in the delta contain shells including *Adamussium colbecki* and *Laternula*

elliptica. The presence of these shells and the sediments and diatom assemblage indicate that the delta formed in a marine environment.

2.6 Ross Sea Drift

While glacial moraine information does not give direct evidence of the rebound along the coastal area, it can provide clues on ice sheet extents and the timing of the glacial advances and retreats. Positively identifying a moraine on a hillside with a particular glacial event (in this case the last glaciation in the area) provides a limiting estimate of the maximum ice sheet elevation in the area. This in turn can be useful in constraining the total size of the ice sheet.

Denton et al. (1989) attempted to provide a constraint for the overall size of the Ross Ice Sheet by this method (see Figure 2.13) using information from the Reedy Glacier, Beardmore Glacier and Hatherton / Darwin glaciers that flow into the Ross Sea from the East Antarctic ice cap. By determining the youngest moraine in each valley and assuming a constant age for these, maximum limits of ice height in the Ross Sea have been obtained since the ice could not have been higher than the moraines at the outlet end of the glacier. Orombelli et al. (1991) examined the glacier profiles and moraines of the Terra Nova Bay region and provided constraints on the Ross Ice Sheet in this area.

The *Ross Sea Drift* is a term given by Stuiver et al. (1981) to the area covered by the last expansion of ice in the Ross Embayment. Aerial photos of the region clearly show the Ross Sea Drift as a covering of sediments around the mouths of the valleys and coastal areas (Figures 7-4 and 7-5 from Stuiver et al. (1981) show this well). The drift sheet, characterised by numerous eskers and minor moraines, has end moraines around the McMurdo Sound region and in the Taylor Valley. The geographical distribution of the terminal moraines has been mapped, along with their heights above current sea level (see Figure 2.14). The Ross Sea Drift is described by Stuiver et al. (1981) in terms of its soil development characteristics (very little development) and its boulder frequency and lithology. The dating of sediments from a pro-glacial lake dammed in the Taylor Valley (Stuiver et al. 1981) and from small ponds (Hall and Denton 2000b) have constrained the time of this drift sheet to the Latest Pleistocene.

2.7 Hjorth Hill Moraines

Moraines from the Ross Sea drift and older drifts occur between Cape Bernacchi and the mouth of the Taylor Valley. This area is large and gently sloping with small valleys and streams that formed after the drift deposition. The height of the lateral/terminal moraine of the Ross Sea Drift is around 300 m (Brook et al. 1995) here on the side of Hjorth Hill (Figure 2.14). The melting of incorporated ice and stream development has

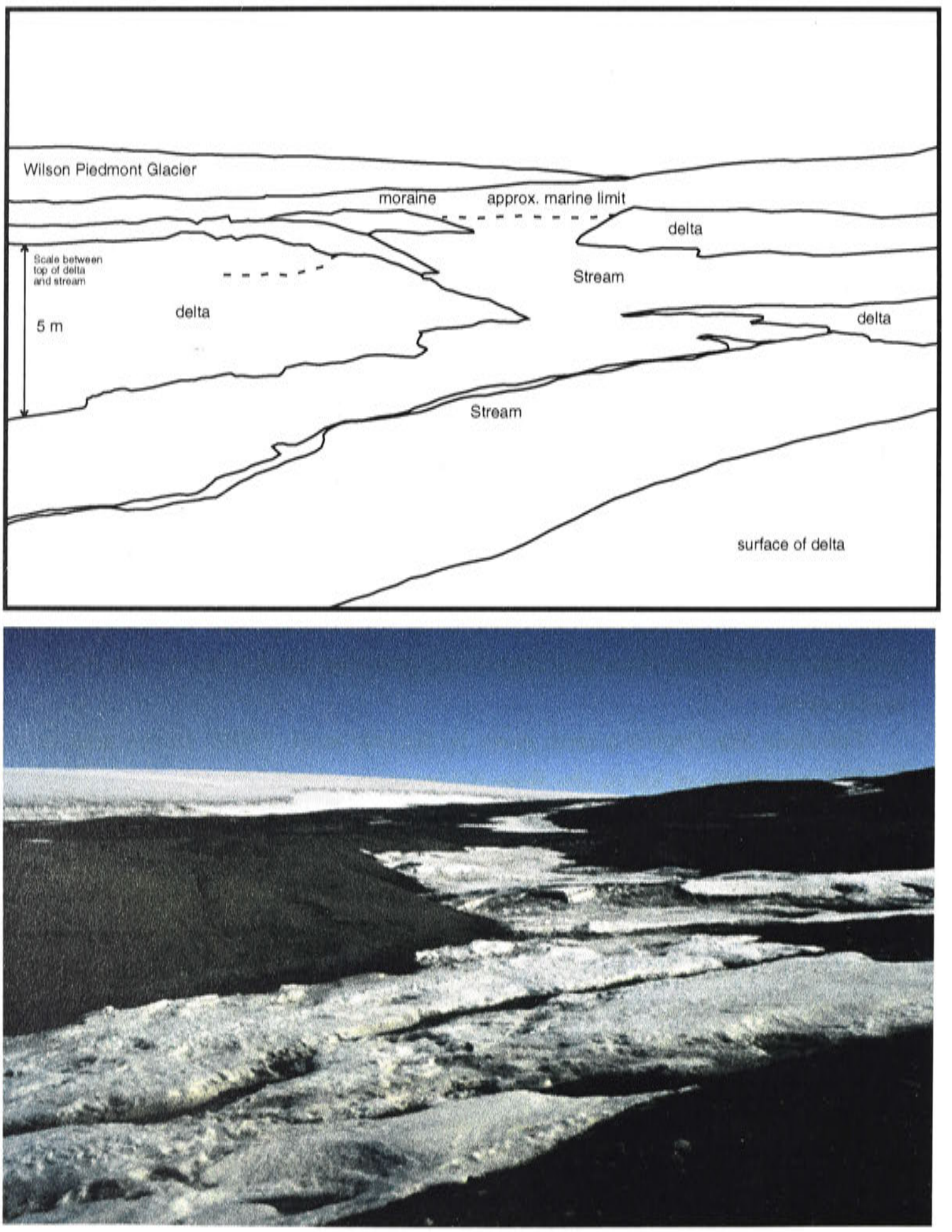

Figure 2.11: Top: Overlay for the photo of the South Stream delta. Bottom: Delta at South Stream. The delta here is cut by modern streams leaving 'islands' of the former delta. Snow covers most of the bed of the stream in the photo. Distance to the Wilson Piedmont Glacier is approximately 1500 m.

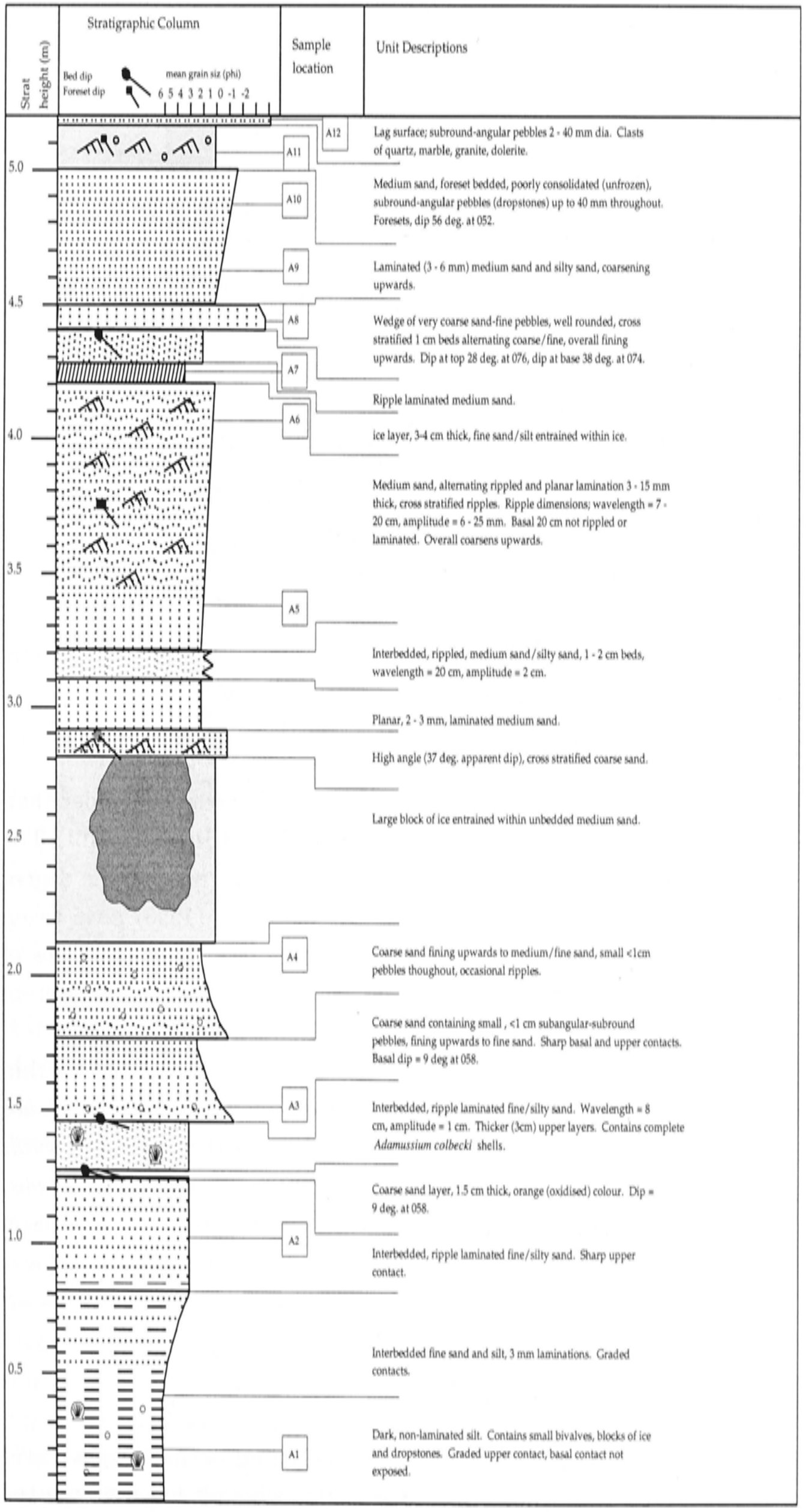

Figure 2.12: Stratigraphic column of section through the South Stream delta. From Webb (1997).

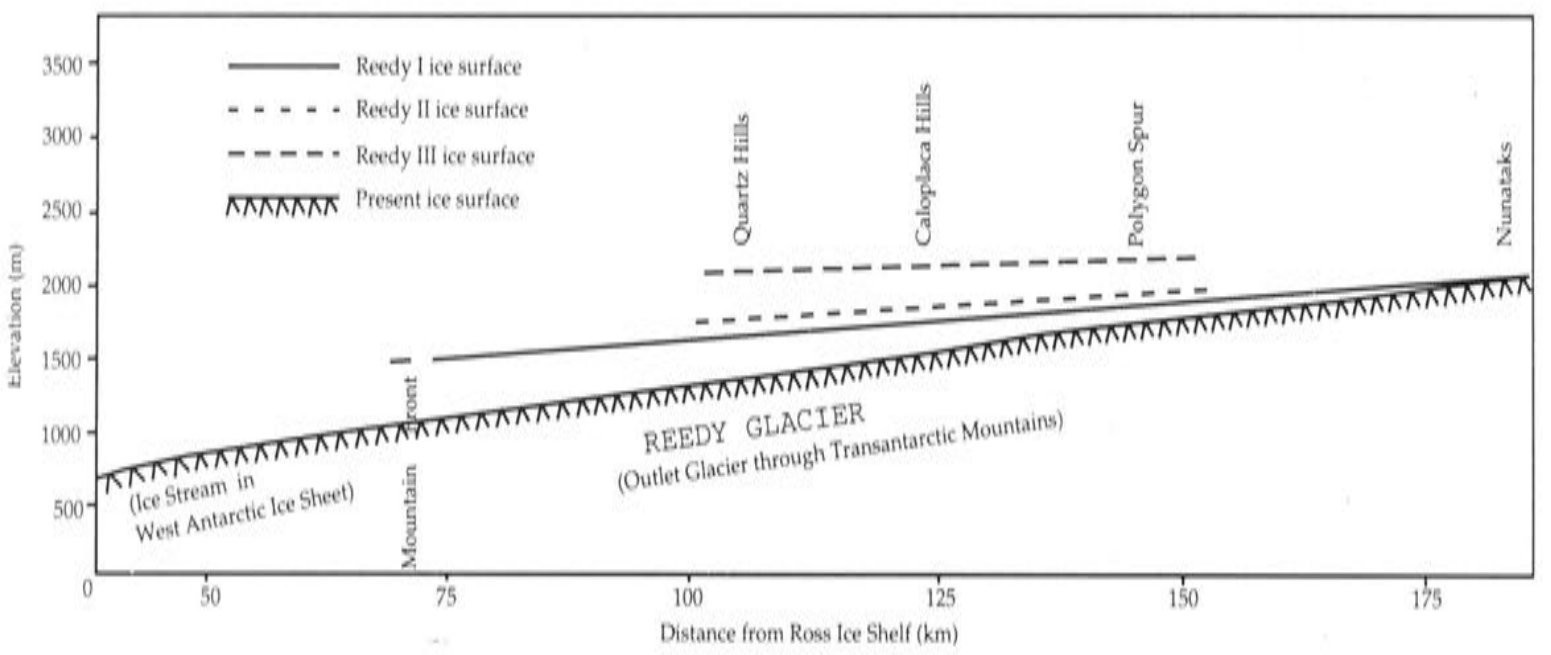

Figure 2.13: Interpreted palaeo-ice surfaces of the Reedy Glacier (flows into the Ross Sea about 86°S) from former glaciations. The former surfaces are only dated by relative dating and are referred to as the Reedy I, Reedy II, and Reedy III ice surfaces. Projections of the ice surface to the Transantarctic Mountain front places a limit on how much ice was in the Ross Sea (it cannot have been higher than the lateral moraine) and likewise at the inland end (approximately where the nunataks are marked). Quartz Hills, Caloplaca Hills, and Polygon Spur are mountain ranges in the Transantarctic Mountains that are cut by the glacier ice. From Denton (1989).

produced a hummocky ground of meltout pits and stream beds. Sediments older than the Ross Sea Drift appear higher on the slopes of Hjorth Hill and Hogback Hill. The lithology of these glacial sediments is the same as the lower sediments but the degree of weathering and soil development is much greater. Brook et al. (1995) have taken 12 surface exposure dating samples from two sites in this area to compare the ages of older and younger moraines. The dates of the older moraine at Hjorth Hill range from 104,000 to 567,000 and the younger moraine range from 8,000 to 106,000.

The moraines on these same hills show there is more than one set of moraines within the younger drift sheet and that there is some overprinting of glacial moraines onto other material. Hall and Denton (2000a) have closely mapped and dated fresh-water algae from the various moraines. This mapping, together with my field observations, suggests that an ice sheet overrode the coast from the east and merged with the Wilson Piedmont Glacier, with various advances and retreats over the Late-Pleistocene and Holocene.

2.8 Wilson Piedmont Glacier

One interesting problem on the Scott Coast of McMurdo Sound is the erosive power of the Wilson Piedmont Glacier and the effect of the glacier where it has over-run the

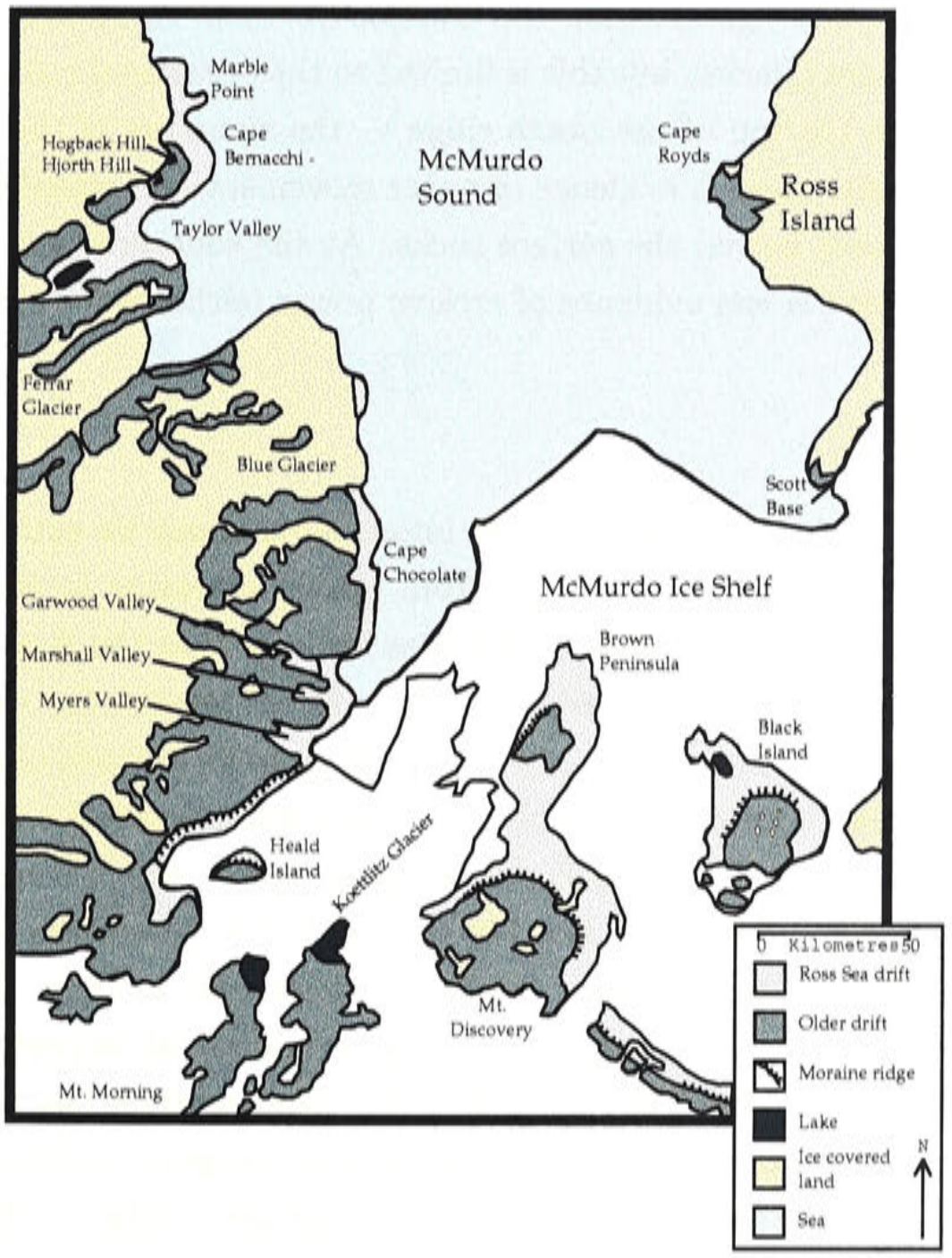

Figure 2.14: Location of Ross Sea drift and older drift sheets. After Brook et al. (1995). The light grey is the Ross Sea drift from the last glacial period which extends up to 300m on Hjorth Hill and Hogback Hill, and into the Taylor Valley where the ice blocked the valley mouth between 23,800 and 8,340 ^{14}C years before the present (Hall, 1999b).

beach ridges. At four field sites visited the beach ridges extend beneath the glacier. In the case of Kolich Point the profile of a sandy beach (shown in appendix A) comes from a point about 20 to 30 m from where this beach extends beneath the glacier. Old aerial photos of this area (from the 1960's) show that the whole area, extending almost up to Kolich Point itself, was covered by the Wilson Piedmont glacier at that time. This suggests that the glacier has very little erosive power, and when it expands and retreats it has a frozen base so moves by projecting ice out from above the base in a

'rolling' motion over the surface and does not move any rock material. Similar evidence for this can be found to the north at Spike Cape and at Cape Roberts. Beaches at Cape Roberts show some sign of minor disturbance for 10 to 15 m away from the face of the Wilson Piedmont Glacier, but this is limited to the occasional rolling of the small boulders/ cobbles on the top of the beach ridge — the structure of the ridge remains unchanged. At this site there is evidence of water movement (silt covering the rocks in places) which may have moved the surface rocks. At the southern part of the Wilson Piedmont Glacier there is less evidence of erosive power (either way) of the glacier.

2.9 Summary

Observations from McMurdo Sound provides information about ice extents and former sea levels in a variety of ways. Evidence from glacial moraines in the surrounding valleys and along the hills of the Scott Coast area indicate that the Ross Sea drift, the ice sheet of the last glaciation, extended some 300 m above present-day sea level on this portion of the coast. Former sea levels are preserved up to an altitude of about 33 m at Cape Ross and decrease southwards to about 11 m at Cape Bernacchi and westwards to about 9 m at Cape Bird on Ross Island. Cape Hallett has a very low recorded marine limit. Below the marine limit raised beaches (typically 3 to 5 beaches) or correlatable rock platforms are found except where the ice-free land ends in cliffs. The formation time, sediment supply, formation energy and preservation are all important features of the beach that must be known before a meaningful interpretation can be made about the local relative-sea-level change. It must have taken a change in conditions to preserve each relict beach, and in most cases the relict beaches are similar to the present-day beach indicating all the beaches have formed in similar conditions. Dates presented in chapter 3 have been obtained from sandy beaches, boulder beaches, boulder pavements, bedrock platforms and a marine delta to show that most of the marine features in this environment can now be usefully employed in determining the relative position of sea level.

Chapter 3

Dating Methods

3.1 Introduction

To date, the history of the ice sheet in the Ross Sea area has been constrained largely by radiocarbon dating of organic material within raised beaches and lakes and ponds dammed by the ice sheet. Much of this material is scarce along these shorelines, leading to a poorly constrained relative-sea-level curve for the various sites along the Victoria Land Coast except for Terra Nova Bay where long a penguin occupation has enabled a good relative-sea-level curve to be inferred by Baroni and Orombelli (1991).

Three Quaternary dating methods have been widely used for establishing chronologies of geological events in low and middle latitudes: the well-developed radiocarbon method and the emerging optical dating and surface exposure age methods. All three methods, however, have limitations at high latitudes. Suitable material for precise and unambiguous ^{14}C dating on and around the Antarctic continent is often scarce. In addition the accuracy of the results is limited by uncertainties in the reservoir correction, a correction for water which has been isolated from the ocean/air ^{14}C exchange and consequently has an anomalously old age. Surface exposure age methods are beginning to provide promising results for Antarctica but the uncertainties arising from rock erosion assumptions and from models of the incident radiation can be large. Few optical dating dates have been obtained for Antarctica and the present results must be considered largely as being experimental. Because of limitations of each, and because of the expanded range of datable materials, a combination of all three methods is desirable.

This study attempts to compare the two other dating methods, optical dating and surface exposure dating using ^{36}Cl, with radiocarbon dating to obtain an improved relative-sea-level curve for the McMurdo Sound area. Optical dating has potential to be useful in the setting of raised beaches because there are some sandy beaches that formed during the austral summer when there is 24 hour daylight (increasing the probability of the grains being reset). Surface exposure dating has potential to be useful in the rockier areas of the coastline. Both large boulders on the beaches and

stepped rock platforms may provide suitable material for this dating method. Using a combination of the three methods can be advantageous because there is a greater chance of obtaining enough dates to form a good relative-sea-level curve. Also, having three independent methods reduces the potential errors from effects such as the ^{14}C reservoir correction not being accurately known.

The next few paragraphs digress from the topic of the dating of the raised shorelines to outline the nature and contribution of the dating to the thesis. A number of people are acknowledged in this chapter because without their expertise and equipment this dating work would not have been possible. Because of the variety of techniques used, I outline that part of the work done by myself and that for which I received assistance.

The accelerator mass spectrometry (AMS) radiocarbon dating preparation and graphitisation was done by myself, except for the initial few samples where I was taught the methodology (by John Head). Measurements were made on the Australian National University facility. I pressed all the samples and made the measurements under the supervision of Drs Keith Fifield and Richard Cresswell from the AMS facility.

All surface exposure dating work was carried out by myself from field sampling to chemistry under the guidance of Dr John Stone. Other people have aided me in learning the techniques and in providing suggestions but did not participate in the sample dating from collection to measurement (excepting the major element analysis and some of the trace element analysis). Drs. Keith Fifield and Richard Cresswell also supervised the AMS runs of the ^{36}Cl samples.

With the optical dating, my role was limited to helping in the initial stages and being present at the running of the samples. A new method was being explored with these samples to improve the accuracy of the younger predicted age of the samples and, due to the complexities of the method, there was not sufficient time for me to contribute to the development of or to use the procedures in production mode.

At the commencement of this project with the fieldwork in 1997 and 1998 little information was available. Unbeknown to me, parallel work had been proposed to the United States Antarctic Program and this led to a substantial amount of additional ^{14}C dates (Hall and Denton 1999, Hall and Denton 2000b, Hall and Denton 2000a). These results are incorporated into this thesis. Had the field work by Hall and Denton not been done or been unsuccessful, the dates from my thesis would have provided more constraints for the relative-sea-level curve in McMurdo Sound than otherwise would have existed.

3.2 Radiocarbon Dating

3.2.1 Introduction

Ten samples from mollusc shells and penguin eggshell were radiocarbon dated using AMS from the McMurdo Sound area and from Cape Hallett further north. I have

assumed here that the reader has a general knowledge of radiocarbon dating and the associated corrections (such as the correction for isotopic fractionation) and this section therefore only highlights any points that are specific to Antarctic samples.

Radiocarbon dates from penguin remains are prolific in the Ross Sea area. There are two species of penguin in the area, the smaller and more abundant Adélie penguin (*Pygoscelis adeliae*) and the larger Emperor penguin (*Aptenodytes forsteri*). The Adélie penguin is more useful for sea-level information as it nests on rocky shores — unlike the sea-ice dwelling Emperor. Samples from within both existing and fossil rookeries have been dated by various researchers (e.g. Heine and Speir 1989, Stuiver et al. 1981, Baroni and Orombelli 1991).

Two types of mollusc were dated from McMurdo Sound, *Adamussium colbecki* and *Laternula elliptica* (Figure 3.1). Both tend to be shallow water species but *Laternula elliptica* typically buries itself deep (up to about 30 cm) in the sediment and allows its feeders to penetrate up through the sea floor while *Adamussium colbecki* (Figure 3.2) is a free-swimming species. Work by Berkman (1994) and Stockton (1984) in McMurdo Sound indicate that *Adamussium colbecki*, in this location, tend to either attach abysally or rarely move except in hyposaline water. Dell (1990) quotes a depth range for this species of 4 to 1335 m water depth.

Figure 3.1: Photo of a *Laternula elliptica*. In growth position with the top of the valves broken off. Width of the shell approximately 4 cm.

Figure 3.2: Photo of an *Adamussium colbecki*. Inside of both valves.

3.2.2 Method

Radiocarbon dating measures the ratio of radiogenic ^{14}C to total C in a sample. In the ocean, water layers do not interact with the air continuously. Because of the fast decay rate of ^{14}C this can mean the ratio of radiogenic ^{14}C to total C in some parts of the ocean can become out of balance with the surface ratio. A correction (ΔR) needs to be applied for the sample location, called the reservoir effect. In the mixed layer of the middle and low latitude oceans this corresponds to a difference of about 400 years, with the ^{14}C being too old by this amount. Water around Antarctica combines with sea ice and there is a seasonal halt in the exchange of CO_2 between the sea and air (Gordon and Harkness 1992). This, together with the water coming from deep in the ocean causes the difference in the ^{14}C to C ratio to be around 1,100 - 1,300 years for Antarctic surface waters. The best method for determining the reservoir effect is to ^{14}C date samples where ages are known by other means (and which pre-date the addition of anomalous ^{14}C into the atmosphere by nuclear explosions, the bomb-spike effect). Fortunately, the early explorers to the continent collected samples of the live fauna that can now be dated. Examples include Weddell seal bones and flesh from seals killed on Inexpressible Island (Northern Victoria Land) in 1912, Emperor and Adélie penguins from Southern Victoria Land at the same time, and penguins from Southern Victoria Land in 1902 to 1904 (Gordon and Harkness 1992). Emperor penguins and a Weddell seal from Cape Evans, Ross Island collected in 1916 (Mabin 1986) and mollusc shells

collected between 1917 and 1940 from West Antarctica and the Antarctic Peninsula have also been dated (Berkman and Forman 1996). These historic dates give best estimates for the reservoir correction of different species in the Ross sea as 1,400 years for seals, 1,130 years for penguins, and approximately 1,300 years for shells and 0 years for algae. The reservoir corrections vary between species as some range over a wider area of the ocean and source food from different 'age' waters (e.g. some food from the mixed layer and some from the up-welling older water). This has been incorporated into the above reservoir estimate for the mollusc shells and penguin eggshell.

The other fractionation measurement required is to account for the differing carbon isotope ratios that different species preferentially take up (δ^{13}C). This has not been measured in this thesis and the estimate of Stuiver and Polach (1977) of -15 ±2.5 ‰for marine organisms has been used instead. This value corresponds to 160 years which is smaller than the uncertainty of the reservoir correction for Antarctica (±200 years).

The procedure for dating of marine shells is routine and is not described here in detail. Dating of penguin eggshell has been attempted by only a few people (one date was found in a literature search). Eggshell from other bird species (such as Moa eggshell) has proven to be a successful material to date (Higham 1994). Long et al. (1983) looked at the different isotopes of carbon in the eggshell of chickens in relation to the isotopic composition of their environment and found that the fractionation in the eggshell is very close to that of the environment. Chickens are closely related to penguins, so this finding can be transferred to the penguins and we can assume that an age from the eggshell will not have an anomalous carbon fractionation. The other issue for the penguin eggshell is the source of the carbon making up the eggshell. The usual carbon source for penguins is marine food but another possible source is gullet stones made of carbonaceous material which is absorbed into the food chain and would make the age appear much older. Observations of the rocks of suitable size at Cape Bird and Cape Hallett - two sites at which eggshell was collected - failed to find anything except volcanic rock but it is possible that the penguins from these rookeries could source their gullet stones from elsewhere along the Victoria Land Coast where carbonaceous material of Pre-Cambrian or Cambrian age occurs as marble bedrock (Gunn and Warren 1962).

The dated penguin eggshell material came from rookeries of the Adélie Penguin at Cape Bird (northern rookery) and Cape Hallett. At both sites penguins have nested on the crests of raised beach ridges for long intervals after formation. Thus, a date from the earliest nests should give a minimum age for the beach ridge. Holes were dug through the penguin nest deposits on a number of beach ridges, and a sample dated from the lowest nest. None of the holes had the dry, dusty characteristics described by Heine and Speir (1989) that occur when a site is abandoned for a number of succeeding seasons. Therefore the deposits dated in this study are believed to have been occupied fairly continuously since the first nest.

The eggshell is typically fragmented into pieces up to 2 cm in size and the eggshell fragments are held together in clumps by partially dried guano. The clumps are separated by nesting stones and solid guano, which clearly defines each eggshell. Thus there is some confidence that only a single eggshell, or single nest, is being sampled. The eggshell was prepared for graphitisation by washing in MQ water and leaching in weak HCl to remove the outer 10% of the shell. Only the sample from Cape Hallett had some brown staining which appeared to extend through the full thickness of the normally white to very pale blue eggshell. Graphitisation of the eggshell was carried out on a graphitisation line at the Australian National University developed by Yokoyama (1999).

3.2.3 Results

Table 3.1 shows the ages obtained for the samples collected at various sites. The conventional ^{14}C ages have been corrected to calibrated ages using the following steps.

1. A fractionation correction of 160 $\pm$40 years for the $\delta^{13}C$ is applied.

2. A partial reservoir correction is applied of 900 years. This consists of the full correction for the Ross Sea area less 400 years for the reservoir effect built into the CALIB4.2.1 program.

3. The age is then calibrated to a calendar age with the program CALIB4.2.1 by Stuiver and Reimer (1993) with the datasets contained in Stuiver et al. (1998) using a marine calibration curve based on U-Th dating of corals from the mixed layer of the ocean. The marine curve has an inbuilt reservoir effect of between 300 and 500 years so that in combination with step 2 will give a 1,300 year reservoir correction.

For estimates of the errors on the ^{14}C age a multiplier of 1.3 was used on the 1 standard deviation initial error to account for scatter in the calibration curves used by CALIB4.2.1 as is suggested in Stuiver et al. (1998). The error on the $\delta^{13}C$ correction and the error on the reservoir correction were combined with the ^{14}C age error using the standard method of error propagation. The propagation of all these errors means that the total errors of the calibrated ages of the samples is typically about 200 years with the major uncertainty coming from the reservoir correction.

3.2.4 Discussion

The Cape Bird area first became ice free before 8,080 $\pm$160 ^{14}C years BP (Heine and Speir 1989) based on a conventional radiocarbon date of an Adélie penguin bone from an abandoned nest site. This abandoned nest site is from part of one of the Cape Bird rookeries that lies above the raised beaches. Because Adélie penguins require open

Sample ANUA	Field ref.	C-14 age	C-14 age - ΔR	Calib. Age with ΔR	Calibration range (1σ)	Location	Sample	Elevation above s.l.
9517	1391	5740 ±230	4440 ±230	5320	4870–5650	South Stream	*L. elliptica*	7.4
9523	1392	6110 ±330	4810 ±330	5720	5310–6180	South Stream	*L. elliptica*	7.4
9519	1395	6180 ±150	4880 ±150	5840	5570–6110	South Stream	*L. elliptica*	7.6
6903	1393	5540 ±220	4240 ±220	5040	4700–5460	South Stream	*L. elliptica*	12.6
6904	1394	5140 ±150	3840 ±150	4530	4220–4850	South Stream	*A. colbecki*	8.4
6901	1396	5440 ±220	4140 ±220	4890	4530–5320	Marble Point	*A. colbecki*	14.2
BLANK	-	25280						
9329	JQ5	2870 ±180	1570 ±180	1900	1580–2290	Cape Hallett	eggshell	2.5
9431	JQ7	880 ±110	modern	modern		Cape Bird	eggshell	3.7
10023	JQ8	1230 ±180	modern	modern		Cape Bird	eggshell	5.4
10024	JQ9	1190 ±110	modern	modern		Cape Bird	eggshell	4.7
BLANK	-	48000						

Table 3.1: Radiocarbon ages obtained from samples in the Ross Sea. Blank samples refer to samples of infinite age run with the samples that precede the blank and the necessary adjustment has been made on the ages where required. Following standard practice, the C-14 ages do not include error estimates from the reservoir correction. This error would uniformly move all the ages in one direction.

water not too distant from their rookeries (Baroni and Orombelli 1994) the penguin bone date indicates that open water was close to the site at this time.

The ages of the penguin eggshells in Table 3.1 suggest that penguins have only recently nested on the raised beaches. The major part of the rookery is above the marine limit and the penguins may have only extended onto the raised beaches in more recent times as the bird population increased. Three dates taken from Cape Bird are all modern once a reservoir correction is applied, even though they come from the lowest stratum.

The single eggshell date from a raised beach at Cape Hallett provides a constraint on sea level, that sea level must have been lower than 2.5 m above present-day at 1,900 years BP. However, this age may be more useful for establishing the time of first occupation of the penguin colony. The only other date from the rookery at Cape Hallett is by Harrington and McKellar (1958), who dated a penguin body at 1,210 ±70 ^{14}C years (uncorrected). This is much younger than the age of 2,870 ±180^{14}C years (uncorrected) from the eggshell in this study. The new age indicates the penguin rookery has been there at least 1,500 years.

The results from the mollusc radiocarbon dates obtained in this thesis indicate that sea level was around 7 to 8 m above present day at 6,000 calibrated years BP, and

ranged between about 15 m to 7 m above present day at 5,000 calibrated years BP. These palaeo-sea-level heights do not include either a correction for the water depth at which the molluscs lived (samples appear to be *in situ*) or a correction for the water depth above the delta surface. The water depths of the samples are taken as a minimum depth range of the species. For *Adamussium colbecki* this is 4 m depth taking Berkman (1994) and Stockton (1984) observations of highest densities at 4 to 6 metres water depth and for *Laternula elliptica* it is 3 m (Dell 1990). Hence the points on the relative sea level curves are minimum heights - sea level may have been higher.

Sediments within the South Stream delta dip between 6^o and 30^o seaward (some of these dips are from sediments within a stratigraphic layer and may be features such as foresets). While it is not possible to assume the surface of the delta is a single stratigraphic layer the dip on the surface is approximately 2^o. Given that this is less than the dip of the sediments 2^o can be used as a conservative estimate of a change in height of a stratigraphic layer from one section of the delta to another. Hence, a correction of 5.2 m water depth would be required between the two sampling locations.

Combining these two corrections suggests that between 5,000 and 5,600 calibrated years BP that sea-level was a minimum of 12.1 to 16.1 metres above present sea level. The high sample from Marble Point (ANUA6901 at 14.2 m) is consistent with an age for an elephant seal buried in a beach dated by Nichols (1968).

Due to its extended ice-free coastlines and relative accessibility, McMurdo Sound has been the focus of a number of studies of the timing of the ice sheet advances and retreats in the area. Hall and Denton (2000b) have obtained ^{14}C dates on freshwater algae within the Ross Sea drift. This determines the age of a pro-glacial lake dammed in the mouth of the eastern Taylor Valley between 23,800 and 8,340 ^{14}C years BP, with a maximum ice advance into the valley from the east occurring between 14,500 and 12,700 ^{14}C years BP (Hall and Denton 2000a) (see Figure 1.3).

Recent work by Hall and Denton (1999) on the raised beaches adds 54 new dates to the beaches. These are from molluscs and elephant-seal skin and fur remains. The molluscs are fragments of *Adamussium colbecki* and were found crushed under boulders buried in the beaches and not in growth position. The shell fragments could be crushed under boulders at any height on a beach but for these to be buried as well probably requires storm action to move the boulders. The elephant-seal skin and fur were found underneath boulders on the surface of the beaches. The seals were probably moulting on the beach during the time of formation (as can be seen today). The beach must have been above sea level at this time. Details of the ages can be found in Hall and Denton (1999); they range from 400 to 5,540 corrected ^{14}C years (480 to 6,310 conventional years BP). Figure 3.3 shows these data and included on this graph are the ages obtained in this thesis. The relative sea level curve plotted on this figure intersects the present day at two metres elevation to account for the average height of the active storm beach which is the modern analogy of the raised beaches. Two metres is an average value

for the Scott Coast of McMurdo Sound taking into account storm beaches facing open sea and beaches with a limited fetch (distance of open water over which waves can develop). The dates on this figure allow limits to be placed on relative-sea-levels in McMurdo Sound from 6,000 ^{14}C years BP to the present.

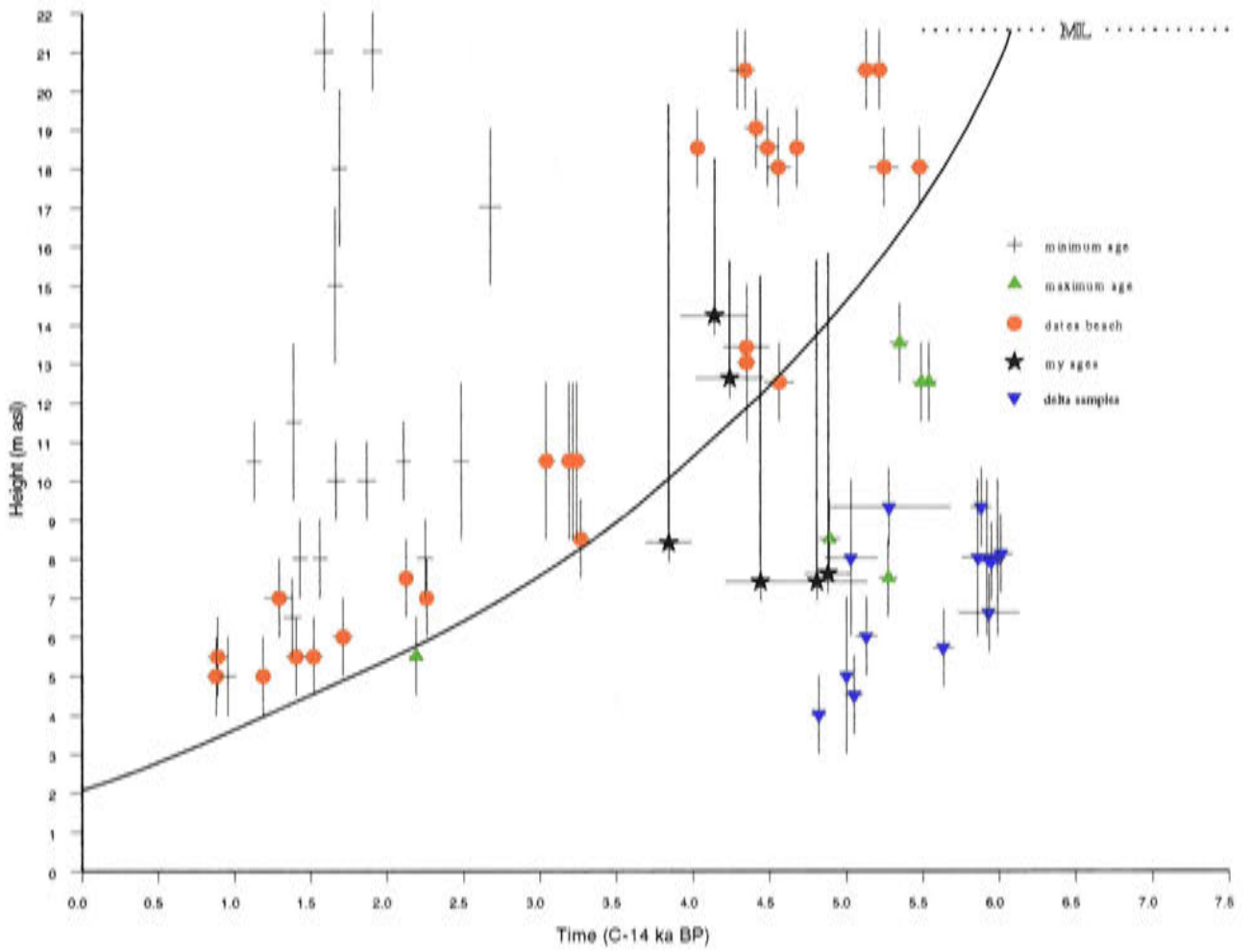

Figure 3.3: Observed relative sea level curve for the Scott Coast from data of Hall and Denton (1999) and this thesis. The radiocarbon ages are plotted on this figure and include a 1,300 year reservoir correction but no other corrections. Crosses are a minimum age from seal fur and skin found close to the surface of the beaches and sea level lies below the points. Triangles indicate a maximum age from non-*in situ* molluscs and sea level must lie to the left of these points. Circles are seal and fur fragments incorporated into the beaches at the time of formation and mollusc fragments crushed under boulders in the beaches and also define upper limits. The inverted triangles are samples from the South Stream delta and define a lower limit. The stars are the data from this thesis for the shells and correspond to lower limits. The line on this curve gives a minimum relative-sea-level curve for the Scott Coast between the present day and 6,000 years BP. This is the relative sea level curve used for comparison with the modelling presented later in the thesis. The letters ML and dotted line indicate the approximate location of the marine limit for McMurdo Sound.

Between 4,000 and 5,000 years BP there is a cluster of dates between 18 and 20 metres above sea level. While Hall and Denton (1999) labelled these samples as dating the beach they also suggest these samples may have been from exceptional storm events depositing material above the active beach level. If this hypothesis is correct, making these samples a minimum age for those beaches lends credibility to the position of the

relative sea level curve through the samples between 10 to 14 m in height between 4,000 and 5,000 years BP.

The cluster of dates from the delta at South Stream is lower than the rest of the dates from the beaches. This suggests that a correction is required for the water depth at which the delta was deposited relative to the mean-sea-level on the beaches. The delta was deposited below sea-level out from the mouth of South Stream, whereas beaches of the same age would occur at a higher elevation. Hall and Denton (1999) describes the dated shells from the delta as a "death-bed" assemblage and therefore we cannot apply a minimum water depth for the shells as described for my samples above. However, to place the "death-bed" shells on the curve in Figure 3.3 approximately 6 metres of water depth would be required.

The inferred relative sea level curve on Figure 3.3 changes slope in an exponential fashion. Because global sea level change in the late Holocene is very small this change suggests the response is due to the removal of local ice in the Ross Embayment or the Antarctic Ice Sheet. This is discussed further in subsequent chapters.

The marine limit from Marble Point is indicated by ML and dotted line on Figure 3.3. In Chapter 2 the marine limits from along the coast have been discussed. If it is assumed that the increase of the marine limit to the north along the edge of McMurdo Sound is a result of a progressive deglaciation or opening of the beaches to the sea (an ice shelf or permanent sea ice may have persisted in the area post-deglaciation) then the intersection of the marine limits with the relative-sea-level curve will give an idea of the timing. These limits suggest that Cape Roberts and Dunlop Island were deglaciated prior to 6,000 years BP, Marble Point around 6,000 years BP and Cape Bernacchi about 4,500 years BP. None of these ages have been confirmed with dates.

Timing for ice-free conditions in this general area comes from two small islands to the north, Beaufort Island (close to Ross Island) and Franklin Island where ^{14}C dating of penguin remains indicate ice-free conditions by 6,000 years BP (Stuiver et al. 1981). Another constraint on grounded ice in the McMurdo Sound area comes from shell samples that have been brought up from the shallow sea floor by internal dynamics of the ice shelf and which are now found on the surface of the floating ice shelves. Grounded ice would not allow marine species to grow beneath the ice sheet. This constrains the grounded ice to 7,750 years BP (Kellogg et al. 1990). The timing of grounded ice extending into the Taylor Valley has been explored by Hall and Denton (2000b). This study has the ice retreating from the valley at 8,340 ^{14}C years BP.

Terra Nova Bay, approximately 400 km to the north of McMurdo Sound has raised beaches that have been dated by Baroni and Orombelli (1991), Baroni and Orombelli (1994), and Orombelli et al. (1991). A mix of shells incorporated into the beaches and penguin remains were ^{14}C dated to provide a relative sea level curve for this area. The curve is shown in Figure 3.4 where the dashed line shows the minimum relative sea level on the coast. Apart from the *in situ* shells, this data only provides a limit on the

relative sea level because the dates are a minimum age. It is interesting to note that the marine limit is about 30 m, higher than on the McMurdo Sound coast, suggesting that this area may have deglaciated earlier.

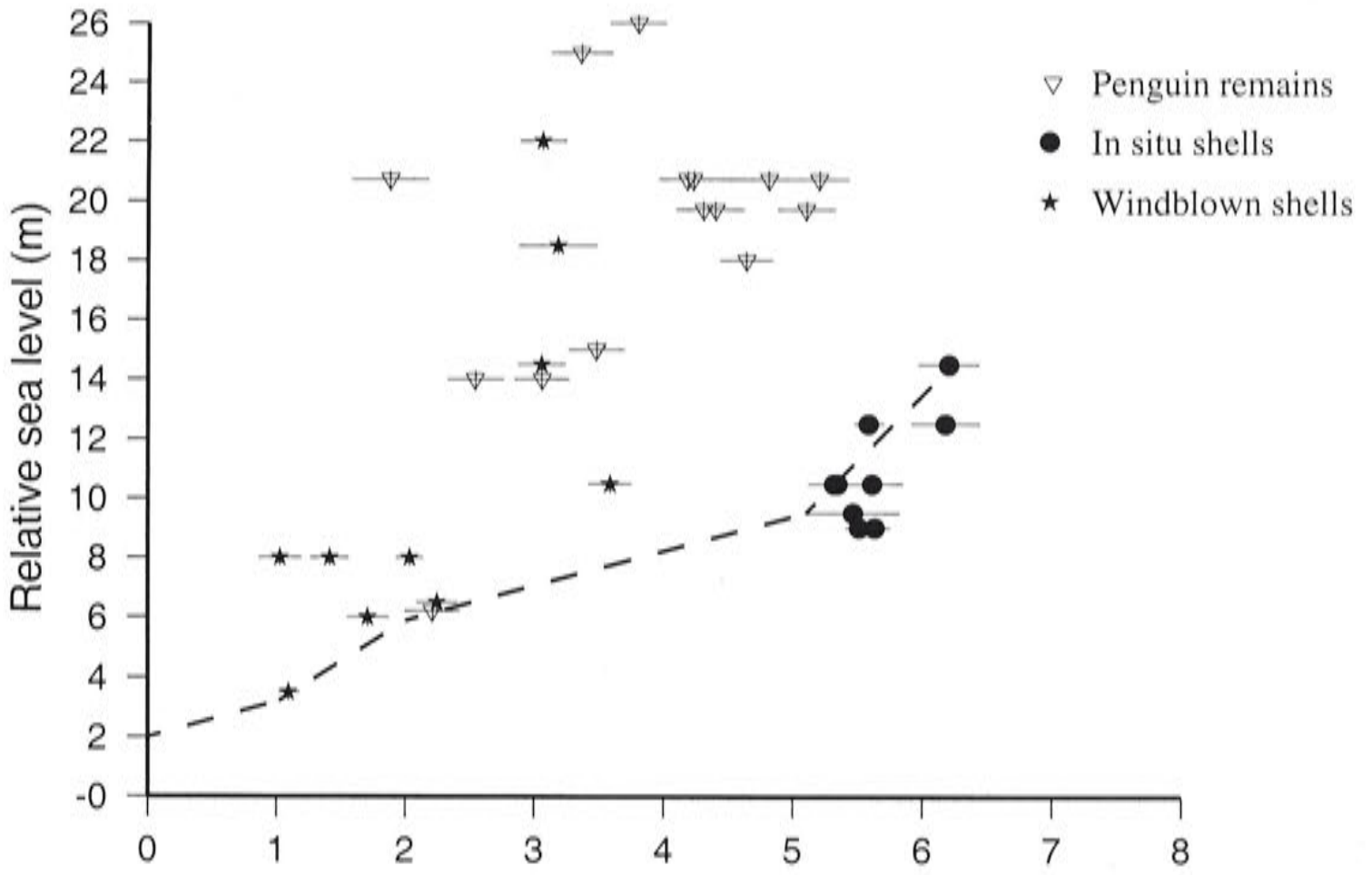

Figure 3.4: The relative sea level constraints from Terra Nova Bay. Circles show the ages from shells found in the beaches (date the formation of the beach) while triangles are penguin remains, which show a minimum age for their height. Stars are wind-blown shells. Therefore sea level lies close to the dashed line. Observations are only found between 7,000 years BP and the present day. Data comes from Baroni and Orombelli (1991), Baroni (1994) and Orombelli (1990). Not shown on this figure is the marine limit about 30 m.

3.3 Optical Dating

3.3.1 Introduction

Optical dating is a numerical method for dating the length of time elapsed since a sediment was buried. Because the sample ages are expected to be Holocene the error on the optical dates may be large as it can take thousands of years for luminescence to build up to measurable levels if the quartz has a low sensitivity to radiation, as is

the case for these Antarctic samples. Hence, the method may only be suitable here as a cross-check against the radiocarbon dating. Consistent dates from both methods would indicate that assumptions made in both methods are valid. Optical dating is also useful for deposits that contain few *in situ* shells or other radiocarbon material, as is often the case in Antarctica. As with the radiocarbon dating section I will assume the reader has a basic knowledge of optical dating and only specific points related to these samples are highlighted. Essentially, trapped charges are removed from their trap sites in a crystal that is exposured to sunlight, but after burial they re-accumulate due to damage from high-energy particles that originate from the radioactive decay of particles in the sediment and also from cosmic rays. The total radiation dose absorbed since burial is termed the Palaeodose.

Two samples were selected for optical dating dating from Marble Point on the coast of McMurdo Sound. Both of the samples were from close to the marine limit and were chosen to complement the radiocarbon-dated samples. There is little sediment movement in the winter because of freezing. Therefore I believe that the sediments were deposited during the austral summer when there is 24 hour daylight, maximising the chances of full bleaching, although there is some possibility of grains moving in the dark, late in the season before complete refreezing of the beaches, lakes and streams.

The first sample (JQTL1) is from a homogeneous unit consisting of sands of a medium grain size and is finely layered in mm to cm scale beds. The sample is interpreted as being formed in a shallow tidal area on the lee side of a small island. The sample height is about 19 m above present-day sea level and 330 mm below the surface.

The second sample (JQTL5) comes from a shallow-water dune made up of two units: a loose dry, medium-grain-size sand with planar and cross-bedding, and a sand with a very fine gravel. The ^{14}C sample ANUA6901 of a shell fragment came from within this dune. The sample height is about 15 m above present-day sea level and 300 mm below the surface.

Both samples were taken from as deep as the permafrost would allow. The fine bedding in both samples (Figure 3.6) indicates that there is a good chance that the samples were well bleached during the deposition stage and that the deposits have not been disturbed since then.

3.3.2 Method

In optical dating the first assumption made is that all sand grains have been reset to zero before burial by exposure to sunlight. Because of the lower light levels at high latitudes it could not be assumed that all sand grains in my Antarctic samples had been reset (bleached), despite the sensitivity of optically stimulated luminescence (OSL) to light. An incompletely bleached grain will give an anomalously old and inconsistent age. Hence, a grain-by-grain optically stimulated luminescence method was chosen in preference to a multiple grain method to allow distinction between bleached and

incompletely bleached grains.

The method used on the samples in this thesis was the 'improved' single-aliquot regenerative-dose (SAR) procedure developed by Murray and Wintle (2000) from the earlier method of Murray and Roberts (1998) and used here for single grains (Figure 3.5). The regenerative-dose curve builds up by giving grains known radiation doses (Figure 3.5) following measurement of the natural OSL signal (the luminescence) as the initial step. The stepwise measurement determines the character of the luminescence-radiation relationship for the sediment and the intercept of the natural OSL (N) onto this curve gives the palaeodose (P) from which the age is calculated.

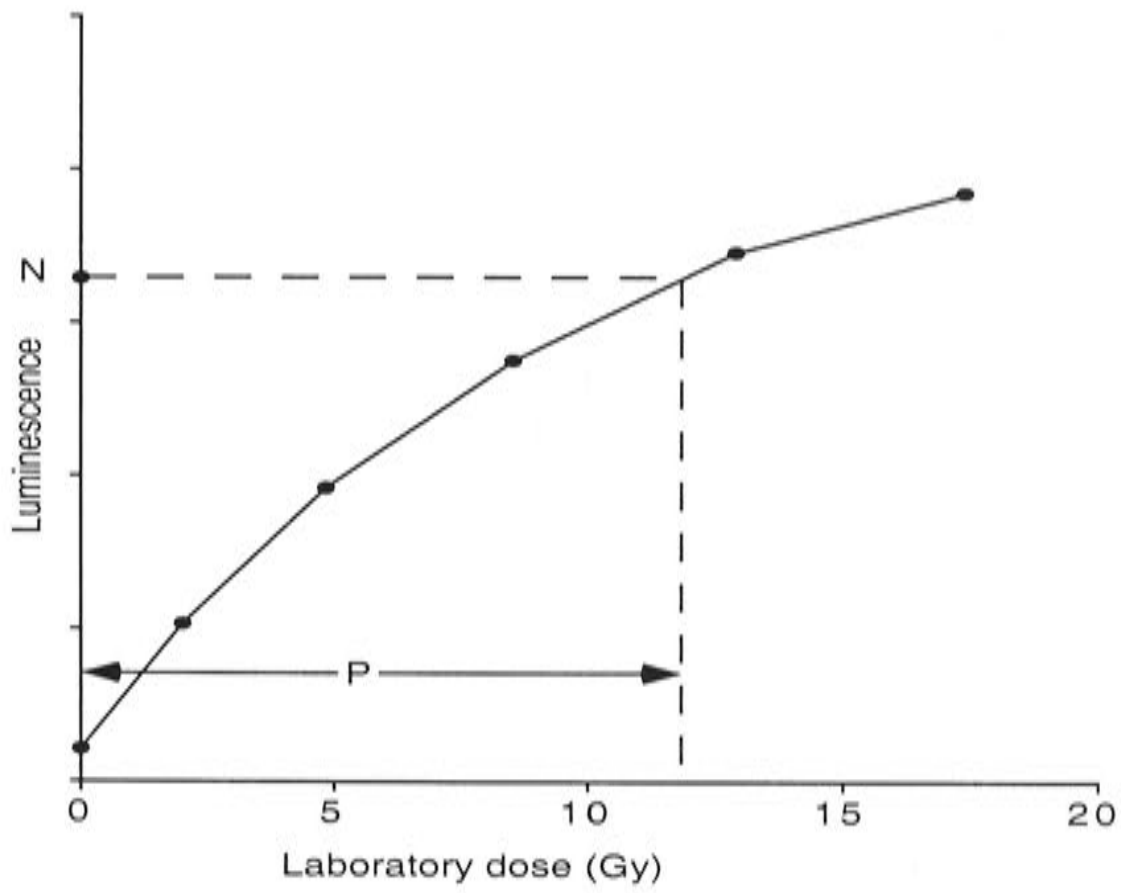

Figure 3.5: Regenerative-dose method of measurement. Aliquots of the sample are given varying doses of radiation and measured for their optically stimulated luminescence. The palaeodose (P) for the sample is calculated from the intercept of the measured natural optically stimulated luminescence (N) with the regenerated-dose curve. Figure after Aitken (1998).

The advantage of the regenerative dose method over the additive dose method is that it does not assume knowledge of the mathematical form of the growth curve. If there are any sensitivity changes within the luminescence, the bleaching and irradiation of the sample may cause the palaeodose to be incorrect but the SAR procedure also makes a measurement of any changes in sensitivity to the test doses applied so that suspect grains can be identified. There have been some recent reservations expressed about the procedure (Spooner et al. 2000) but it is still considered to be the most reliable of the existing single-grain optical dating methods.

Only two samples were considered appropriate for analysis because sample prepa-

ration and measurement for optical dating is time consuming and complex. Thus I did not perform the physical analysis myself. Instead, Norman Hill was responsible for nearly all the preparation (with my assistance), Daniele Questiaux performed the analysis, and Nigel Spooner was responsible for the measurement method choice and the measurements themselves.

To calculate the time, T, of burial for an OSL sample it is necessary to know the annual dose-rate which is received both from external sources and local radioactive decay and the palaeodose age is then the palaeodose/dose rate. The gamma ray component of the dose-rate (from any local radioactive decay) is measured in the field using a gamma scintollometer (Labelled Field gamma spectrometry on Table 3.2). The estimate of the annual dose-rate can be incorrect if the water table has moved relative to the sample position. Water absorbs some of the radiation resulting in a lower annual dose if the water table has been above the sample site. Sites may also have seasonal water table fluctuations, but for Antarctica it is difficult to sample below the summer water table due to permafrost.

To determine the dose rate that the quartz grains have received, the samples are also measured in the laboratory for U, Th, and K contents. The radioisotope activities of these and other radioactive isotopes were measured using high-resolution germanium gamma-spectrometry (by Dr Jon Olley, CSIRO Division of Land and Water, Canberra, Australia), and the parent isotope concentrations were calculated (labelled High-resolution gamma spectrometry on the table). There was no significant U-series disequilibrium apparent which suggests that there has been no removal of Uranium by water. The potassium contents of the sediments were measured using X-ray fluorescence (XRF) with an estimated error of ± 2 % (by the Department of Geology, Faculties, Australian National University and labelled XRF on the table). In addition, neutron activation analysis and delayed neutron activation (NAA/DNA) were used to measure U, Th and K (at Becquerel Laboratories, Lucas Heights, Australia and also labelled NAA/DNA on table). The weighted means of the radioisotope concentrations measured by these methods were calculated and used in the age evaluation.

The contribution from cosmic rays is only a small fraction of the total dose (the samples are from about 30 cm deep) and this contribution was calculated using the data of Prescott and Hutton (1994) (headed Cosmic ray dose-rate on Table 3.2).

Based on previous results for quartz-rich sediment (Questiaux 1990), the concentration of radioisotopes contained within the quartz grains was assumed to be 10 % of the bulk sediment concentration, and the efficiency with which resulting internally-emitted alpha-particles induced luminescence within the host grain is assumed to be $0.05 \pm 0.02\%$.

Water is an effective absorber of radiation so the *in situ* water content was measured during the sample unpacking procedure (headed In-situ water content on Table 3.2), along with sample mass and volume which are necessary to calculate sediment porosity.

Estimated ages are given in Table 3.2 and in the table, palaeodoses and ages which are very similar are joined together to produce an average palaeodose or age. For example JQTL1 had 75 grains measured with 37 grains averaging 0.5 ±0.11. The number of grains averaged for each age is given in the brackets. The range of ages is discussed in more detail below.

The optically stimulated luminescence measurements for the Marble Point samples were made using a Type TL-DA-15 Risø "Minisys" reader, with an optical stimulation waveband of 420-560 nm provided by a filtered halogen lamp. Emissions were detected by an EMI 9235QA photomultiplier tube shielded by two 2 mm Hoya U340 filters from the scattered stimulation light. For each sample around 40 grains were measured to get a representative population from the sample. The optically stimulated luminescence measurement for each grain ("aliquot") consists of the following steps.

1. Before any measurement is made on the grains a trial dose is applied to ensure that there is sufficient luminescence sensitivity to measure the grain (this dose is subsequently corrected for).

2. The aliquot is pre-heated at 240 °C for 10 seconds to empty thermally-unstable traps.

3. The natural OSL (N) is measured while the aliquot is illuminated for 125 seconds while being held at 125 °C. For each "shine" curve an integral of the final 20 seconds of the measurement is subtracted as a background from an integral of an early portion of the measurement (<20 seconds) to isolate the natural OSL from the background.

4. A test dose (3 Gray (Gy) here) is applied to the aliquot.

5. The aliquot is pre-heated to 160 °C, to empty the thermally-unstable shallow traps while measuring the 110 °C thermoluminescence (TL) peak. This TL can be used to correct for effects of any change in sensitivity during the SAR procedure.

6. The OSL induced by the test dose is measured, as per step 3. This OSL can be used as a means of correction for sensitivity changes during the SAR procedure.

7. Apply the first (typically of 5) regenerative-dose.

8. Pre-heat as per step 2.

9. Measure regenerative-dose OSL as per step 3.

Repeat steps 4 to 9, another 4 times, each time with an incrementally larger regenerative-dose, in order to construct a regenerative-dose growth curve. This is the curve from which the paleodose (P) is determined.

Sample	JQTL 1 ANU_{OD}114a	JQTL 5 ANU_{OD}114e
Sample burial depth (m)	0.33	0.30
Quartz grain diameter (μm)	387.5±37.5	387.5±37.5
Field gamma spectrometry (μGy)	712±36	783±39
High-resolution gamma spectrometry (activity Bq)		
U-238	27.51±1.93	18.43±2.42
Ra-226	24.74±0.35	22.30±0.48
Pb-210	19.80±0.28	17.84±0.39
Th-228	32.79±0.43	25.77±0.59
Ra-228	32.68±0.71	26.86±1.06
Th-232	32.76±0.37	26.03±0.52
K-40	652.6±9.7	603.0±13.5
High-resolution gamma spectrometry (concentration)		
U (ppm)	2.00±0.03	1.80±0.04
Th (ppm)	8.05±0.09	6.39±0.13
K (%)	2.06±0.03	1.91±0.04
Weighted means of isotope concentrations		
U (ppm)	1.99±0.07	1.83±0.04
Th (ppm)	7.76±0.08	6.63±0.09
K (%)	1.98±0.02	1.90±0.03
XRF		
K (%)	1.872±0.037	1.906±0.038
NAA/DNA		
U (ppm)	1.92±0.08	1.93±0.08
Th (ppm)	7.07±0.14	6.92±0.14
K (%)	1.72±0.12	1.73±0.12
Cosmic ray dose-rate (Gy/ka)	0.202±0.030	0.202±0.030
Internal alpha dose-rate (Gy/ka)	0.055±0.022	0.048±0.02
Internal beta dose-rate (Gy/ka)	0.035±0.004	0.033±0.003
External alpha dose-rate (Gy/ka)	0.014±0.007	0.012±0.006
External beta dose-rate (Gy/ka)	1.588±0.035	1.534±0.033

Sample	JQTL 1	JQTL 5
External gamma + cosmic ray dose-rate (Gy/ka)	1.217±0.033	1.149±0.032
Total dose rate (Gy/ka)	2.909±0.060	2.777±0.056
In-situ water content (%)	5.4±1	3.6±0.7
Saturation water content (%)	44±9	35±7.0
In-situ fraction of saturation	0.12±0.03	0.10±0.03
Alpha particle efficiency	0.05±0.02	0.05±0.02
Palaeodose (Gy)	77±22	153.0±5.1
Palaeodose (Gy)	10.06±2.81	110.6±4.7
Palaeodose (Gy)	4.59±1.15	68.8±8.0
Palaeodose (Gy)	1.06±0.32	31.7±13.9
Palaeodose (Gy)	1.46±0.32*	17.3±3.4
Palaeodose (Gy)		11.3±1.0
Palaeodose (Gy)		5.1±0.8
Palaeodose (Gy)		0.88±0.36
Age (ka)	(1) 26.5±7.6	(1) 55.1±2.1
Age (ka)	(4) 3.46±0.97	(1) 39.8±1.9
Age (ka)	(5) 1.58±0.40	(1) 24.8±2.9
Age (ka)	(28) 0.36±0.12	(1) 11.4±5.0
Age (ka)	(37*) 0.50±0.11	(1) 6.2±1.2
Age (ka)		(8) 4.05±0.38
Age (ka)		(6) 1.85±0.29
Age (ka)		(29) 0.32±0.13

Table 3.2: Results of the optically stimulated luminescence measurements and associated radioisotope measurements. Bracketed are the number of grains included in each age calculation. The * indicates the age is the sum of all grains, excluding one outlier, giving an age of 26.5 ka. Gy is a Gray where 1 Gray = 1 Joule/kg = 100 rads.

The TL sensitivity correction is particularly important for the Marble Point samples where the natural OSL was faint. However, following laboratory dosing most grains showed readily detectable OSL, indicating that the faint signal of optically stimulated luminescence from the 'natural' grains was a result of their generally young ages or a low-level activation of sensitivity (from the test doses) or no 'natural' signal at all. The low levels of natural OSL in some grains has meant that the errors on the palaeodose are large (errors are derived from counting statistics and also incorporate calibration uncertainties for the laboratory beta source). The ages were evaluated using the AGE program of R. Grün (Australian National University), incorporating the updated dose-

rate conversion factors of Adamiec and Aitken (1998).

Figure 3.6: Site of sample JQTL1. Note the undisturbed nature of the sediment. Hammer handle approximately 300 mm long.

3.3.3 Results and Discussion

The results from the two samples are shown in Figures 3.7 and 3.8. Both these plots illustrate the scatter in the estimated palaeodoses of the individual grains. This is also shown in Table 3.2 where the individual grains have been placed into groups of similar ages. The figures show that while most of the grains show mid- to late-Holocene ages a few grains are much older. These are typical of grains that are only partially bleached and were probably incorporated into the deposit without being completely bleached at the time of deposition (Murray et al. 1995) but the possibility of some later disturbance such as an introduction of older grains by frost-wedge activity cannot be ruled out. However, later disturbance is unlikely because the deposits consist of fine-scale, undisturbed bedding. The partially bleached grains were possibly deposited during dark periods or at a time when the clarity of the water was insufficient for bleaching (possibly thin ice cover). However, there are sufficient numbers of grains with a Holocene age to be confident that the two samples were deposited during the Holocene.

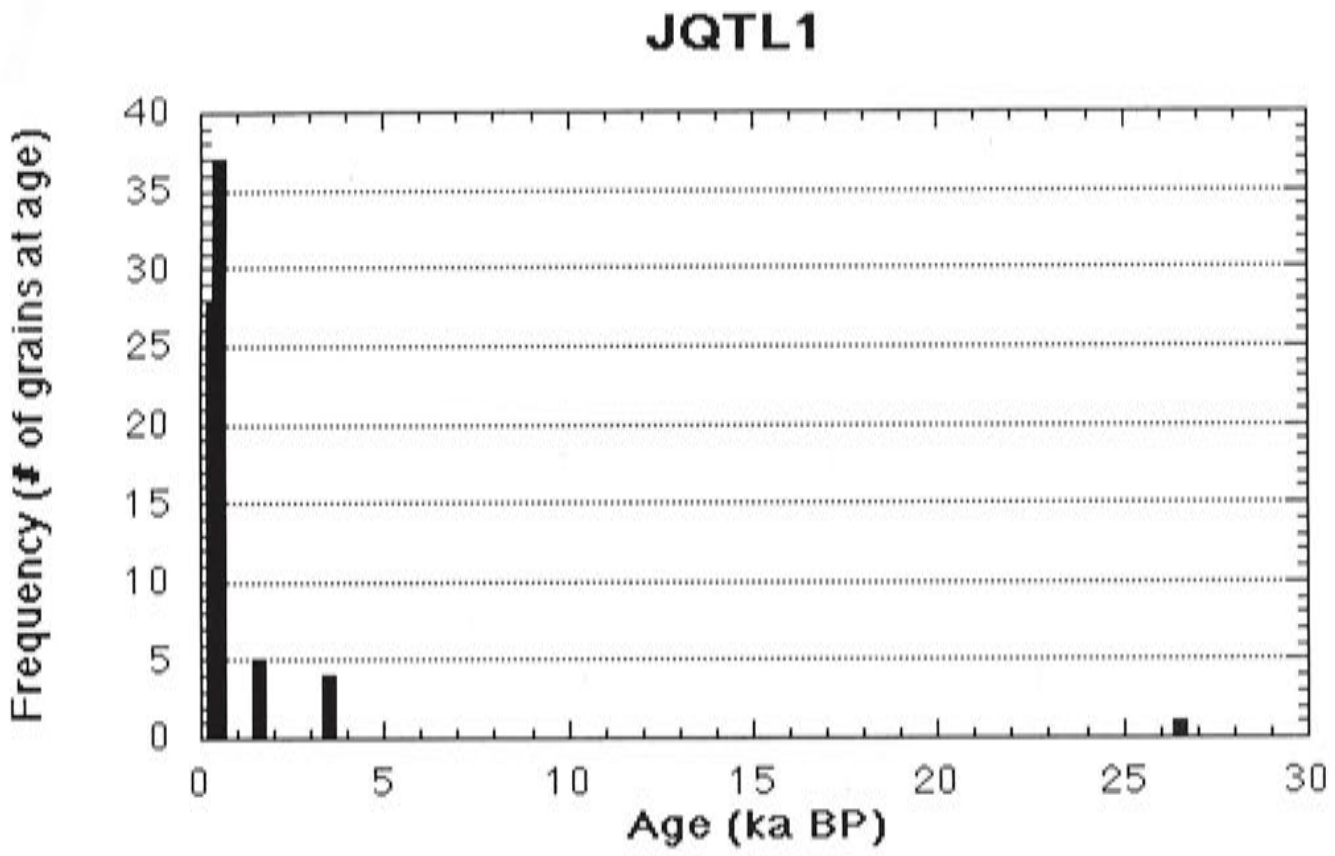

Figure 3.7: Plot of sample JQTL1. The figure shows clearly the young age of the sample with the one outlier.

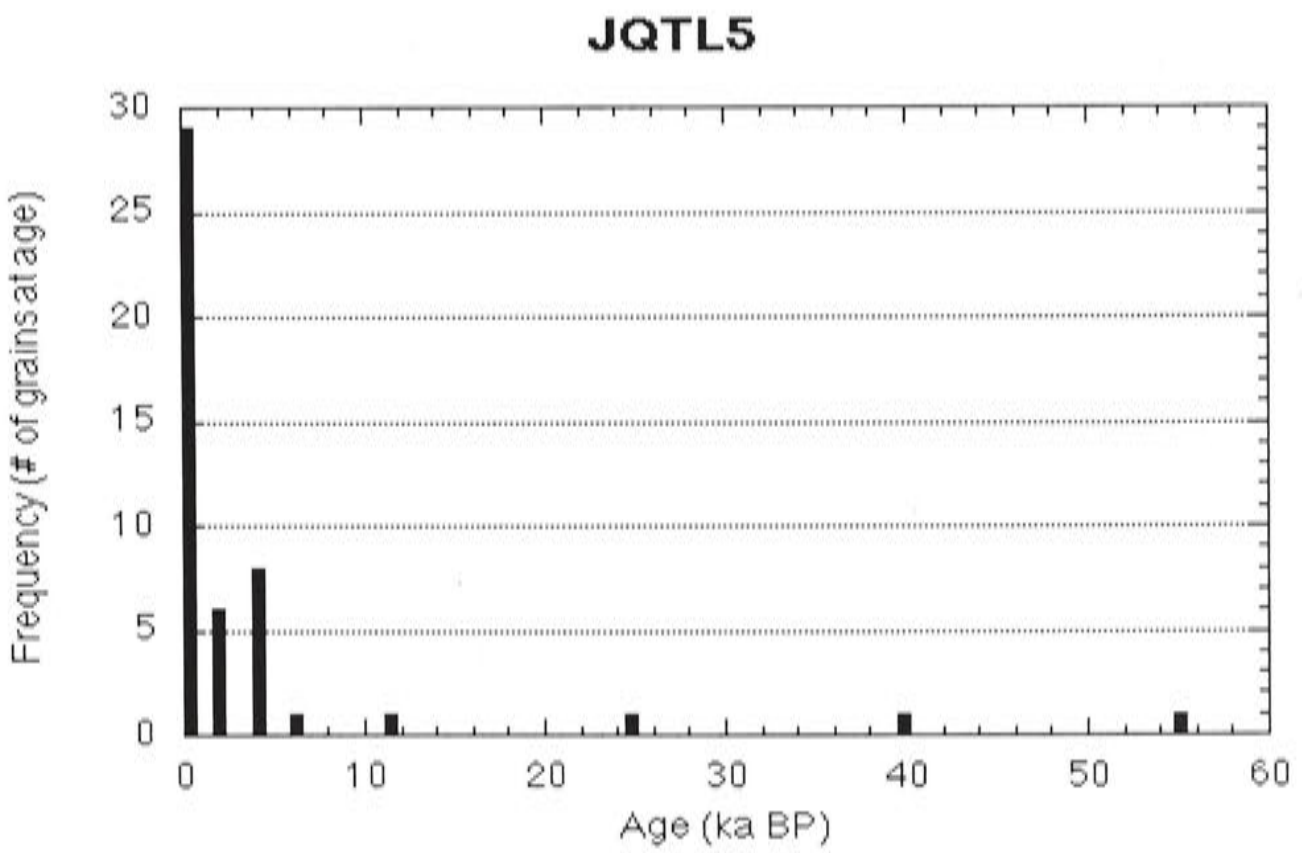

Figure 3.8: Plot of sample JQTL5. The figure shows clearly the young age of the sample with the outliers.

sensitivity from test doses or of the pre-heating treatments. In particular the single-aliquot regenerative-dose protocol may be underestimating the ages of the sediment grains dated, as outlined in Spooner et al. (2000). While there is a risk of removing true

data, if these grains, as well as the grains with obvious partial-bleaching characteristics (e.g. palaeodoses of 77 Gy), are removed, the ages for the samples are calculated as 2,420 ±970 years for JQTL1 and 3,120 ±380 years for JQTL5. The most severe estimates of the underestimating of the ages by the SAR method (Spooner et al. 2000) is 40%, so the age of the Marble Point sediment must still be mid-Holocene.

The older sample, JQTL5, comes from a lower elevation (15 m above sea level) than the younger sample (JQTL1 — 19 m above sea level). For a coastline with a falling relative-sea-level these ages would expect to be inverted. Both the samples come from water-lain sediments so were below mean sea level at the time of deposition, but the exact water depth at this time is unknown. Thus, in view of the uncertainty surrounding the palaeodoses and the sample elevations it may be best to give an estimate of sea level from the optical dating as between 15 and 19 m above present-day sea-level between 2,400 and 3,100 years BP.

The radiocarbon date of the shell fragment from the same pit as JQTL5 is 4,890 (between 4,530 and 5,320) calibrated years before the present. This maximum age for the beach is not inconsistent with the optical dating age despite the large uncertainty of the latter. Thus, what can be drawn from this optical dating work is that the samples are Holocene, probably mid- to late-Holocene, in age. This is an important point for the implications of the dating work for this thesis. The radiocarbon dates obtained are all mid- to late- Holocene in age and yet the surface exposure dating (see next section) suggests that the ages of the raised beaches are much older. Hence, the Holocene optical dates support conclusions from the radiocarbon dating method.

3.4 Surface Exposure Dating

3.4.1 Introduction

Surface exposure dating is, as the name suggests, a method for determining the length of time for which a rock surface has been exposed at the surface to cosmic rays. The technique is based on the build-up time of isotopes formed by reactions between cosmic rays and target nuclei in rock surfaces. In this study, the rock types available were best suited to ^{36}Cl measurements. ^{36}Cl, with a half-life of 301,000 years, accumulates comparatively rapidly in calcium- and potassium-rich minerals (such as calcite and K-feldspar), making it an ideal isotope for dating Late-Pleistocene to Holocene samples that are rich in these minerals. Samples were taken from a number of emerged coastal rock platforms, glacially derived erratic beach boulders and boulder pavements along the coast of McMurdo Sound and from Cape Ross in an endeavor to date sea-level changes and ice retreat histories on the emerging coastline.

3.4.2 Method

The energetic particles producing cosmogenic isotopes are absorbed in the upper layers of the material and do not penetrate deep into the ground. Absorption is characterised by an attenuation parameter Γ, that determines the depth over which the surface production rate is reduced by a factor of 1/e. Because denser materials are more effective at absorbing energetic particles, the attenuation parameter is quoted as a depth scaled by the density of the material subjected to the radiation. Γ has a value of approximately 150 g/cm^2, which corresponds to a depth of about 150 cm of water ($\rho = 1$), about 165 cm of ice ($\rho = 0.9$) or 50 cm of rock ($\rho = 3.0$).

The cosmic ray flux (and hence production rate) at a sample site is affected by its geomagnetic latitude (because the Earth's geomagnetic field deflects the incoming rays), and atmospheric pressure due to altitude (because of absorption by the atmosphere) (Cerling and Craig 1994). The atmospheric pressure effect is usually expressed in terms of elevation but in Antarctica where sea level atmospheric pressure is low, higher production rates (by approximately 20 to 25 %) result than at equivalent altitudes elsewhere (Stone 2000). Hence, sites at high latitudes and high altitudes receive the highest cosmic ray fluxes. For the samples in this study an altitude correction is not needed as they are all located close to sea level.

The cosmic flux rate varies over the surface of the Earth in response to deflection of incoming cosmic rays by the Earth's geomagnetic field. The amount of deflection is related to the incident angle and the rigidity (rigidity = momentum x velocity of light / charge of the particle) and is lowest at the poles (Cerling and Craig 1994).

The exposure geometry of a sample can affect the amount of cosmic ray flux that a sample receives. Surrounding features, such as hills or nearby boulders, can block incoming rays (Figure 3.9). Because most of the flux is concentrated in a cone about 45° above the horizon, objects within this cone block a significant portion of the flux from reaching a sample. Careful sampling can minimise this potential problem.

The build-up of ^{36}Cl through a rock is variable because there are a number of different reactions that produce the isotope. The major part of the cosmic-ray flux at ground level consists of neutrons which, because of their high energy, cause spallation reactions by splitting the target nuclei into various by-products through the removal of neutrons and protons. In the case of ^{36}Cl studies it is the direct spallation of ^{39}K and ^{40}Ca that is most important. Neutrons emitted in the spallation reactions loose energy in elastic collisions. When the electron reaches a low enough energy state (<0.5 eV) they can be captured by atoms (thermal neutron capture). It is the thermal neutron capture by chlorine-35 that produces the chlorine-36. Non-cosmogenic isotope production (from natural radioactive sources) and muon reactions (mainly important at depth) are other more minor sources of ^{36}Cl.

As indicated by the depth-profile in Figure 3.10 ^{36}Cl concentrations initally increase

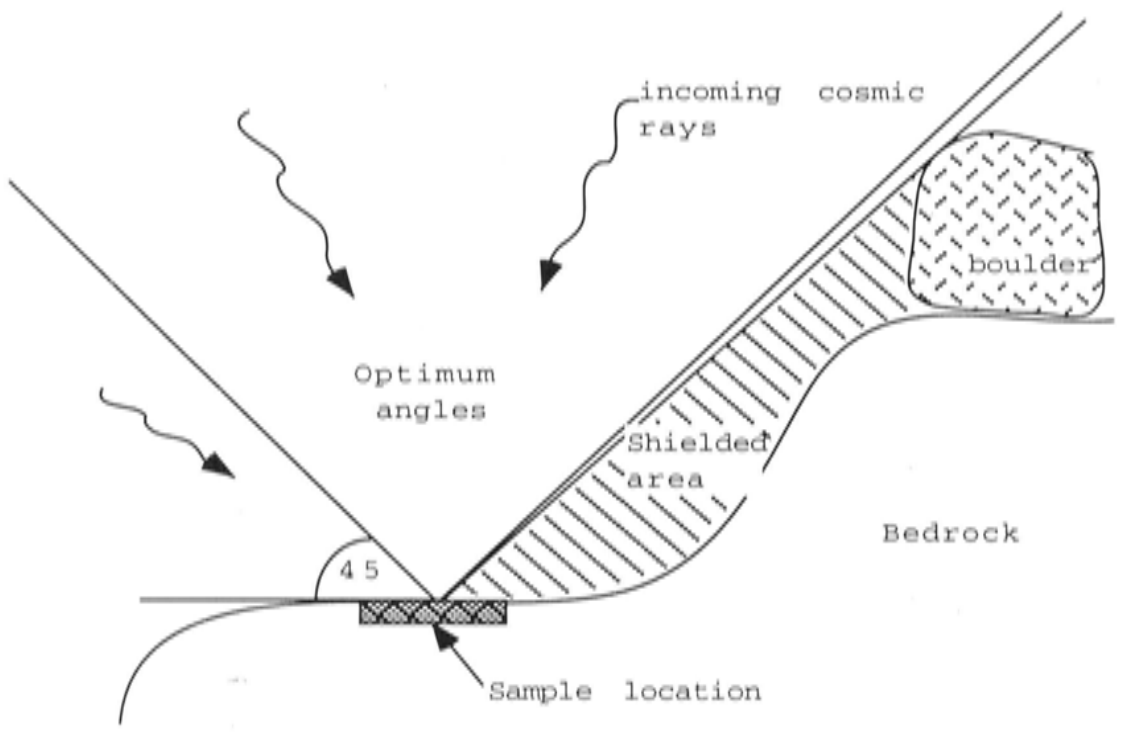

Figure 3.9: Schematic illustration of the incident angles of the incoming cosmic rays on a rock surface showing the angles at which the majority of the rays enter and the effect of shielding.

with depth, reaching maximum values at depths of about 10 cm. Therefore, erosion of the rock surface can have an important effect on the age determination but this can be corrected for if the erosion history is known.

In the field sampling only bedrock surfaces that retained a surface polish from the ice were selected. Boulder samples with a smooth surface rather than a rough crystalline surface are also likely to have been subjected to minimal erosion since deposition. A good indicator for the occurrence of surface erosion is the existence of a 'tail' of crystals downwind of a boulder or outcrop.

Sampling boulders from the top of a beach or sampling very large boulders minimises the risk that the surfaces have been buried which would lead to an apparently younger age being recorded. For the bedrock platforms the best sample sites to assure non-burial are far from sand deposits (to minimize wind-blown or water-washed sand covering the rock), and preferably close to the front of the platform as sand deposits are more typically found at the back of the platforms.

Constant orientation of the sample to ensure that a constant flux has been received is easy to establish for the bedrock sites but this condition is less obvious with the boulder samples. Choosing the large and stable boulders on a beach maximises the chances of them not having moved since their final deposition. If a boulder has rotated 90° (onto one of its sides) immediately prior to sampling the exposure age will only be half of the real exposure for the pre-rotated time (assuming a cubic shape). If the boulder rotates by 180° the amount of ^{36}Cl on the new top surface will depend on the thickness of the boulder, but will be about half of the real exposure for a 70 cm rock thickness.

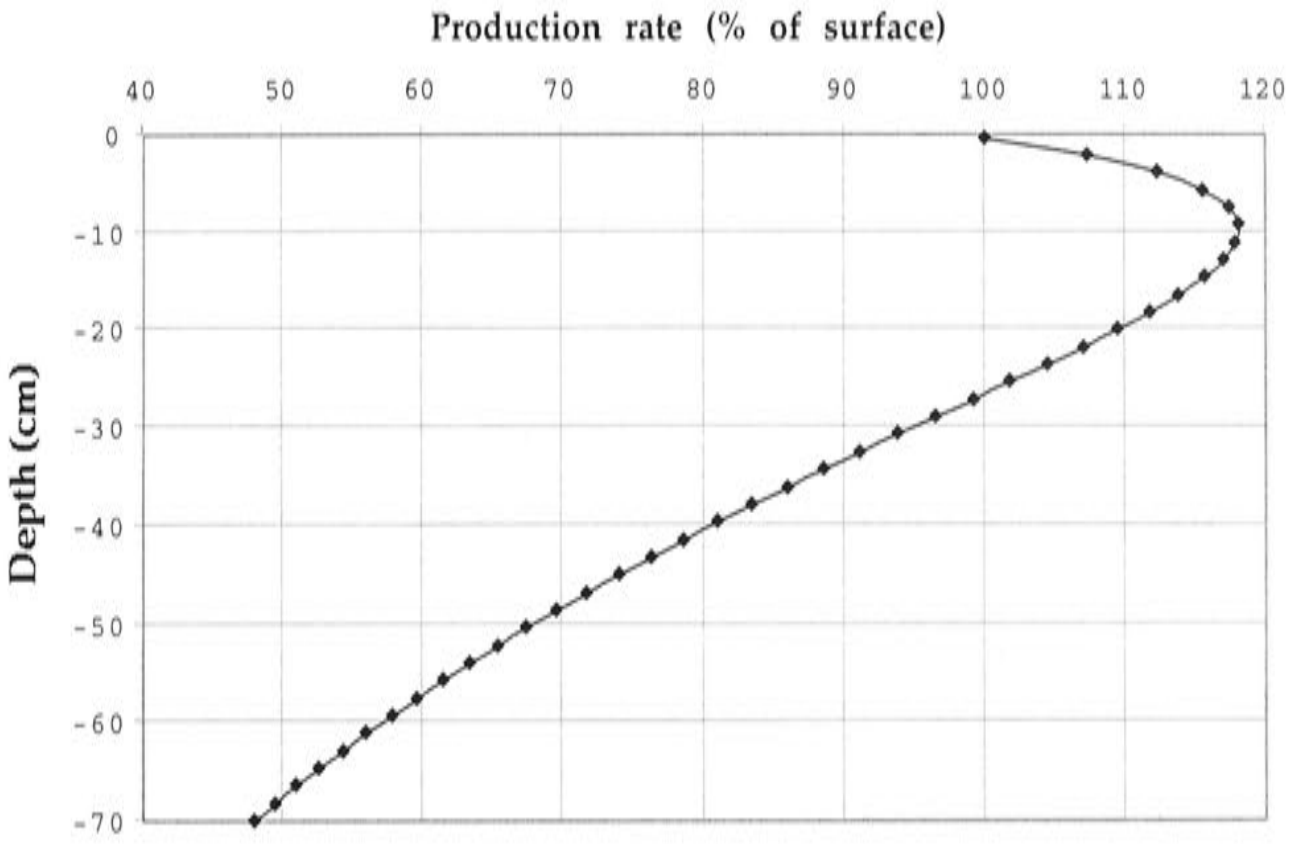

Figure 3.10: Build-up of Chlorine-36 through a rock. 0 cm is the rock surface and 100% is the production rate at the surface. The production actually increases in the rock for the first 10 cm of depth.

Annual snow cover needs to be estimated because snow has a shielding effect by absorbing some of the cosmic rays resulting in a decrease in the apparent age. However, snow cover in Antarctica is small because the annual precipitation is low and the high winds rapidly remove snow build-up on exposed surfaces. Even with one metre of snow cover for five months of the year, an unlikely amount for exposed locations, the effective age will only decrease by about 12%. A more realistic estimate is a few percent (a few hundred years for a mid-Holocene age beach). Because of the difficulty in estimating the snow cover now and in the past, and the small difference made to the ages, this correction has not been applied to these samples.

The measurement method followed standard practice for both carbonate and silicate rock types (Evans et al. 1997). The carbonate rock is crushed and dissolved. The sample is spiked with ^{36}Cl-free carrier to increase the chlorine yield, precipitated, and cleaned of any contaminants, especially sulphur. The ^{36}S isotope can lead to false counts in the accelerator mass spectrometer if it is not removed from the sample because it has the same mass as ^{36}Cl. The preparation of the silicate rocks follow the same procedure except that the K-feldspar is separated after crushing and it is this portion that is used. More details of the method are outlined in Stone et al. (1996). Major element analysis, trace elements (with high neutron capture cross-sections) and neutron producers, and potassium concentrations in the K-feldspar samples are measured using a flame photometer (K-feldspar) or an isotope dilution method (carbonate) to determine

the composition of the rock for estimating neutron absorption and contributions from internal radioactive sources to the ^{36}Cl producing reactions.

Ages are calculated assuming production rates at a standard pressure (1013 mbar) and high latitudes (>60°) given in Table 3.3. Note that the production rates estimated at sea level in Antarctica are expected to be approximately 23% higher than for standard pressure sites at the same latitude due to the low air pressure over the continent (Stone 2000). Samples in this thesis have this correction for low air pressure.

Method	Reaction	Rate	References
Ca spallation	^{40}Ca(n,2n3p)^{36}Cl	48.8 ± 1.7 atom/g Ca/yr	1,2,3
K spallation	^{39}K(n,2n2p)^{36}Cl	178 ± 14 atom/g K/yr	1,2,4
P_f(o) [Secondary neutron production in air]	^{35}Cl(n,γ)^{36}Cl	586 ± n/g air/yr	2,5
Negative muons from Ca	^{40}Ca(μ^-,α)^{36}Cl	4.8 ± 1 atom/g Ca/yr	6,7
Negative muons from K	^{39}K(μ^-,$p2n$)^{36}Cl	9.4 ± 0.9 atom/g K/yr	John Stone (pers. comm.)
Neutron yield from muon capture in calcite or K-feldspar	—	0.5 n/stopped muon	6,7

Table 3.3: Chlorine-36 production rates. References: (1) Zreda et. al. (1991), (2) Phillips et. al. (1996), (3) Stone et. al. (1996), (4) Evans et. al. (1997), (5) Liu et. al. (1994), (6) Stone et. al. (1998), (7) Charalambus (1971).

Five sites from the western side of McMurdo Sound from Cape Ross to Cape Bernacchi (Figure 3.11) were chosen for surface exposure dating because they provided a complete sequence of samples from sea level to the marine limit. In contrast, the surface exposure dating sampling done by other workers (Brook et al. 1995, Webb 1997) around McMurdo Sound was all done on glacial erratics above the marine limit to establish the age of the Ross Sea Drift (LGM) and earlier drift sheets.

Bedrock was sampled in locations where it was eroded into steps that could be correlated with the raised beaches. At Marble Point the marble bedrock was sampled rather than the beach boulders because the marble contains large quantities of calcium, one of the target minerals for the spallation reaction. Weathering caused difficulties in sampling at the higher end of the outcrop because much of the bedrock had lost the surface polish and showed evidence of surface erosion. This required careful sample selection and, in places, an estimate of the amount of erosion. In both locations where the bedrock was sampled (Marble Point and Dunlop Island) the beach boulders in the area were small (<20 cm diameter) and probably unstable. At neither location were both surface bedrock and erratics identified.

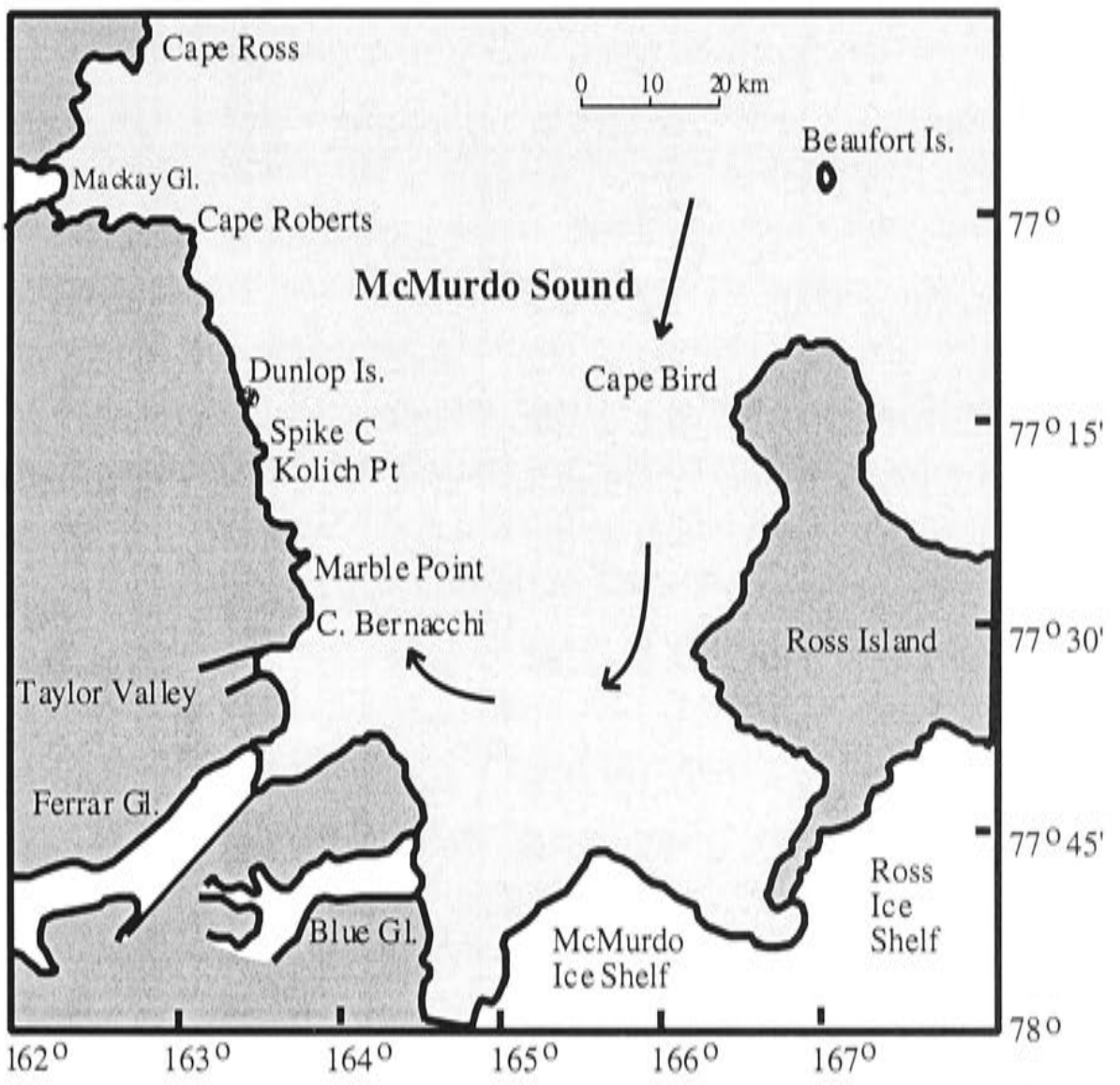

Figure 3.11: Location map for McMurdo Sound and the Scott Coast. Arrows indicated the proposed ice flow directions for Last Glacial Maximum ice into the McMurdo Sound area. (Kellogg et al. 1996).

The beach boulders which were sampled came from suites of raised beaches facing north-east, the direction of greatest wave energy. For each sample, the boulder's likely history was noted (e.g. a boulder on a beach much larger than most of its companions may have been ice-rafted) to give an idea of any potential prior exposure or insufficient erosion. In the case of the boulder pavements at Cape Roberts only samples with smooth flat tops that were indicative of sea-ice erosion were sampled. Cape Ross was sampled for both boulders and bedrock with the ages of the highest beaches being of most interest (boulder samples) because their elevations are much higher than elsewhere along the coast of McMurdo Sound. Hence, only the boulders were dated.

3.4.3 Results

Table 3.4 summarizes the results. At all sites similar trends are observed with the higher beach ridge/rock platform samples being older than the low elevation samples. Also, all sites show approximately the same range of ages, suggesting a similar exposure history for the localities as would be expected over the short section of coastline covered by the sites. However, the ages for the lowest samples appear to be older than expected

(e.g. cbc18/1 is 4,380 ±630 years at only 1.2 ±0.2 m — the storm berm of the active beach).

Sample	Age	Height	Sample	Age	Height
Cape Bernacchi			Cape Roberts		
cbc18/1	4,380 ± 630	1.2 ± 0.2	crc1	6,950 ± 1,200	2.5 ± 0.5
cbc18/2*	655 ± 440	3.2 ± 0.2	crc2	12,020 ± 1,600	2.7 ± 0.5
cbc18/3	5,210 ± 700	5.1 ± 0.2	crc3	11,950 ± 1,730	3.3 ± 0.5
cbc18/4	12,050 ± 150	7.0 ± 0.2	crc4	5,840 ± 960	4.9 ± 0.5
cbc18/5	15,830 ± 310	8.2 ± 0.2	crc5*	6,810 ± 1,050	7.0 ± 0.5
South Stream			crc6	8,630 ± 1,200	7.1 ± 0.5
ssc2	30,230 ± 390	8.6 ± 0.3	crc8	16,210 ± 1,200	11.9 ± 0.5
Marble Point			crc9	19,520 ± 2,540	12.3 ± 0.5
ac4071	5,100 ± 430	1.1 ± 0.8	crc11	17,820 ± 2,240	14.1 ± 0.5
ac4073	7,240 ± 520	4.7 ± 0.8	crc12	16,040 ± 1,920	14.1 ± 0.5
ac4075*	13,130 ± 180	10.7 ± 0.8			
ac4076	11,060 ± 830	11.2 ± 0.8	Cape Ross		
ac4077*	5,660 ± 1,000	4.5 ± 0.8	ross12	11,320 ± 1,890	26.7 ± 1.0
ac4079	9,720 ± 820	9.2 ± 0.8	ross13	36,850 ± 4,830	30.2 ± 1.0
ac40710	10,540 ± 740	13.9 ± 0.8	ross14*	10,960 ± 1,690	31.7 ± 1.0
ac40712*	17,080 ± 2,370	16.5 ± 0.8	ross15	13,010 ± 6,370	27.4 ± 1.0
ac40715*	24,100 ± 3,440	22.3 ± 0.8	ross16*	8,430 ± 1,480	23.3 ± 1.0
Dunlop Island			ross17	10,100 ± 2000	28.4 ± 1.0
dis1	14,770 ± 2,150	13.0 ± 0.6			
dis4	10,470 ± 1,200	12.4 ± 0.6			
dis6*	3,500 ± 990	6.2 ± 0.6			
dis9	5,460 ± 930	3.5 ± 0.6			
dis10	6,210 ± 1,170	2.5 ± 0.6			
dis12*	6,700 ± 1,010	9.4 ± 0.6			

Table 3.4: Ages for surface exposure dating of boulders and rock platforms. Sample names, cbc = Cape Bernacchi boulders, ssc = boulder sample on top of the delta at south stream, ac4 = Marble Point bedrock, dis = Dunlop Island bedrock, crc = Cape Roberts boulders, ross = Cape Ross boulders. Chlorine values for the starred samples are only estimates. Changing the chlorine contents does not change the age significantly for any sample except cbc18/2 (discussed below). An estimate of 70 ±10 ppm was used for all except cbc18/2 where 80 ±10 ppm was used. Details of these components can be found in Appendix B.

Several assumptions are made in estimating ages from the measured ^{36}Cl contents. Taking the uplift rate for the McMurdo Sound area based on the radiocarbon dating of

Taking the uplift rate for the McMurdo Sound area based on the radiocarbon dating of 20 m in 6,000 years, the sample will only be in the water attenuation zone for about 500 hundred years before being fully exposed. These effects, as well as uncertainties arising from shielding of the sample, dip of the sample, sample movement, and measurement errors are all included where necessary in the age uncertainty calculations. This is done by field measurements of the current boulder orientation and calculation of the percentage of visible sky. Underestimation of these parameters will increase the age of the sample. However, the degree to which this estimation would need to be changed to agree with the radiocarbon ages is larger than is plausible. It is difficult then to explain the ^{36}Cl ages presented here other than the occurrence of a period of prior-exposure followed by insufficient erosion. This possibility is examined in more detail below.

The boulder from the first raised beach at Cape Bernacchi (cbc18/2) is anomalously young and must have been uncovered recently (Figure 3.12). The young age indicates that the beaches can be formed by boulders that contain no prior cosmogenic isotopes. This conclusion is important because it indicates that it is possible to date the age of the beaches by using cosmogenic isotopes. Of course care needs to be taken on raised beaches to ensure boulder stability since deposition in the beach otherwise the true age for the beach formation may not be measured.

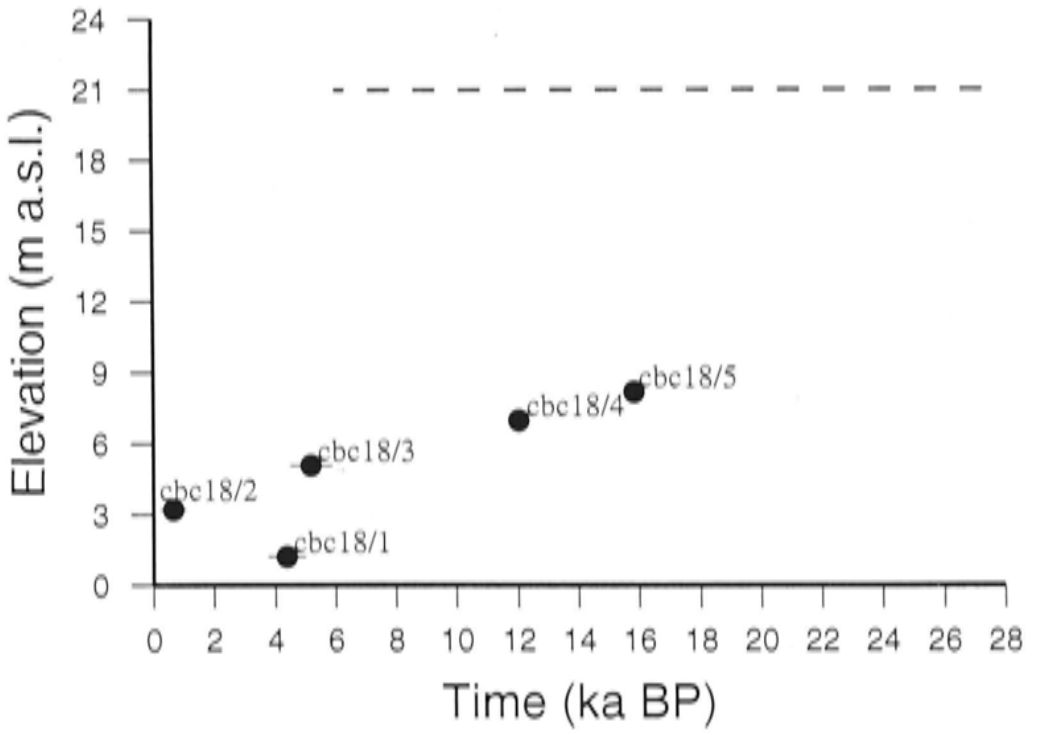

Figure 3.12: Chlorine-36 ages from Cape Bernacchi are the black dots with error bars. Samples are K-feldspar splits from granitic boulders on the raised beaches. Shown on the Figure is the average marine limit for McMurdo Sound (dashed line).

Bedrock platforms are good sites for testing the assumption that erosion of the

bedrock prior to exposure is sufficient to remove any pre-existing cosmogenic isotopes (1 to 2 m of material needs to be removed — at 2 m depth there is only 5 % of the surface amount of ^{36}Cl). Such platforms have been successfully used previously in Western Scotland to constrain the timing of higher relative sea levels (Stone et al. 1996). If the erosion has been sufficient to reset all the samples there should be a significant difference between samples from platforms at different heights, and this is the case for Marble Point (excepting sample ac40710 which, according to the field observations, may have been buried at some stage, resulting in a younger age) (Figure 3.13). However, the sample from the lowest platform (ac4071), which occurs at the elevation of the first raised beach, has an age (5,100 ±430 years) that is older than expected (1,000 to 2,000 years), indicating that the platform has not experienced sufficient erosion to completely reset the cosmogenic isotopes at the surface.

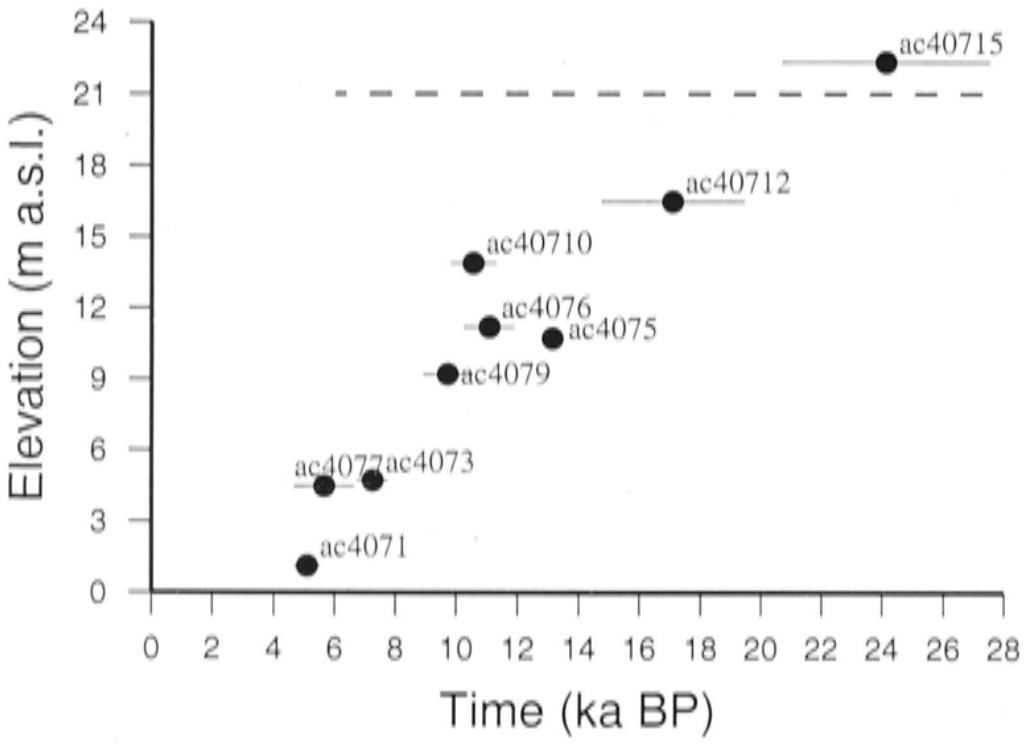

Figure 3.13: Chlorine-36 ages from Marble Point. All samples are all from near marble bedrock platforms from sea-level to above the marine limit (dashed line).

One sample (ac40715 — 24,301 ±3,440 years) was taken from above the marine limit (about 20 m above sea level) at Marble Point. The age of this sample falls on the same linear trend as the rest of the samples from Marble Point. This sample could record the time of retreat of the ice sheet from this location, and if so would suggest the coast became sufficiently ice free to form beaches soon after the retreat. However, the age of this sample does not fit with other deglaciation evidence from both Antarctica (e.g. Hall and Denton 2000b; Kellogg et al. 1990). What is more likely is that it too has a component of prior exposure.

Unfortunately the distance from the front of each rock platform was not recorded for

each sample. Hence, it is not possible to model any erosion scenarios (e.g. insufficient erosion at the front of a platform to reset the ^{36}Cl to zero content in the rock).

A similar situation exists for Dunlop Island and is shown in Figure 3.14. Again this is a bedrock platform site although the levels are not as clear as the Marble Point platforms, especially as the overall steepness of the site is much greater. Like Marble Point the samples located just above present-day sea-level were older than expected. One sample (dis6) in particular shows a young age for the sample height suggesting possible erosion from the surface (burial is considered unlikely for this sample).

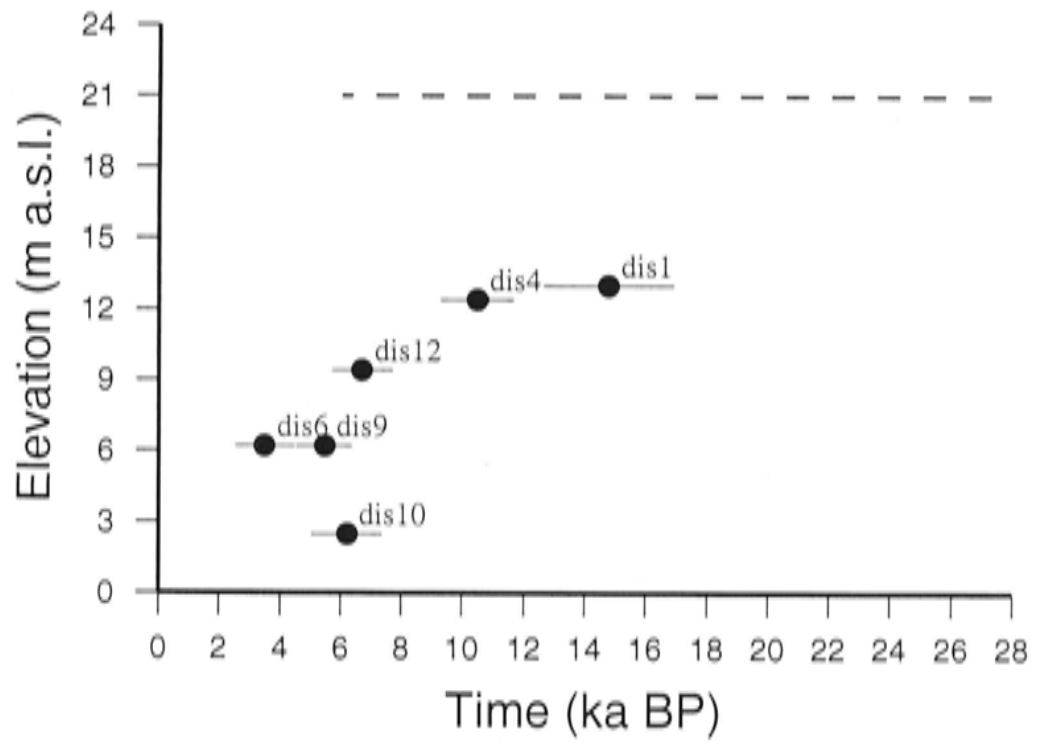

Figure 3.14: Chlorine-36 ages from Dunlop Island are the black dots with error bars. K-feldspar samples from granitic bedrock platforms. A definite trend of older ages with height despite the few ages. Shown on the Figure is the average marine limit for McMurdo Sound (dashed line).

The old ages of the boulder pavement at Cape Roberts (see Table 3.4, Figure 3.15) suggest that although the boulder pavement is well-developed, the rocks that make up the pavement experienced some exposure before they were formed into the pavement and/or that the pavement may have formed over several glacial cycles. The former scenario could be possible as all the rocks are of a similar composition suggesting a local origin. If the rocks have been re-worked by ice or water with only decimetres of erosion it is possible to have a situation of an apparently young, well-developed boulder pavement yielding an anomalously old ^{36}Cl age. Some of the age inversions seen at Cape Roberts could possibly be a function of erosion having occurred but which was not detected during the sampling. If erosion, in the form of a flake (with a parallel top and bottom), had occurred then the surface underneath would give a younger age.

To ensure that a flake had not been removed from crc12, another sample crc11 from the same height was measured and the ages were found to be similar, confirming the date.

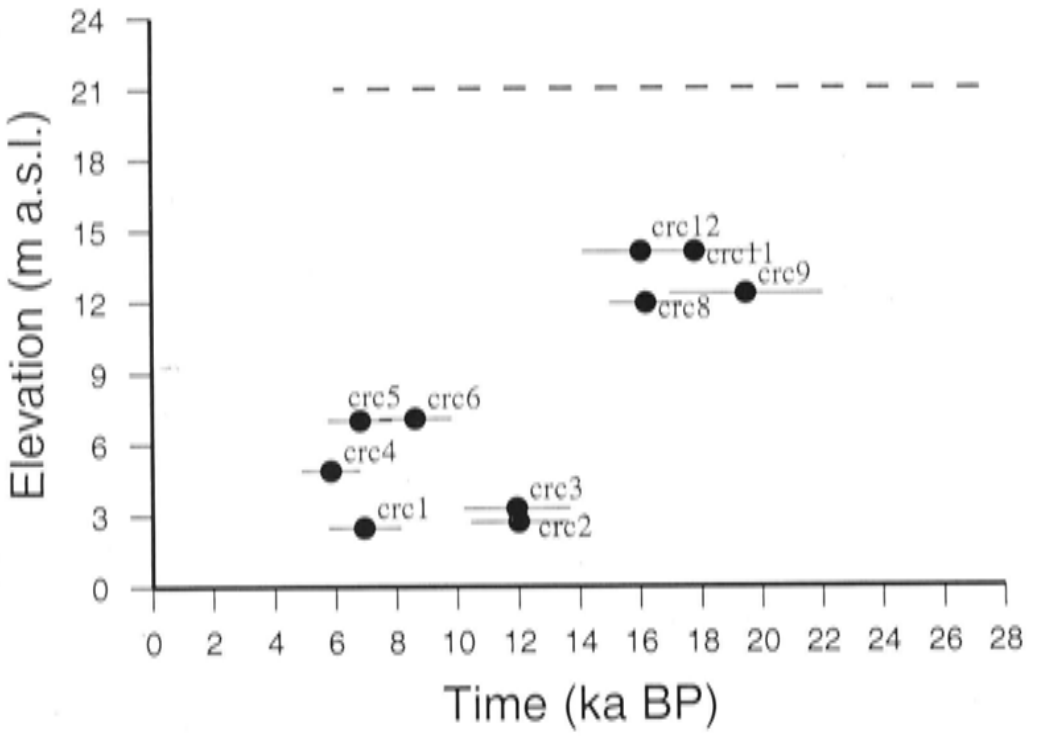

Figure 3.15: Chlorine-36 ages from Cape Roberts. Note the age inversions as well as the general trend of older ages with height. These samples are K-feldspar splits from a well-developed boulder pavement. Shown on the Figure is the average marine limit for McMurdo Sound (dashed line).

Cape Ross samples yield similar ages to the McMurdo Sound samples despite the higher elevation of the beach ridges. The similar ages suggest that this site may have been uplifted further than McMurdo Sound over the same time interval (compare Figure 3.15 to Figure 3.16).

Figure 3.17 shows the ^{14}C dates from a fossil penguin rookery (Baroni and Orombelli 1994) together with the ^{36}Cl dates from Cape Ross. Again, like the other sites there is a disparity between the two dating methods. Also plotted on this figure is the relative sea level curve from the sites further south. If extrapolated this curve falls close to the ^{36}Cl dates but well clear of the ^{14}C dates. However, because the ^{14}C are from a fossil penguin rookery these provide only a minimum age for the site and it is possible that the extrapolation of the relative sea level curve is appropriate, in which case Cape Ross must have deglaciated around 8,000 years BP, close to the deglaciation time of Terra Nova Bay to the north and some time before the rest of McMurdo Sound.

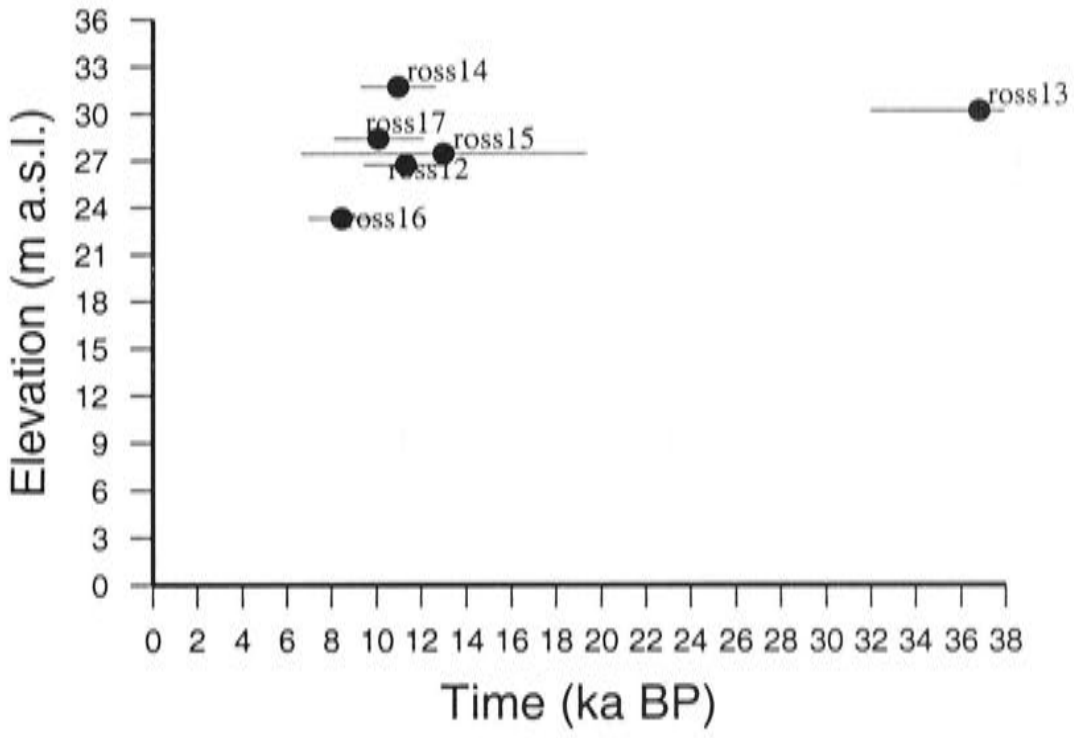

Figure 3.16: Chlorine-36 ages from Cape Ross are the black dots with error bars. Samples are K-feldspar splits of granitic boulders from the high, well-developed beach ridges. Ross13 must have been exposed at some earlier time and gives a disproportionately old age.

3.4.4 Discussion

Prior exposure

Unless a rock has just been formed (e.g. volcanic) or has never been exposed at the surface (e.g. formed beneath the sea) it will contain ^{36}Cl. However the cosmogenic rays only penetrate the surface of the rock up to approximately 2 m depth and if the rock is eroded to at least this depth the 'clock' can effectively be reset to zero. It was assumed when the rock was being sampled for this dating process that there had been sufficient erosion while the rock was beneath either ice or water to reset the clock. However, the ^{36}Cl ages show otherwise and in the following discussion I will explore several ways of determining a component of prior exposure. With the final amount of ^{36}Cl being the only accurately known parameter it is not possible to determine a unique history with multiple parameters of exposure, burial and erosion. However it is possible to describe a range of possible histories that are consistent with the ^{36}Cl measurements.

Three methods of determining the history of the cosmogenic samples (and coastal area) are explored:

1. Constant offset: Determining a prior exposure by fitting the cosmogenic dating results to the radiocarbon dates for McMurdo Sound. This method assumes that there is a constant period of exposure, burial, erosion and final exposure for all samples.

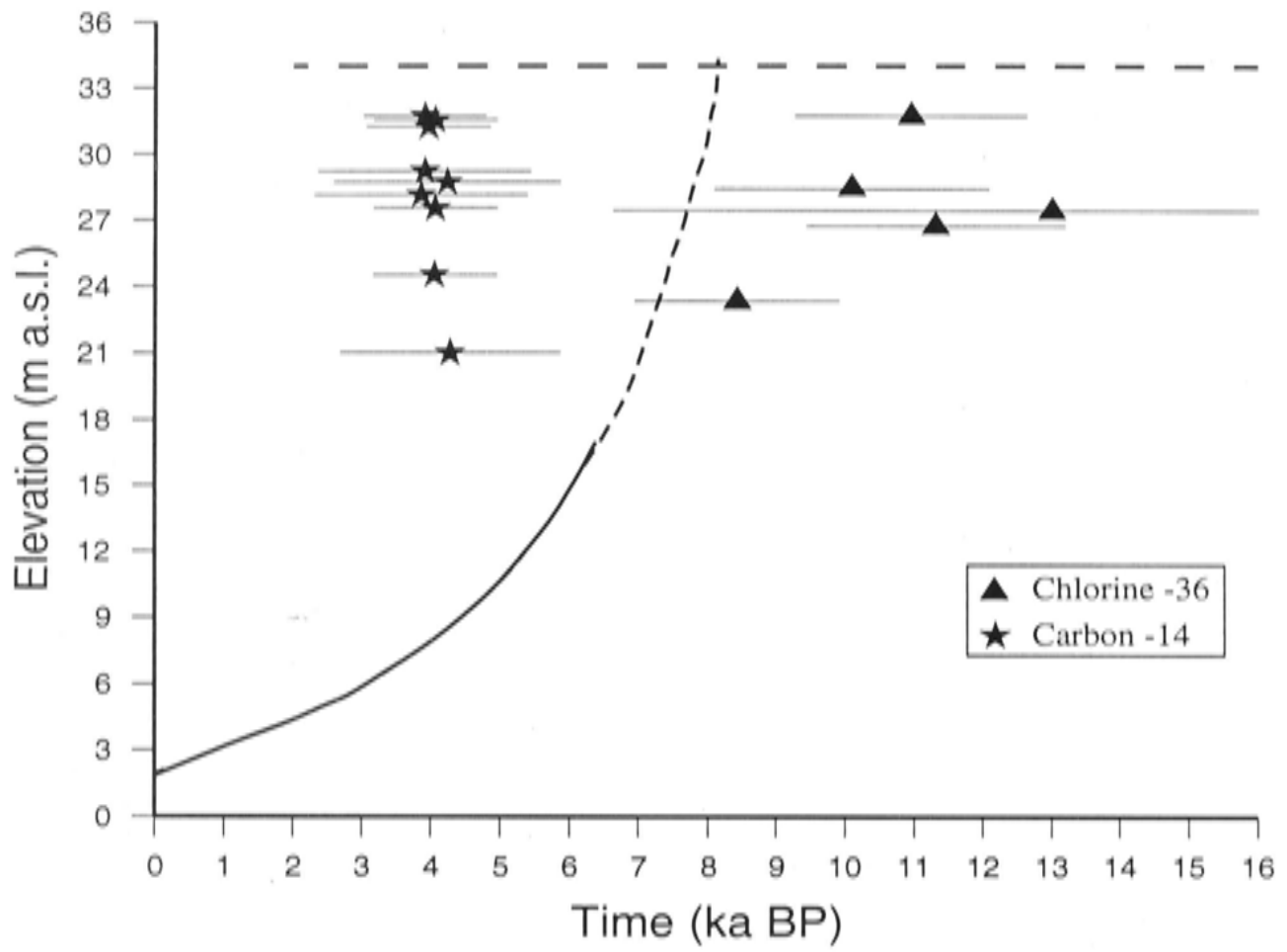

Figure 3.17: C-14 and Cl-36 ages from Cape Ross. These samples do not overlap in time. The curve is the relative sea level curve from the sites further south in McMurdo Sound and the dashed part of the line is an extension up to the observed marine limit at Cape Ross. For clarity sample *ross13* has been removed from this plot.

2. Non-constant offset: Determining a prior exposure history by applying a non-constant offset to the cosmogenic dates. This method does not assume the same history for all samples, but also may not be geologically plausible.

3. Forward modelling of the results of prior-exposure scenarios: Because any prior-exposure will involve at least one period of exposure and burial it is possible that more than one combination of exposure and burial times may fit a given sample. Included in any prior-exposure scenario must also be a component of erosion.

To be able to compare the cosmogenic isotope data with the radiocarbon data some elevation adjustments were necessary for the samples from bedrock platforms. As outlined in Chapter 2 it is thought that a bedrock platform corresponds to a beach approximately two metres higher in elevation. Hence to be able to compare the bedrock samples to beach samples, and also to the radiocarbon samples, the bedrock sample elevations need two metres added (e.g. a platform at an elevation of +3 m a.s.l. has an equivalent beach height of +5 m a.s.l.). Figure 3.18 shows the cosmogenic samples together with the relative sea level curve determined from the radiocarbon dating. Initally the cosmogenic dating results are compared visually to the radiocarbon dating rather than applying any numerical fits to the data. Given the number of assumptions

already made in the modelling a visual data fit is an adequate approximation.

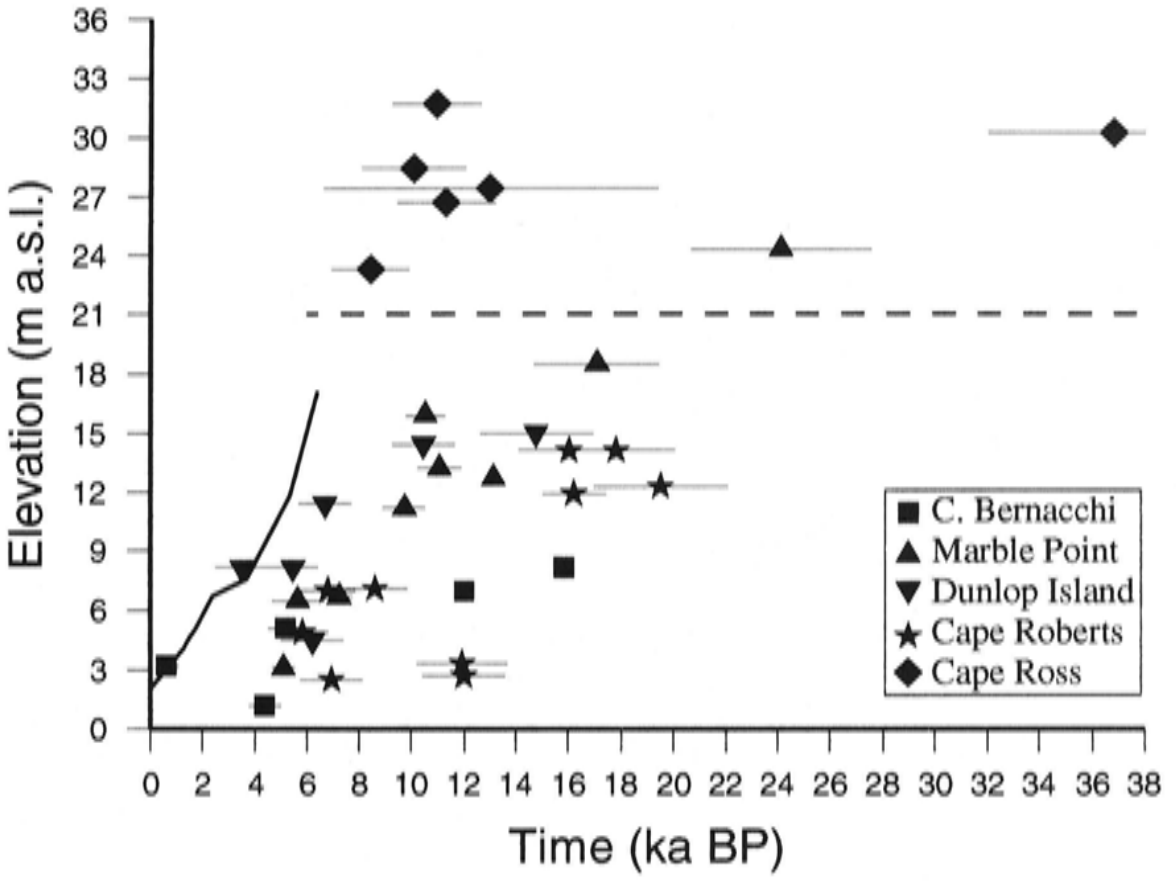

Figure 3.18: ^{36}Cl ages from all McMurdo Sound sites together with the radiocarbon dating (black line). Heights of the bedrock samples have 2 m added to enable direct correlation with the beaches. The dashed line is the marine limit for McMurdo Sound.

Constant offset

A constant offset of the ^{36}Cl ages from the radiocarbon ages implies that there has been a common exposure history for all cosmogenic samples collected from McMurdo Sound. Figure 3.19 shows the same set of cosmogenic and radiocarbon dating data but with 5,000 years subtracted from the age of the cosmogenic samples.

When comparing the relative sea level curve from the radiocarbon dating to the cosmogenic dates the two data sets overlap more closely than in Figure 3.18. The relative sea level curve fits with some of the cosmogenic data but there is scatter in the cosmogenic ages and the visual 'best fit' curve is uncertain. The data from Marble Point (upright triangles) and Dunlop Island (inverted triangles) fit the radiocarbon curve better than the data from Cape Bernacchi (squares) and Cape Roberts (stars). A difficulty in using a constant offset for all samples along the coast is that some of the samples (e.g. from Cape Bernacchi) become negative in age.

To interpret Figure 3.19 further the marine limit for McMurdo Sound is shown at approximately 21 m elevation. At some point in time the relative-sea-level curve must reach this height because there is evidence of a marine influence below this level.

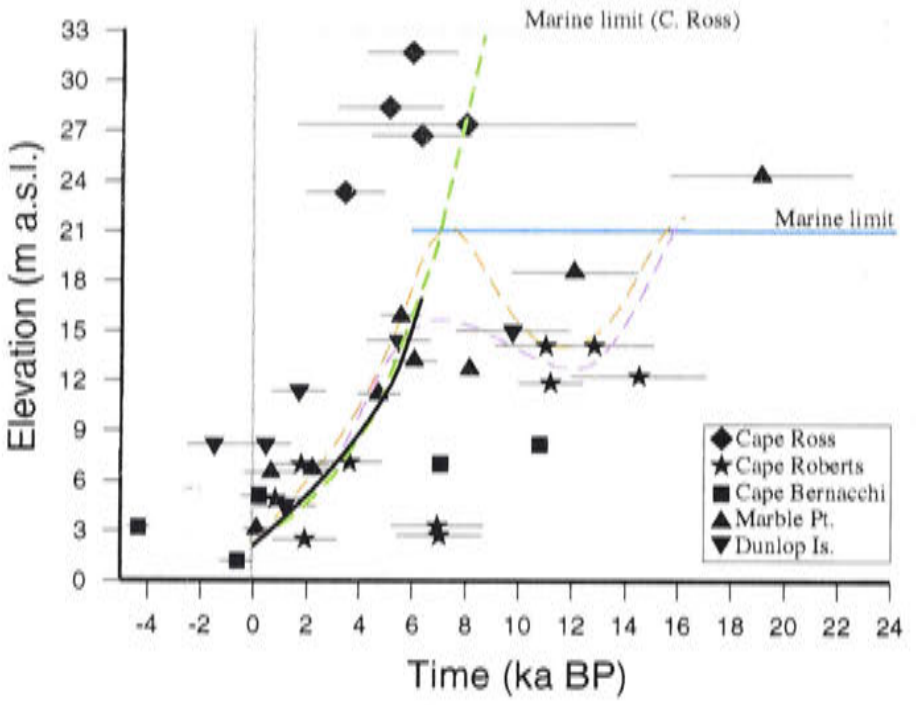

Figure 3.19: Chlorine-36 ages from all McMurdo Sound sites together with the radiocarbon dating. Ages of the Chlorine-36 samples have had 5,000 years removed. Heights of the bedrock samples have 2 m added to correlate to the beaches. A grey reference line has been put at 0 years, the marine limit for McMurdo Sound in blue and a light blue line for the marine limit at Cape Ross. The Cape Ross marine limit is higher than all the other sites and relates only to the Cape Ross samples (diamonds). Several curves have been plotted on this figure: the solid black line is the radiocarbon curve and the dashed green, orange and purple lines are possible curve fits to the adjusted chlorine-36 data. The Cape Ross, Cape Roberts and Cape Bernacchi samples were from beach boulders while the samples from Marble Point and Dunlop Island were from bedrock platforms.

Several interpretations are possible using the scatter of the data and these are sketched onto the figure in dashed green, orange and purple.

Firstly, it would be possible to extend the radiocarbon relative-sea-level curve (black line) through the marine limit around 7,000 years BP in a simple linear extrapolation (green line). This would provide an age for the marine limit and intersect some of the data from Cape Ross. This curve will also intersect the Cape Ross marine limit about 8,000 years BP. Because Cape Ross is at the northern end of McMurdo Sound with a big bay (Granite Harbour) between it and Cape Roberts, the northern-most point on the Scott Coast, it is possible for Cape Ross to have become ice free before the rest of McMurdo Sound. The oldest ^{14}C dates from Terra Nova Bay, to the north, have a maximum age of 7,000 years BP (Baroni and Orombelli 1991) which is younger than inferred from from the Cape Ross marine limit. The age of the marine limit at Terra Nova Bay would need to be older than 7,000 years BP in order to lend credibility to

the claim that Cape Ross deglaciated about 8,000 years BP.

The second curve (orange dashes) on Figure 3.19 also touches the marine limit in McMurdo Sound at about 6,000 to 7,000 years BP, following the trend of the radiocarbon curve (black line). However there are several points below the marine limit with older ages (triangles and stars to the right of the radiocarbon curve on Figure 3.19) that may be legitimate ages. Because this site is within the boundary of the Last Glacial Maximum ice sheet the relative sea level curve from this site may be complex (typical relative sea level curves from such localities are discussed in more detail in Chapter 4). Sites from similar situations in East Antarctica have relative sea level curves with a maximum in the Holocene. The Vestfold Hills is an example where the relative sea level curve has a maximum in the Holocene (about 6,000 years BP (Zwartz 1995) Figure 3.20) and prior to this there was a period of several thousand years where the trend of the relative sea level changed from falling to rising. The orange curve on Figure 3.19 follows a similar trend with a reversal in the trend of the relative sea level between 12,000 years BP and 6,000 years BP. Including this reversal provides an explanation for earlier ^{36}Cl dates in the area.

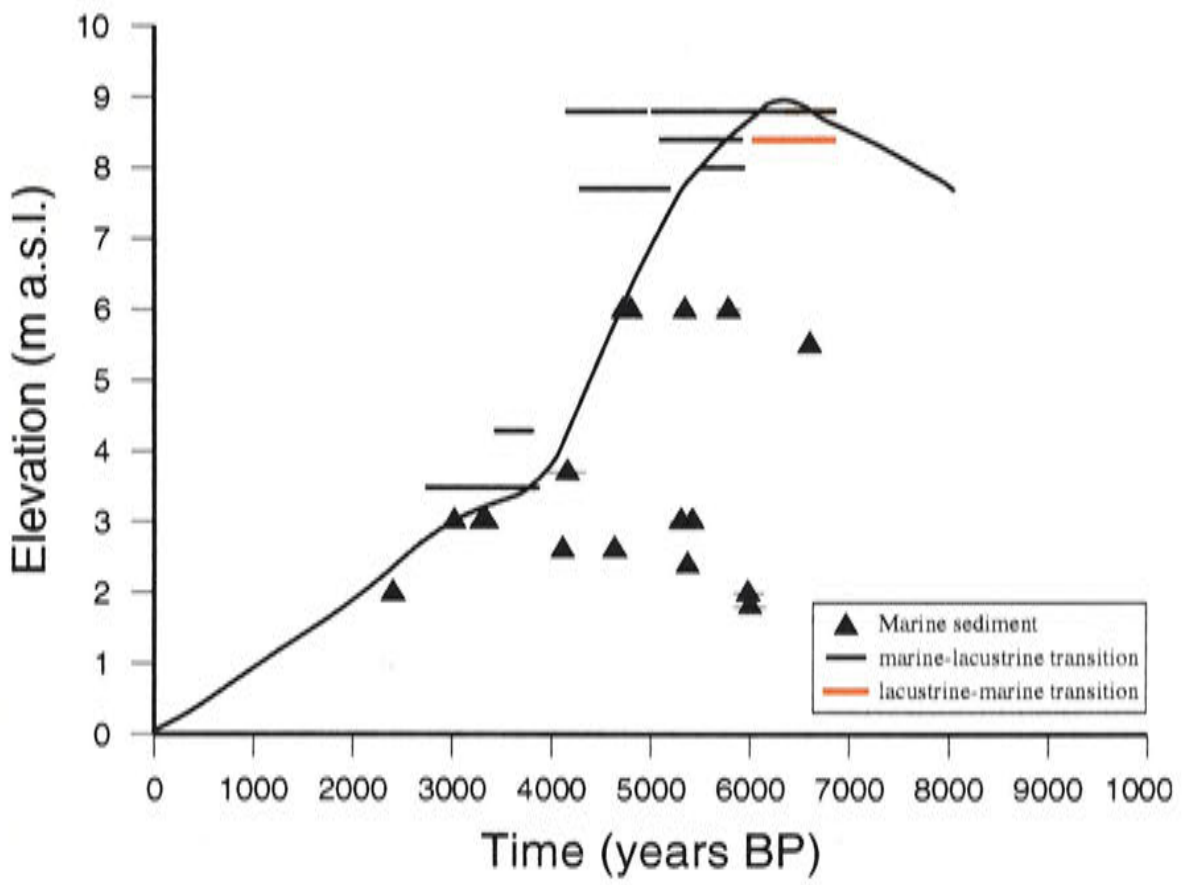

Figure 3.20: Relative sea level curve from Vestfold Hills, East Antarctica (Zwartz:1995). This curve is based on lake isolation observations which date the time the lake became isolated from the sea due to a relative sea level drop.

Finally, the purple curve on Figure 3.19 provides a third option for the relative sea level curve following the modified ^{36}Cl data. This curve once again follows the trend of the radiocarbon dates but instead of reaching the marine limit about 6,000 years BP the curve follows the other ^{36}Cl points. Like the orange curve there is a

small reversal in the trend of the relative sea level curve between 6,000 years BP and 12,000 years BP. However in this case the overall relative sea level rise is only 4 metres rather than 7 metres. At 12,000 years BP this curve trends upwards to reach the marine limit at 16,000 years BP. If this curve was valid it raises questions about why no radiocarbon samples have been found between 16,000 years BP and 6,000 years BP at higher elevations where the sea level has not covered since 16,000 years BP (between 16 metres and the marine limit). However, the purple curve also provides less radical changes in relative sea level than the orange curve.

If one of the three functions described is valid for McMurdo Sound what does this mean in terms of the prior exposure of the ^{36}Cl samples? Removing 5,000 years from all the ages implies an identical history for the entire area prior to the final exposure since the Last Glacial Maximum. If it has taken approximately 6,000 years of falling sea level to expose the beaches it is unlikely that a falling and rising sea level would give the uniform 5,000 years of prior exposure across the coast. Instead we would expect more prior exposure higher up the beach. Thus, local coverage by ice may be a more likely scenario, possibly with the Wilson Piedmont Glacier having advanced further than at present on the Scott Coast. If the coastal area was covered by ice a brief local or global climate change could rapidly uncover the area for a short period of time. The several samples with negative ages may not have received the same 5,000 years of exposure, either through these boulders being ice rafted in at a later date (in the case of the two Cape Bernacchi samples) or because of a greater degree of weathering than expected (in the case of the Dunlop Island bedrock sample).

In conclusion, while there is still much scatter in the data, a correction of 5,000 years is consistent with the relative-sea-level scenarios of the ^{36}Cl data as well as being in agreement with ^{14}C relative-sea-level curve.

Non-constant offset

An alternative to a constant offset between the ^{14}C and the ^{36}Cl dates is to apply a correction proportional to the age of the sample. This is equivalent to dividing the ages by a constant and Figure 3.21 shows the best visual fit. In fact this fit requires quite a large correction equivalent to dividing the cosmogenic ages by three. This is numerically more attractive than removing 5,000 years because it eliminates the problem of some samples having negative ages. This correction is less readily justified, but might be explained, for example, by a substantial error in the environmental parameters used in the data reduction.

Correcting the age of the cosmogenic samples in this way moves all the points closer to the radiocarbon ages. Hence, it is possible to fit the relative-sea-level curve of the radiocarbon dates to the cosmogenic dates, although the scatter of all the cosmogenic ages remains large. The marine limit is also shown on Figure 3.21 and it is not difficult to extrapolate the relative-sea-level curve to the marine limit using this scenario.

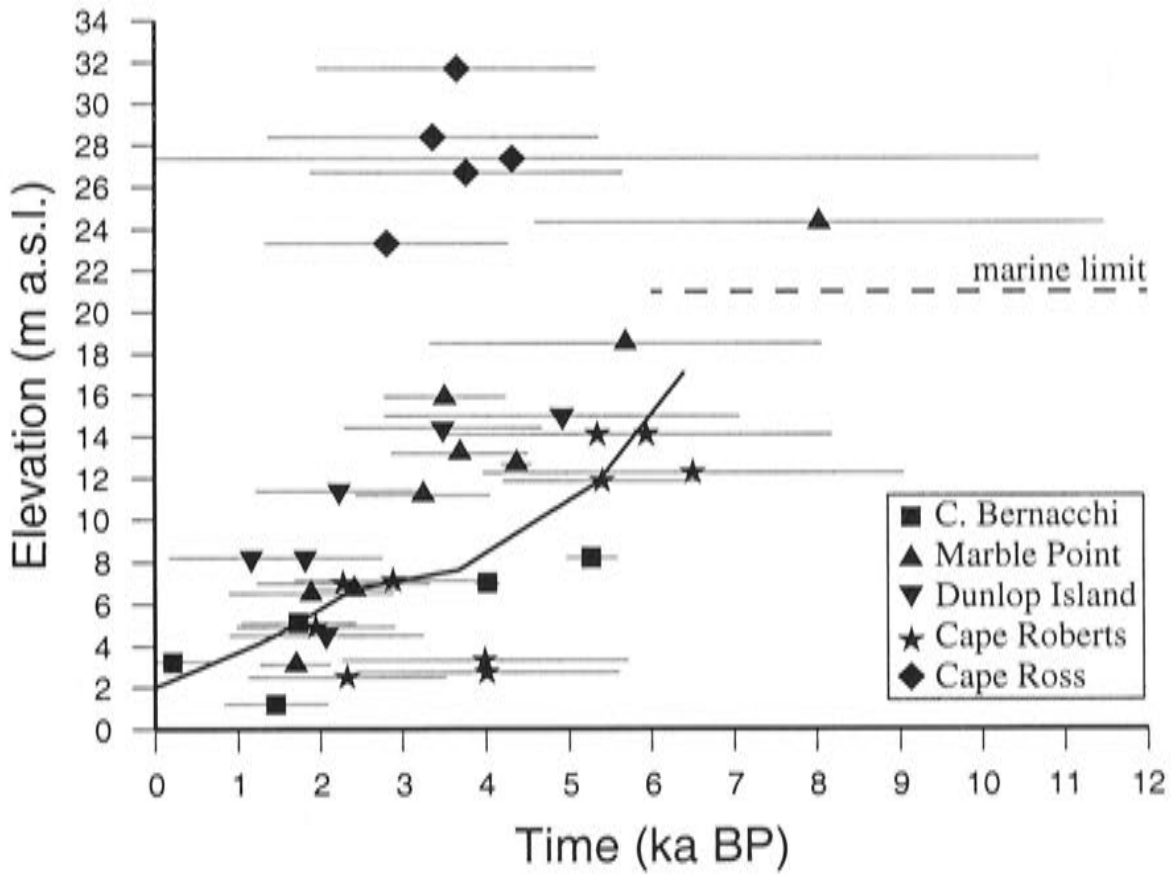

Figure 3.21: Chlorine-36 ages from all McMurdo Sound sites together with the radiocarbon dating. Ages of the Chlorine-36 samples have been divided by three. The error bars appear larger on this figure because of the shorter time scale (errors remain the same).

Using a non-constant offset, such as this, implies that either the exposure history is very complex or there is an error in the age calculation or parameters. The age calculation appears to be robust and has been used successfully in a range of environments (Stone et al. 1996, Brook et al. 1995, Stone et al. 1997, and Stone et al. 2003). Any plausible changes in the constants would not affect the ages to any significant degree (certainly not enough to match the cosmogenic and radiocarbon curves).

Other parameters such as more erosion than estimated or coverage by snow have been investigated to determine the effect of any error in them. However, uncertainties in these parameters all tend to make the ages older rather than younger.

Hence it is difficult to find a sound reason to divide the ^{36}Cl ages by a value as high as three and this option is not favoured.

Forward modelling

Forward modelling the radiogenic isotope content of samples allows various scenarios to be tested for prior-exposure histories. When considering the exposure history of a sample it is necessary to consider not only the periods of exposure of the sample but also the periods of burial. Because ^{36}Cl is a radioactive isotope it will decay while the rock is buried as well as while it is being exposed, reducing the total amount of ^{36}Cl

and therefore the estimate of the age. The half life of ^{36}Cl is 300,000 years and the chlorine builds up more quickly during periods of exposure than it decays when buried.

Another factor necessary to consider when modelling the history of a sample is whether the rock surface has been eroded at the time of exposure or at some point between then and when the surface was sampled. Erosion of the rock surface will effectively mean the sample is taken from deeper in the rock than the original surface. Because the production of ^{36}Cl falls with depth in the rock it will also have the effect of reducing the amount of ^{36}Cl in the sample, and hence the age.

Initally, the adopted forward model assumes a constant value for the production rate of ^{36}Cl at the surface, 21.4 atoms/gram/year (Stone et al. 1996). The production rate is dependent on the rock composition and the cosmic ray flux and this value is for calcite at sea level at a high latitude (e.g. Marble Point samples). The cosmic ray flux is more constant with time at high latitudes than at low latitudes (Noller et al. 2000) so this is an appropriate simplification to make for modelling Antarctic samples. While the rock composition for the McMurdo Sound samples is variable, the average for all the samples is 23.3 atoms/gram/year. However the average production rate for the Marble Point samples used in the first two series of models is also 21.4 atoms/gram/year and hence the production rate suggested by Stone et al. (1996) is appropriate to use. For the final forward model the calculated production rate for each sample is used.

Another simplification of the forward modelling used here is to only have a single period of prior-exposure and burial. It is possible to have multiple periods of exposure and burial, and this may be the case for McMurdo Sound. However, it is best to start with this simpler model.

Initally, it is assumed that there is no erosion between the two exposure times. This is probably incorrect given the field observations of the beach and platform development in McMurdo Sound but it provides a way of testing the importance of the initial period of exposure and burial without adding a third factor.

Exposure and burial patterns are a significant consideration here. Which part of the beach is exposed first when the ice retreats? When sea level falls there is a progressive exposure from the top. However, while less likely to occur, in a previous exposure cycle the coastal area may have been buried by ice and not covered by the sea. In this situation the area could be exposed on the seaward side first. For this modelling exercise the exposure and burial patterns have been kept constant with the relative-sea-level rising to cover the samples and falling to expose samples. This means that higher samples are buried last and exposed first. If the samples had been covered by ice expanding and retreating in the opposite direction (retreating away from the sea) there would be a consistent over-estimate of the ages of the higher samples and vice versa for lower samples.

The final exposure period (approximately 6,000 years BP to present day) is dependent on the height of the sample above sea level. To account for this, the height of

each sample was matched to the radiocarbon relative-sea-level curve to determine a 'radiocarbon' age for each sample (see Table 3.5). This age (after conversion from ^{14}C years to calibrated years) was used as the time of final exposure for each sample.

Sample	Cl-36 atoms	Age	C-14 based age
AC4073	201600	5100	1,800
AC4075	339200	13130	4,100
AC4076	294200	11060	4,400
AC4077	142900	5660	1,500
AC4079	253500	9720	3,800
AC40710	272100	10540	5,000
AC40712	453500	17080	5,500

Table 3.5: Chlorine-36 ages for samples from Marble Point together with the radiocarbon age at the same height from the curve in Figure 3.3.

In applying a constant adjustment to all the samples a constant history for McMurdo Sound is being assumed. This scenario has been investigated above so will not be looked at again in this section.

The first step with the forward modelling is to determine whether it is possible to obtain the same age with a number of different first-exposure and burial histories. Figure 3.22 shows three exposure histories for a single sample that give the same final amount of ^{36}Cl (and hence the same inferred age). Table 3.6 shows exposure and burial times for the three exposure histories.

	Exposure 1	Burial 1	Exposure 2
History 1	64,000	52,000	4,400
History 2	27,000	16,000	4,400
History 3	15,000	-	-

Table 3.6: Exposure and burial histories for three scenarios using the same sample.

This first series of forward models show that it is possible to obtain the same final age estimate from a number of different scenarios. If all the information available is one isotopic age estimate on one sample it is not possible to distinguish between these scenarios. If another cosmogenic isotope was measured with a different half-life it would be possible to distinguish between the scenarios by the different decay rates when the sample is buried. Aluminium and Beryllium are often used in this manner, but because of difficulties in measuring these isotopes on the Australian National University accelerator mass spectrometer at the time of dating, it was not possible to use another isotope.

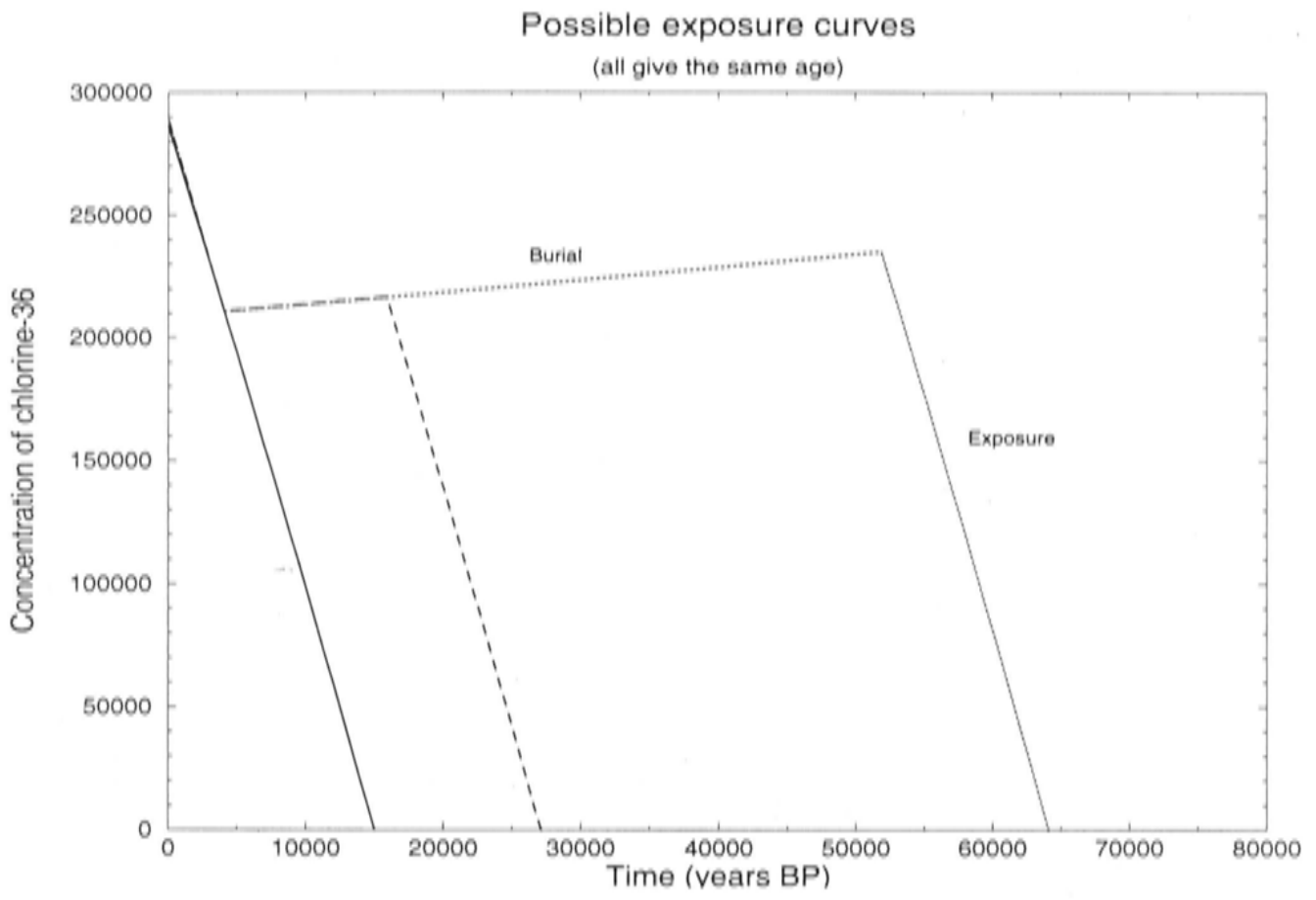

Figure 3.22: Three possible exposure histories that give the same final age. This is a simplified model and does not include any erosion during the burial periods.

The second series of models use two samples from Marble Point to illustrate that it is possible to have two similar prior-exposure histories and end up with the spread in ages that we see at this site. The two samples, AC4073 and AC40712, were assumed to have the initial exposure, burial and final exposure histories shown in Table 3.7. These times of exposure and burial are assumed to represent the progressive exposure and burial of a coastal area by the sea. Hence, sample AC40712 is exposed first at 65,000 years BP and sample AC4073 is exposed later at 62,450 years BP as sea level falls. Sample AC4073 is buried before sample AC40712 as sea level rises again. These assumed times of exposure and burial are not linked to any known sea level falls or rises because, as was shown with the first forward model, it is not possible to constrain this time.

In the modelling, the time of final (second) exposure was kept constant and matched to the radiocarbon curve and the initial exposure time (65,000 and 62,450 years) was altered in a series of iterations until the final age of the sample was correct. Table 3.7 also shows the calculated final times of exposure and burial.

Figure 3.23 shows the results of the second series of models. The figure shows that it is possible to model these two samples, which are 9,800 ^{36}Cl years apart with a very similar exposure and burial history. The additional curve, marked c, with a first exposure time of 32,550 years BP is a reminder that it is actually possible to expose the samples at many different times to achieve the same result. In fact, the prior exposure

Sample	^{14}C Age	^{36}Cl Age	Initial Exp. time	1st Exp. time	Burial time	2nd Exp. time	Total Exposure	Total Burial
AC40712	4980	17080	65000	68250	55000	4980	18230	50000
AC4073	2450	7240	62450	62950	57550	2450	7850	55100
AC4073	2450	7240	62450	32550	27550	2450	7450	25100

Table 3.7: Times of exposure (years) and burial for two samples from Marble Point. Using these values it is possible to model the chlorine-36 ages.

contained in these rocks may even date from the last interglacial period. A possible solution is for the older sample to be exposed first at 68,250 years BP and the younger sample at 32,550 years BP.

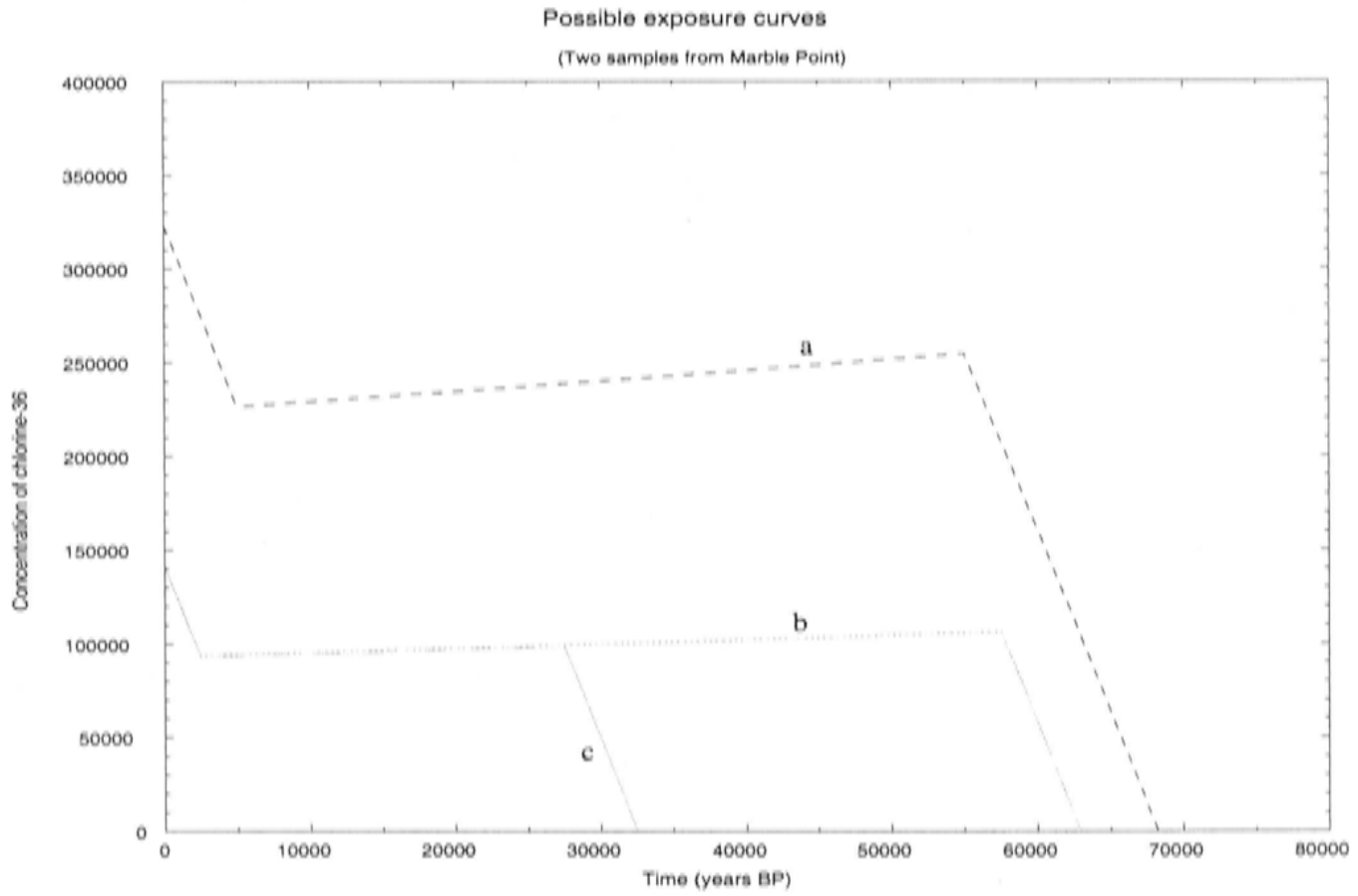

Figure 3.23: Possible exposure histories for samples from Marble Point. Samples are exposed at times indicated in the above Table. The final exposure times are based on radiocarbon dating. This simplified model does not contain any erosion during burial. Curve "a" is sample AC40712, curve "b" is sample AC4073 and curve "c" is an alternative history for sample AC4073.

The above models have not included the possibility of erosion in the final ^{36}Cl age. By eroding the rock, the top surface that contains the greatest portion of ^{36}Cl will be removed reducing the amount of ^{36}Cl in the portion sampled. Erosion therefore reduces the amount of prior-exposure required given the measured ages. Erosion can be caused in two ways. If the samples are beneath the ice sheet gradual erosion by ice over the entire burial period is possible. The other way is if the samples are below sea-level

then the maximum erosion rate is likely to occur as the sample is exposed (beach or rock platform development). For the McMurdo Sound samples the erosion may be a combination of these two, but for the purposes of the forward modelling I have assumed the point in time at which erosion occurs while the sample is buried will not affect the result.

In the third series of forward models, which include erosion, the times of exposure and burial vary with each sample. The radiocarbon ages indicate a progressive exposure of the coastline during late Holocene time so I have assumed a similar trend for the first exposure, and a reverse trend for the time of burial such as would be expected from exposure and burial by sea level fluctuations. The timing of the exposure and burial is linked to the McMurdo Sound radiocarbon relative sea level curve. For each sample a radiocarbon age is determined by the sample height (e.g. a sample at 10 m elevation would intersect the radiocarbon curve at 4,050 years BP). The radiocarbon age is calibrated to conventional years. Table 3.24 gives the equivalent ^{14}C age for each sample (e.g. sample cbc18/1 with a ^{36}Cl age of 4,380 and a height of 1.2 m above sea level has an equivalent ^{14}C age of 1,500 years BP) For the initial exposure, the time of exposure is taken as 40,000 years BP plus the ^{14}C years at the height of the sample (e.g. a sample with a ^{14}C age for its height of 4,100 years will have an initial exposure age of 44,100 years BP). The time of burial is 30,000 years BP minus the ^{14}C years at the height of the sample (e.g. 25,900 years BP for the sample quoted above). All the McMurdo Sound samples with ^{36}Cl ages have been modelled in this way, and these are shown on Figure 3.24. Note the progressive exposure and burial of each sample on the figure.

An exposure time of around 40,000 years and burial time of around 30,000 years has been applied to all samples. For three samples this does not provide sufficient prior exposure to reach the final age. In this situation, these samples must have had an extra period of exposure.

From the exposure and burial time the amount of erosion required after the initial exposure for each sample to reach the measured amount of ^{36}Cl has been calculated. This means that on Figure 3.24 the buildup of ^{36}Cl in the rock is calculated for the depth to which the rock will be eroded during burial. The amount of erosion averages about 61 cm (but with a standard deviation of 53 cm). Table 3.8 lists the samples and required erosion in this model.

An example is sample AC4076 from Marble Point (orange curve in Figure 3.24-B). This sample is exposed at 44,160 years BP for 18,320 years then it is buried at 25,840 years BP for 18,320 years. It is exposed for a final time at 4,160 years BP. For this amount of prior-exposure sample AC4076 requires 47 cm of erosion during burial to produce the measured ^{36}Cl age of 11,060 years. If 47 cm of rock is eroded during burial it will be the rock that was at 47 cm depth during the first exposure cycle that gets exposed at the surface on the final exposure cycle. Therefore we need

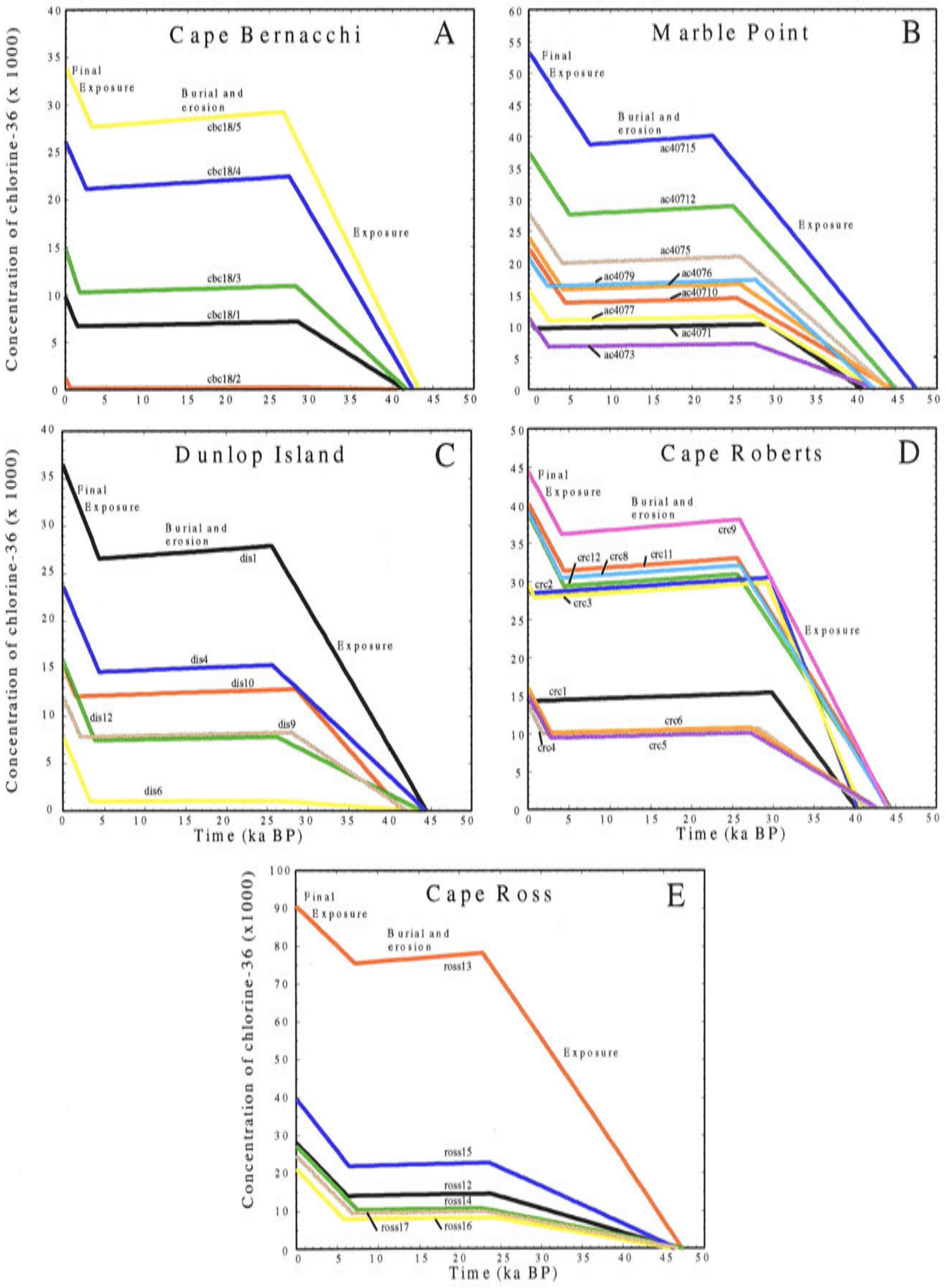

Figure 3.24: Exposure histories predicted from the third forward model for each site along McMurdo Sound. The rate of accumulation during the first exposure period is determined by the amount of erosion the rock received during burial. The higher samples are exposed first and buried last, and the final exposure time is determined by their relationship to the radiocarbon relative sea level curve.

Sample	Production rate	^{14}C age (calibrated)	^{36}Cl age	Chlorine concentration (x100)	Total erosion required (cm)
C. Bernacchi					
cbc18/1	22.3	1,500	4,380	98	78
cbc18/2	20.1	620	655	13	>200
cbc18/3	28.6	1,770	5,210	149	70
cbc18/4	21.7	2,550	12,050	261	19
cbc18/5	21.5	3,300	15,830	340	9
Marble Pt.					
ac4071	22.0	800	5,100	112	50
ac4073	21.8	2,450	7,240	158	56
ac4075	21.2	4,100	13,110	278	32
ac4076	21.7	4,160	11,060	240	47
ac4077	19.8	2,450	5,660	112	78
ac4079	21.3	2,280	9,720	207	31
ac40710	21.1	4,460	10,540	222	56
ac40712	21.9	4,980	17,080	374	21
ac40715	22.1	7,480	24,100	533	15
Dunlop Is.					
dis1	24.7	4,450	14,770	356	27
dis4	22.6	4,380	10,470	237	55
dis6	22.3	3,300	3,500	78	199
dis9	22.0	2,080	5,460	120	73
dis10	25.0	1,500	6,210	155	50
dis12	23.5	3,850	6,700	157	92
C. Roberts					
crc1	21.0	170	6,950	146	18
crc2	24.3	350	12,020	292	insuff.**
crc3	24.8	800	11,950	296	insuff.**
crc4	23.6	1,770	5,840	138	61
crc5	23.6	2,750	6,810	161	67
crc6	21.9	2,750	6,830	150	67
crc8	24.2	4,050	16,210	392	15
crc9	22.8	4,100	19,520	445	3
crc11	22.6	4,400	17,820	403	12
crc12	24.3	4,400	16,040	390	20

Sample	Production* rate	^{14}C age (calibrated)	^{36}Cl age	Chlorine concentration	Total erosion required (cm)
C. Ross					
ross12	24.8	6,250	11,320	281	73
ross13	24.6	7,200	36,850	907	insuff.**
ross14	24.8	7,450	10,960	272	96
ross15	30.5	6,450	13,010	397	61
ross16	25.1	5,800	8,430	212	104
ross17	24.4	6,800	10,100	246	97

Table 3.8: Amounts of erosion required for a forward model with prior exposure beginning approximately 40,000 years BP, a burial phase beginning approximately 30,00 years BP and a final exposure time based on the sample's age determined from the radiocarbon relative-sea-level curve. Erosion required is given in centimetres. Samples with less than 26 cm erosion have two values that may be eroded because of the nature of the production rate curve near the surface and here the lesser value has been taken.

** Insufficient exposure.

to calculate the rate of accumulation at 47 cm depth for the first exposure cycle. This accumulation curve will have a different slope to the surface because accumulation rates fall with depth into the rock (see Figure 3.10). Because the amount of erosion required is calculated for each sample the slope of the accumulation stage of ^{36}Cl for the initial exposure will be different for each sample.

This forward model illustrates that it is possible to suggest a consistent history for exposure and burial for the McMurdo Sound samples. There is no need to postulate that erosion has been faster for the higher sites than for the lower sites. For a longer initial exposure more erosion would be required to decrease the amount of chlorine at the surface after erosion. Because the decay rate during burial is much slower than the accumulation rate during exposure, the length of the burial time is less important for the final ^{36}Cl concentration than the length of the exposure time or the amount of erosion.

It would be possible to estimate a uniform amount of erosion that every sample received (e.g. 50 cm) and alter the length of time of the initial exposure to match the measured ^{36}Cl. However, over the coastal area with the development of rock platforms and boulder beaches the amount of erosion is likely to vary more than the time of exposure, especially for samples in a fairly close proximity so this approach has little merit.

It is also possible to extend this model to reproduce several exposure, burial and erosion cycles. However, without additional information about the likely history of the

McMurdo Sound coastal area adding further cycles of unknown duration is not helpful.

In summary, forward modelling provides illustrations of the possible history of the McMurdo Sound ^{36}Cl samples. The modelling shows how a prior history of exposure, burial and exposure can produce the difference between the ^{36}Cl ages and the ^{14}C ages. However, because only one isotope has been measured it is not possible to distinguish between different scenarios.

3.5 Summary

Ten sites around McMurdo Sound and Cape Hallett were visited to obtain observational evidence of the timing of relative-sea-level retreat to compare with the glacio-hydro-isostatic model results. The sites all have raised shoreline deposits from which material was collected for dating. The sites vary greatly in their characteristics; from a raised delta deposit at a palaeo-stream mouth, to raised beach ridges (both sand and boulder ridges), to sea-ice cut bedrock platforms, to raised boulder pavements, and finally Adélie penguin rookeries on raised beaches.

Three dating techniques were applied — radiocarbon, optical dating, and surface exposure dating. Radiocarbon dates were obtained from a raised delta deposit, a beach ridge, and from penguin nests on top of beach ridges. 10 samples provided ages between the present day and 5,840 calibrated years before the present and were combined with dates from Hall and Denton (1999) to form a relative sea level curve for McMurdo Sound (Figure 3.3).

Two samples were optically dated using a single-grain regenerative-dose method. The two ages obtained, 2,420 and 3,120 years, compliment the radiocarbon ages and confirm the Holocene age of the raised beaches.

The cosmogenic isotope ^{36}Cl was used to surface exposure date both rock platforms and boulders from the raised shorelines around McMurdo Sound. Samples from six locations were dated with ages ranging from 655 to 36,850 years with the majority of the ages older than the radiocarbon and optical dates. There is no difference between samples from bedrock and boulders. It is interpreted that there is a component of prior exposure in these samples and a series of possible histories were modelled. However, without a second isotope to constrain the time duration of burial it is not possible to draw further conclusions.

Chapter 4

Ice sheets, crustal rebound and sea-level change

4.1 Introduction

This chapter outlines the concepts that are used in the rest of this thesis to define the former limits of the Antarctic Ice Sheet. A glacio-hydro-isostatic modelling method is used to constrain the former ice sheet in Antarctica. The main discussion in this chapter is about how this method is used to model the Antarctic Ice Sheet and what conclusions can be drawn about it.

The Earth's geoid is an equipotential surface whose shape is determined by the mass distribution of the planet. As mass is redistributed, either by deformation of the planet and internal mass redistribution or by redistribution of surface mass such as ice and water, the external gravity field changes and hence the equipotential surfaces also change. In the absence of other forces such as winds and water currents, the surface of the ocean is an equipotential surface. Therefore changes in the mass distribution and equipotential surfaces cause the shape of sea level to change.

The shape of the sea level equipotential surface (the geoid) is defined as the position of this surface relative to the centre of mass of the earth. However, this absolute position of the sea surface cannot be measured from the geological record and instead, what is measured is the change in sea level relative to the crust. This measurable change is used in the glacio-hydro-isostatic modelling.

When an ice sheet grows or melts, three effects combine to determine the change in sea level relative to the crust:

1. Firstly, there is a radial displacement of the crust as the masses of ice and water change the loading on the Earth's crust. Relative sea level is modified by the Earth's internal redistribution of mass and change of shape.

2. The second is a change in gravitational attraction to the movement of ice and

water loads on the Earth's surface in the form of ice sheets and oceans. This redistribution causes a change in the shape of the equipotential surface.

3. Thirdly, there is a change in the volume of the oceans as water is taken up or melted by the ice sheet. This changes the mean level of the sea with respect to the land.

The first and second effects are referred to as the isostatic contributions and are the combined displacement and gravitational effects. These can be divided into a glacio-isostatic term which is the part due to the change in the ice load, and the hydro-isostatic term, which is the part due to the change in water load. Hence the term glacio-hydro-isostasy for the relative sea level change caused by the growth or decay of ice sheets.

The movement of water between ice and the ocean (effect number 3 above) is termed the eustatic sea level or the ice-volume equivalent sea level, which represents the globally averaged sea level change due to the change in ocean volume. Hence, the equivalent sea level is position independent and can be represented mathematically by (Lambeck et al. 2000):

$$\Delta\zeta_e(t) = \frac{\rho_i}{\rho_o} \int \frac{1}{A_o(t)} \frac{dV_i dt}{dt} \tag{4.1}$$

Where ρ_i is the average density of ice, ρ_o is the average density of the oceans, and $A_o(t)$ is the area of the oceans at time t. $A_o(t)$ is also ocean volume change (V_i) dependent because the area of the oceans changes with the amount of water frozen into or melted from the ice sheets (Lambeck et al. 2000).

The surface loads of ice and water are related through the changing geometry of the ocean basins, the need to conserve mass, and the need to keep the sea surface at an equipotential. This relationship is defined by the sea level equation of Farrell and Clark (1976) in the first approximation or by the more precise definition of Johnston (1993) (see also Lambeck et al. 2003). The equation for a tectonically stable area is:

$$\Delta\zeta_{rsl}(\Phi, \lambda, t) = \Delta\zeta_e(t) + \Delta\zeta_i(\Phi, \lambda, t) + \Delta\zeta_w(\Phi, \lambda, t) \tag{4.2}$$

For any given site at co-latitude Φ (degrees of latitude from the north pole), longitude λ, and time t, the relative sea level is a combination of the equivalent sea level change ($\Delta\zeta_e(t)$), the isostatic crustal response to the ice load at the site ($\Delta\zeta_i$), the isostatic crustal response to the water load at the site ($\Delta\zeta_w$) and the change in the gravitational component (included in both the $\Delta\zeta_i$ and $\Delta\zeta_w$ terms). Each of these components is discussed further below.

The glacio-hydro-isostatic method of modelling allows different parameters to be determined. If the ice models are known, the observations of the relative-sea-level change can be inverted to estimate the rheological parameters of the Earth. If the rheology is known but the ice history is not, then this inversion method can be used to estimate ice sheet parameters. In most situations both the parameters for the Earth's

rheology and the ice sheet are partly known. Using the glacio-hydro-isostatic modelling method both can be improved through an iterative process.

For Antarctica it is the ice history that is considered to be most uncertain. Thus, for Antarctica we assume that the Earth is radially symmetric in its physical properties and that the rheology inferred from the better constrained inversions of the Northern Hemisphere is also valid for the mantle beneath Antarctica. The models for the Earth are explored in further detail later in this chapter, however these Northern Hemisphere models appear to work for Antartica and the variations in the rheological parameters have less consequence than do any errors arising from the uncertain knowledge of the ice sheet.

Because there were a number of ice sheets on Earth during the last glacial cycle we need to differentiate between the Antarctic Ice Sheet and the Northern Hemisphere ice sheets. Schematically this can be written as:

$$\Delta\zeta_{rsl}^{obs} = \Delta\zeta_e + \Delta\zeta_{rsl}^{Ant} + \Delta\zeta_{rsl}^{ff} \tag{4.3}$$

where $\Delta\zeta_{rsl}^{obs}$is the observed relative sea level, $\Delta\zeta_{rsl}^{Ant}$ is the glacio-hydro-isostatic effect of the Antarctic Ice Sheet and $\Delta\zeta_{rsl}^{ff}$ the glacio-hydro-isostatic effect of the Northern Hemisphere far-field ice sheets. If $\Delta\zeta_{rsl}^{ff}$ can be assumed to be known and $\Delta\zeta_e$ is established, then by an iterative process using relative sea level data from sites far from any of the ice sheets (e.g. Barbados) an equation can be generated that gives information about the ice sheet and Earth:

$$\Delta\zeta_{rsl}^{obs} - (\Delta\zeta_e + \Delta\zeta_{rsl}^{ff}) = \Delta\zeta_{rsl}^{Ant}(E, I) \tag{4.4}$$

Where $\Delta\zeta_{rsl}^{Ant}$ is a complex function of the earth (E) and ice (I) parameters. Inversion of this equation, assuming the Earth function is known, determines aspects of the Antarctic Ice Sheet at a given point in time. This is essentially the process used in this thesis, using the field data from McMurdo Sound to estimate the ice parameter for the Ross Sea Embayment.

4.1.1 Modelling process

A glacio-hydro-isostatic model of the Earth is used in this thesis to predict changes in relative sea levels from both the Antarctic and Northern Hemisphere Ice Sheets. The predicted relative sea level changes are then used to constrain ice location, volume, and melting in the Antarctic Ice Sheet. There is an potential for circularity in the process which is necessary to combine the disparate evidence into a consistent whole. The modelling method requires an ice sheet, a model for the Earth and a growth/melting history for the ice sheet. Figure 4.1 shows a flow chart of the modelling process.

The ice sheets input into the glacio-hydro-isostatic modelling program are defined in terms of an ice load change with time. The ice sheets are located on the Earth by

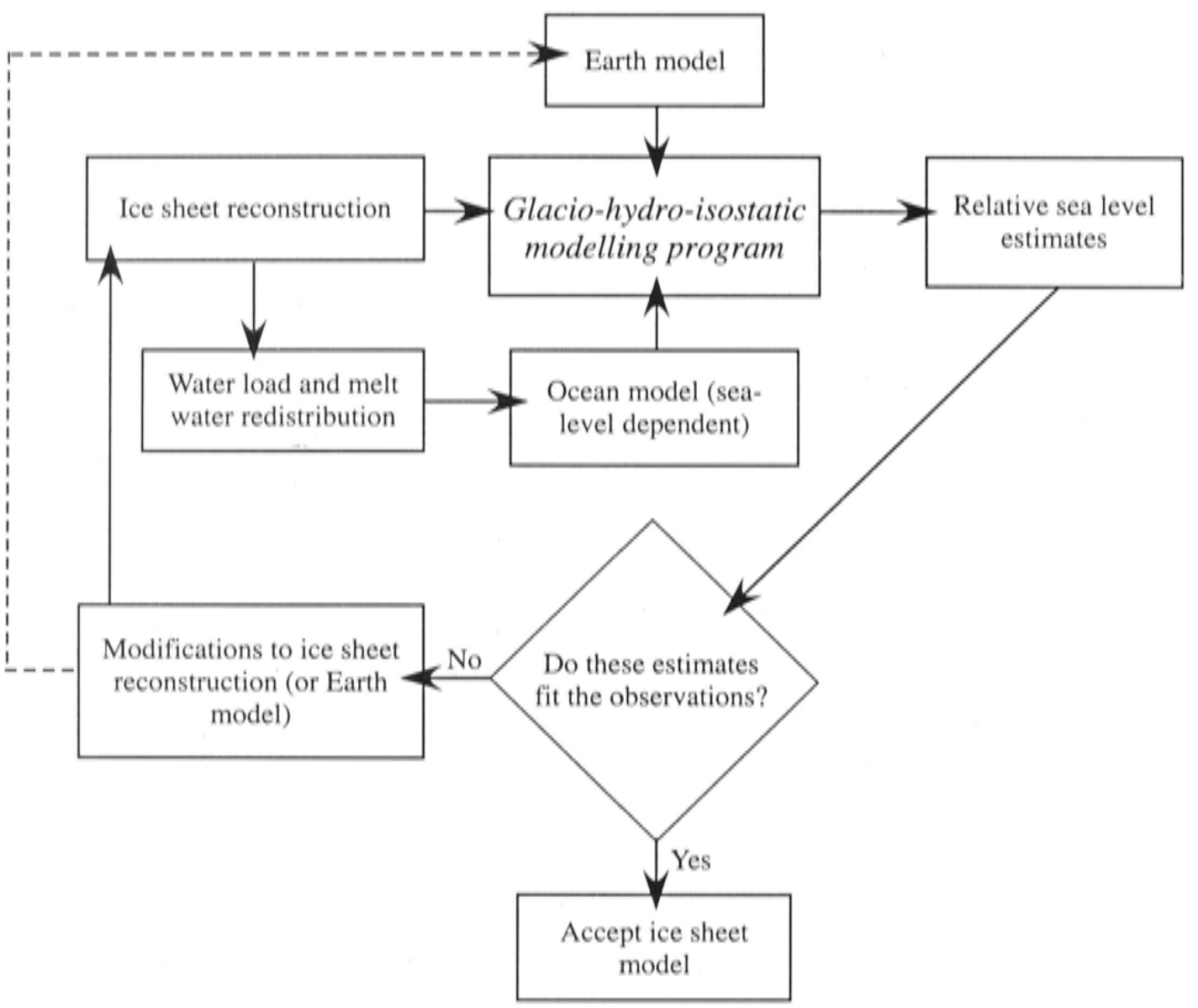

Figure 4.1: Flow chart showing the process of obtaining a reconstruction of an ice sheet using the glacio-hydro-isostatic modelling program.

colatitude and longitude. The oceans are defined as well to model the water loading. In the model used, the ice sheet surface is defined every 0.2 degree (approximately 22 km^2). At each of a series of time steps the change in height of each defined point in the ice sheet is given in metres. For example a change of -3 m means that the ice sheet has melted at this point by 3 metres since the previous time step. A linear interpolation is made between the time steps. A simple model might define only a few time steps (e.g. a maximum ice sheet and a final time step where the ice sheet is at a minimum). However, more time steps allows for a more complex and more realistic melting history.

4.1.2 Ocean basins

In defining the hydro-isostasy or water load, the ocean basins must be known and the change in the shape and volume of the ocean basins through time must be computed for all epochs, even when all ice sheet melting has ended. The ocean basin continues to deform because the visco-elastic flow of mantle material in response to the changing load

is slower than the melting of the ice sheet. Thus, ocean water is redistributed within the ocean and this is included in the formulation of the relative-sea-level equation.

Some special problems occur in the definition of the ocean basins at the ice margins when ice encroaches onto the shelves. The glacio-hydro-isostatic modelling code used in this thesis has the ocean function defined by the ice margin irrespective of whether the ice is grounded or floating. But, the ice sheets in these models are only defined by grounded ice and do not incorporate the floating ice which is treated the same as if it was melted and is included in the oceans.

However, a much more suitable solution is to evaluate the grounding line position at each point in time on the shelves and define the ocean basin from this. On melting, as the ice thins or eustatic sea level rises, it may float off and the grounding line is redefined.

The load from the ice sheets and from the water in the ocean basins are separated in the glacio-hydro-isostatic modelling. The ocean water load is determined by the ocean depth function $h_o(\Phi, \lambda, t)$ (Figure 4.2). This (h_o) is the distance from the ocean floor to the geoid at the point Φ, λ (latitude and longitude) and at time, t. Where there is no water this is zero. The ice thickness function is $h_I(\Phi, \lambda, t)$ and is the distance from the lower-most to the upper-most surface of the ice load at the point Φ, λ and at time, t. Thus, for grounded ice there is no water load so the ice thickness function is used for these areas.

The calculation can be made more complex during deglaciation when some areas of the grounded ice sheet melt and start floating. Floating ice can be incorporated into the ocean model through a modified ocean depth function $h_o^*(\Phi, \lambda, t)$. This (h_o^*) is the distance from the ocean floor to the water/ice interface. Where there is floating ice of thickness h_I the load (L) at this point can be written as (see Figure 4.2):

$$L(\Phi, \lambda, t) = \rho_w h_o^*(\Phi, \lambda, t) + \rho_i h_I(\Phi, \lambda, t) \tag{4.5}$$

Where ρ_w is the density of water and ρ_i is the density of ice. During deglaciation the change in the surface load $\Delta L(t)$ is calculated:

$$\Delta L(\Phi, \lambda, t) = L(\Phi, \lambda, t) - L(\Phi, \lambda, t_0) = \rho_w[h_o^*(t) - h_o^*(t_0)] + \rho_i[h_I(t) - h_I(t_0)] \tag{4.6}$$

Both equations are from Lambeck et al. (2003).

4.1.3 Ice and water load terms

Returning to the relative sea level equation (4.2), the ice load term, $(\Delta\zeta_i)$ is the response of the Earth to the change in the local ice load $(\Delta\zeta_{rsl}^{Ant.})$ and the change in any ice load of the distant ice sheets $(\Delta\zeta_{rsl}^{ff})$. Also included in the ice load term is the gravitational attraction of the ice. Close to the ice sheet the gravitational attraction of the ice sheet is large (up to 70 m for an ice sheet with melting similar to the Last Glacial Maximum

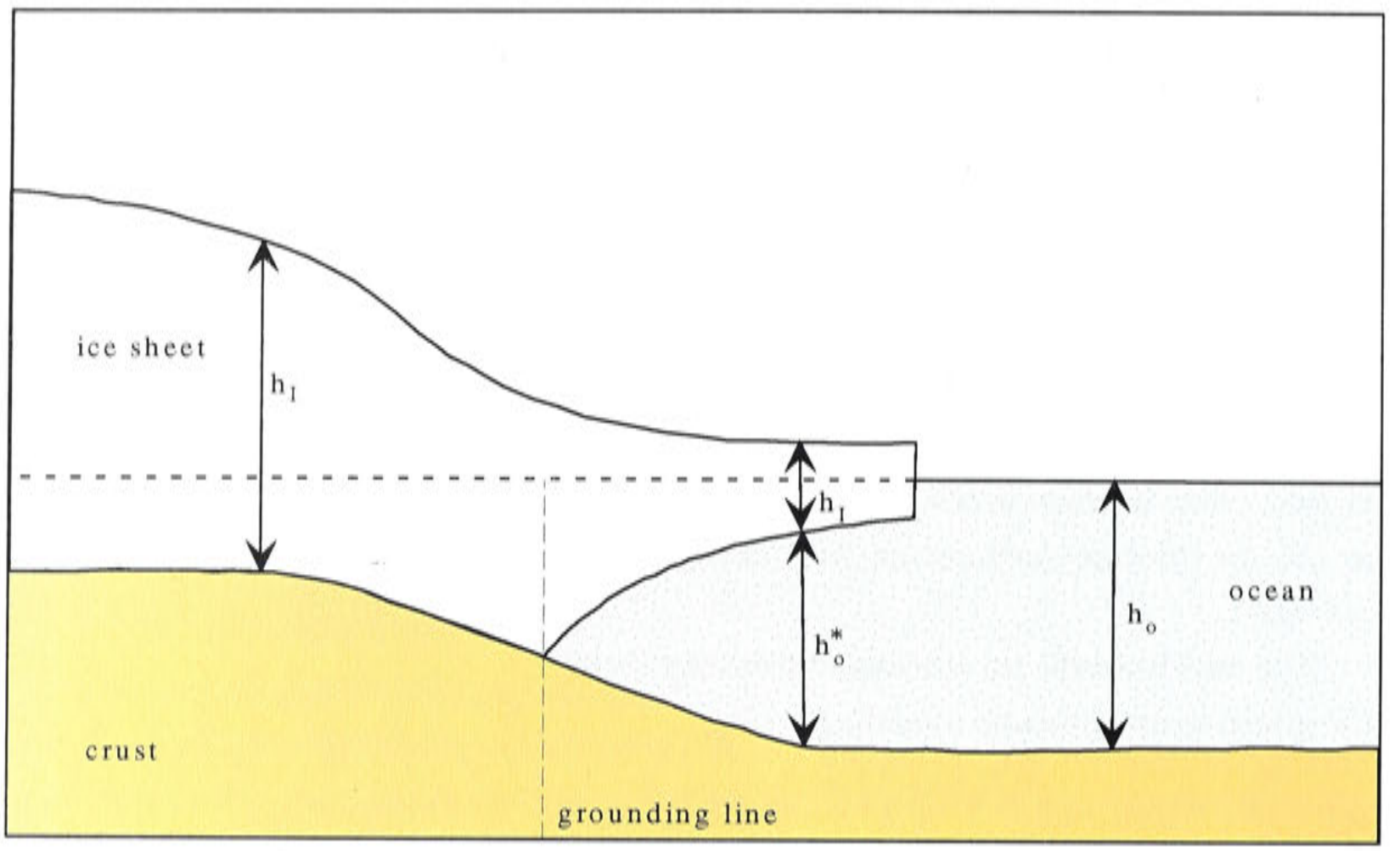

Figure 4.2: Schematic diagram of how grounded ice below sea level is treated in the calculations of isostasy. h_o is the ocean depth, h_I is the ice thickness, and $h*_o$ is the ocean depth below the ice. The load $L(\Phi, \lambda, t)$ is calculated using the floating ice thickness from the grounding line together with the water depth below the ice.

Antarctic Ice Sheet). Figure 4.3 shows schematically the effect of the gravitational attraction by the ice sheet. The gravitational component is generally small compared to the radial deformation of the surface by the ice load term and in some places where the two terms are opposite such as close to the ice sheet margin the radial deformation component dampens the response of the gravitational attraction.

The ocean basins change size and shape with the addition or removal of water. On ice sheet melting the first iteration of the glacio-hydro-isostatic modelling program only places the extra water load into the oceans. Subsequent iterations take into account coastline alterations. Hence it is important to do at least two iterations of the modelling.

Figure 4.4 illustrates the ice and water components for a schematic axially symmetric load. The ice term shows the effects of the ice load only. The water load term illustrated here also includes the effects of the gravitational attraction of the ice load and of the mass redistribution within the Earth. The eustatic sea level change for this model is approximately 90 metres. The relative sea level (final curve) on figure 4.4 shows the combination of the ice load, the water load and the eustatic sea level.

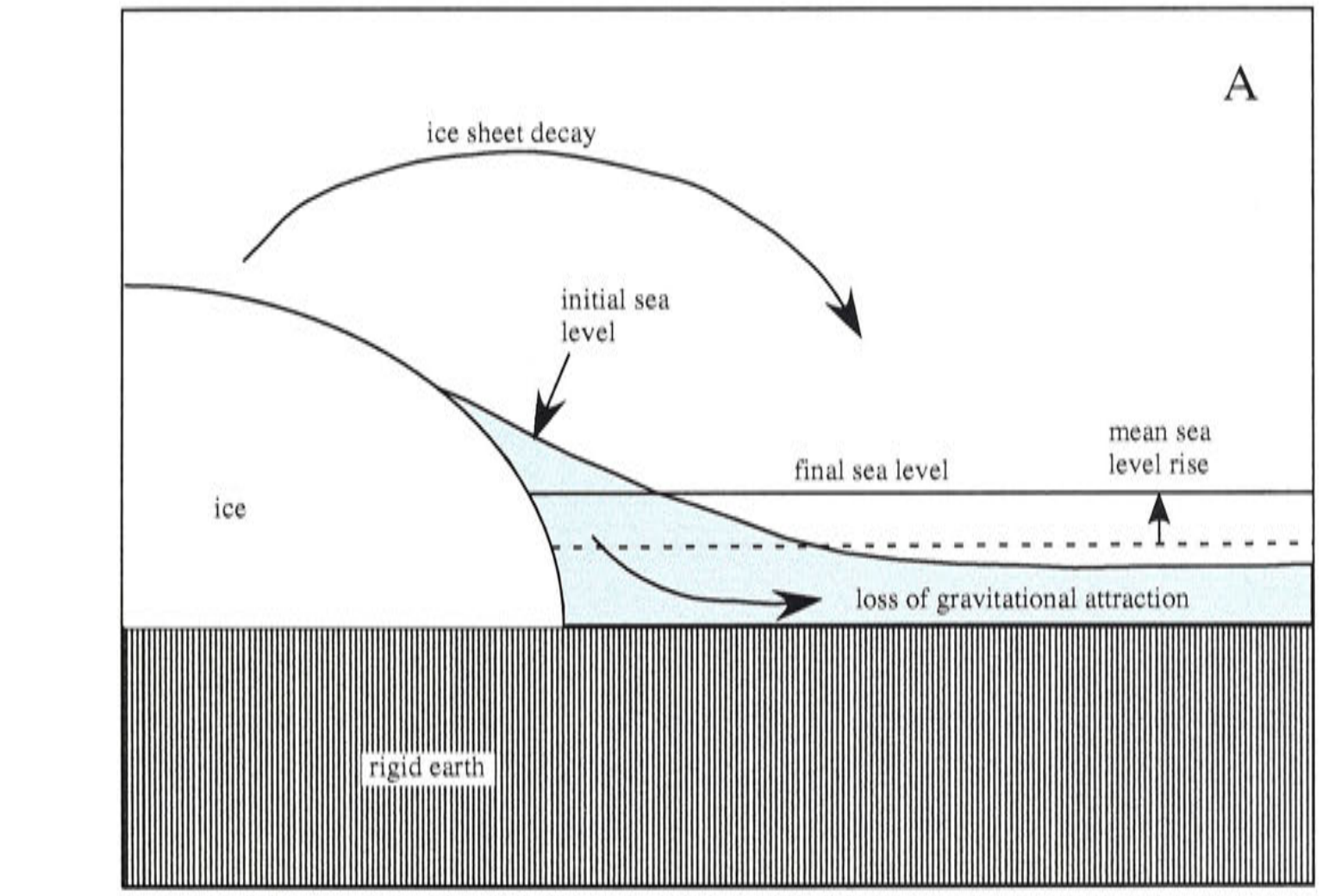

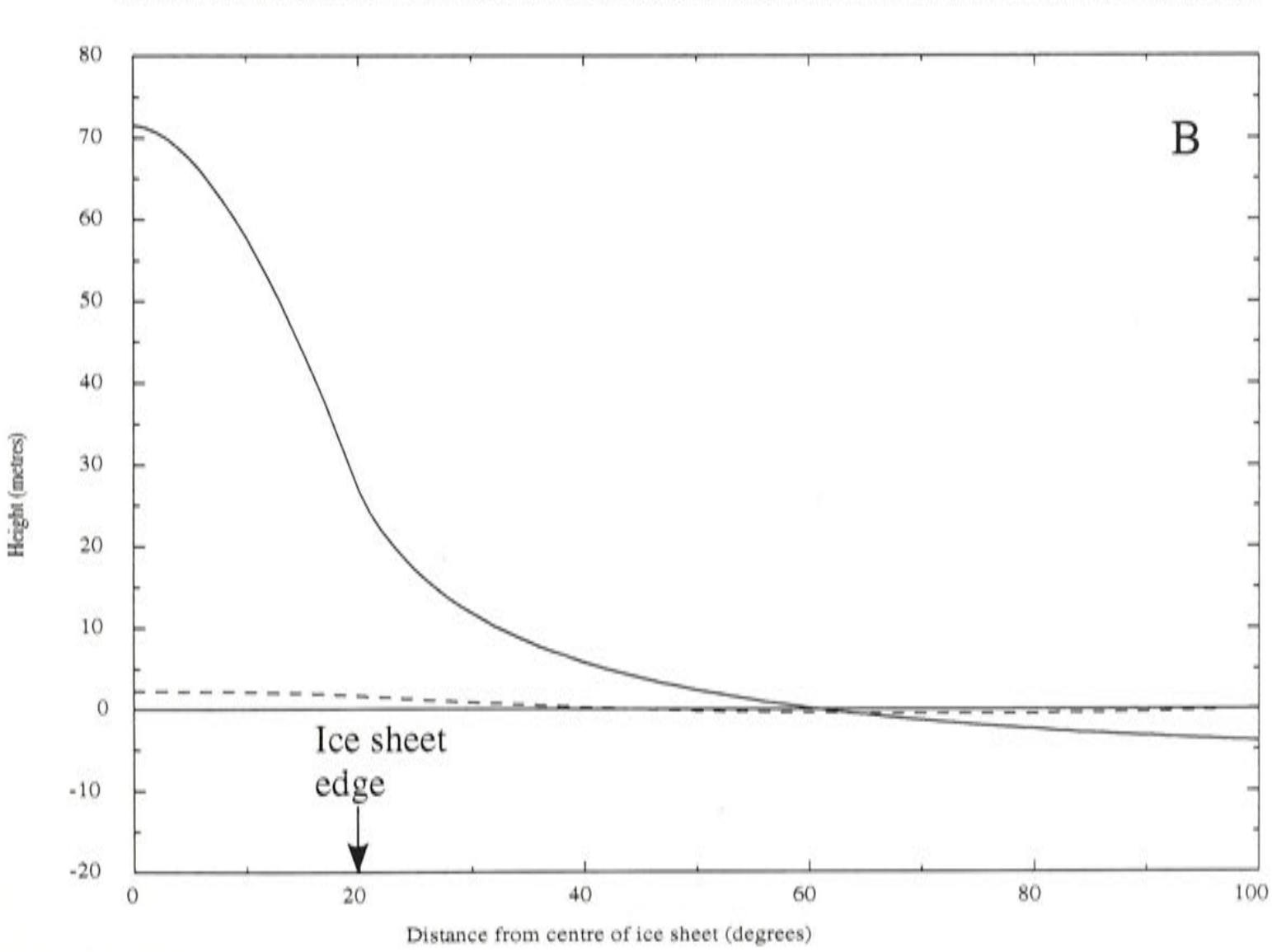

Figure 4.3: A. Schematic illustration showing the gravitational attraction of sea level to an ice sheet, modified from Stirling (1996). B. Calculated gravitational attraction of an ice sheet containing about 30 m equivalent sea level. The edge of the ice sheet is at 20° on top of a continent. The solid curve is the attraction of the ice load and the dashed curve is the gravitational attraction of the water load.

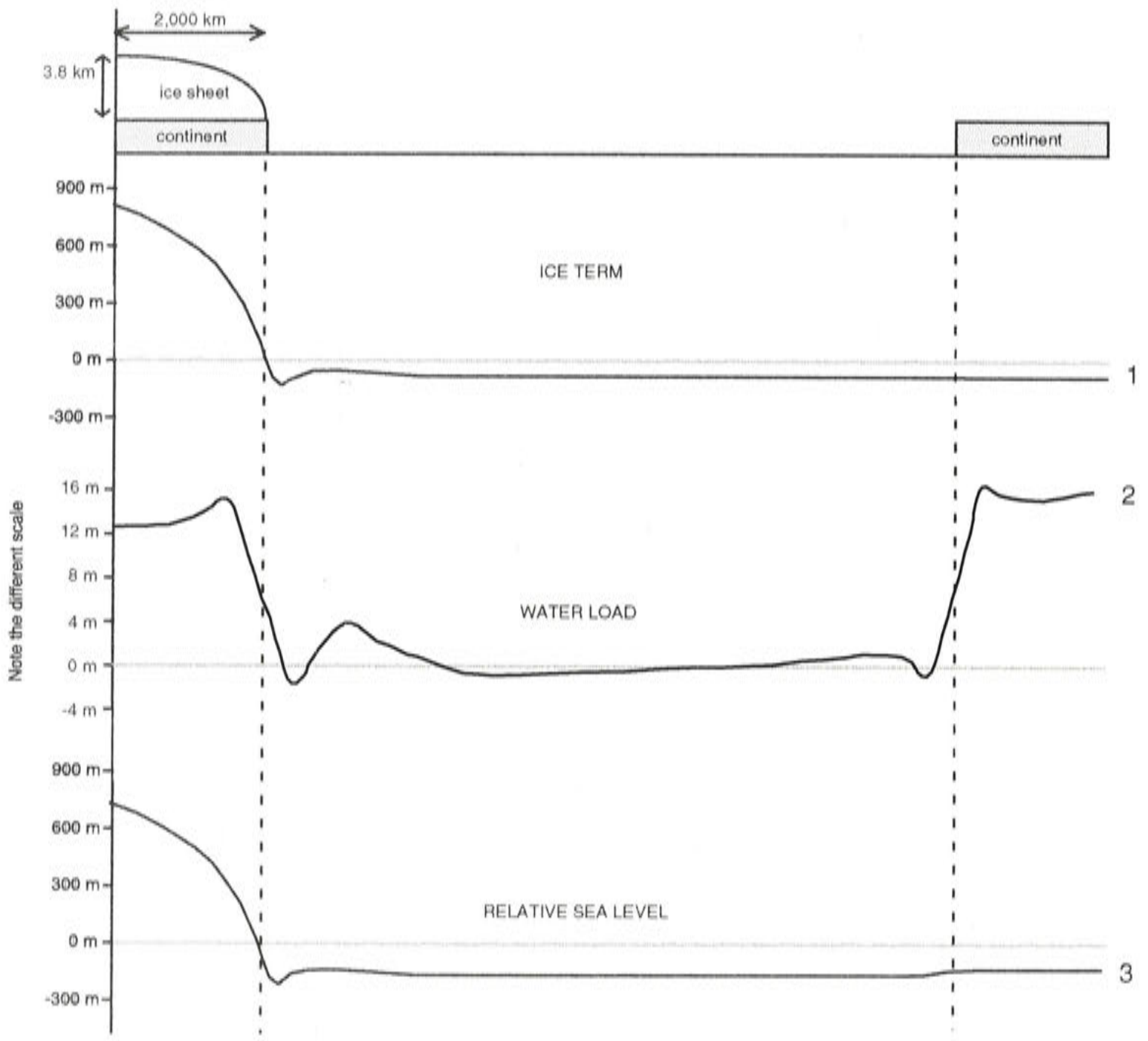

Figure 4.4: Schematic diagram illustrating the two major contributions in relative sea level modelling. While not to scale the figure shows a transect through the Earth radially outwards from the centre of an ice sheet placed on one of the continents. This figure shows the difference between two near-equilibrium situations - with and without an ice sheet loading the left-hand continent. Below the top drawing there are three lines; the ice load term, the water load term and the combined relative sea level. On each of the panels is a horizontal grey reference line to indicate how far the sea level has deviated from the equilibrium position prior to loading. The ice term contains the effects on the geoid from the loading of the ice and subsequent mantle flow. The water term includes the gravitational attraction of the ice and the changing gravitational attraction caused by mantle flow but does not include the equivalent sea level change (90 m for this ice sheet). The relative sea level term is the sum of the two plus the equivalent sea level.

4.2 Earth deformation

Ice sheet loads cause a glacio-hydro-isostatic deformation of the Earth that varies with distance from the region of loading. The deformation is measured by using relative-

sea-level changes but the deformation is initally discussed here in terms of crustal, lithospheric and mantle movement.

The response of the Earth is approximated by that of a Maxwell visco-elastic body (Johnston 1993). In this approximation the Earth is radially divided into the lithosphere (which includes the crust) and the mantle, where the mantle may have one or more layers. The Earth is divided in this manner because the outer portion, the lithosphere, tends to have an elastic response to loading and a high flexural rigidity whereas the mantle tends to deform viscously under stress. The mantle may be divided into layers with increasing viscosity with depth. The viscosities of the mantle regions typically used in the glacio-hydro-isostatic modelling are around (1-5)x10^{20} Pa s for the upper portion of the mantle and approximately 10^{22} Pa s for the lower portion of the mantle (Lambeck et al. 1996).

With a visco-elastic approximation for the Earth, when a load is placed on the Earth there is an immediate elastic deformation of the lithosphere and mantle. If the load duration is long (such as an ice sheet load may be) then the stresses in the mantle relax and the load may be finally carried by the flexural rigidity of the lithosphere and by the buoyancy forces in the lithosphere and mantle. The characteristic response of the Earth in this situation is defined by the flexural rigidity which is a measure of the distance over which load stresses are distributed.

The effects of an ice load on the mantle depends on load size. The stresses from a small ice sheet may only propagate into the more shallow regions and hence the response is determined mainly by the upper mantle viscosity. A larger ice sheet will propagate stress into the deeper mantle as well as the shallower area. Because of the lower viscosity the upper mantle stresses relax more rapidly than the lower mantle giving a different time scales of relaxation dependent on the load size. If a load is very small the stresses do not propagate beyond the lithosphere and only an elastic response will be seen.

It is important to know how long the ice sheet has been at its maximum extent. If the ice sheet grows and melts within a few thousand years then the Earth would not have had time to fully adjust to the loading of the ice sheet. Hence, the final record of the response of the Earth to the load will provide a solution to glacio-hydro-isostatic modelling that contains less ice than the actual volume of the load.

In terms of ice sheet melting, assuming the ice sheet melts instantaneously for illustrative purposes only, we can explore the immediate elastic responses of the Earth and the delayed responses of the viscous mantle. Later, the effects of non-instantaneous melting will be discussed. Figure 4.5 shows a schematic diagram of an ice sheet loading the Earth together with a series of time steps showing the Earth re-establishing an equilibrium after melting of the ice sheet. Figure 4.6 shows characteristic relative sea level curves with time for different sites. This second figure does not make the assumption of instantaneous ice sheet melting and shows the relative sea level curves

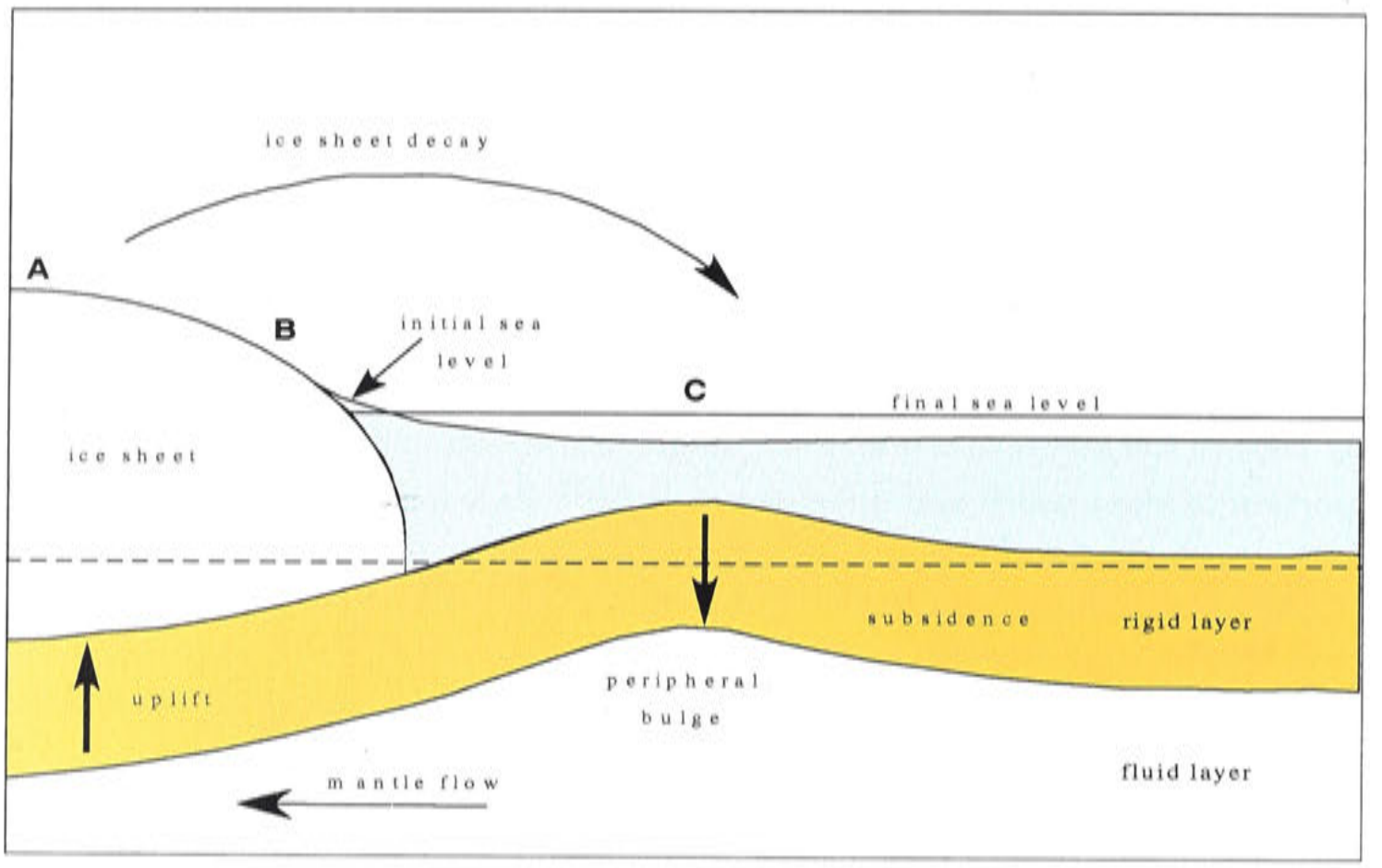

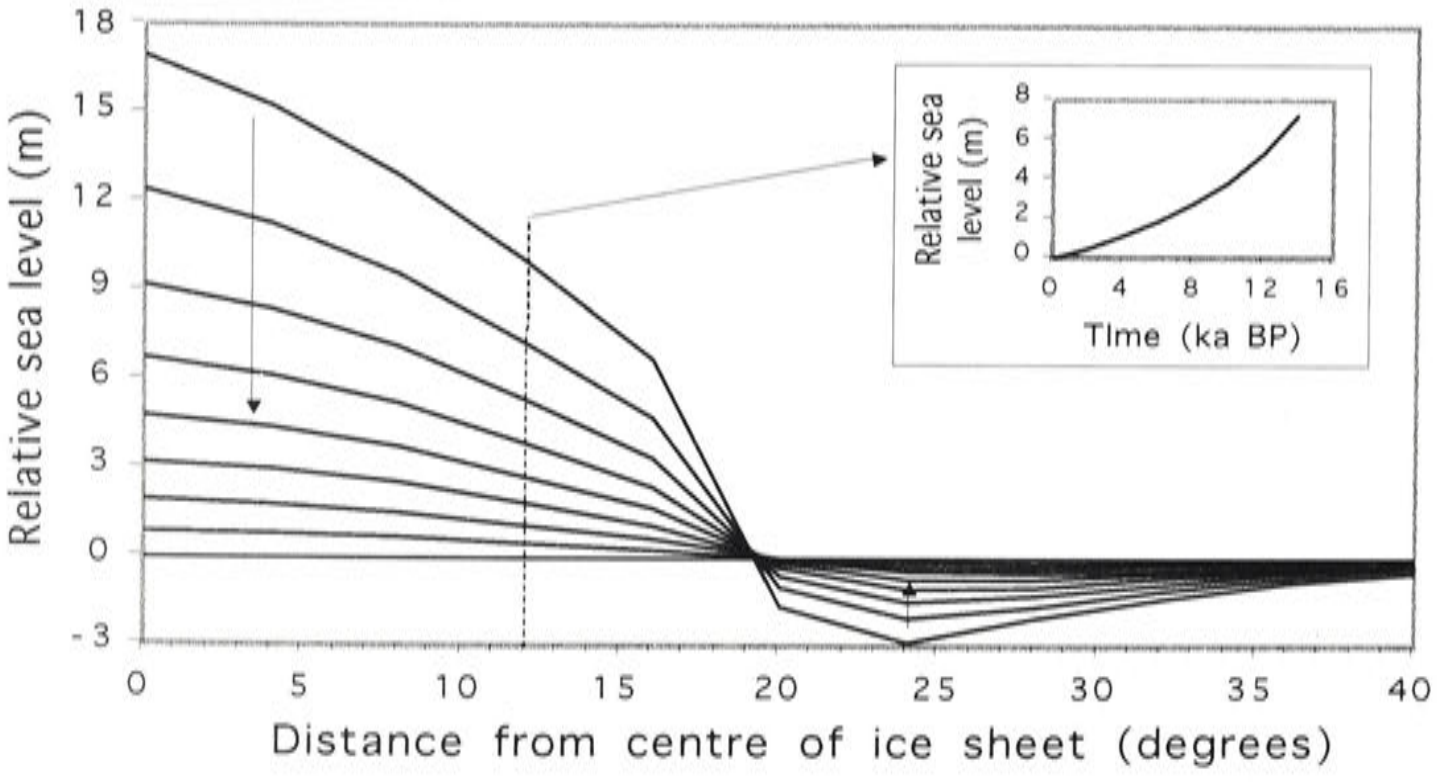

Figure 4.5: Top: Schematic diagram showing the rebound direction of the Earth after the melting of an ice sheet. Bottom: An example of a series of time steps as the Earth re-establishes an equilibrium after the melting of an ice sheet. All time steps are calculated relative to the final time step (0). This shows how each time step (2,000 years in this case) moves closer to equilibrium as is shown by the arrows. If a vertical line is traced through any value for x (degree), this represents the change in relative sea level at a single location. An example for 12 degrees is shown in the insert.

that would be measured from ideal field observations. The following paragraphs outline the changes that would be seen from the loading of an ice sheet.

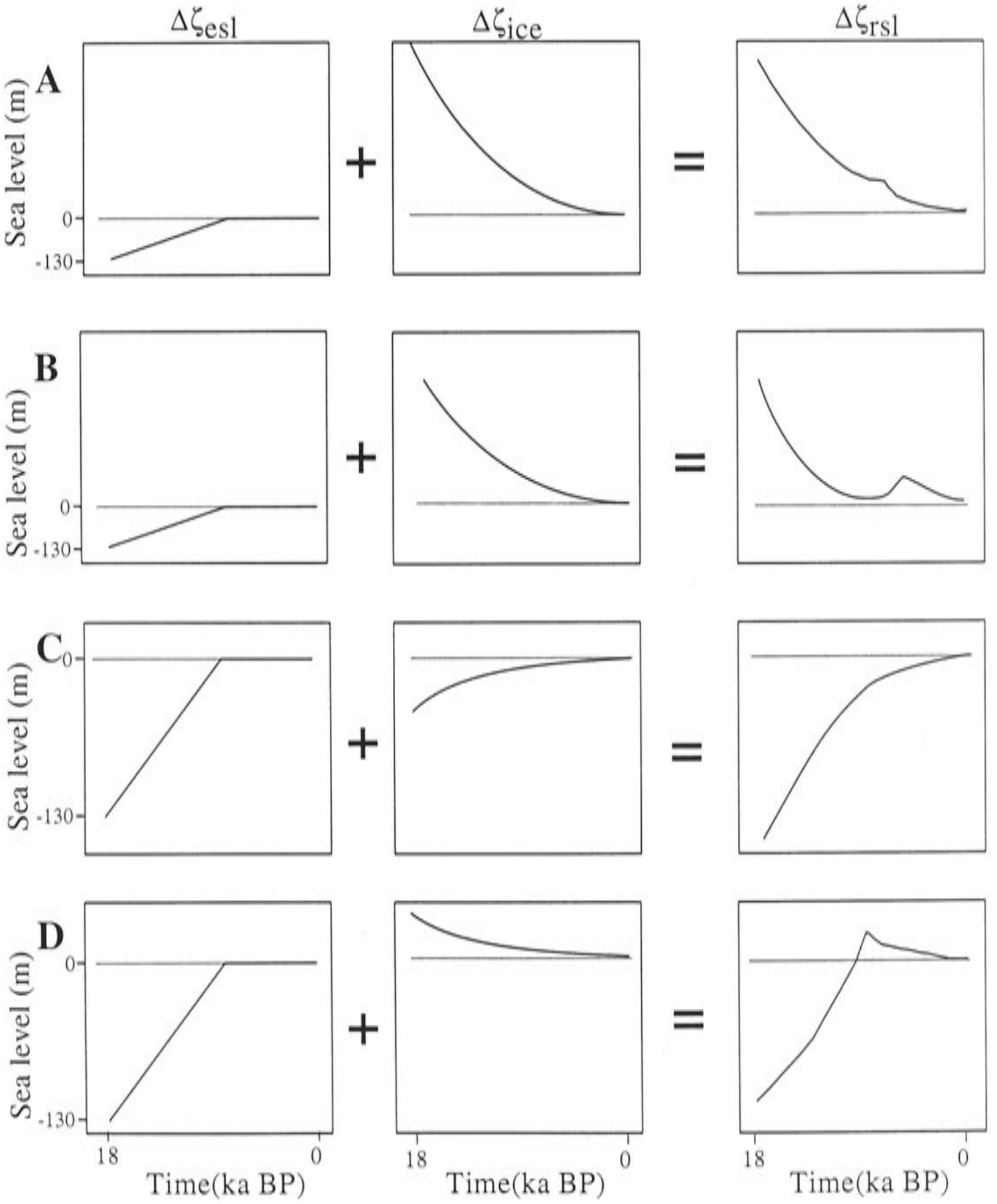

Figure 4.6: Diagram showing the equivalent sea level $\Delta\zeta_{esl}$, ice load $\Delta\zeta_{ice}$ and combined relative sea levels $\Delta\zeta_{esl}$ of different locations from an ice sheet. A is beneath an ice sheet, B is close to the edge but within the boundary of an ice sheet, C is outside the boundary of the ice sheet and D is in the far-field. Diagram after Yokoyama (1999)

1. Beneath the ice sheet:

   Directly beneath the ice sheet (label A on Figure 4.5) the mass of the load causes a depression approximating the size of the local isostatic limit. The local isostatic limit is defined as:

   $$limit = -\rho_i/\rho_e H \tag{4.7}$$

   where ρ_i is the density of ice, ρ_e the density of the Earth and H the height of the column of ice. For a change in ice load of 900 m the local isostatic limit would be about 270 m. Under a large ice dome, such as in Antarctica, this depression can amount to hundreds of metres. As the stresses in the mantle relax to the load, only buoyancy forces will respond.

   On instantaneous melting there will be an immediate response with the lithosphere and mantle elastically rebounding. The gravitational attraction of the ice mass will be gone too and may be replaced by an attraction to water if the sea encroaches the area. Both effects cause a drop in the relative sea level within the boundary of the ice sheet. After the initial relative sea level drop there will be a further relative sea level drop as the Earth rebounds and the mantle material moves back beneath the former ice sheet. In a place that has been beneath the former ice sheet, such as Hudson Bay or the Gulf of Bothnia, the relative sea levels have fallen from the Last Glacial Maximum to the present day, continuing after the ice sheets melted.

   Closer to the edge of the ice sheet the elastic properties of the lithosphere help to support some of the load causing less depression than in the centre of the load.

   In an area close to the edge of a former ice sheet (B on figure 4.5), but within the boundary of the ice sheet, is an area that forms the relative sea level curve in B on Figure 4.6. At this location the crustal rebound is less, mainly because both the ice load and the flexural deformation of the lithospheric response to the load are less. A complex signal of a falling relative sea level followed by a rising relative sea level and again followed by a falling relative sea level is developed. This complex response is seen in East Antarctica (Zwartz 1995) and may also be present in the Ross Embayment.

2. Adjacent to the ice sheet:

   Adjacent to the ice sheet the load will be regionally supported (illustrated at C in Figure 4.5). In a first approximation the Earth may be considered incompressible (this is not assumed in the realistic modelling) so that the volume of the solid Earth is conserved. Hence as subsidence occurs below the ice, uplift occurs outside the ice sheet. This creates a broad regional bulge of uplifted crust that may extend thousands of kilometres beyond the ice margin. While the width is large, the amplitude of the bulge is usually small, of the order of tens of metres.

Where the peripheral bulge occurs in an oceanic environment it displaces water and hence modifies sea level. The sea level change in this area is a combination of the radial deformation, the reduction in the gravitational attraction to the water and an increase in the gravitational attraction towards the ice. The contribution is a relative sea level rise as the ice sheet melts and is shown by line C on Figure 4.6.

The amplitudes of the different contributions change quite rapidly near the ice margin and the resulting relative sea level immediately outside the ice margin will vary rapidly with changes in the ice sheet. Observations of relative sea level change from sites adjacent to the ice sheet will be very sensitive to the ice loads and the relative sea level change will quickly vary over a distance of tens of kilometres from the characteristic curve shown on line B to line C on Figure 4.6. Observations from these sites as well as from immediately inside the edge of the ice sheet will be representative of what is observed in the Ross Embayment.

3. At a distance from the ice sheet and on a continental margin (far-field):

   On a continental margin the response from a melting ice sheet is from the water loading. There will be a relative sea level response from the water added to the oceans as well as the time delayed subsidence of the crust from mantle relaxation in the same way as for a mid-ocean site.

   As the stress from the water loading is transmitted into the Earth the mantle will flow away beneath the continent causing the crust to rise in continental areas and tilt on the shelf. The size of the viscous component is in the order of metres when the eustatic sea level rise is of the order of tens to hundreds of metres.

   There is also a flexural signal across the continental margin caused by the elastic lithosphere supporting some of the load. The lithosphere supports some of the load giving a more gradual change in relative sea level than would be the case for pure local isostasy. This gives a characteristic relative sea level response shown in Figure 4.7 of a raised relative sea level at the continental edge, to a point where relative sea level does not change, to a falling relative sea level offshore.

4. At a distance from the ice sheet and at an ocean island (far-field):

   There are still influences of an ice sheet at a great distance from it. As the ice sheet melts there is a large volume of water added to the oceans forming a horizontal sheet load across the oceans. This added water is the largest influence on relative sea levels in the area. As the mantle stresses relax from this load there will be a general flow of mantle from beneath the oceans to under continental areas causing subsidence of the sea floor and a change in the gravitational attraction of the Earth. Combining the effects of additional water in the oceans, the gravitational attraction of this water, and the corresponding hydro-isostatic response, has an

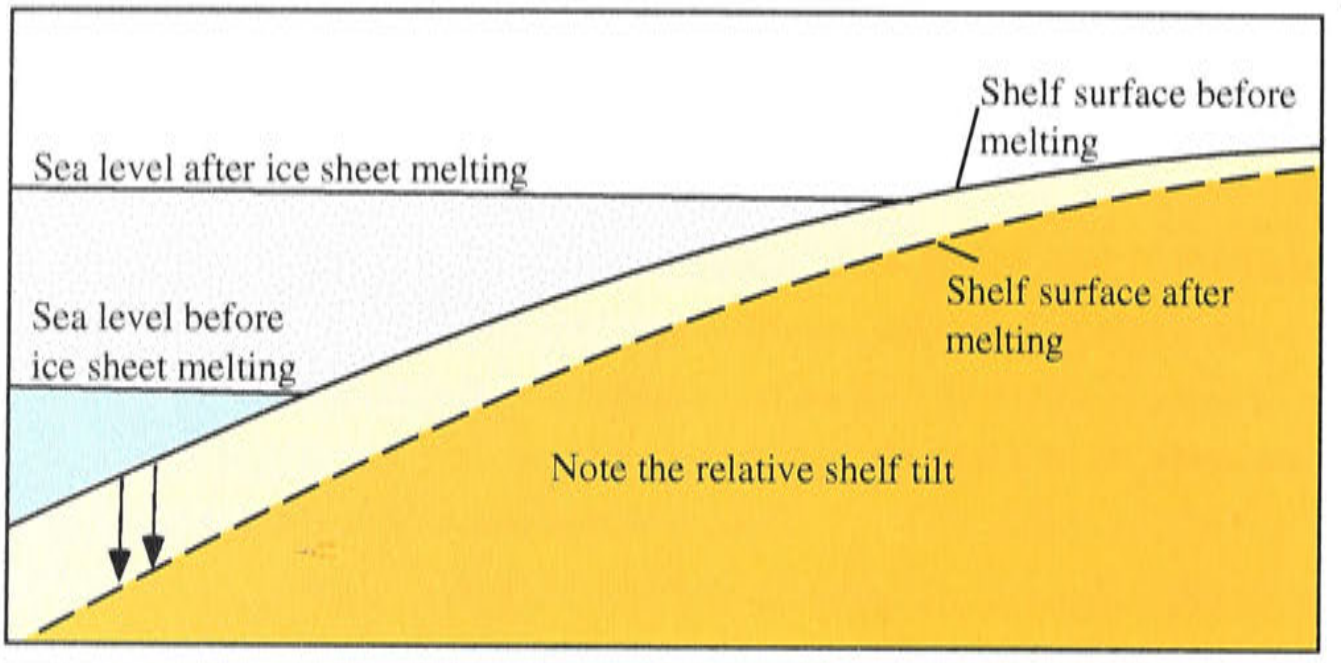

Figure 4.7: Schematic diagram of relative sea level changes from an initial equilibrium position with an ice sheet to a new equilibrium position after an ice sheet has melted. This diagram shows the loading on a continental shelf at a distance from the ice sheet. The mass of the water change causes a relative tilting of the shelf. The solid line is the crust before water loading (from the melting ice sheet) and the dashed line is where the crust is situated after the melting of the ice sheet and mantle relaxation.

overall influence of causing the relative sea level to rise, but not as much as if the hydro-isostatic effects are ignored. This leads to a characteristic sea level curve from these areas that initally rises steeply and falls gently to the present day. See D on Figure 4.6.

4.3 Characteristics of the Antarctic Ice Sheet

In terms of the response to ice sheet melting, Antarctica has some characteristics not found in most of the Northern Hemisphere ice sheets (excepting Greenland). Because ice still exists in Antarctica the melting pattern of the ice sheet will be different from the Northern Hemisphere ice sheets. In the Northern Hemisphere, the ice sheets were for the most part thickest close to the centre of the ice sheet. With such an ice load this is the area of greatest depression, and hence, the greatest rebound occurs in these central areas. In Antarctica however, the bulk of the ice sheet remains, perhaps 8 to 30 % smaller in volume. The greatest changes in the ice volume of this ice sheet occur at its edges where the grounding line/margin has retreated from the Last Glacial Maximum. Hence, the margins will be the areas of greatest rebound towards a new equilibrium with the current ice sheet. Figure 4.8 illustrates in cross section how the ice sheet would be expected to melt, assuming a parabolic shaped ice sheet, showing the

relatively greater volume melted at the periphery of the ice sheet along with a sketch of the expected relative-sea-level response.

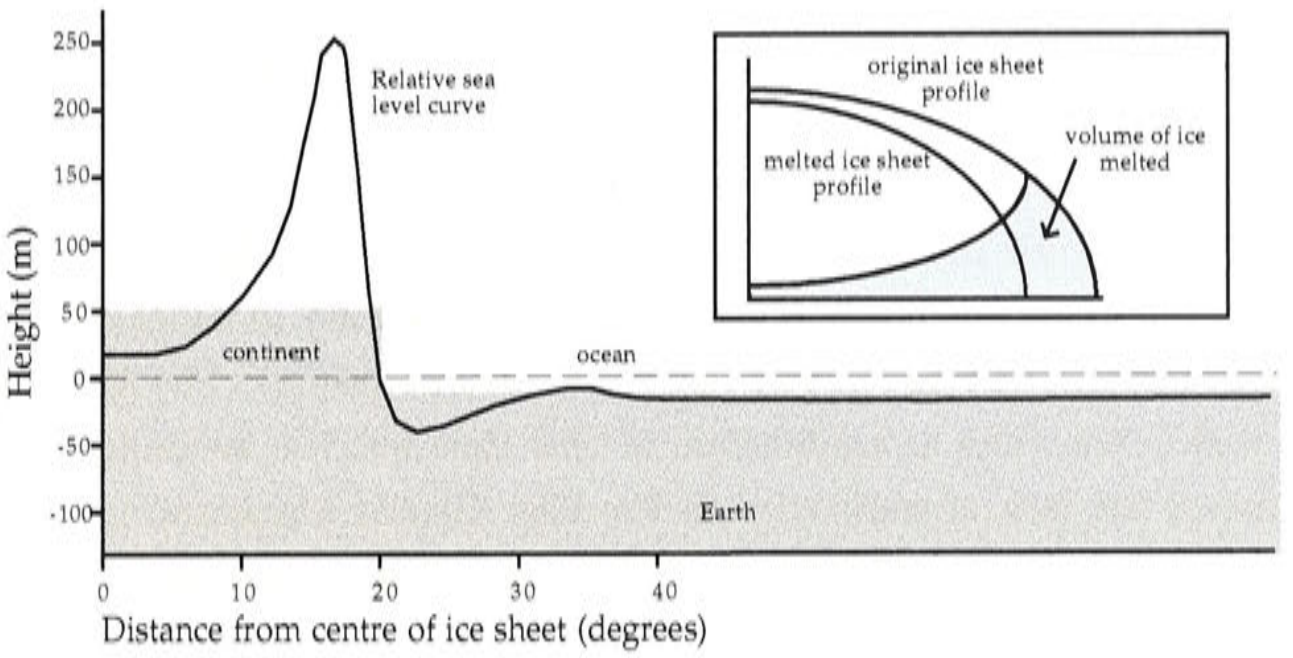

Figure 4.8: Schematic diagram showing the effects of an ice sheet on a continent. Relative sea level (includes both the ice term and the water term) is shown for the Last Glacial Maximum. In this case the ice sheet does not melt entirely (as is the case in Antarctica), so the volume of ice melted is a maximum at the edge of the continent and the maximum relative sea level change occurs near the ice margin. This schematic diagram is for a simplified model with a block continent and ocean.

The relative sea level response for the melting of the Antarctic Ice Sheet at the Last Glacial Maximum is expected to occur in a zone of uplift (relative sea level drop) around the periphery of the existing ice sheet where the ice load and the crustal rebound reach their maximum values. It decreases with distance away from the ice margin as well as towards the centre of the ice sheet where the reduction in ice volume is minimal. This pattern is strongly dependent on the details of actual melting and this means that the relative sea level data near and within the boundary of the former ice sheet (e.g. McMurdo Sound) is important for estimating past ice volumes.

Even though only the Ross Embayment section of the Antarctic Ice Sheet is being modelled the load change from the rest of the Antarctic Ice Sheet must be considered too because it too will impact on the field site. Also concurrent to the melting of the Antarctic Ice Sheet is the melting of the Northern Hemisphere ice sheets. While these ice sheets are at a great distance from Antarctica they too have an impact on the Ross Embayment. Firstly, they release large volumes of water into the oceans as they melt. Secondly, the Earth isostatically reacts to the extra load in the ocean basins and to the load removal of the Northern Hemisphere ice sheets. Hence, it is important to take a holistic view to the modelling of the ice sheet in the Ross Embayment and include

ice sheets from elsewhere. To do this I have taken existing Northern Hemisphere and Antarctic models and evaluated these to determine their relative impacts on the Ross Embayment. Two possible models are considered for the Northern Hemisphere ice sheets and three possible models considered for the Antarctic Ice Sheet surrounding the Ross Embayment. The predicted relative sea levels for each of these is examined and conclusions drawn about their influence on local relative sea levels in the Ross Embayment and specifically in McMurdo Sound.

In this thesis it is assumed that the ice sheet was at a maximum limit for a long time interval such that the isostatic state was one of regional isostasy in which the load stresses are supported by the lithosphere only (i.e. it was at equilibrium). The Antarctic Ice Sheet was probably not quite at equilibrium at this time but the assumption has been made because of the lack of sensitivity to Pre-Last Glacial Maximum ice sheet fluctuations in the late-Holocene observations (this is demonstrated in Chapter 5).

To be able to define the change from the Last Glacial Maximum in the ice sheet for Antarctica it is necessary to first know the ice volume and location at the present-day. The chosen model for the present-day ice sheet comes from a folio by Drewry (1979). This is also the model chosen by Huybrechts (1990) for his present day model for the ice sheet in Antarctica. In the case of the maximum reconstruction by Stuiver et al. (1981) used in this thesis, the present day model used has a different ice surface from the Drewry (1979) model. This has the consequence that the present day ice thicknesses exceeds the Last Glacial Maximum ice thicknesses in a few locations. In order to avoid this anomaly, some ice was added to the Stuiver et al. (1981) reconstruction in a few places in East Antarctica in order to contain at least the same thickness of ice at all points as the adopted present day model.

The temporal response of the melting ice sheet will be complicated by a non-instantaneous melting. The Last Glacial Maximum ice sheets in the Northern Hemisphere melted over a period of about 10,000 years (Peltier 1998). This means some of the response to the initial melting will be occurring while the final melting is taking place. This type of melting can be difficult to model accurately because responses to the later melting may mask responses from the earlier melting, but by looking at sites far from the ice sheets some ideas can be obtained on periods of rapid melting such as melt-water pulses (Andrews et al. 1994). These records will give ice-equivalent volumes of water melted but not the location of where the ice melting has occurred. Fortunately for the modelling of the Antarctic Ice Sheet, it is not necessary to know which Northern Hemisphere ice sheet melted at what time because the effect of them all is only that of water being added to the ocean in the coastal areas around Antarctica. The timing of Antarctic Ice Sheet melting is much more significant here, and its effects are investigated as questions in the final chapter.

4.4 Earth Models

This section outlines the importance of the different Earth model parameters and, by comparing to alternative Earth models, explains why the particular Earth model used here was chosen.

The outer part of the Earth is divided into the lithosphere and the mantle. The lithosphere is the cold, rigid outer layer, approximately 50 to 100 km thick, and in terms of the modelling includes the crust. The lithosphere is treated as an elastic medium because its viscosity is several orders of magnitude greater than the mantle (Johnston 1993). The mantle is divided into a number of layers with differing viscosities. Lambeck et al. (1996) explored the response of the mantle beneath the British Ice Sheet using models of between three and five layers for the Earth, and varying the viscosities of the mantle and the thickness of the lithosphere. They show that the three layer Earth model (comprising an upper and a lower mantle with a boundary at the 670 km seismic discontinuity) approximates the sea level data almost as well as a five layer model. Hence, a three layer style of Earth model is chosen in this thesis for modelling rebound in Antarctica.

Table 4.1 shows a selection of possible Earth model lithospheric thicknesses and mantle viscosities for an Earth of three homogeneous layers. This selection covers the range of these parameters found from previous rebound and sea-level analyses for different parts of the world.

Earth model	Lithospheric thick. (km)	Upper mantle viscosity (Pa s)	Lower mantle viscosity (Pa s)	comment
ma4A	65	4×10^{20}	1×10^{22}	Standard model
mb4A	50	4×10^{20}	1×10^{22}	Thin lithosphere
md4A	100	4×10^{20}	1×10^{22}	Thick lithosphere
ma1A	65	1×10^{20}	1×10^{22}	Low upper mantle visc.
maAA	65	1×10^{21}	1×10^{22}	High upper mantle visc.
ma41	65	4×10^{20}	1×10^{21}	Low lower mantle visc.
ma4E	65	4×10^{20}	5×10^{22}	High lower mantle visc.

Table 4.1: Earth models used to determine Earth model dependency

At some distance from the centre of the load a thicker lithosphere will support a greater load and less deformation will occur. Hence, the thickness of the lithosphere becomes important around the edges of the ice sheet.

Figure 4.9 shows the relative sea levels predicted from an ice sheet reconstruction with a number of models for the Earth. An average model for the Earth determined by Lambeck et al. (1996) is shown together with several others in which one Earth parameter is adjusted to a limit of its reasonably expected range. The extreme models

contain respectively a thick lithosphere, a thin lithosphere, a low viscosity upper mantle, a high viscosity upper mantle, a low viscosity lower mantle, and a high viscosity lower mantle. The relative sea level range from all of these models equates to around 25 m at 6,000 years BP. A number of conclusions can be drawn from Figure 4.9 regarding the characteristics of these models for a site such as McMurdo Sound. A thicker lithosphere has a small influence in reducing the amount of maximum deformation but overall there is not a great deal of difference between a lithosphere of 50 km and a lithosphere of 100 km thickness (Table 4.2). The greatest difference between all of these models is the one with a low viscosity upper mantle. This model re-equilibrates much quicker (by around 1,000 years) than the other models (solid green line on Figure 4.9). The viscosity of the lower mantle does not cause a great deal of variation, except in the relative sea level close to the Last Glacial Maximum.

Earth Model	ma4A	mb4A	md4A	ma1A	maAA	ma41	ma4E
8ka	91.9	95.9	80.6	73.2	81.9	87.7	85.8
7ka	75.3	78.7	65.6	52.0	70.1	68.1	70.9
6ka	59.3	62.1	51.3	35.1	57.8	50.7	56.2
5ka	44.7	47.0	38.4	23.1	45.7	36.4	42.6
4ka	32.7	34.5	27.9	15.4	35.0	25.5	31.4
3ka	22.6	23.9	19.2	10.1	25.2	17.0	21.8
2ka	14.0	14.7	11.8	6.1	16.2	10.2	13.5
1ka	6.5	6.9	5.5	2.8	7.8	4.6	6.3

Table 4.2: Predicted relative sea levels from 8,000 years BP to 1,000 years BP (all converge on zero for the present day). Relative sea levels are in metres.

Because there is not a great deal of variation in the past 8,000 years between the different models for the Earth parameters (except the model with a low upper mantle viscosity), it was decided that a single model would be adopted against which to test the various ice models. In terms of the relative sea level outcome, the uncertainty in the ice models is much larger than the uncertainty in the Earth models.

In other studies, the three-layered Earth models have been tested mostly in regions of tectonic stability without major lateral variations in upper mantle structure. They may not be ideally suited to the Ross Embayment because the geology of the area consists of a stable craton to the east of the Transantarctic Mountains and a high mountain range bordering an area of extension (horst and graben structures) in the Ross Embayment. Active volcanos are also present in Marie Byrd Land and Victoria Land suggesting that viscosities may be lower and lithospheric thicknesses may be thinner in those areas. However, refining the Earth model for the Ross Embayment

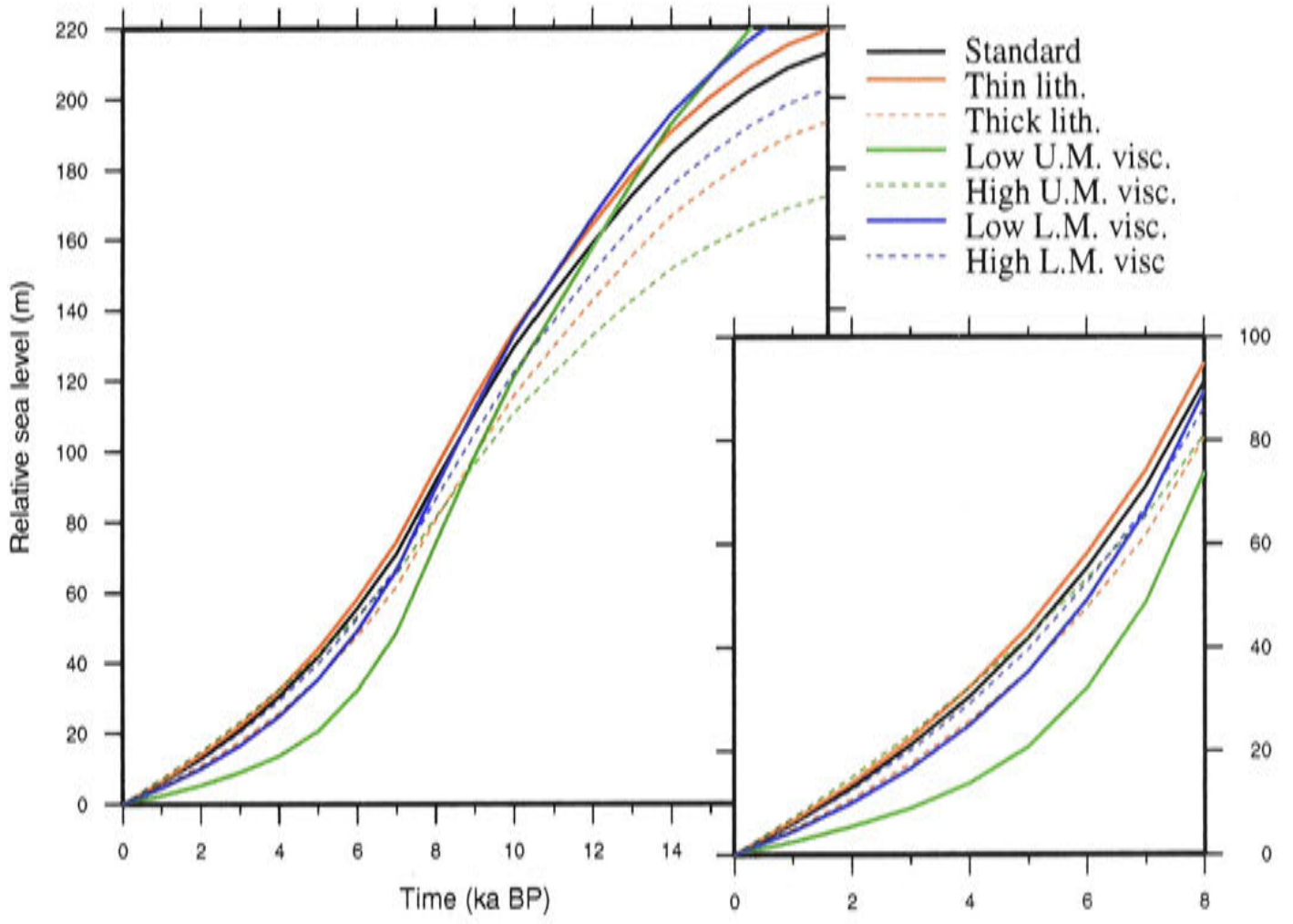

Figure 4.9: Predicted relative sea levels for McMurdo Sound using the glacio-hydro-isostatic modelling method and the Huybrechts (1990) ice reconstruction and melting history. Each line represents one of the Earth models from Table 6.1, as per the key (see also Table 4.1).

leads into a circular problem because it relies on knowledge of the ice model which is what what we are trying to determine. In addition any lateral variation in the properties of the crust, lithosphere and mantle cannot be incorporated into the Earth model for the glacio-hydro-isostatic modelling due to the added complexities and available computing power and time. Therefore it is appropriate to use a standard model that has been proven to be a reasonable fit to elsewhere on the Earth.

Since the original development of the glacio-hydro-isostatic modelling program of Johnston (1993) another feature has been added to the model (Johnston and Lambeck 1999) to refine the calculations. As ice sheets grow and melt on the earth, and the Earth deforms in response, the centre of mass of the Earth moves. The effects of this change are small in comparison to the changes of the ice sheet but are incorporated into the modelling to remove any possible error from this source, and illustrate the detailed and comprehensive accounting for known physical effects in the modelling.

4.5 Ice models and constraints

This section looks at some specific aspects for the modelling in the Ross Embayment area. The ice-sheet unloading is broken down into three components; the Northern Hemisphere ice sheets, the Antarctic Ice Sheet outside the Ross Embayment and the local ice sheet within the Ross Embayment. In the following discussion the Antarctic Ice Sheet outside the Ross Embayment will be referred to as the distal ice.

As mentioned above, it is necessary to include the effects of melting of Northern Hemisphere ice sheets. Although the details of the spatial distribution of Northern Hemisphere ice does not affect the Antarctic coast, the magnitudes and timing of the equivalent sea level rise does, so two possible models are investigated to compare their effect on the relative sea level at McMurdo Sound.

Three models for the Antarctic distal ice are investigated to determine the sensitivity of the Ross Embayment to this ice.

By combining the Northern Hemisphere Ice Sheets with the distal ice it is possible to determine the plausible range of relative sea level changes due to the contribution from all ice outside the Ross Embayment. This is determined and the relative errors on the predicted relative sea levels calculated.

The melting histories of the ice sheets can also have an influence through the timing of water input into the oceans and isostatic rebound. This is discussed and several possible melting histories shown.

4.5.1 Ice models for the Northern Hemisphere

The ice sheets of the Northern Hemisphere include the Laurentide, Cordillerian, Innuitian, Greenland, British, Fennoscandinavian, and Barents-Kara Ice Sheets. These are relatively well constrained in their ice extents and Holocene melting, and have contributed approximately 110 m (Lambeck et al. 2000) of equivalent sea level to sea-level rise since the Last Glacial Maximum. The main effect in the Antarctic of these Northern Hemisphere ice sheets is that of adding water to the oceans and producing a hydro-isostatic response to the rising sea level around Antarctica.

Two reconstructions were used to examine the range of the predicted relative-sea-level change in the Ross Embayment from the Northern Hemisphere ice sheets. The first one, called 'fennice.new+nhewice.new' here, is used for all of the subsequent modelling in this thesis. In this model the ice sheet over Fennoscandia and the small ice sheet over the Barents-Kara Sea are from Lambeck et al. (1998) and are combined with a reconstruction for North America and Greenland based on the ICE1 reconstruction of Peltier and Andrews (1976) as modified by Nakada and Lambeck (1987).

The other ice sheet reconstruction, called 'arc3s' here, is larger. It is also based on the ICE1 reconstruction but includes a large ice dome over the Barents-Kara Sea. Both use a pre-Last Glacial Maximum ice sheet history based on the $\delta^{18}O$ isotope curve of

Shackleton (1987). There is now general agreement that there was an ice sheet covering the Barents Sea but some debate still remains about how much ice there may have been in the Kara Sea region. Lambeck (1995) proposed a maximum and a minimum ice sheet for the region based on glacio-hydro-isostatic modelling. The maximum ice sheet covers both the Barents and the Kara Seas while the minimum has little ice in the Kara Sea, although the conclusion is that there must have been more ice than the minimum model suggests. Svendsen et al. (1999) also proposed a maximum and minimum model with a dome over the Barents Sea. Their maximum model has the Barents Sea dome extending over the Kara Sea while their minimum model only has isolated ice domes over small areas. It is agreed that the Last Glacial Maximum ice sheet did not persist for a long time with melting having occurred about 15,000 to 13,000 years BP.

Wherever the ice was situated around the Barents and Kara Seas it is more important for the Antarctic Ice Sheet modelling to know the amount of ice (and hence eustatic sea level) than the exact location. The difference between the two models is essentially the eustatic sea level difference.

The Scott Coast predicted relative-sea-level contributions from the two reconstructions for the Northern Hemisphere ice sheets are shown on Figure 4.10 (this figure includes no ice contribution from Antarctica). The largest difference, of about 12 m relative sea level, occurs between 18,000 years BP and 14,000 years BP. By the Holocene the two reconstructions give essentially the same prediction of relative sea level (maximum difference of 0.28 m). For the present purpose, as our observations from Antarctica are only from the Holocene, it appears that the choice of Northern Hemisphere ice model is not important. Figure 4.10 indicates that the relative sea level from 6,000 years BP to present is above present day, typical of observed relative sea levels along continental margins far from the former Northern Hemisphere ice sheets (e.g. Antarctica — Zwartz (1995)).

4.5.2 Ice models for the area outside the Ross Embayment

Three models were investigated to see what effects ice from the portion of the Antarctic Ice Sheet outside of the Ross Embayment area has on the predicted relative sea levels at McMurdo Sound. The first is a reconstruction by Stuiver et al. (1981), one of the earlier reconstructions for the ice sheet which is a maximum reconstruction at the Last Glacial Maximum. This reconstruction is probably an overestimate of ice volumes but is useful as an end-member for the range of models used in this thesis. The maximum reconstruction (Figure 4.11), developed by Stuiver et al. (1981), is also the ice sheet used for the CLIMAP reconstructions. This reconstruction is based mainly on field work from the Ross Embayment and Transantarctic Mountains and hence the East Antarctic portion of the ice sheet is not well constrained. In this reconstruction, a higher surface for the East Antarctic Ice Sheet is assumed in response to the lateral expansion of about 75 to 90 km beyond the present day margin, on the edge of the continental shelf (this

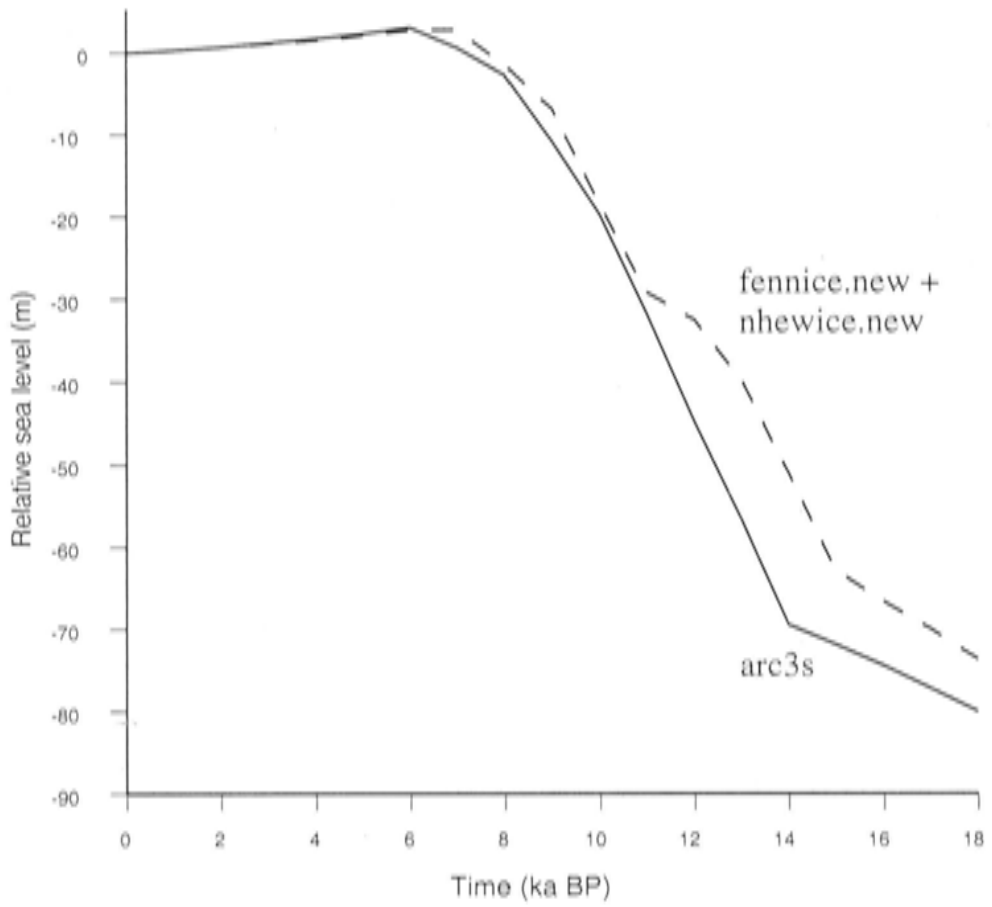

Figure 4.10: Contribution to the relative sea level in McMurdo Sound from two different reconstructions of the Northern Hemisphere ice sheets and uses the Earth model ma4A. Shown is the relative sea levels predicted for a maximum (arc3s) reconstruction (dashed) and the standard (fennice.new + nhewice.new) reconstruction (solid). Observations in the field only cover the time period 7,000 years BP to the present day.

may not be an appropriate assumption - e.g. Jouzel et al. (1989) calculate a 60 % lower accumulation rate at the Byrd ice core in central West Antarctica). The equivalent-sea-level contribution calculated here from the Stuiver et al. (1981) reconstruction is about 25.5 m.

The second reconstruction used here is an intermediate one by Huybrechts (1990) (Figure 4.12). This reconstruction uses a glaciological model that defines the ice sheet by a set of equations and varies the ice sheet over a glacial cycle through changing one or more of the controlling parameters. Ice shelves are included in the model as well as grounding line dynamics, basal sliding and isostasy. Three main variables can be changed, either individually or in combination. Accumulation rates can be changed, global temperatures can be varied, and global sea levels can rise and fall. At a full glacial maximum the Huybrechts (1990) model has about a 16 m sea level drop from ice added to the Antarctic Ice Sheet. Melting occurs very late in the Huybrechts (1990) reconstruction and continues up to the present day.

Finally, a small reconstruction by Nakada et al. (2000) is used. This reconstruction was developed to fit the observed relative-sea-level data from around the Antarctic continent and has a minimum contribution compared with the previous two models to sea-level rise since the Last Glacial Maximum. It has an enlarged ice dome situated

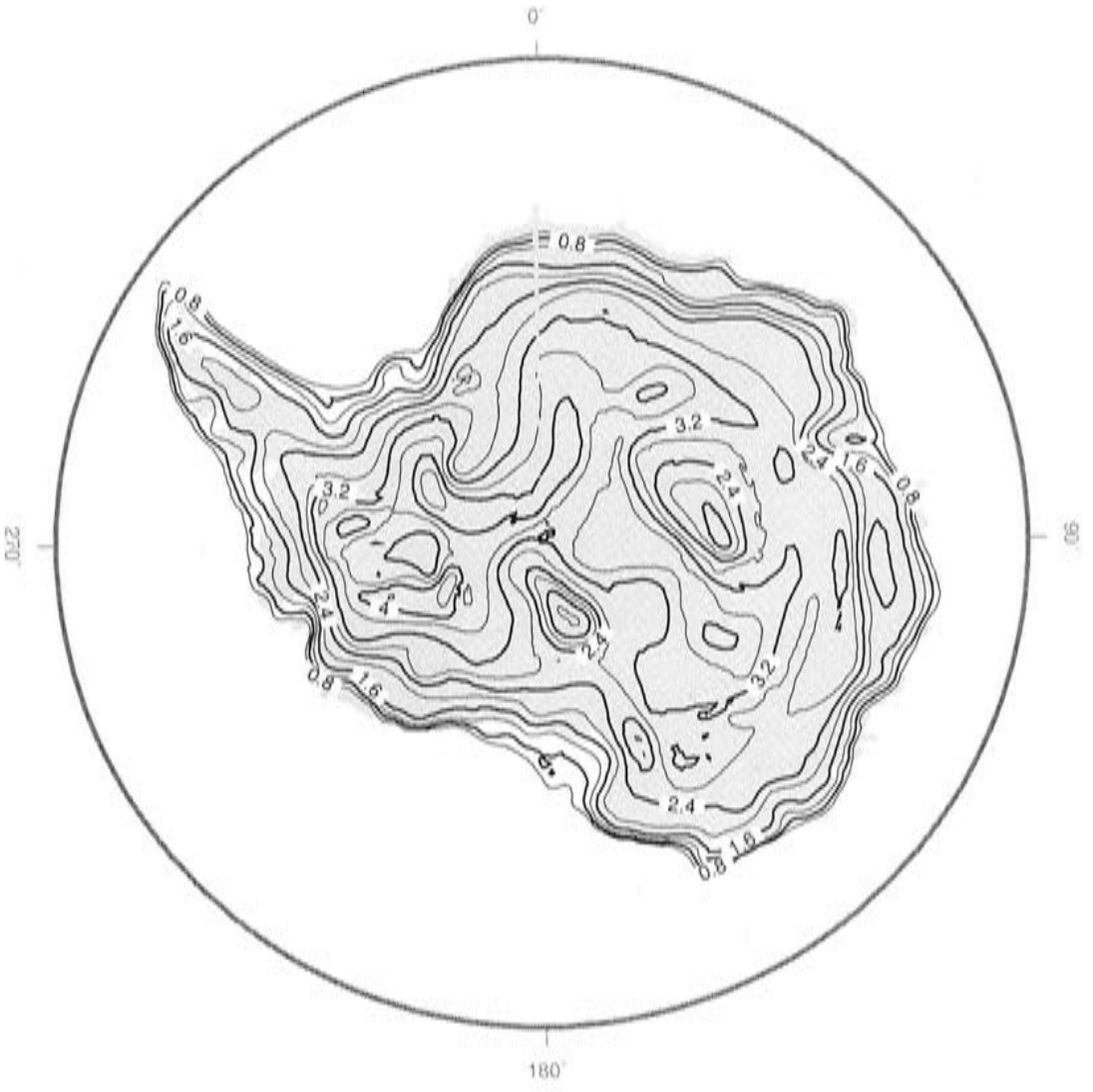

Figure 4.11: Maximum ice thickness reconstruction from Stuiver et al (1981) at the Last Glacial Maximum. Contour interval of 0.4 km.

over the Antarctic Peninsula, consisting of about 1,000 m more ice than the present day, and other enlarged domes (smaller than the Antarctic Peninsula) at the Last Glacial Maximum over Enderby Land and Law Dome in East Antarctica (Figure 4.13). Ice has only been placed over regions where relative-sea-level observation data has been collected. The small amounts of extra ice Nakada et al. (2000) place in this reconstruction lead to a low estimate of only about 5 m of equivalent sea level rise from the Antarctic Ice Sheet since the Last Glacial Maximum. The Nakada et al. (2000) reconstruction is probably unrealistic in not having ice sheet expansion over the entire continent but is plausible on the assumption that a cooler, drier climate will result in less precipitation reaching the interior. This reconstruction provides a minimal reconstruction for comparison with the other models.

Figure 4.14 shows the predicted relative sea level in McMurdo Sound from the three reconstructions without any Ross Embayment ice sheet change. The models all predict a lower than the present-day relative sea level since the Last Glacial Maximum for the

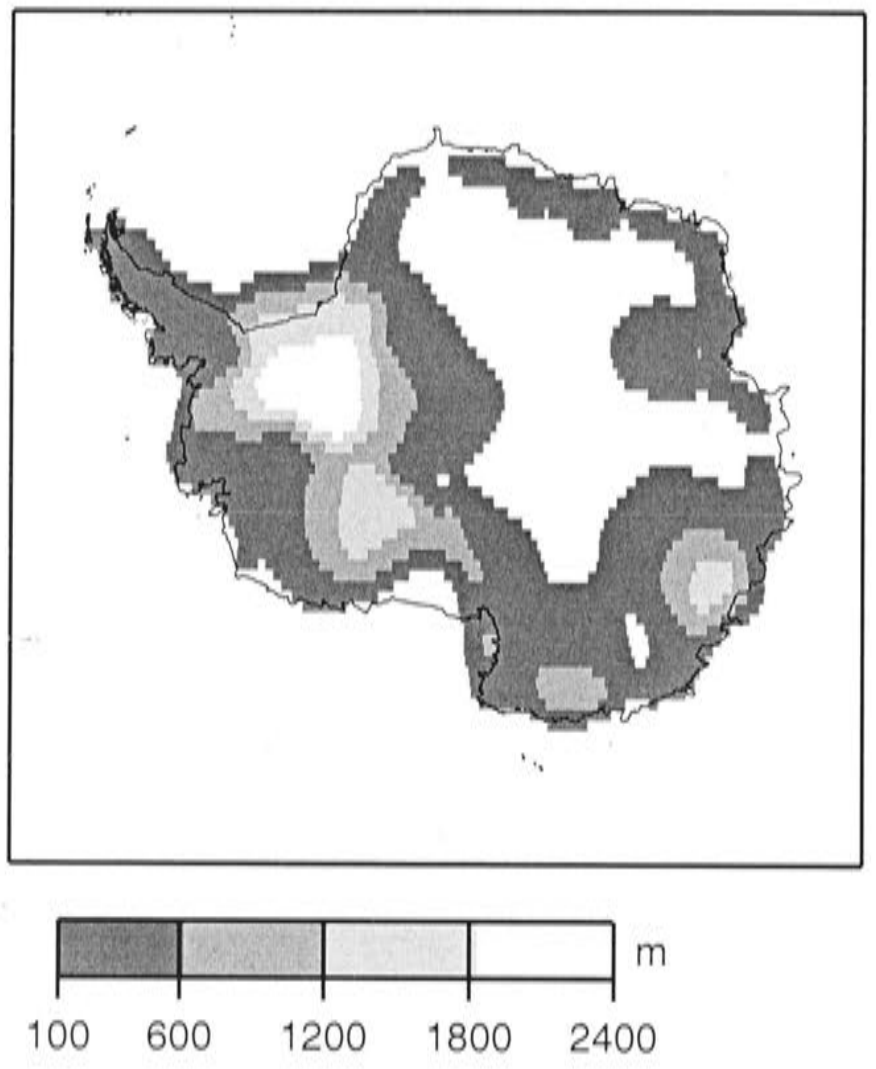

Figure 4.12: Ice sheet reconstruction of Huybrechts (1990) for Antarctica at the Last Glacial Maximum. Ice shown here is extra ice on top of the present day ice sheet. 0° longitude is at the top of the figure. The resolution of this reconstruction is on a 1° x 1° grid.

McMurdo Sound area. This is because the Ross drainage basin lies in the peripheral area of the ice sheet covering the rest of the continent. When the ice sheet melts the peripheral bulge will collapse and over-deepen the Ross Embayment. But, to be able to form beaches in the Ross Embayment higher than the present day, we need a local contribution that forces the relative sea level higher than the present day. Because the contribution from the Northern Hemisphere and distal ice has the opposite effect to local ice, the local contribution needs to be larger than if the external ice is ignored.

The sea-level prediction based on the Stuiver et al. (1981) reconstruction for the distal part is significantly greater in magnitude than the predictions based on the other two models (4.14). In the Stuiver et al. (1981) reconstruction the relative sea level is nearly -17 m at 18,000 years BP and is still -6.5 m at 6,000 years BP. The Huybrechts (1990) reconstruction and Nakada et al. (2000) reconstruction of ice outside the Ross Embayment make only small contributions to the sea-level change in the Ross Embayment, with a minimum of -3 m and -1.5 m relative sea level respectively.

To fully establish the effects of ice outside the Ross Embayment on the relative sea

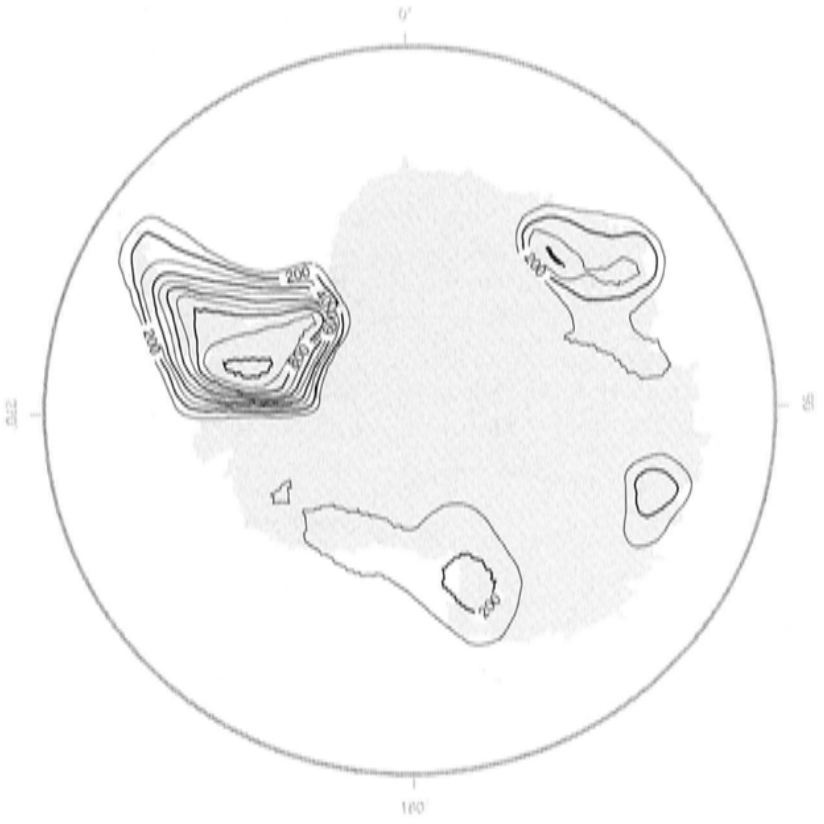

Figure 4.13: Nakada et al. 1999 reconstruction showing the additional ice thickness (on top of the present day ice) at the Last Glacial Maximum. Contour interval of 100 m.

levels in McMurdo Sound we must add the contribution from the Antarctic Ice Sheet (outside the Ross Embayment) and the Northern Hemisphere Ice Sheets. Figure 4.15 shows the predicted relative sea level contributions from this combination using the Stuiver et al. (1981) reconstruction. The solid line is the combined effect of both these ice sources and the relative sea level (without the Ross Embayment contribution), and is below present levels during the entire deglaciation.

Figure 4.16 shows the relative sea level predictions for the two alternate Northern Hemisphere ice sheet reconstructions combined with the three Antarctic Ice Sheet reconstructions (Maximum: Stuiver et al. (1981), medium: Huybrechts (1990) and minimum: Nakada et al. (2000)). On this figure the solid lines show the contribution from the standard Northern Hemisphere reconstruction (fennice.new + nhewice.newice.new) and the dashed lines show the contribution from the larger Northern Hemisphere reconstruction (arc3s). For the Holocene period sea-level predictions based on these two reconstructions are nearly identical whereas their dependence on the distal Antarctic ice contribution is greater. Combining the two ice sources means there is a maximum of +2 to -4 m predicted relative sea level from 6,000 years to the present. This value is to between -21 and -30 m relative sea level at 10,000 years BP. To produce an ice sheet reconstruction with the observed marine limit of +20 m at 6,000 years on the Scott Coast, the removal of the local ice load will need to contribute between +18 m and +24 m of relative sea level change at this time.

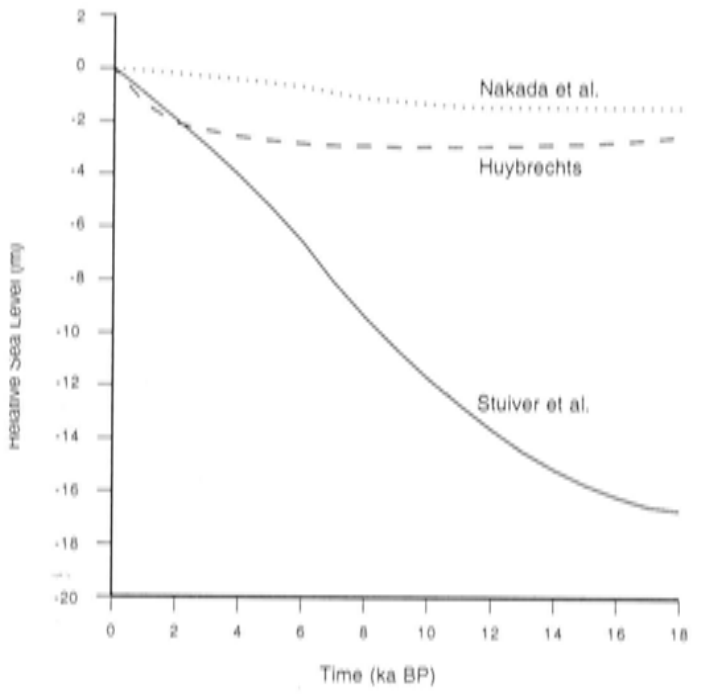

Figure 4.14: Predicted relative sea level in McMurdo Sound from Antarctic ice outside of the Ross drainage basin. No ice or water components are present from the Ross drainage basin or the Northern Hemisphere and these predictions use the Earth model ma4A. Maximum reconstruction (solid line) comes from Stuiver et al. 1981, Minimum reconstruction (dotted line) from Nakada et al. 1999 and the other (dashed line) from Huybrechts, 1990b.

4.5.3 Melting histories

The ice reconstructions used here assume model melting histories based on models such as those of Nakada and Lambeck (1988), Nakada et al. (2000), Huybrechts (1990). Figure 4.17 shows these three melting histories. The Nakada and Lambeck (1988) melting histories assume that the melting of the Antarctic Ice Sheet is synchronous with the melting of the Northern Hemisphere ice sheets. This melting history starts at 18,000 years BP and is almost complete by 6,000 years BP. The Huybrechts (1990) melting history, derived from his ice sheet reconstruction, is driven by the rising sea level from the melting of the Northern Hemisphere ice sheets. This leads to later melting, with most of it occurring in the latest Holocene. The Antarctic contribution is therefore out of phase with the Northern Hemisphere contributions to global sea level rise. The Nakada et al. (2000) melting occurs between 14,000 and 6,000 years which grounding line evidence (e.g. Licht et al. (1996)) suggests is the period of greatest melting in the Ross Embayment.

Sea level curves from far-field places such as Barbados or Huon Peninsula (Shackleton (1987); Chappell and Polach (1991)) can provide some useful constraints on melting histories. These curves indicate the volume of melt water entering the oceans at any point in time.

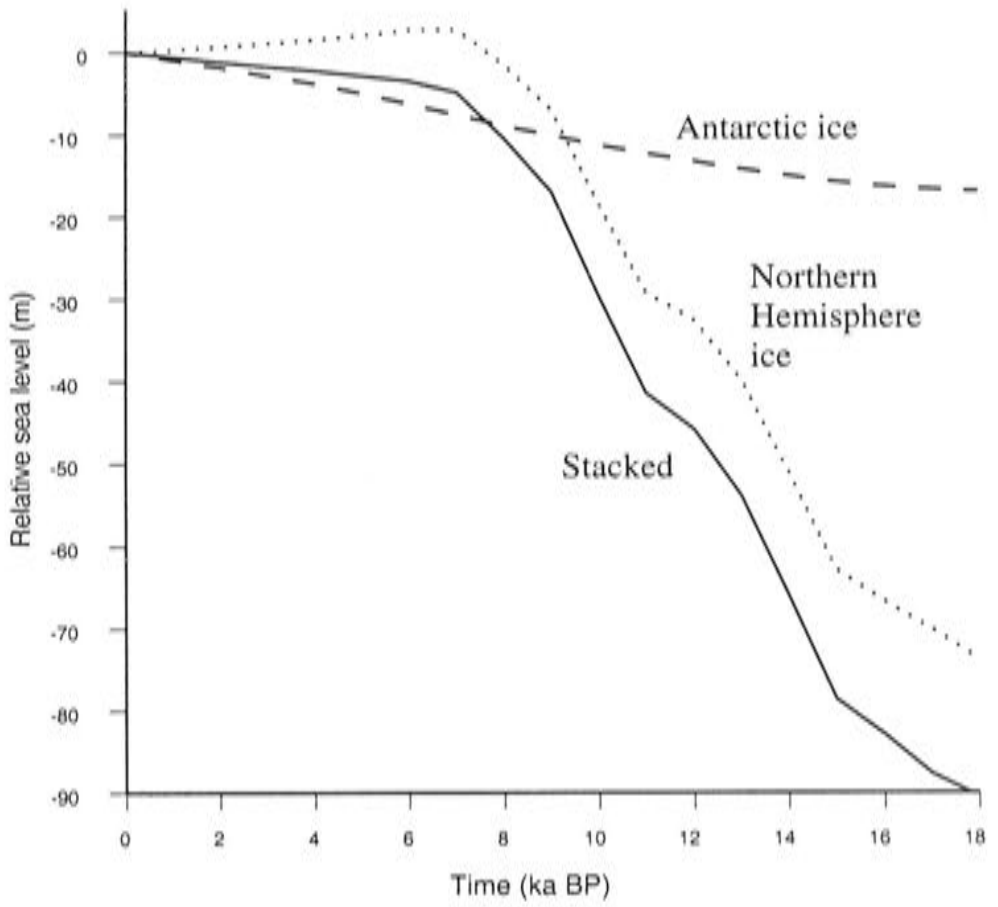

Figure 4.15: Components of the predicted relative sea level from the maximum reconstruction of ice from Antarctica (Stuiver et al. 1981) and the standard reconstruction (fennice.new + nhewice.new) for the Northern Hemisphere (Lambeck et al. 1998). This plot shows the ice contribution from Antarctic ice outside the Ross drainage basin (dashed), ice contribution from the Northern Hemisphere (dotted) and from the total ice outside of the Ross drainage basin (solid).

4.6 Summary

To summarise, the modelling used on the Ross Embayment portion of the Antarctic Ice sheet in this thesis is done using a glacio-hydro-isostatic method. The method uses an assumed model for the Earth to predict the responses of changing ice and water loads. Because the Earth behaves like a visco-elastic material, responses occur, not only spatially over the Earth, but also there is a time-delayed component.

Also when dealing with the Earth it is unrealistic to model the Ross Embayment in isolation. Contributions from two models for the Northern Hemisphere ice sheets and three models for the distal Antarctic ice were calculated on the relative sea level in the Ross Embayment. There is a contribution of between +18 and +24 m of relative sea level required from the removal of the local ice load.

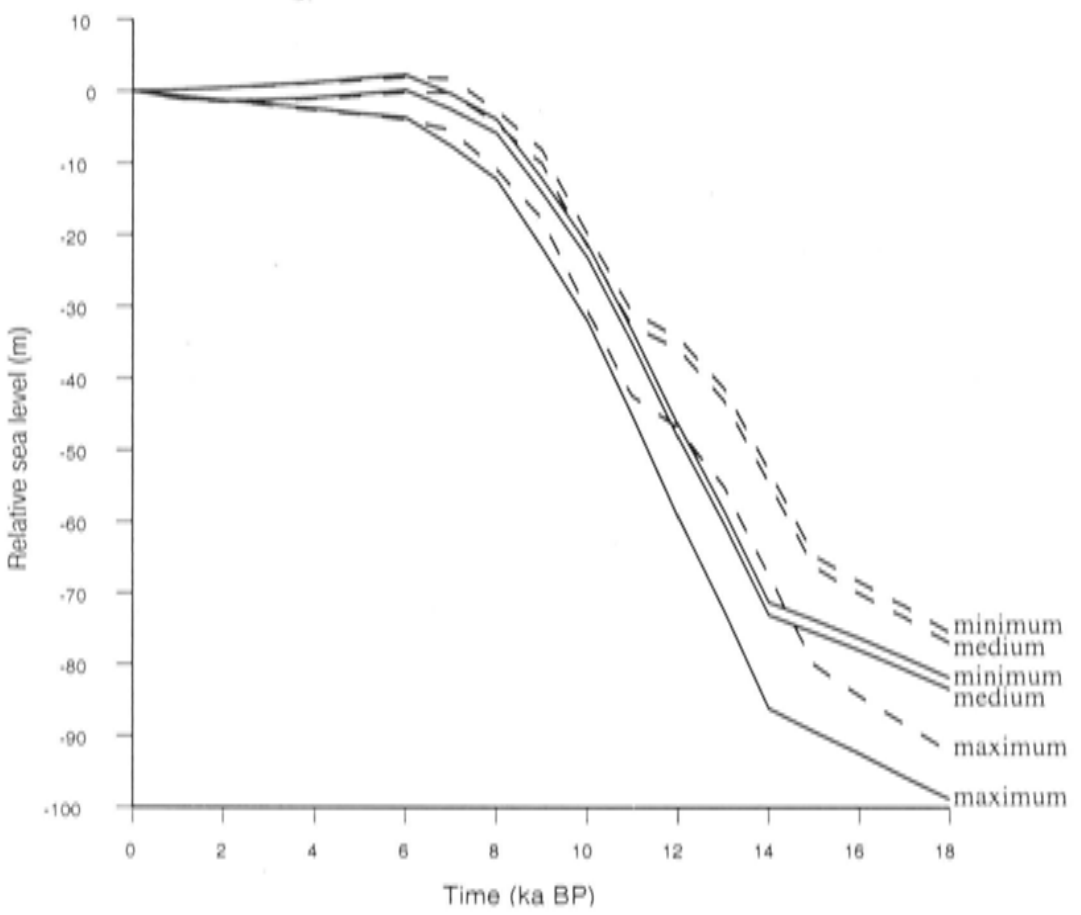

Figure 4.16: Predicted relative sea level curves for McMurdo Sound from the combined effects of all deglaciation outside of the Ross Embayment. Dotted lines show a maximum reconstruction for the Northern Hemisphere (arc3s) while solid lines show the Standard Reconstruction (fennice.new+nhewice.new). Reconstructions for Antarctica are: minimum is the Nakada et al. (1999) reconstruction, medium is the Huybrechts (1990) reconstruction, and the maximum is the Stuiver et al (1981) reconstruction.

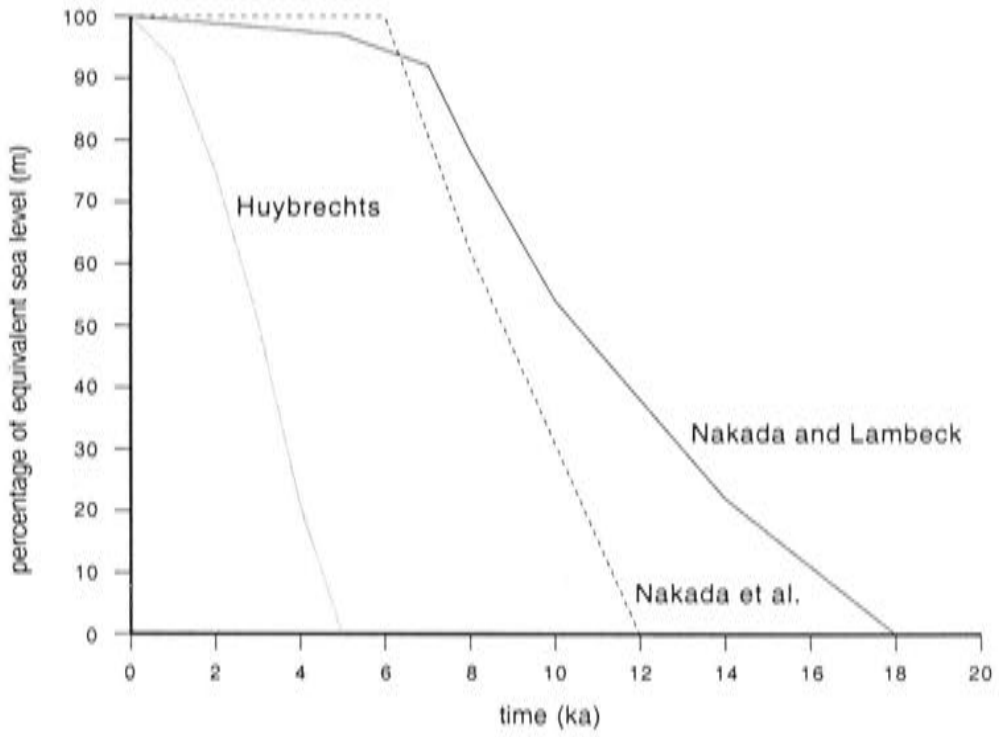

Figure 4.17: Three possible melting histories from 18,000 years BP to present day for the Antarctic Ice Sheet expressed as a percentage of ice melted in a given time period (e.g. 100% in 5,000 years in the case of the Huybrechts (1990) model).

Chapter 5

Ice reconstructions for the Ross Embayment

5.1 Introduction

This chapter presents modelling of the ice sheet in the Ross Embayment portion of the Antarctic Ice Sheet. All the modelling described in this chapter is of the glacio-hydro-isostatic style introduced in the previous chapter. Because it is not possible to model a portion of an ice sheet in isolation, the first section in this chapter evaluates the influences of Antarctic ice and water that lies outside of the Ross Embayment area. This determines how much of the isostatic rebound observed in the Ross Embayment is a consequence of the outside glacio-hydro-isostatic influences and how much must be due to local ice and water changes. The second section outlines the limitations of the Ross Embayment models. These include the limits determined from the available field data, the effects of approximating the drainage basin as a rectangle, the treatment of the grounding line, and the melting of the ice sheet. The third section of this chapter examines the details of the ice reconstruction including the location of the ice, the ice volume in the reconstruction, and the timing of the ice sheet melting. A simple block model illustrates how information from field observations is modelled. Finally, the reconstruction, selected as most plausible on the basis of current evidence, is presented for the Ross Embayment at the Last Glacial Maximum.

5.2 Outside Influences

It is not possible to investigate a single portion of the Antarctic Ice Sheet in isolation to other sites because of the response of the Earth at a distance to changes in surface loads. These external influences have been discussed in the previous chapter so only an outline is given here where it relates to the Ross Embayment ice sheet modelling.

Since the Last Glacial Maximum, not only has the Antarctic Ice Sheet receded but

the Northern Hemisphere ice sheets have faded from vast, continent-covering ice sheets to a few scattered mountain ice fields. This had a large effect on the Antarctic Ice Sheet because approximately 90 m (equivalent sea level) of water had been put into the oceans. In the Ross Embayment area this raised sea levels and has also caused a small amount of isostatic depression (from the load of the extra water). Figure 5.1 shows the effects due to both the Northern Hemisphere Ice Sheets and that part of the Antarctic Ice Sheet outside the Ross Embayment (again referred to as the 'distal' Antarctic Ice Sheet in this chapter). The Ross Embayment lies in the intermediate field of the distal Antarctic Ice Sheet and the isostatic response to the waning of this ice sheet causes a relative-sea-level rise in the Ross Embayment area (a rise of 7 m from 6,000 years BP to the present day at McMurdo Sound). When combined with the effect of the Northern Hemisphere Ice Sheets (See Chapter 4.5.1) the sea level from these sources alone in McMurdo Sound is about −4 to +2 metres. Therefore, the local ice needs to produce between +18 and +24 m of relative sea level change to match observational constraints.

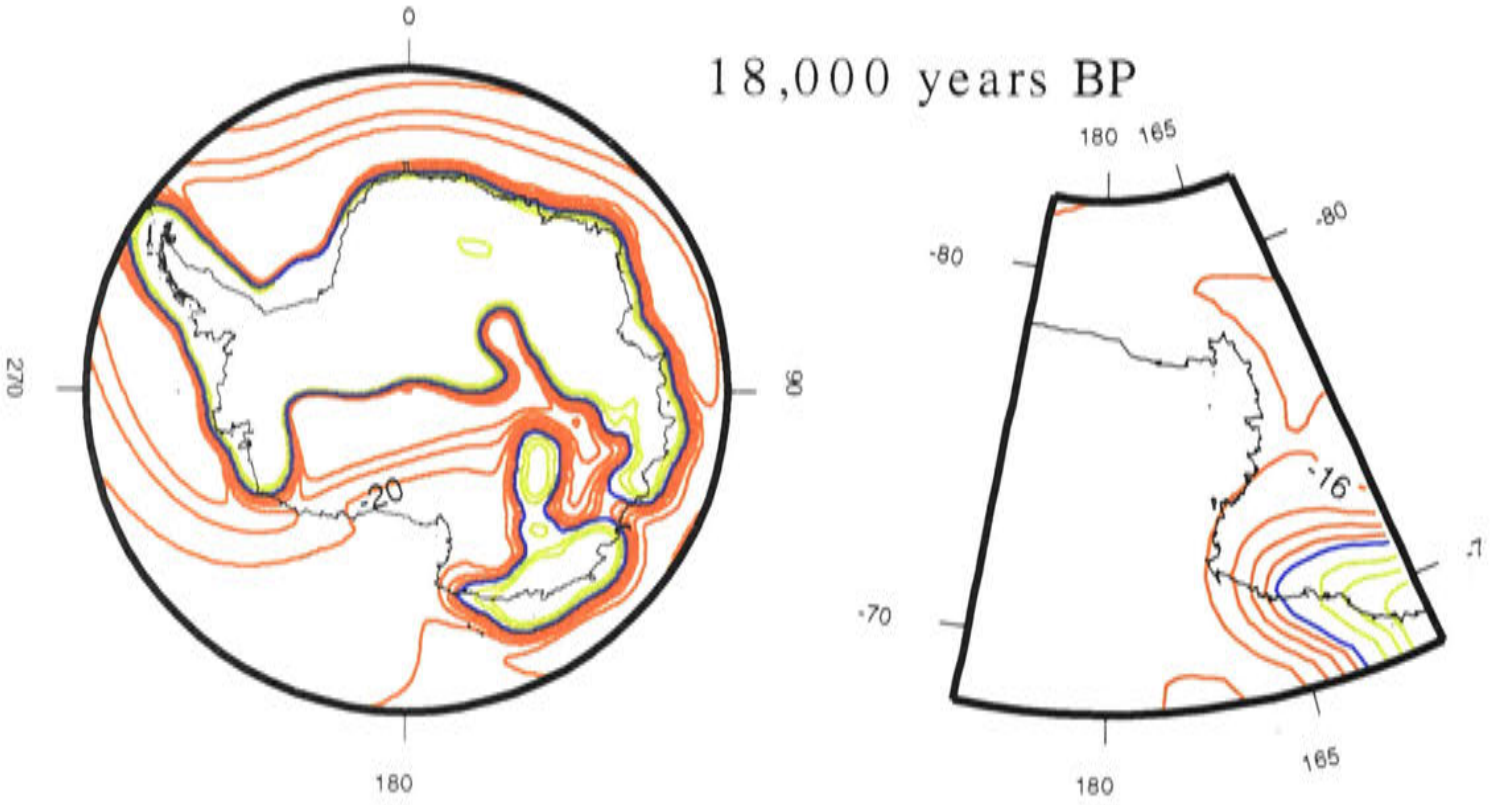

Figure 5.1: Contour plots of predicted relative sea level at the Last Glacial Maximum from all ice outside of the Ross drainage basin (distal Antarctica and the Northern Hemisphere contributions). This plot shows only the results for the maximum reconstruction in Antarctica and the standard Northern Hemisphere reconstructions (fennice.new + nhewice.new). The plot does not contain any ice change in the Ross Embayment and this can be seen by the steep contours in an approximately rectangular box around the area. Red contours indicate sea levels below present and a rising predicted relative sea level. The contours are at a 5 m spacing with the blue contour being the zero contour. On the right is an enlargement of the Western Ross sea and Victoria Land areas. McMurdo Sound is located at approximately 78°S and 165°E.

5.3 Limitations on the reconstruction

To be able to effectively test different ice sheets in the Ross Embayment some limitations have been placed on the reconstruction of this part of the Antarctic Ice Sheet. Three different reconstruction for the rest of the Antarctic Ice Sheet (the distal section) have been used that span a range of plausible models. Differences between the three have been outlined in Chapter 4. From this Antarctic reconstruction a rectangular section that approximates the drainage basin for the Ross Embayment has been removed. This allows various Ross Embayment reconstructions to be inserted for testing.

The effects of approximating the shape of the drainage basin are investigated below but before discussing the details of the approximations in the modelling, the limitations from the field observations that are used to constrain the reconstructions must be considered.

5.3.1 Field observations providing ice sheet constraints

There have been various studies in the Ross Embayment area both on-land and off-shore to determine where the ice sheet was at the Last Glacial Maximum, how thick it was and where it flowed (Figure 5.2). These types of constraint are important in the glacio-hydro-isostatic modelling because they provide limitations on where ice may or may not have been located.

Considered first is evidence for the Last Glacial Maximum position and retreat of the ice sheet. Surface sediments collected by piston cores in the Ross Sea identify possibly locations of the grounding line and high resolution seismic, swath bathymetry and side-scan sonar records of the sea floor help distinguish different sediment packages associated with ice sheet growth and retreat, as well as ice-contact features such as the grounding line (e.g. Shipp et al. 1999; Anderson et al. 1992).

Licht et al. (1996) described core data from the Ross Sea on the basis of the nature of the sediments and suggested that the ice was not grounded to the edge of the continental shelf but that the grounding line occurred near Cape Washington, 100 to 200 km south of Coulman Island. Seismic work by Karl (1989) on the characteristics of the sediments drew the same conclusion. In other areas of the Ross Sea, sediments from piston cores taken by Licht and Andrews (1997) are not as conclusive on the grounding line location due to variations in the nature of the sediments and variable ages of the surface sediments (e.g. Andrews et al. 1999 and Domack et al. 1999). These variations have caused difficulty in the interpretation. However, general consensus is that the grounding line extended out close to the shelf edge in the eastern and central Ross Embayment.

For much of the central and eastern part of the Ross Sea there is little firm evidence for movement of the grounding line with time. Despite this, Conway et al. (1999) from radiocarbon dating in Victoria Land and the Hatherton Glacier (Transantarctic

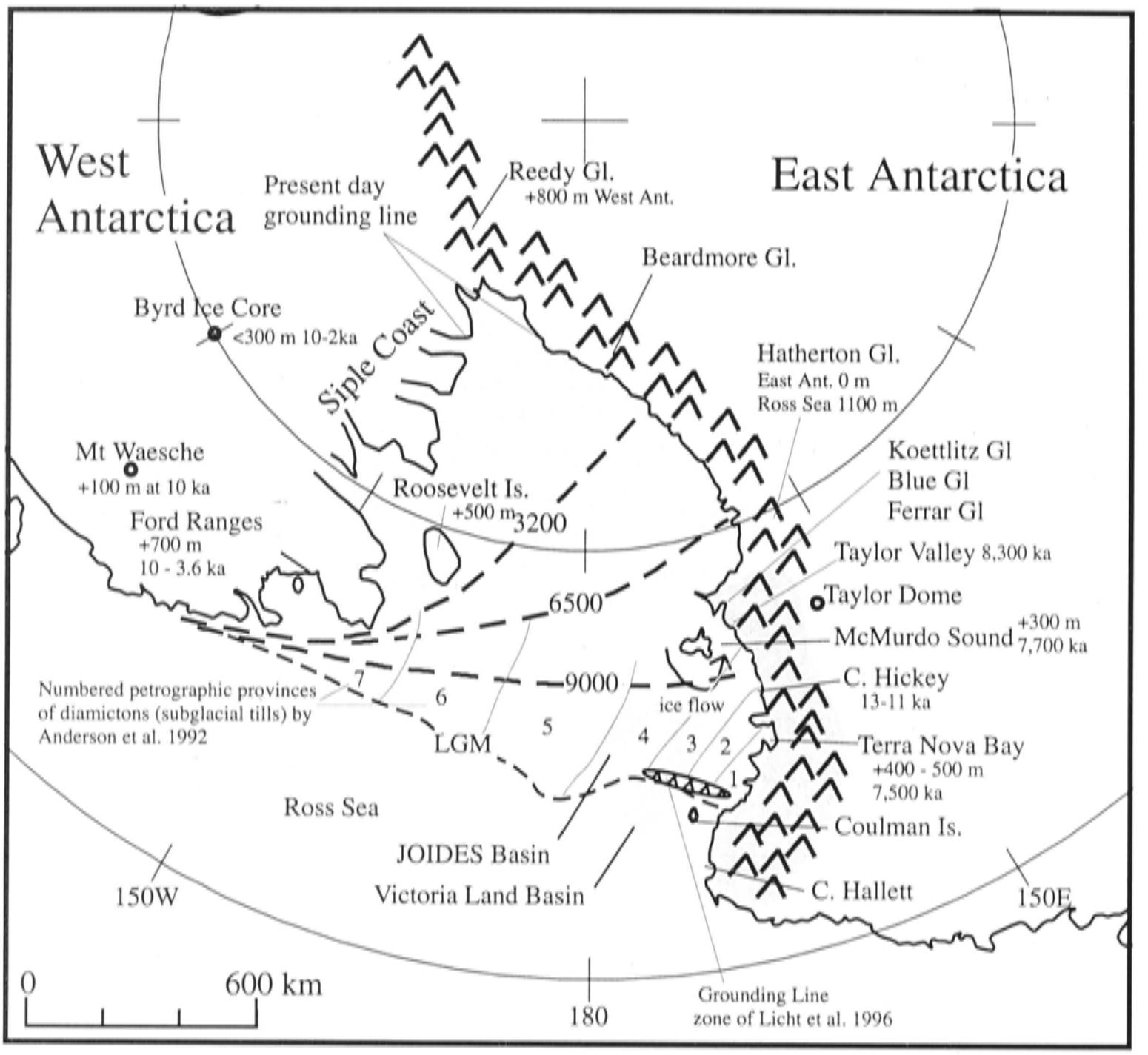

Figure 5.2: Field observations from the Ross Embayment. Glaciers flowing through the Transantarctic Mountains are shown with trimline heights. Glacial trimlines are also labelled for McMurdo Sound and Terra Nova Bay (with respect to present-day sea level). Ages beside sites give a time for ice sheet retreat at this location. These ages may be a minimum or maximum age as outlined in the text. The petrographic provinces of Anderson et al. 1992 indicate ice flow directions in the Ross Sea. Ice sheet heights are given for two sites in West Antarctica and a maximum ice height is given in the Ford Ranges with a time of deglaciation. The Last Glacial Maximum grounding line is labelled and is based on the combined evidence outlined in the text. The approximate retreat lines at 9,000, 6,500 and 3,200 years BP are from Conway et al. 1999.

Mountains about 80°S) and glaciological modelling of ice features on Roosevelt Island in the eastern Ross Sea have estimated the retreat of the grounding line in the Ross Sea of nearly 1,300 km from Coulman Island to the present-day position along the Siple Coast of West Antarctica (see grounding line positions of Figure 5.2).

The ice height can sometimes be determined by the lateral moraines left by glaciers

and drift sheets (glacial deposits from beneath the ice sheet). Denton et al. (1989) (updated in Denton and Hughes 2000) examined the glacier profiles of the Koettlitz, Blue and Ferrar glaciers and used these to constrain the height of the ice sheet (Figure 2.13 gives an example of a glacier profile from the Reedy Glacier). They created a map showing the flowlines in the McMurdo Sound area which includes ice sheet flow from the south (the interior of the Ross Embayment) over most of the islands on the southern and south-eastern sides of McMurdo Sound. Kellogg et al. (1996) have since investigated trimlines on Black Island and White Island (south of Ross Island) and conclude that the ice did not extend as high over these islands as Denton et al. (1989) proposed. Denton and Hughes (2000) agree with the Kellogg et al. (1996) value of about 600 m for the ice surface height to the south of Ross Island.

The damming of a lake by the Ross Ice Sheet in one of the Dry Valleys (Taylor Valley) has provided evidence for the presence of ice in McMurdo Sound and the timing of its retreat. Hall and Denton (2000b) dated algae and shells from the former ice dammed lake. The results constrain the ice to its maximum position about 2 km into the valley between 12,700 and 14,600 ^{14}C years BP and shows that ice blocked the valley mouth from 23,800 years BP to around 8,300 years BP. It has also been suggested that at the Last Glacial Maximum ice in McMurdo Sound flowed around Ross Island and entered the Sound from the north. This is based on stable oxygen isotope data and boulder provenance from the McMurdo Ice Shelf (Kellogg et al. 1996).

Further north from McMurdo Sound, heights of trimlines from Last Glacial Maximum glaciers have also been used by Orombelli and Denton (1990) to establish grounded ice sheet heights around Terra Nova Bay. They classified the major landscapes and traced trimlines from glacial drifts. It appears that the Terra Nova Bay drift postdates 25,600 ^{14}C years BP and is older than the 7,500 ^{14}C year age of the highest beach.

The glacial geology and marine data can be combined into a series of ice reconstructions of plausible ice sheet configurations. It is not possible to resolve questions such as how the ice may have flowed in the McMurdo Sound area for two reasons. Firstly, because the characteristic flexural wavelength of the lithosphere is about 150 km it is not possible to resolve loads smaller than this distance. Secondly, an observed relative sea level curve is available from only one side of McMurdo Sound. The ages of known former sea levels on Ross Island (other side of the sound) are very young and do not help to constrain sea level except in the latest Holocene. However, the timing of retreat from the maximum extent and some indication of the timing of ice retreat from McMurdo Sound form important inputs for the ice reconstruction.

5.3.2 Modelling Considerations

Models of the glacio-hydro-isostatic rebound are functions of the Earth's response function to loading and of the geometry of the ice load (the ice margins and the ice thickness

through time). The former is assumed known (see Chapter 4.4) and in this section the isostatic consequences of some different scenarios for the latter are examined.

The drainage basin for the Ross Embayment is outlined on Figure 5.3 and the approximating rectangle is also shown. There will be some edge effects caused by the rapid change in ice thickness across the boundary between the ice sheet used for the rest of the Antarctic Ice Sheet and some of the ice sheets used for the Ross Embayment, particularly when a minimum-sized ice sheet is assumed for the Ross Embayment. As Figure 5.1 shows there is a large gradient across the edge, but minimal effects a short distance from the edge of the approximating rectangle. Thus, the western boundary has been placed sufficiently far from the Victoria Land Coastline to remove boundary effects from the coastal Victoria Land area and the relative sea level predictions in McMurdo Sound and Terra Nova Bay are edge effect free.

In the glacio-hydro-isostatic modelling program it is possible to keep the ice sheet margin fixed for a period of time and thin the ice sheet. The effects of this were investigated to determine whether it was necessary to move the margin of the ice sheet. Figure 5.4 shows the predicted relative sea level in McMurdo Sound from two reconstructions that are the same except that in one the margin is kept fixed until the last time step and in the second the margin moves back at each time step. On the figure, between 6,000 years BP and the present day, the two curves diverge by several metres indicating a potential source of error in the predicted relative sea levels if the margin of the ice sheet is not moved at the same time as the ice sheet is thinned. McMurdo Sound is located in the zone between where the ice sheet grounding line is located today and where the ice sheet grounding line was at the Last Glacial Maximum. Evidence from McMurdo Sound (Hall and Denton 2000b) suggests that the grounding line retreated from the McMurdo Sound area between 8,300 and 6,000 ^{14}C years BP. If we did not model the movement of the margin, the relative sea level estimates for McMurdo Sound would be incorrect.

The model for the Earth's response was discussed in the previous chapter and Figure 4.9 shows the dependence of sea level predictions on the choice of Earth model parameters. While this influence can be significant, we only have field data from 6,000 years BP to present and in this time interval the difference between the predictions for different Earth models is smaller than uncertainties arising from the load distribution and timing of the ice retreat.

5.4 Ice in the Ross Embayment

This section examines possible ice configurations for the Ross Embayment that differ in the total volume of ice, in the location of ice and in the melting rates of ice. A series of questions are addressed:

1. Starting from an existing maximum reconstruction for the Ross Embayment, how

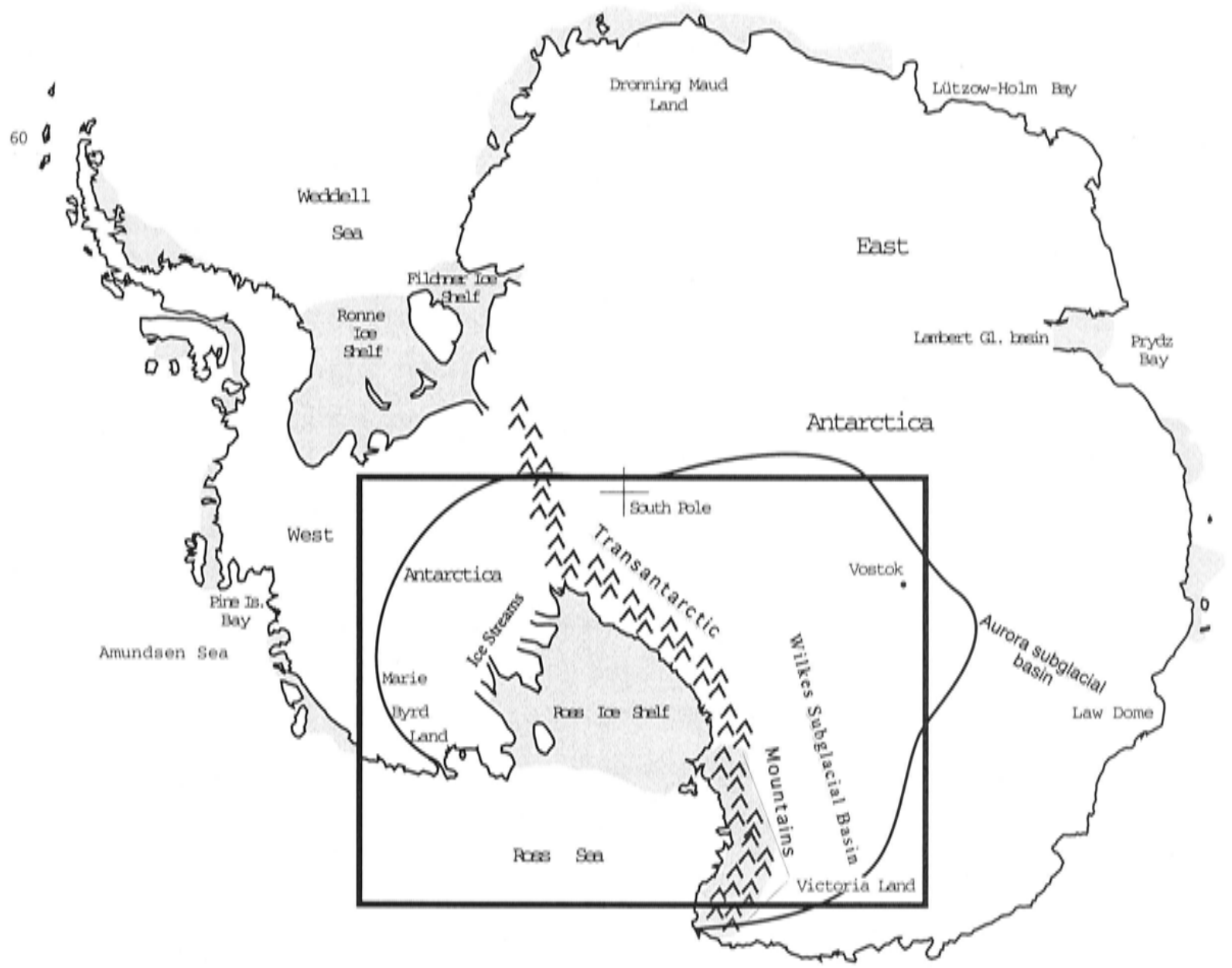

Figure 5.3: Ross Embayment drainage basin (solid line) and the approximating rectangle (thick line).

much of this ice is required in order that the predicted sea levels agree with the field evidence?

2. What is the dependence of the relative sea level predictions on the melting rates of the ice sheet? What is the effect on the predictions, for example, if we lengthen the entire melting time but melt the same volume? Are the predicted sea levels similar if the ice is melted earlier or later?

3. How does adding small areas of ice directly over the field site affect the predicted relative sea level?

4. What happens when we add a large volume of ice at a distance from the field

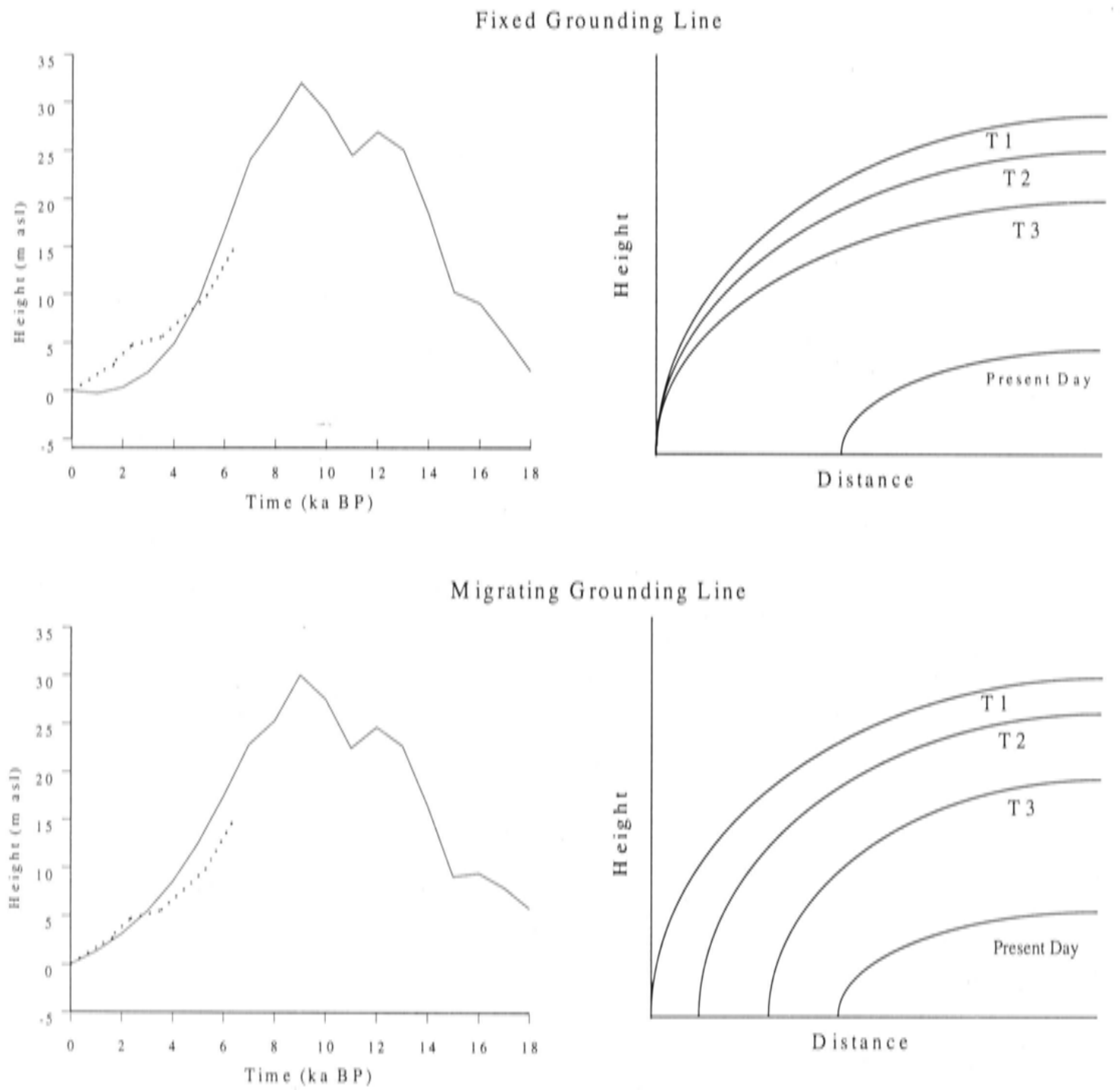

Figure 5.4: Left: A pair of relative sea level predictions in McMurdo Sound from 18ka to the present. Both figures have the same ice sheet reconstruction but with the ice sheet margin of the reconstruction stepping back with each melting time step in the lower figure. The dotted line is the observed relative sea level curve for McMurdo Sound. Right: Profiles of a hypothetical ice sheet showing retreat at times T_1, T_2, and T_3. The fixed grounding line (top) only thins until the final time step when the margin retreats whereas the migrating grounding line (bottom) continuously moves.

site? Will this have the same effect as a small volume specifically located?

5. Is the predicted uplift at all sensitive to the pattern of ice flow around McMurdo Sound?

The answers to these questions will provide a basis for a reconstruction of the ice history in the Ross Embayment, that will be consistent with the observed relative sea

level curves from McMurdo Sound and Terra Nova Bay. A unique solution may not be possible using observational evidence from two sites only but, by ensuring that the mass distribution is consistent with other field evidence the solution should be plausible. The solutions should also give some insight into the limitations of the modelling.

The previous chapter outlined three ice reconstructions for Antarctica by Stuiver et al. (1981), Huybrechts (1990) and Nakada et al. (2000) (Figures 4.11, 4.12, and 4.13 respectively). Before answering the first question of how much ice is required from the maximum reconstruction, the predicted relative sea levels from each of these reconstructions are shown. All the models shown in this chapter use the Northern Hemisphere ice sheets *fennice.new* and *nhewice.new* outlined in Chapter 4.5.1. The Stuiver et al. (1981) reconstruction is a maximum reconstruction and is used here for the portion of the Antarctic Ice Sheet outside of the Ross Embayment. This reconstruction has the grounding line close to the edge of the continental shelf and has no ice streams. Thus, this ice sheet is characterized by a convex shape.

The full Antarctic Ice Sheet reconstruction of Stuiver et al. (1981) predicts high Holocene relative sea levels for McMurdo Sound. Ice from this Antarctic Ice Sheet raises the predicted relative sea level by 40 m at 6,000 years BP compared to the observed elevation of about 20 m (Figure 5.5). This discrepancy requires that either (or both) the amount of ice in the reconstruction must be reduced or the time of melting must change.

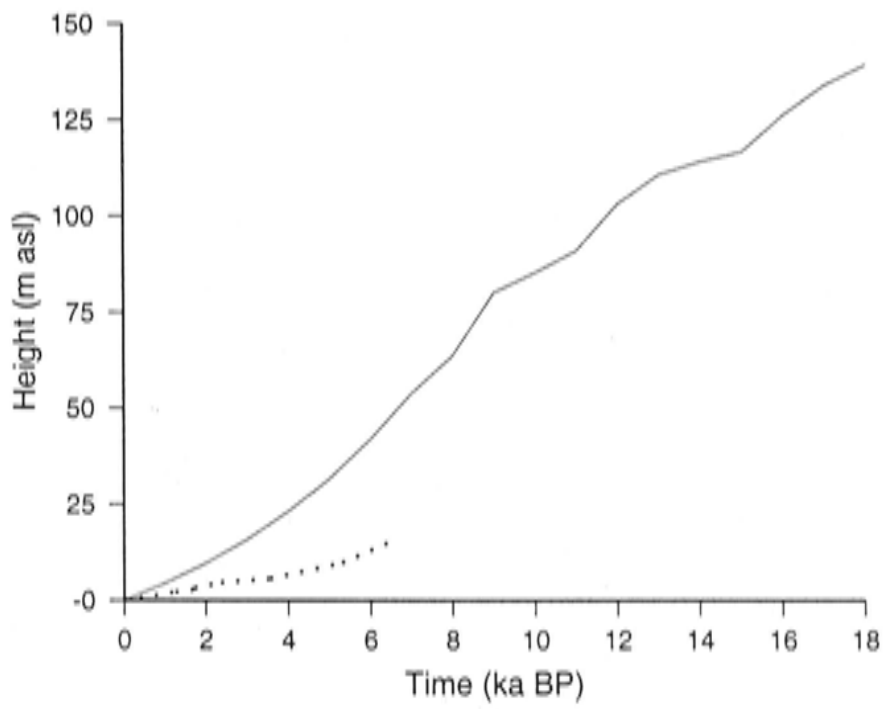

Figure 5.5: Predicted relative sea level curve for the maximum reconstruction of Stuiver et al. (1981). The dotted line is the observed relative sea level for McMurdo Sound.

The Huybrechts (1990) reconstruction predicts an even higher relative-sea-level peak of 70 m at 7,000 years BP in McMurdo Sound (Figure 5.6). This is despite the ice sheet

having a lesser volume of ice at the Last Glacial Maximum than the Stuiver et al. (1981) reconstruction. The high relative sea levels are a consequence of the late melting characteristic of this model.

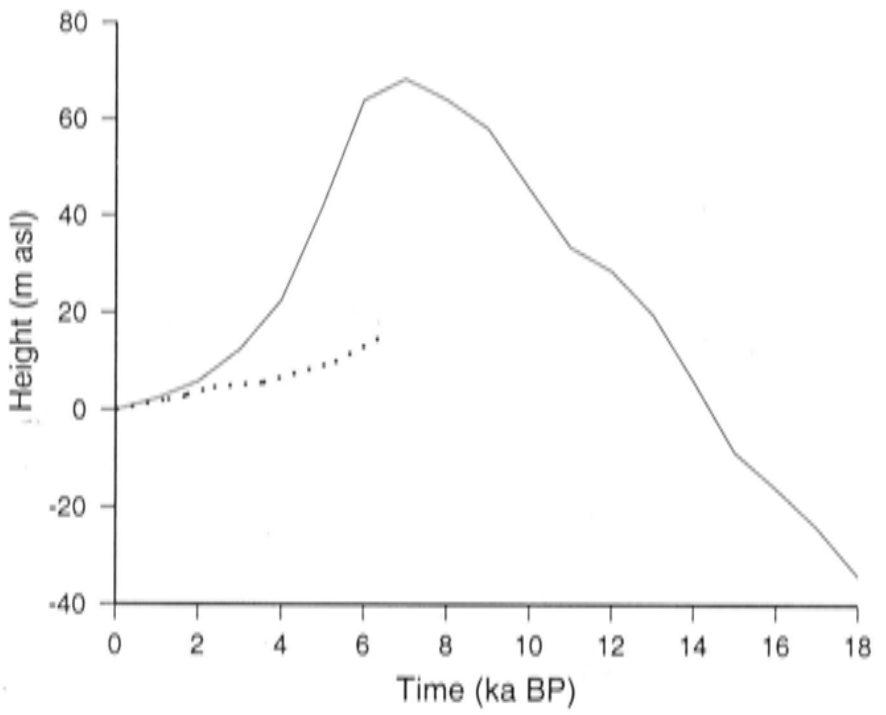

Figure 5.6: Predicted relative sea level curve from the reconstruction of Huybrechts (1990). The dotted line is the observed relative sea level for McMurdo Sound.

The small ice sheet reconstruction of Nakada et al. (2000) is an attempt to fit observed relative sea level curves from around the Antarctic continent with ice placed in specific locations only close to where sea level observations are located. The reconstruction predicts a relative sea level curve that is very close to the observed relative sea level in McMurdo Sound (Figure 5.7) as expected. However, this reconstruction only contains an extra 5.3 metres equivalent sea level of ice in the entire Antarctic Ice Sheet compared with 25.35 metres for Stuiver et al. (1981) and 16 metres for Huybrechts (1990). If this reconstruction is to be used for the Antarctic Ice Sheet then a location for a large volume of ice would be required elsewhere in Antarctica.

Returning to the first question of the amount of ice of the maximum existing reconstruction, we begin with the Stuiver et al. (1981) reconstruction. The amount of ice that this reconstruction contained in the Ross Embayment was reduced, scaling the reconstruction by a constant factor. Figure 5.8 shows the predicted relative sea levels using 17% and 27% of the original amount of ice in the Ross Embayment. Using only 17% of the original amount of ice predicts relative sea levels in McMurdo Sound which are too low when compared to the observations. However, ice volume reduction in the Ross Embayment to 27% of the Stuiver et al. (1981) reconstruction predicts relative sea levels that are consistent with observations between 6,000 years BP and the present day. A more rapid drop in relative sea level between 6,000 and 4,000 years BP would fit

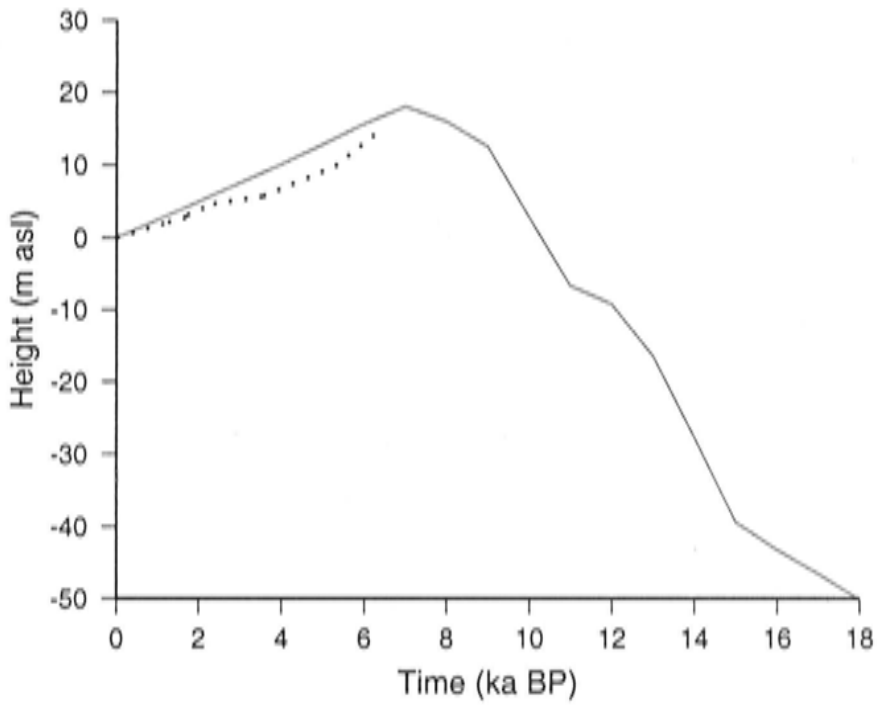

Figure 5.7: Predicted relative sea level curve based on the Antarctic Ice Sheet reconstruction of Nakada et al. (2000). The dotted line is the observed relative sea level for McMurdo Sound.

the observed data better and produce a sea level closer to the observed marine limit at 7,000 years BP, but as the observed data contains some scatter this is still a reasonable reconstruction. A problem in simply scaling the Stuiver et al. (1981) reconstruction occurs with the far-field predicted relative sea levels. 27% of the total volume of ice melted from the Stuiver et al. (1981) reconstruction is only 7 m equivalent sea level which is less than the required amount of melting from the Antarctic Ice Sheet since the Last Glacial Maximum. Thus, each part of the Antarctic Ice Sheet would need to be considered in isolation such that the Ross Embayment is scaled by this amount (27%) but other portions of the ice sheet considered against relative sea levels and other evidence from those areas.

But what happens if we alter the melting time? To demonstrate the effects of changing the melting times the reconstructions of Stuiver et al. (1981), Huybrechts (1990), and Nakada et al. (2000) are used. These three reconstructions use quite different melting histories to represent the Antarctic Ice Sheet while also using different ice volumes. Figure 4.17 in the previous chapter compares the melting histories of the three reconstructions.

Two modifications to the melt timing of the Stuiver et al. (1981) reconstruction are applied, to examine what effect they have on the relative sea levels predicted in the late Holocene. In the first modification, melting commences at 18,000 years BP and ends by 10,000 years BP (compared with the original reconstruction of melting between 18,000 and 6,000 years BP). Thus, Antarctic Ice Sheet melting leads the melting of the Northern Hemisphere ice sheets. The early melting results in reduced amplitudes for

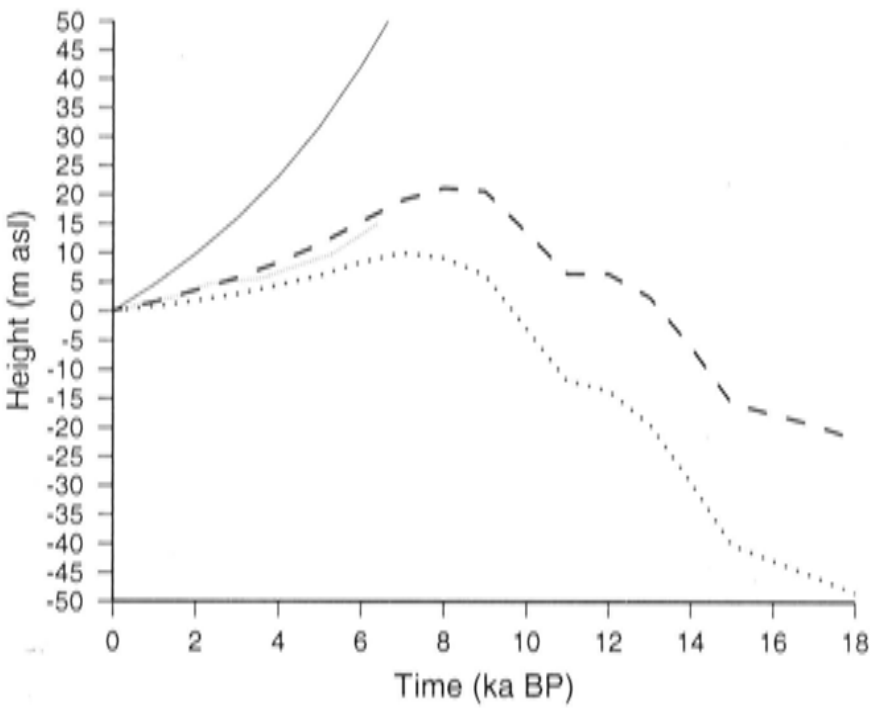

Figure 5.8: Predicted relative sea levels from 27% (dashed line) and 17% (dotted line) of the original amount (solid line in Holocene) of ice in the Ross Embayment of the Stuiver et al. (1981) reconstruction. The grey line shows the observed relative sea level.

the predicted relative sea levels (Figure 5.9) in the Holocene because a larger part of the exponentially decreasing rebound has occurred before 6,000 years BP. Hence by moving the melting time earlier, the response seen in the late-Holocene will be smaller. This is in part due to the competing effect of melting in the Northern Hemisphere, but is made possible by the viscosity of the mantle, which produces a response time to melting that is of the order of 10,000 years. Hence, if some of the melting is close to the Last Glacial Maximum it will be difficult to see much effect from it in the late-Holocene. If, on the other hand, the melting occurs late, the effects will be magnified in the late-Holocene period. Despite the smaller late-Holocene response from early melting, the relative sea level predicted with this early melting still significantly overestimates the observed relative sea levels as can be seen on Figure 5.9.

A late melting pattern is also considered, with melting commencing at 10,000 years BP and continuing until the present day (Figure 5.10). Late melting causes the predicted relative sea levels in the Late Holocene to be grossly over-estimated (e.g. 145 m at 6,000 years BP) and must be rejected if ice volumes are maintained.

The above two examples demonstrate that if we have observations from only a short period of time, and not over the entire melting period, we can adjust the time that the ice sheet melts to match the predictions with the observations. So, what happens if the melting history is 'stretched' to melt over a longer period of time? Because the Huybrechts (1990) reconstruction invokes a relatively brief and late melting scenario (from about 5,000 years to present) this reconstruction was chosen to investigate this

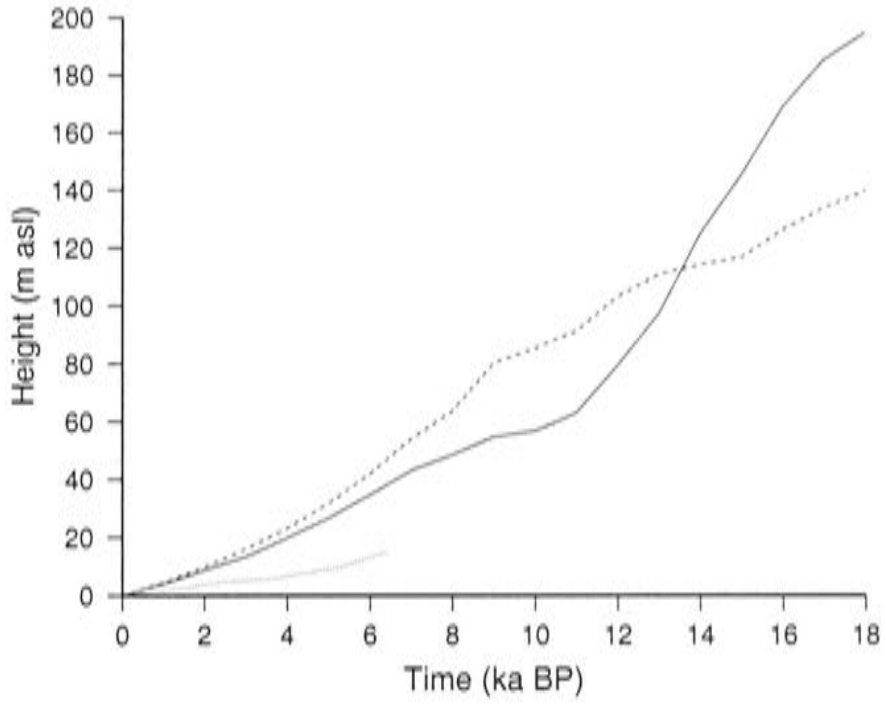

Figure 5.9: Early melting predictions of the relative sea levels in McMurdo Sound from the Stuiver et al. (1981) reconstruction. The solid line is the early melting and the dashed line is the unmodified Stuiver et al. (1981) reconstruction. The dotted line shows the observed relative sea level.

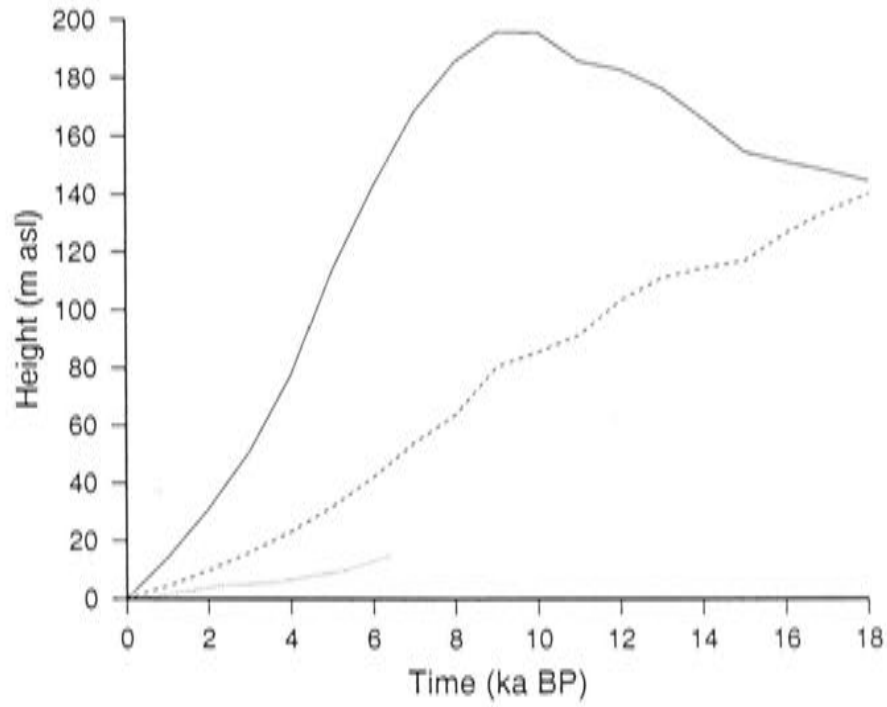

Figure 5.10: Predictions of the relative sea levels in McMurdo Sound from late melting of the Stuiver et al. (1981) reconstruction. The solid line is the late melting and the dashed line is the unmodified Stuiver et al. (1981) reconstruction. The dotted line shows the observed relative sea level.

effect. There is evidence from places such as the Taylor Valley in Antarctica (Hall and Denton 2000b) that the Antarctic Ice Sheet was melting prior to 5,000 years BP, but there is little evidence to indicate when melting stopped. Therefore, it may not be unreasonable to modify the Huybrechts (1990) reconstruction such that melting occurred over a longer time interval. In the modified melting scenario the onset of melting is assumed to start at 10,000 years BP and continue to the present day. The predictions for the relative sea levels in McMurdo Sound with this modified melting history (Figure 5.11) are lower than with the original melting history (40 m peak relative sea level at 9,000 years compared to a 70 m peak at 7,000 years BP) and are much more consistent with the observations for the last 6,000 years. This demonstrates that stretching the melting time will dampen the predicted relative sea levels over the entire period since melting began. Because the melting began late in the case of the Huybrechts (1990) reconstruction, the stretched melting time also shifts the timing of the peak in relative sea level to an earlier time.

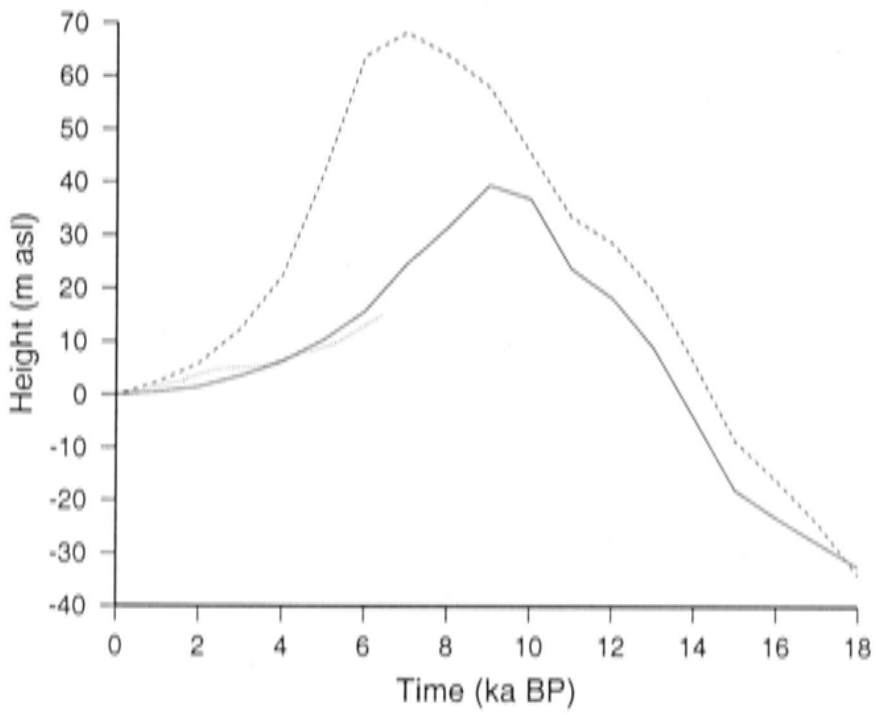

Figure 5.11: Predictions of relative sea levels from the modified melting history of the Huybrechts (1990) reconstruction. The solid line is the prediction from the modified melting while the dashed line is the original melting. The dotted line shows the observed relative sea level.

However, the Huybrechts (1990) reconstruction melting is driven by a prescribed eustatic sea level and background temperature change. Thus, for this modified melting history to be valid another forcing mechanism for the melting would have to be invoked for the melting or parameters defining the ice sheet response to the sea level rise would need to be modified.

A useful method for testing the validity of a melting history is to compare predicted sea levels with observed values since the Last Glacial Maximum at sites far from the ice

sheets and where isostatic effects are small. Figure 5.12 shows the far-field predicted relative sea levels from the Huybrechts (1990) reconstruction and the 'stretched' melting modification (solid line). Both models include the effect of the Northern Hemisphere ice sheets. Both models also under-predict the observed late-Pleistocene relative sea levels, indicating that ice volumes melting at that time are insufficient. The longer melting period, however, better predicts the mid- to late-Holocene observed relative sea levels in the far-field. Using the far-field observations in this way provides valuable information that we cannot get directly from the Antarctic observations (if we assume models of the Northern Hemisphere ice sheets are accurate). In this case it suggests that some ice needs to be melted even earlier somewhere in the world, even though this melting does not show up in the predictions for McMurdo Sound in the mid-Holocene.

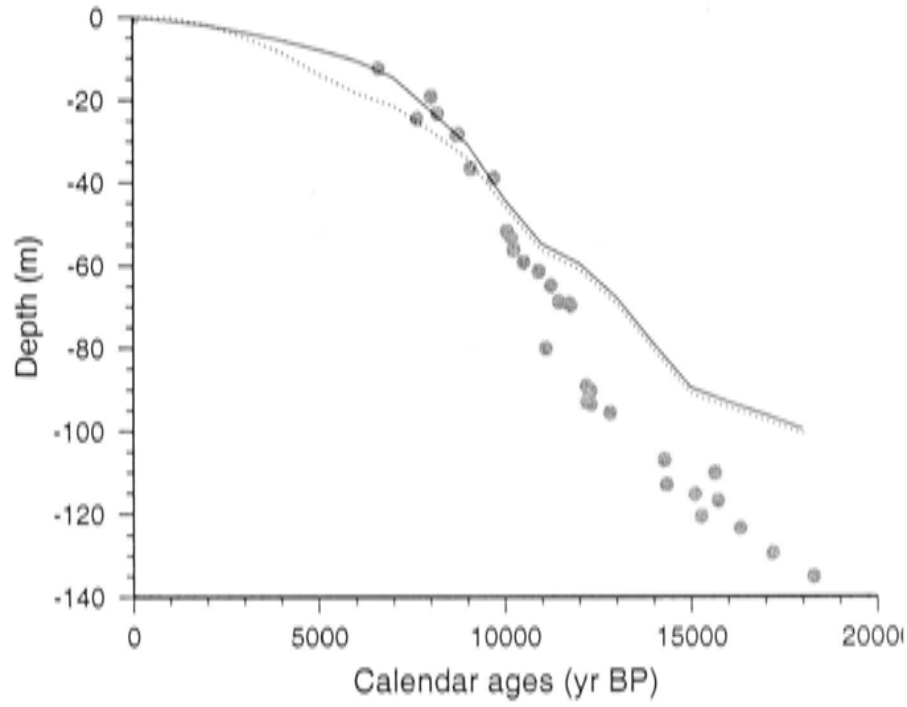

Figure 5.12: Predicted relative sea level curve of Huybrechts (1990) in the far-field. Curves from the original melting history (dotted line) and from the stretched melting history (10,000 years BP to the present day — solid line). Both model predictions fail to fit the early melting but the stretched melting history is a closer match to the Barbados relative sea level in the mid-Holocene.

Next, the location of the ice is considered. How does adding small areas of ice directly over the field site affect the relative sea level? If a small block of ice is added over a site there will be a depression of the crust beneath the block and 'peripheral bulges' to the sides of the block (Figure 5.13). This is the same as for a full-sized ice sheet, apart from the flexural rigidity of the lithosphere supporting a greater proportion the load. Hence, if we place small blocks directly over the locations of observed relative sea level we should be able to predict the relative sea levels. This is essentially the method used by Nakada et al. (2000) in their reconstruction. Additional ice was

placed over McMurdo Sound and Terra Nova Bay to fit the field observations (see Figure 4.13). The field observations of relative sea level vary between McMurdo Sound and Terra Nova Bay (by nearly 10 m at the marine limit) so it may also be possible to use a strategically located smaller block to achieve the same appropriate predicted relative sea level while ignoring any field constraints. This is what the following section demonstrates.

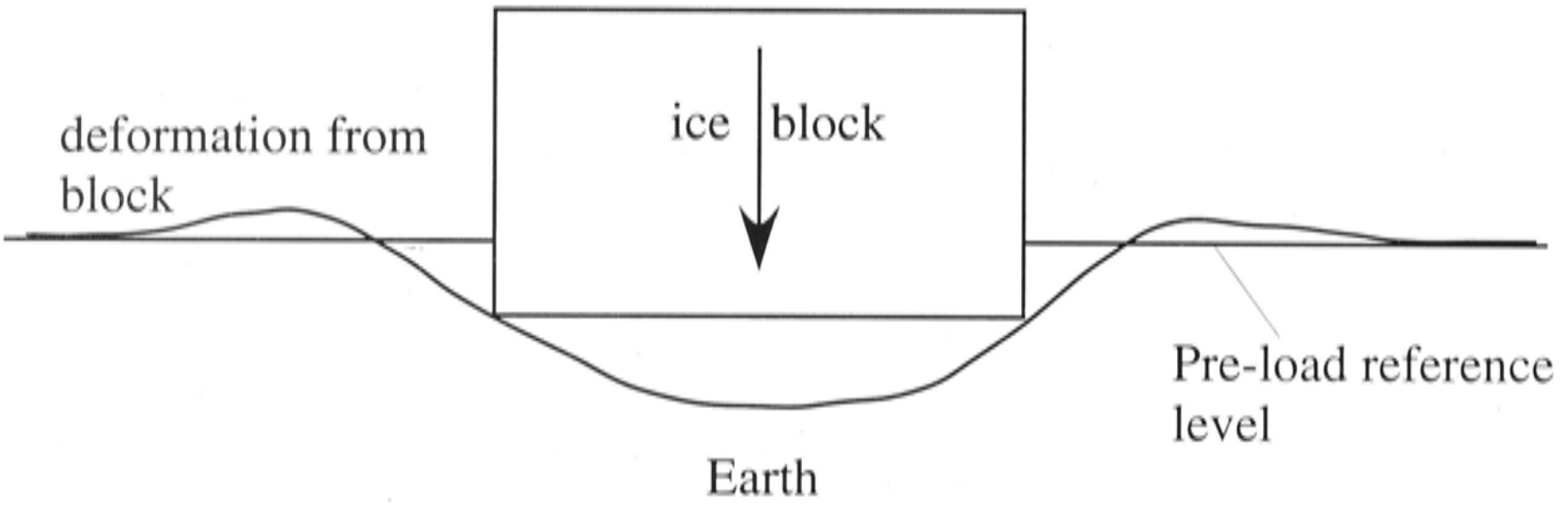

Figure 5.13: Schematic diagram of a block of ice sitting on the crust. The resulting crustal deformation due to the block is shown.

Small blocks of ice (approximately 0.2 to 0.4 m equivalent sea level) are used in different locations here to illustrate the ways that ice can be placed strategically into an ice sheet. The blocks of ice are placed into the Nakada et al. (2000) model because this model already predicts well the observed relative sea levels and deviations from this are viewed easily on the relative sea level prediction figures.

First, a block of ice of dimensions 400 x 400 x 1 km (approximately 0.4 m equivalent sea level) is placed over McMurdo Sound and to the area north of McMurdo Sound (see Figure 5.14 block 1). Figure 5.15 shows the predicted relative sea levels from adding ice directly over a site. Because McMurdo Sound is directly beneath the block there is a larger amount of isostatic rebound on melting causing approximately 25 metres more relative sea level at 7,000 years BP than the Nakada et al. (2000) model only. The block of ice extends north and covers Terra Nova Bay. Because Terra Nova Bay lies near the edge of the block a smaller change in the predicted relative sea level, with respect to the Nakada et al. (2000) model, would be expected. The difference is only about 10 m relative sea level at 7,000 years BP and is shown on the lower plot of Figure 5.15.

Next, a block of ice (dimensions 400 x 400 x 0.4 km - approximately 0.2 m equivalent sea level) is placed to the south of McMurdo Sound (illustrated on Figure 5.14 as block 2). McMurdo Sound is still close to the block (less than 100 km) so the relative sea level is approximately 10 metres higher at 7,000 years BP than the Nakada et al. (2000) model. However, because Terra Nova Bay is now close to 400 km from the edge of the

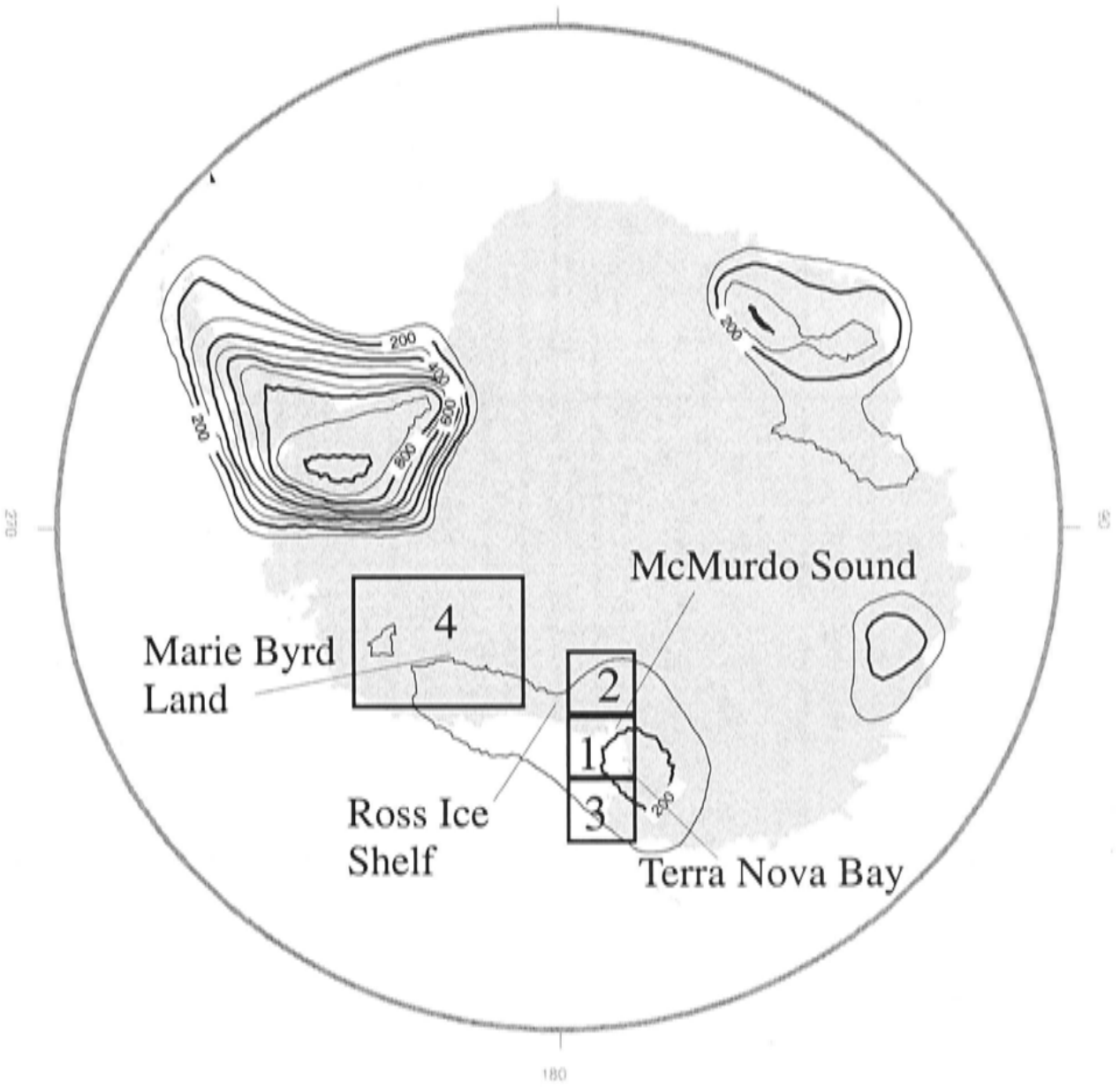

Figure 5.14: Location of ice blocks on the Nakada et al (2000) reconstruction. Three blocks are labelled, each of which will be discussed in turn in the text. At any one time only a single block is modelled.

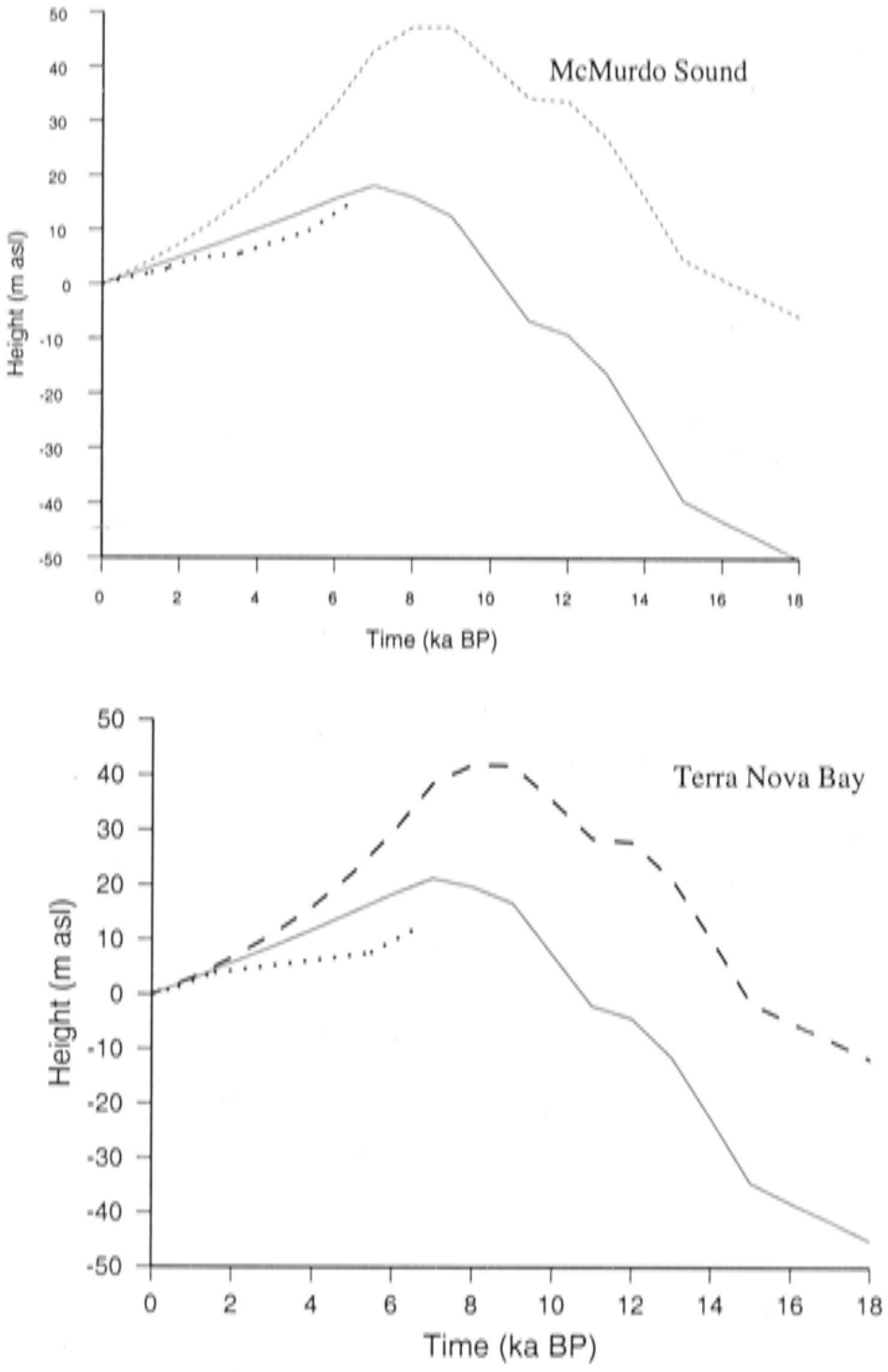

Figure 5.15: Relative sea level curves at McMurdo Sound (top) and Terra Nova Bay (bottom) for the reconstruction of Nakada et al. (2000) with a block of ice added. The solid line shows the unmodified ice reconstruction predictions and the dashed line shows the same reconstruction but with a block of ice directly over and to the north of McMurdo Sound. The dotted lines show the observed relative sea level.

block there is almost no change in the predicted relative sea levels. This illustrates how it is possible to achieve a difference in predicted relative sea levels between two sites.

Finally, a block of ice (dimensions 400 x 400 x 0.4 km - approximately 0.2 m equivalent sea level) is placed to the north of Terra Nova Bay (illustrated on Figure 5.14 as block 3). Essentially this is the same exercise as above but with the ice close to Terra Nova Bay and far from McMurdo Sound. This block predicts an additional 5 metres of

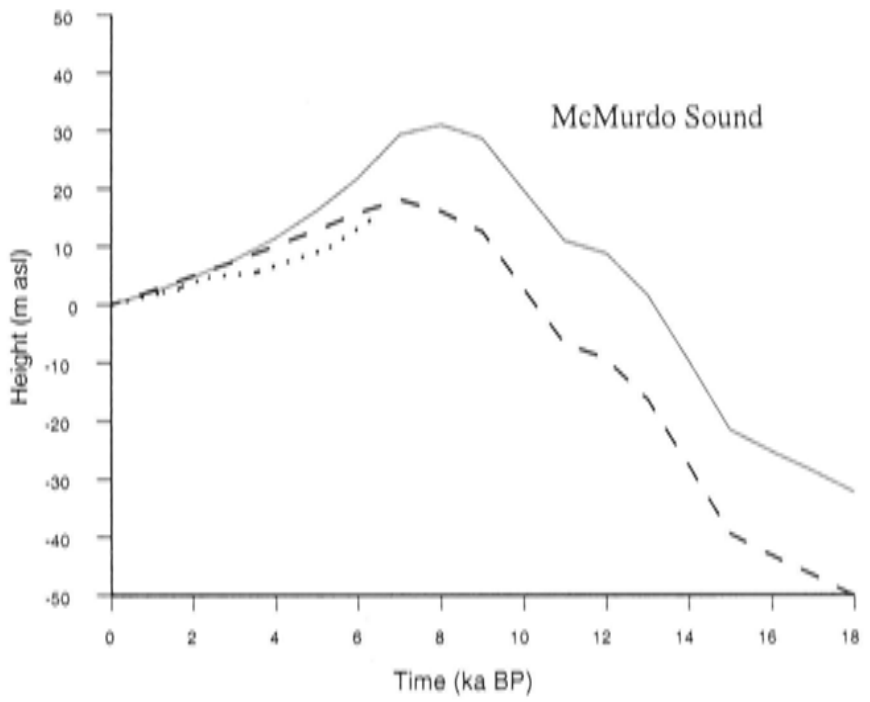

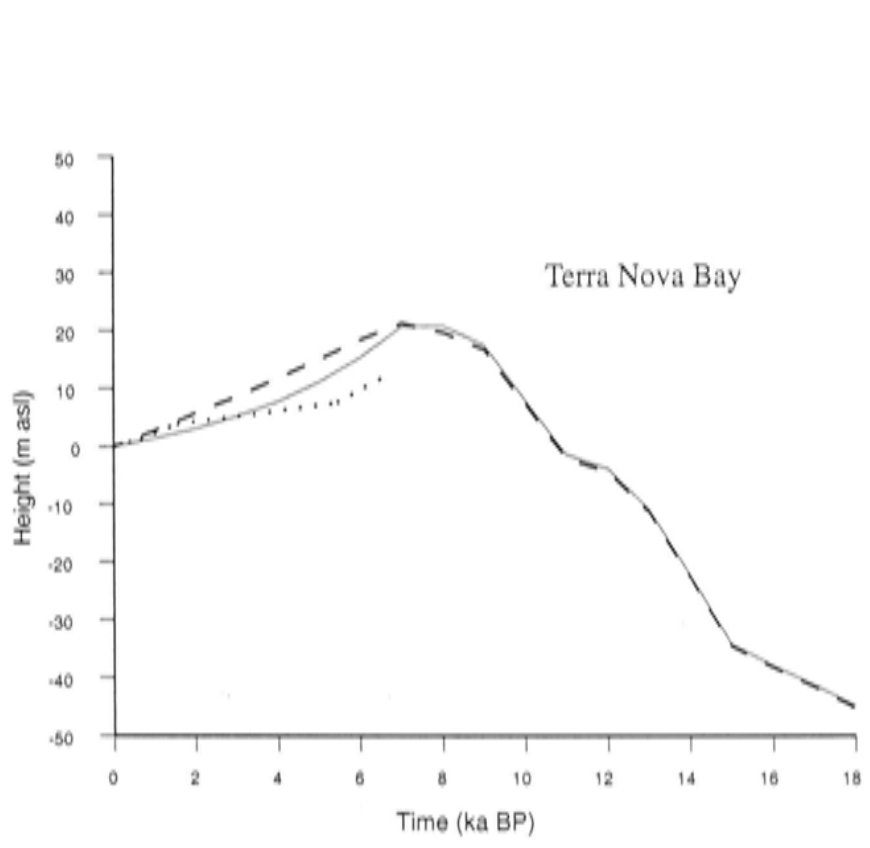

Figure 5.16: Predictions of the relative sea levels from the Nakada et al. (2000) reconstruction with a block of ice placed to the south of McMurdo Sound. The upper graph is the prediction for McMurdo Sound and the lower graph for Terra Nova Bay. The dotted lines show the observed relative sea level, the solid lines the prediction with the block of ice and the dashed lines the original prediction of Nakada et al. (2000).

relative sea level at 7,000 years BP over the Nakada et al. (2000) model at Terra Nova Bay, but no additional relative sea level is predicted at McMurdo Sound. Once again this illustrates how blocks can be placed to match predictions with observed relative sea levels. These results are used in combination with field observation constraints later in the construction of a full block model for the Ross Embayment area.

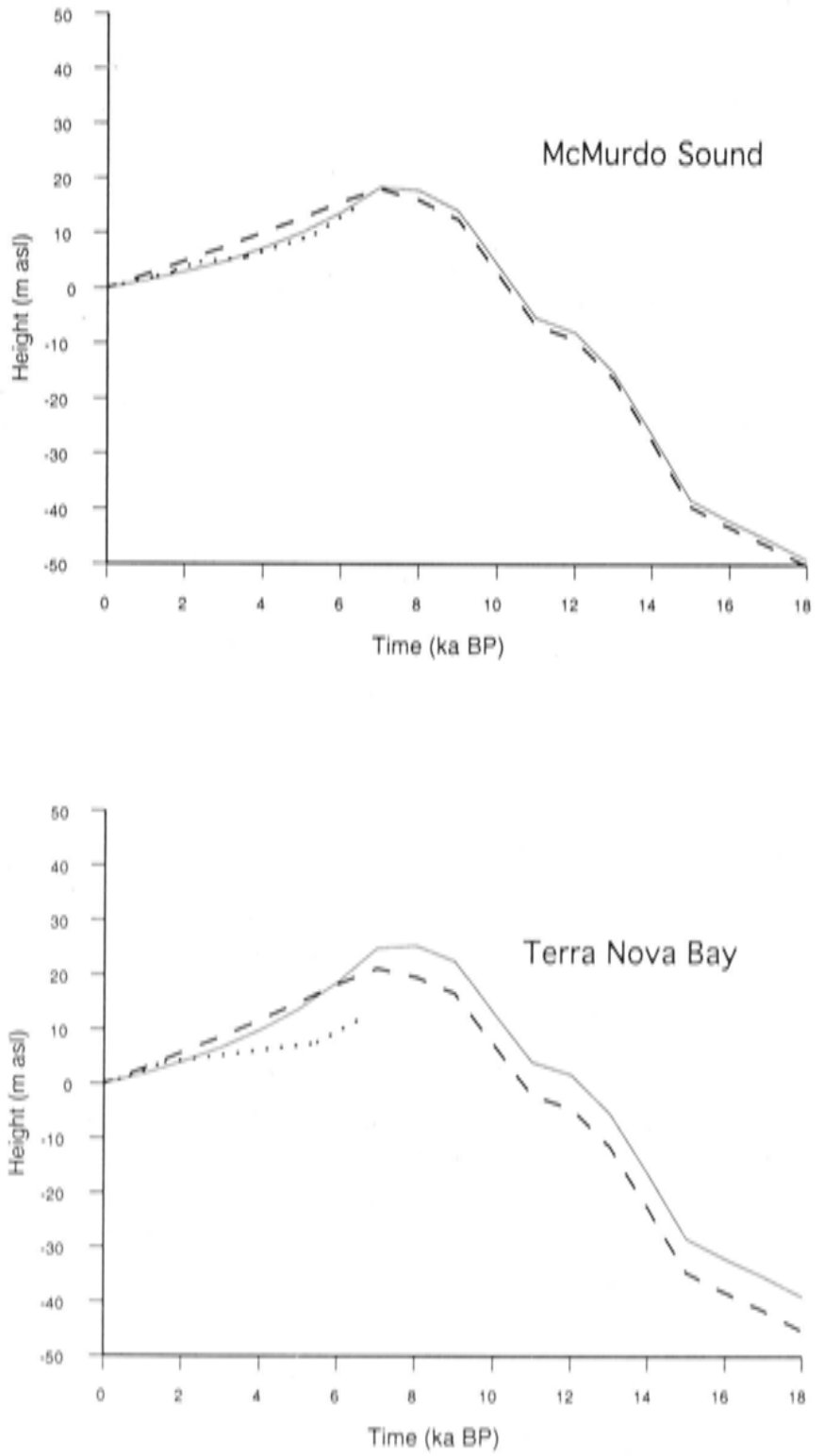

Figure 5.17: Predictions of the relative sea levels from the Nakada et al. (2000) reconstruction with a block of ice placed close to Terra Nova Bay to the north of McMurdo Sound. The upper graph is the prediction for McMurdo Sound and the lower graph for Terra Nova Bay. The dashed lines show the unmodified ice reconstruction predictions and the solid lines show the same reconstruction with the block of ice. The dotted lines show the observed relative sea level.

Does placing a block of ice further away from both McMurdo Sound and Terra Nova Bay have a significant effect? To test this a larger (dimensions 1000 x 1200 x 0.5 km - approximately 1.9 m e.s.l.) block was placed over Marie Byrd Land in West Antarctica (Figure 5.14, block 4). The predicted relative sea level due to this block of ice is shown in Figure 5.18. Essentially there is little change in the predicted relative sea levels in McMurdo Sound because this site is far enough outside the edge of the block to have no crustal movement caused by the block, emphasising the importance of the local ice over the regional ice (until the regional ice volume is very large).

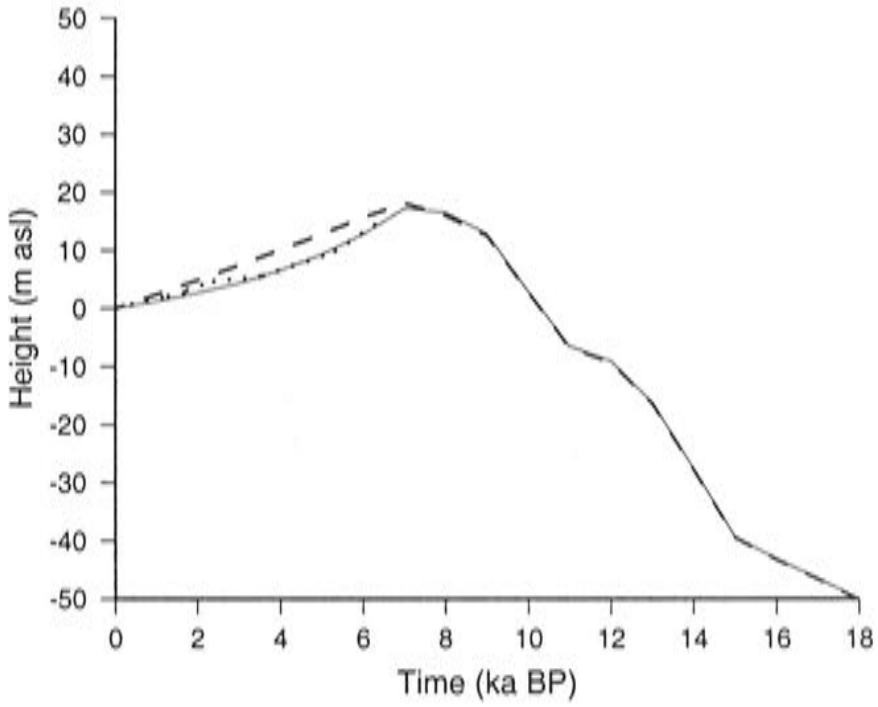

Figure 5.18: Predicted relative sea level curve for McMurdo Sound and the Nakada et al. (2000) reconstruction. This prediction has a large block of ice added to Marie Byrd Land on the eastern side of the Ross Embayment. The dotted line shows the observed relative sea level, the solid line shows the prediction with the block of ice and the dashed line shows the original prediction of Nakada et al. (2000).

Using blocks of ice it is possible to change the predicted relative sea levels for sites around Antarctica. This demonstrates the need for more than two sites of observed relative sea level in the Ross Embayment so that the location of any 'blocks' of ice can be constrained through the isostatic responses seen at varying distances (illustrated by the blocks north and south of McMurdo Sound). The size of any additional blocks of ice may also be constrained by local trimlines and glaciological plausibility. It is also possible to place ice at a distance from a site of observed relative sea level without a major change in the predicted relative sea levels which again demonstrates the need for more observations of relative sea level and ice sheet limits over a widespread area.

Modelling small volumes of ice lead into the question of modelling the ice flow around McMurdo Sound. Because McMurdo Sound is bounded by mountains on the

western, eastern and southern sides the ice flow in this area must have been more complex than the simple expansion of ice out of the Ross Embayment to the south. Glacial erratics of kenyte sourced from Cape Royds on Ross Island (eastern side of McMurdo Sound) have been found on the opposite side of McMurdo Sound (see Figure 5.19). This indicates that there must have been some flow across the sound, possibly in an anti-clockwise fashion. Because of the blocking effect of the mountains to the south of the sound it is believed (e.g. Kellogg et al. 1996, Denton and Hughes 2000) that most of the ice probably flowed south into the Sound. Unfortunately, it is not possible to clearly distinguish between different possible flow models for ice into the Sound because the wavelength of the flexural rigidity of the lithosphere relative to the size of McMurdo Sound as outlined earlier in this chapter.

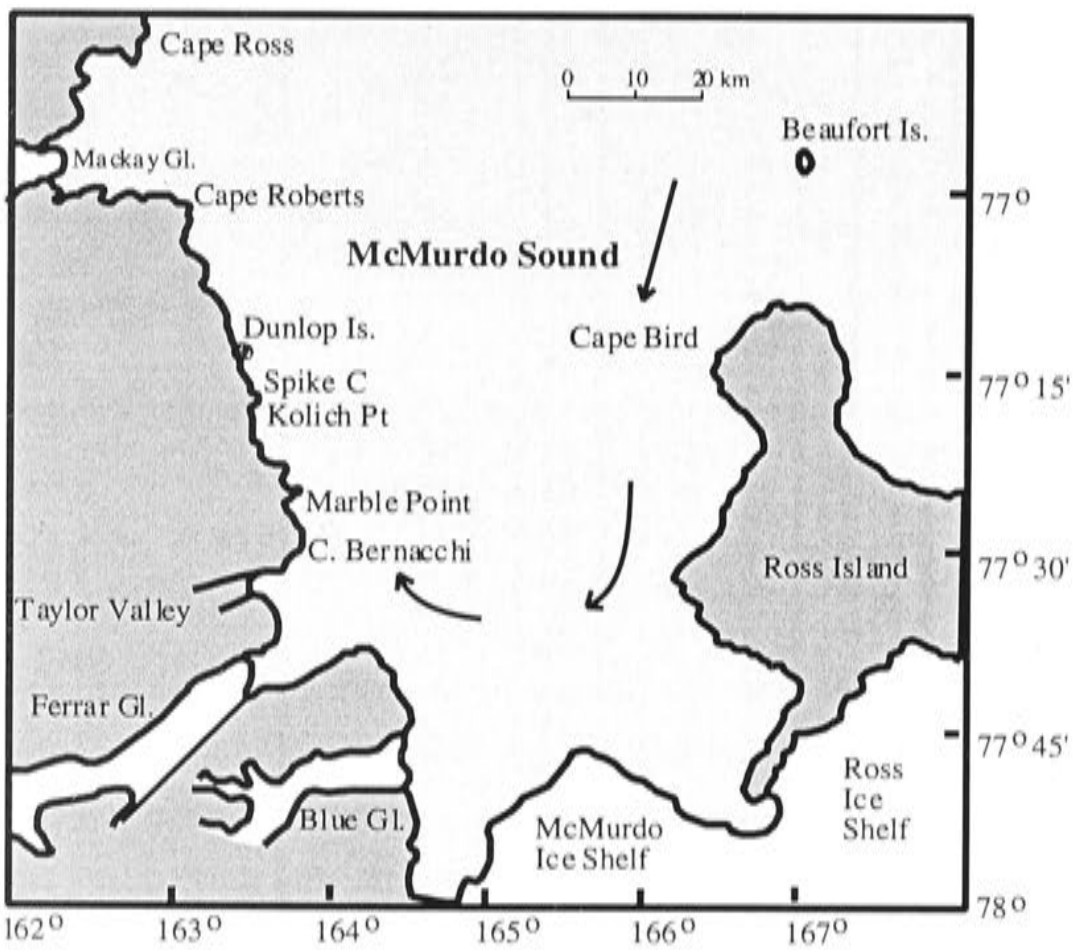

Figure 5.19: McMurdo Sound with proposed ice flow direction indicated by the black arrows.

5.5 A preliminary block model

A simple model is presented in this section for the Ross Embayment. It has been constructed from a series of blocks at the Last Glacial Maximum and three intermediate time steps at 12,000, 8,000, and 7,000 ^{14}C years BP to the present day. In between these time steps there is a linear reduction in the height of each block. The ice margin moves only at each time step. Using a block model of ice thickness allows ice to be freely moved around in the modelling process between iterations, and hence allows many variations to be tried. While this model may appear crude, it fairly accurately

represents different portions of the ice sheet where there is field evidence. This model attempts to fit all the field observations possible in the Ross Embayment.

Ice thicknesses over some areas at the Last Glacial Maximum may appear much greater than the glacial trimlines suggest (e.g. trimlines in McMurdo Sound are at 300 m above present-day sea level with an ice thickness over the same area of 600 m). However, in the formulation of the relative sea level equation the ice load is defined as the ice thickness measured with respect to the crust. If the ice is grounded below sea level, as is the case in the Ross Embayment, then the ice thickness is still defined as the total ice column. Therefore we must include this ice into our reconstruction by adding the present-day water depth to the trimline height above present-day sea level (e.g. 300 m for water depth + 300 m for the height of the trimline).

Figure 5.20 shows the simple block model at the Last Glacial Maximum and each time step and Figures 5.21 and 5.22 show the predicted relative sea levels at McMurdo Sound and Terra Nova Bay. This model was chosen as the best fit from a suite of models tried and refined. Throughout the iterations the earth model was kept constant (the standard ma4A model used throughout this chapter). It would be possible, if time and computing resources allowed, to perform these iterations on many models of the Earth to see if the same model was reached. Instead the suite of earth models was only tried on the chosen block model. For this block reconstruction a model for the Earth with a thinner lithosphere (50 km instead of the standard 65 km) provides a better match of predicted relative sea levels at both McMurdo Sound and Terra Nova Bay because of the shorter flexural wavelength of the thinner lithosphere.

At McMurdo Sound, a maximum relative sea level is predicted at 9,000 ^{14}C years BP and passes through the marine limit at 6,500 ^{14}C years BP. The curve also passes through many of the points obtained from dating of the beaches. At Terra Nova Bay the predicted relative sea level passes through the marine limit about 8,000 ^{14}C years BP and below many of the observed maximum sea level points. It would be preferable to have a shallower slope on this curve (as also desired for the 'stretched' melting model of Huybrechts 1990). However, the models that achieved this had either more ice than field evidence suggests (e.g. Orombelli and Denton 1990, Orombelli et al. 1991) (or is glaciologically plausible) at Terra Nova Bay, or the relative sea level predictions for McMurdo Sound are no longer valid.

Because Terra Nova Bay is relatively close to the ice margin at the Last Glacial Maximum and appears to have deglaciated early (by 11,000 years BP) many models were attempted in order to fit a predicted relative sea level of 30 m. Attempts at fitting were made by:

1. placing ice to the south of Terra Nova Bay. Placing more than about 600 m ice to the south of Terra Nova Bay does not fit field observations and raises the relative sea level predictions at McMurdo Sound above about 25 m which is beyond realistic levels.

2. placing ice to the north of Terra Nova Bay. However, placing more than about 600 m of ice over Northern Victoria Land, which is close to the ice margin, is unrealistic because ice sheets have a glaciological tendency to thin towards their edges.

3. placing more ice inland towards the East Antarctic Ice Sheet from Terra Nova Bay. But, trimlines from glaciers that flow from East Antarctica through the Transantarctic Mountains indicate minimal thickening of the East Antarctic Ice Cap at this time too (Orombelli and Denton 1990). Thus it would be unrealistic to place much more ice inland of Terra Nova Bay.

The compromise found through various iterations of the block models is 600 m of extra ice over Northern Victoria Land and 500 m of extra ice inland of the Transantarctic Mountains.

Relative sea level predictions are made for Cape Ross, on the northern edge of McMurdo Sound between McMurdo Sound and Terra Nova Bay. Cape Ross has been discussed in Chapter 3.2.3 with respect to dating at this location and the high marine limit. A challenge with the block model was to try to match the observed marine limit of approximately 33 m about 8,000 years BP. Cape Ross, assuming it becomes ice free sooner than McMurdo Sound, needs to have had a relative sea level at least as high as Terra Nova Bay. This is difficult to match while retaining both the ice thicknesses that trimlines suggest to the south in McMurdo Sound and to the north at Terra Nova Bay and the suggested melting rate from the field observations at both sites. Figure 5.23 shows the predictions of this model fall short of reaching the marine limit in this area.

This block model is favoured as an initial representation of the true ice distribution of a model because it fits the relative sea level observations well at McMurdo Sound and fairly well at Terra Nova Bay and because the volumes of ice and retreat times have been kept as close as possible to field observations. However, it is only a block model so suffers from edge effects at the side of the blocks, there are limitations in ice placement by using blocks, and the retreat of the ice is non-linear. The following ice sheet reconstruction incorporates the block model findings while addressing some of these limitations.

5.6 The reconstruction

The previous sections outlined how, for a given ice sheet, the ice volume, the ice location and the melting history can be altered to produce a predicted relative sea level that matches the observed relative sea level. An example was given using a simple block model. Here my preferred model for the ice sheet in the Ross Embayment is presented, the *Ross5* model. It is a model that is based on all the types of information that can be brought to bear in such a reconstruction, and takes into account all of the diverse

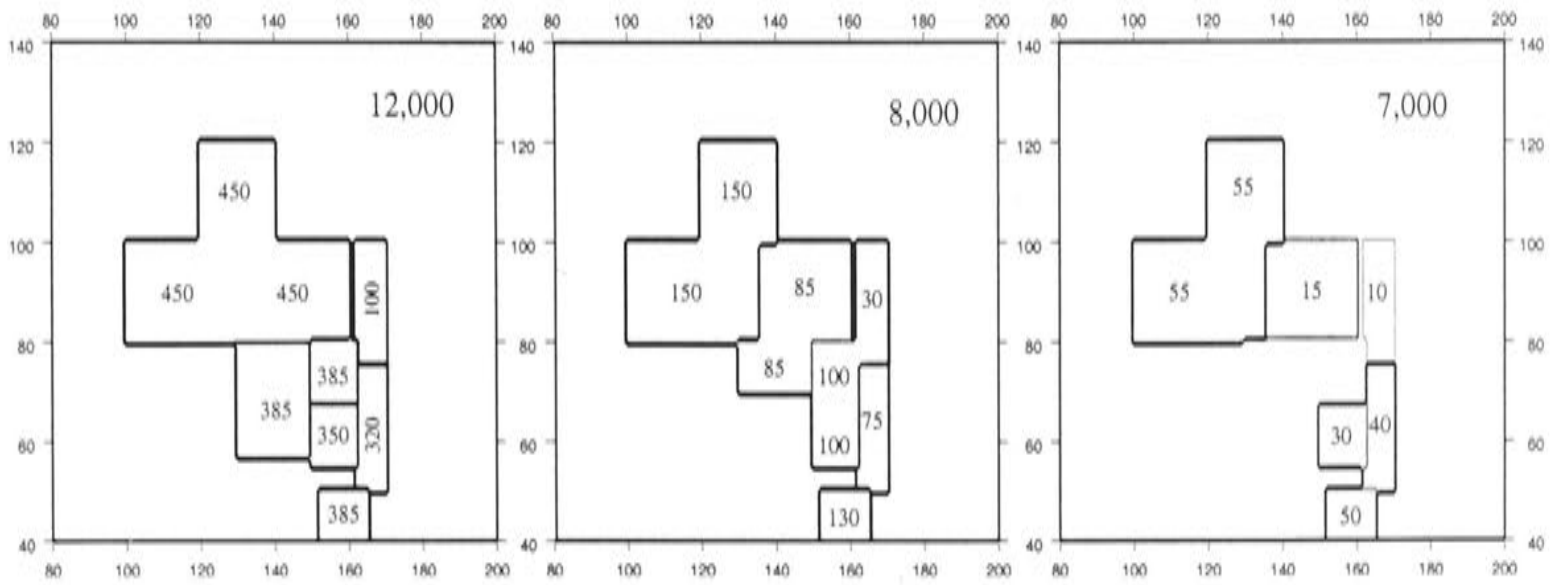

Figure 5.20: Top: Ice thicknesses at the Last Glacial Maximum for the simple block model. Some ice thicknesses have been placed into the model for separate blocks. Some boundaries do not show on this model due to the contour interval of 300 m. Bottom: Blocks for the time steps 12,000, 8,000 and 7,000 years BP are shown below with ice thickness values.

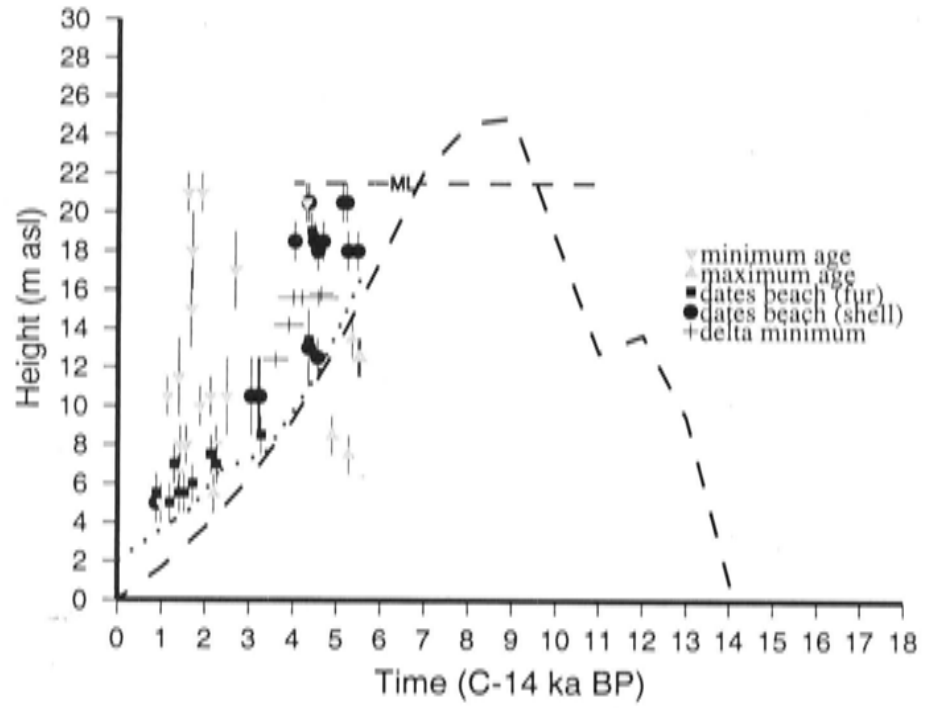

Figure 5.21: Predictions of the relative sea level in McMurdo Sound for the simple block model. The dotted line shows the observed relative sea level while the dashed line shows the predicted relative sea level. The marine limit does not have a confirmed age and therefore is drawn as a horizontal dashed line labelled ML.

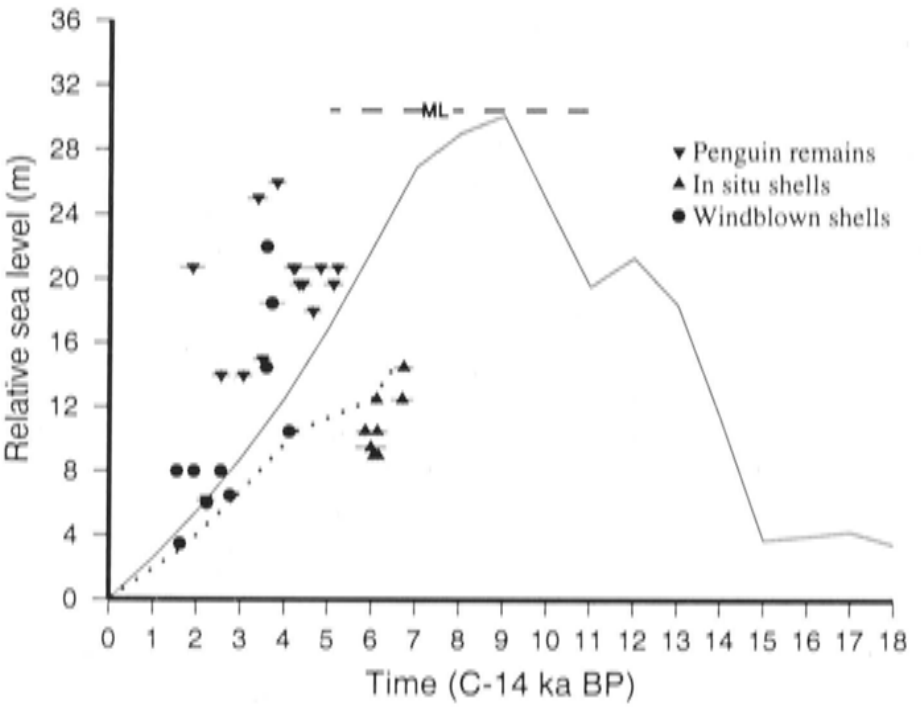

Figure 5.22: Predictions of the relative sea level in Terra Nova Bay for the simple block model. The dotted line shows the observed relative sea level while the solid line shows the predicted relative sea level. The marine limit does not have a confirmed age and therefore is drawn as a horizontal dashed line labelled ML.

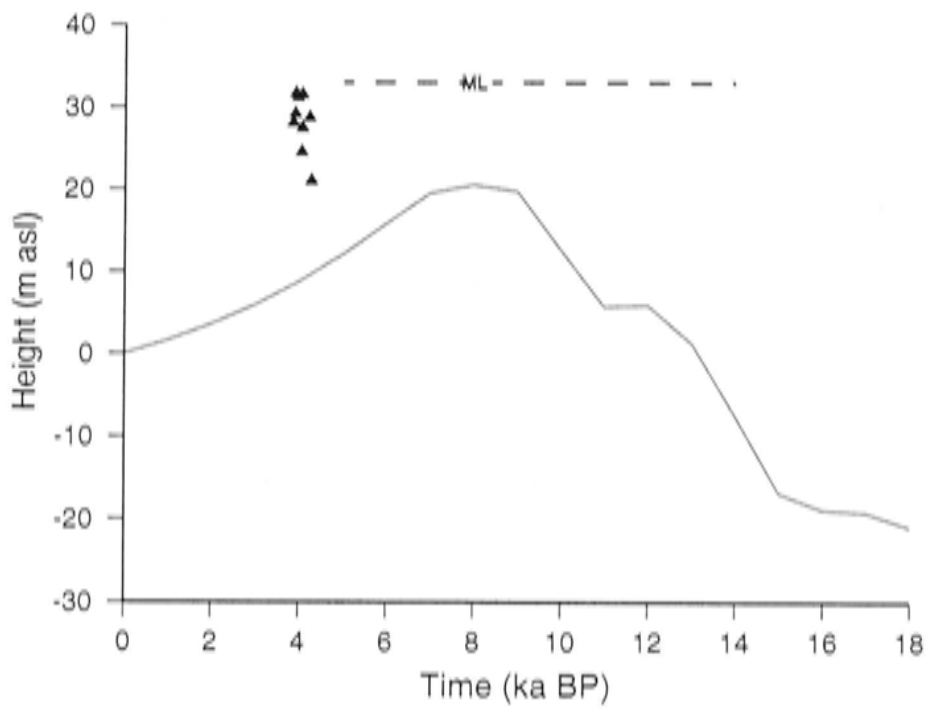

Figure 5.23: Predictions of the relative sea level at Cape Ross for the simple block model. Penguins nested above present-day sea level as shown by the triangles (Baroni and Orombelli 1994) indicating the area was ice free at that time and sea level lay below these points.

loading and timing effects illustrated in section 5.4. Most importantly the predicted relative sea level for both McMurdo Sound and Terra Nova Bay closely match the observed relative sea levels.

Because there are several variables that can be manipulated in the glacio-hydro-isostatic modelling method, such as the trade-off between the ice model and the earth model, it is not possible with this method to provide a unique solution. However, using the chosen Earth model and ice sheets for the Northern Hemisphere and distal Antarctica I believe this model is the best solution.

The Ross5 reconstruction contains 8.4 m equivalent sea level in the Ross Embayment, and 34 m overall when added to the Stuiver et al. (1981) reconstruction outside the Ross Embayment. Outside Antarctica this reconstruction uses the fennice.new+nhewice.new reconstructions for the Northern Hemisphere ice sheets (see Chapter 4) and the ma4A standard Earth model (Lambeck et al. 1998, Nakada and Lambeck 1987, and Lambeck et al. 1996). When the Ross5 model is added to the Huybrechts (1990) model, the overall reconstruction contributes 19.4 m equivalent sea level.

The Ross5 reconstruction is shown in Figure 5.24 as contour plots at the Last Glacial Maximum. The top plot is the ice surface height and the bottom plot is the ice thickness. The Ross5 model adds between 400 and 800 m extra ice at the Last Glacial Maximum over most of the Ross Embayment as the block model suggests. They only deviation from the block model values is in central West Antarctica where

1600 to 2000 m extra ice is added. This is done to enhance the fit of the Last Glacial Maximum reconstruction with the Stuiver et al. (1981) model used for the distal Antarctic Ice Sheet. It was shown earlier in the chapter that ice at a distance from the sites of relative sea level observation will not alter the predicted relative sea levels by a significant amount. The recent observations of Last Glacial Maximum ice thickness from the coastal Ford Ranges in West Antarctica by Stone et al. (2003) agree with the ice modelled in Ross5.

Ross5 is a model where the Last Glacial Maximum surface is determined based on the collated evidence from both the field observations and the preliminary modelling. From this surface the ice thickness change between the Last Glacial Maximum and the present day was calculated by subtracting the surface of the land and present-day ice sheet. This leads to the mountain peaks not receiving as much additional ice as the valleys and basins as naturally occurs. Adopting this method of calculating the ice thickness is more accurate than the method used for the preliminary block model.

The Ross5 model retreats across the Ross Embayment at the same time as for the western Ross Sea. Figure 5.25 shows time steps at 10,000 and 6,000 years BP. Ice in the Ross5 model does not retreat in the western Ross Sea as quickly as the glacio-marine evidence suggests, with ice remaining fairly close to the grounding line until about 10,000 ^{14}C years BP. Marine evidence suggests that Terra Nova Bay may have deglaciated approximately 12,000 ^{14}C years BP. Some ice remains around McMurdo Sound a little later than is likely (until 6,000 ^{14}C years BP). This retreat is different to the model proposed (subsequent to the modelling of Ross5) by Conway et al. (1999) in not pinning the ice sheet at Roosevelt Island until the very late Holocene. However, the retreat timing in this part of the Ross Embayment will not affect the predicted relative sea levels at either McMurdo Sound or Terra Nova Bay because of the great distance from these two locations.

Figure 5.26 shows the relative sea level predictions at McMurdo Sound and Barbados in the far-field using this Ross Embayment reconstruction. Predicted relative sea levels for the Ross5 model at McMurdo Sound from 6,000 ^{14}C years BP to the present day match the observations well with the marine limit at approximately 6,500 ^{14}C years BP and the curve passing through or very close to many of the observed points dating the raised beaches. It cannot be expected that the curve would match the observations perfectly because the beaches are formed mainly during storm events and not in perfect timing with a gradual relative shoreline uplift.

At Terra Nova Bay a compromise needs to be made in matching a high marine limit (approximately 30 m) and the *in situ* shell evidence. The Ross5 model does this fairly well coming close to the marine limit and below most of the maximum height dates. Ideally this curve would have a slightly flatter slope between 7,000 ^{14}C years BP and the present day.

The Ross5 model predicts a maximum relative sea level at Cape Ross of 39.3 m at

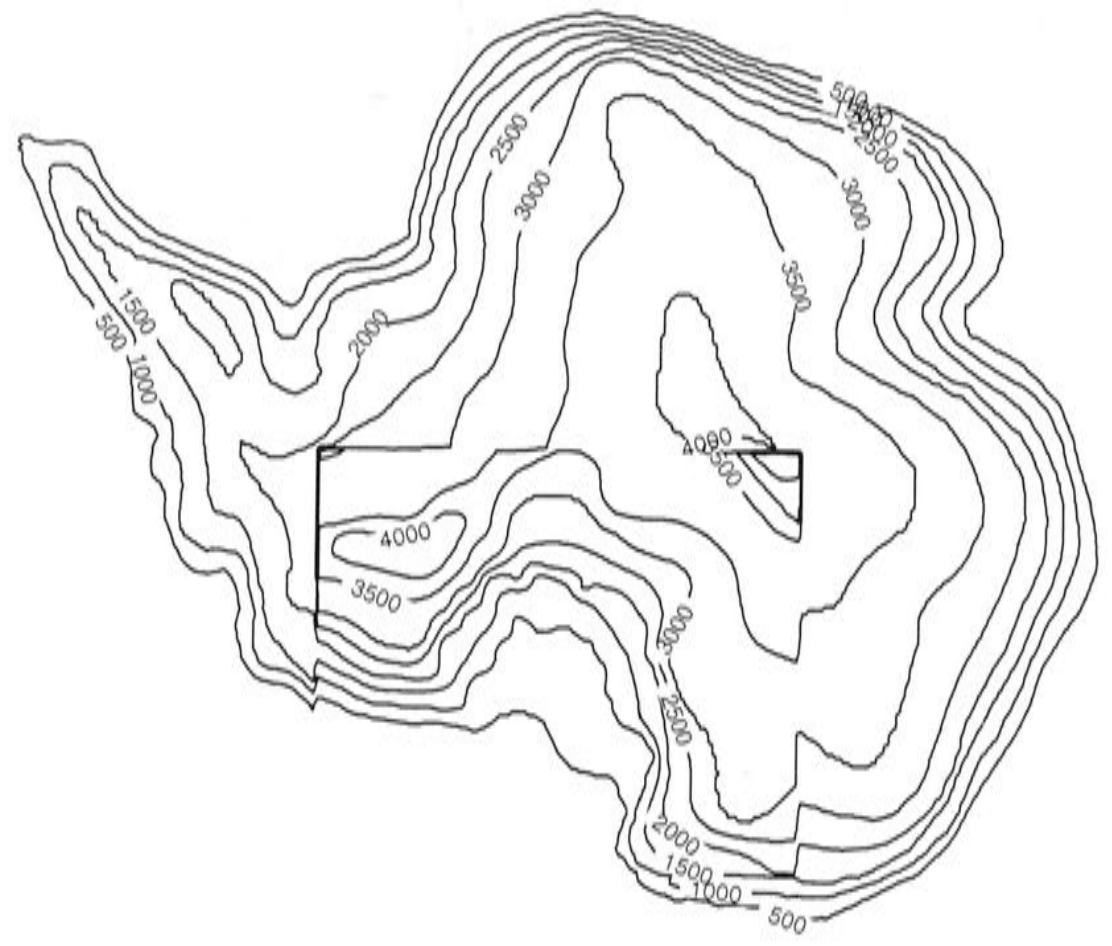

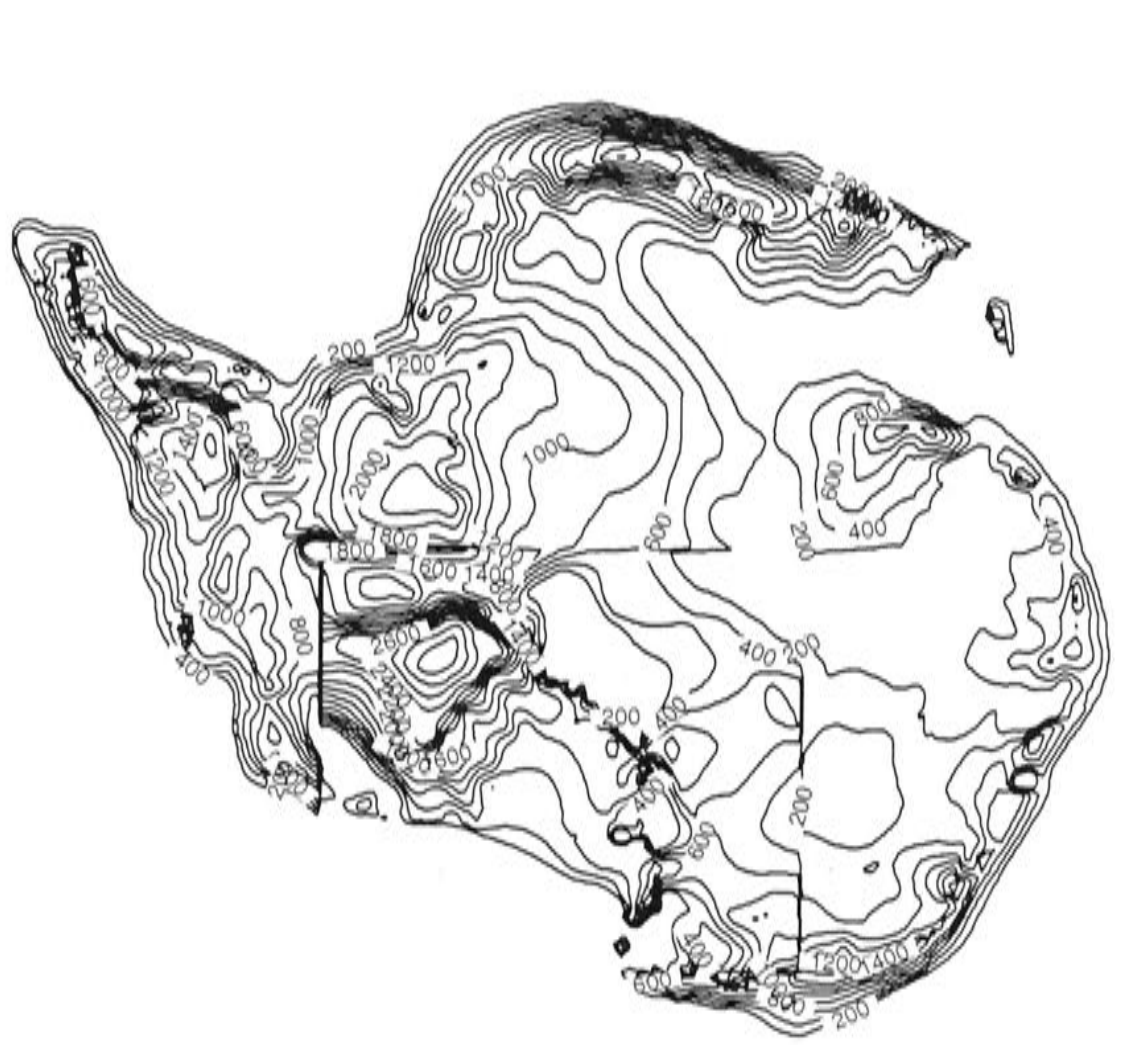

Figure 5.24: Contour plots of the Ross5 ice sheet reconstruction for the Ross Embayment. Top figure is the ice surface and the lower figure is the ice thickness.

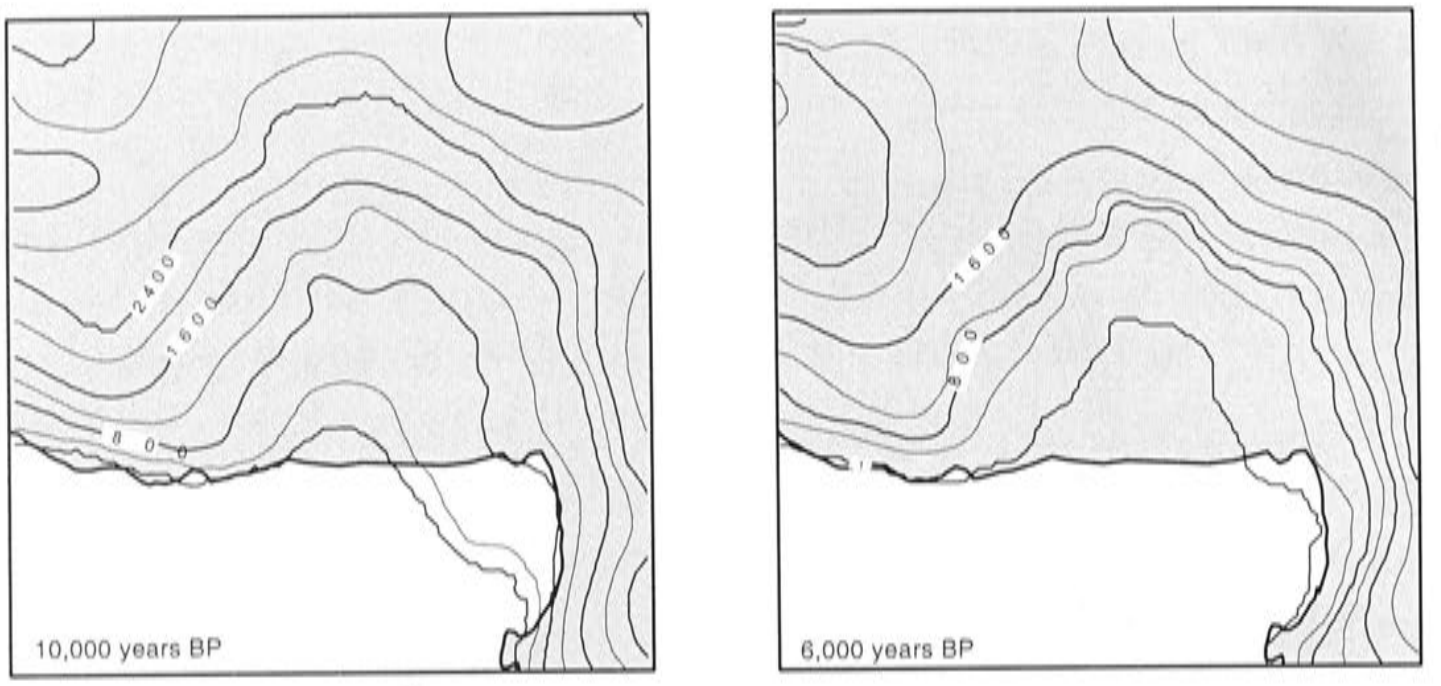

Figure 5.25: Contour plots of time steps 10,000 years BP and 6,000 years BP from the Ross5 ice sheet reconstruction for the Ross Embayment. Only the Ross Embayment is shown here. The Stuiver et al. (1981) model is used for all times steps in the distal part of the Antarctic Ice Sheet.

9,000 ^{14}C years BP and 33 m at 8,000 ^{14}C years BP suggesting that a deglaciation/ice-free time of 8,000 ^{14}C years BP would reproduce the observed marine limit.

The Ross5 model is an appropriate model for the Ross Embayment because it provides a realistic model for the Ross Embayment portion of the Antarctic Ice Sheet without extra ice over mountain tops, and it provides a good fit to the observed marine limits and relative sea levels for McMurdo Sound and Terra Nova Bay.

5.7 Summary

The various aspects of the structure and retreat of an ice sheet have been investigated to see what effects they have on predicted sea levels in the Ross Embayment. By combining the spatial and temporal distribution of data points in the Ross Embayment and the far field it is possible to constrain many of these aspects.

The influence of ice sheets melting in the Northern Hemisphere (fennice.new + nhewice.new) and the distal Antarctic Ice Sheet (Stuiver et al. 1981) is about 4 metres above present-day sea level at 6,000 years BP. Hence, +18 to +24 metres of isostatic response to local ice is required to match observed relative sea levels.

Limitations on ice sheet extent and timing are available from other field observations in the Ross Embayment. General consensus places the grounding line at the shelf edge in the central and eastern Ross Sea at the Last Glacial Maximum and south of Coulman Island in the western Ross Sea. Observations of 300 to 1,100 metres of ice-

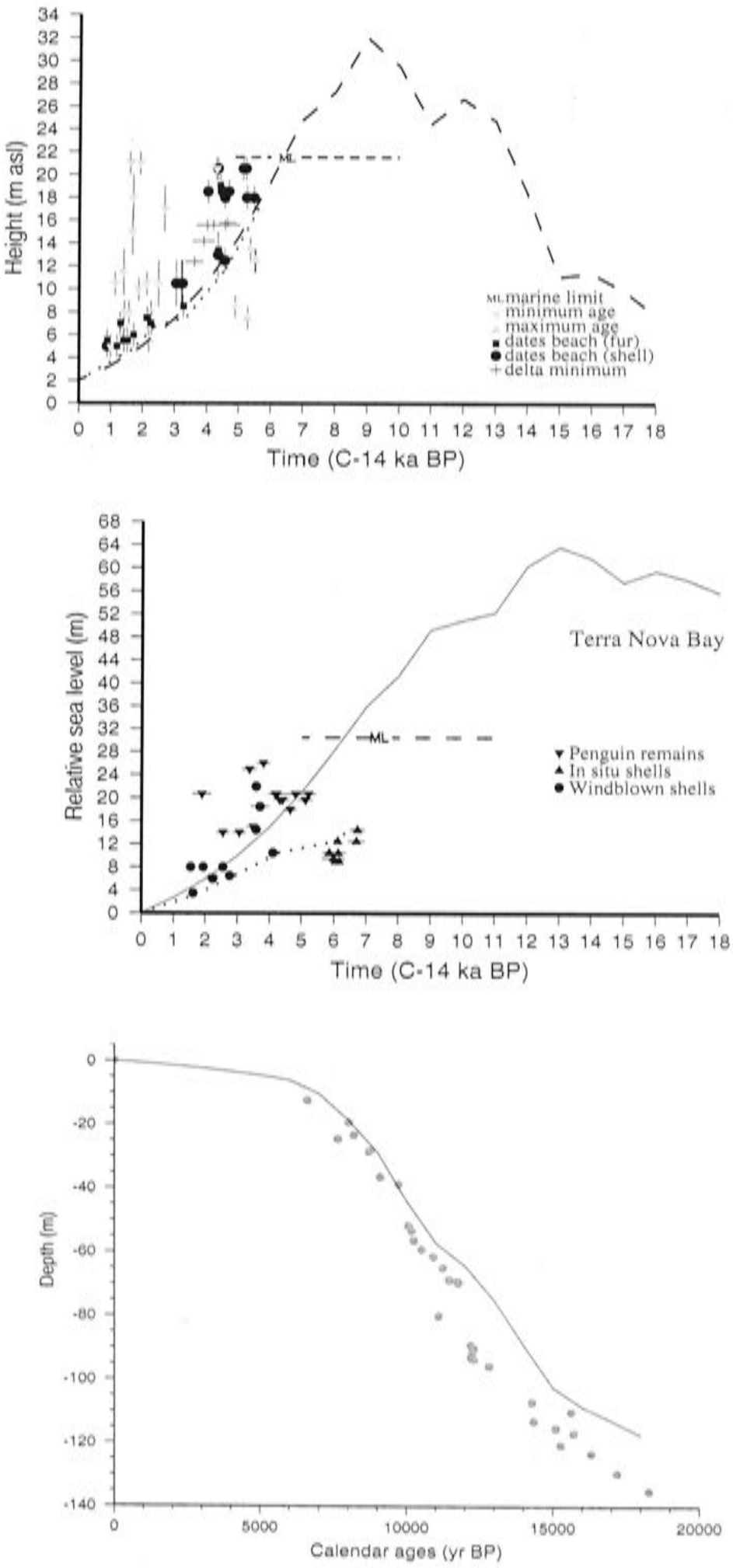

Figure 5.26: Predicted relative sea levels for the Ross5 reconstruction in McMurdo Sound, Terra Nova Bay and Barbados (far-field). The dotted lines show the observed relative sea level while the dashed (McMurdo Sound) and solid (Terra Nova Bay) lines show the predicted relative sea levels. The ML and dashed line on the plots indicates the marine limits. At Terra Nova Bay the penguin remains and the windblown shells represent an upper bound on relative sea level.

sheet thickening are recorded around the Ross Embayment, although in many situations a correction for ice grounded below present-day sea level must be made which gives a thicker ice sheet.

The ice sheet has been shown to be sensitive to the timing of the grounding line retreat in the Ross Embayment with a migrating grounding line required.

The Stuiver et al. (1981) ice sheet used for the distal Antarctic Ice Sheet is shown to overpredict the relative sea levels when used for all of Antarctica (including the Ross Embayment), but if the ice sheet in the Ross Embayment area is scaled to 27% of the original the predictions match the observations well.

The importance of the timing of melting was illustrated using the Huybrechts (1990) model. This is a late melting model that overpredicts the relative sea level in the Ross Embayment. Stretching the duration of melting by commencing melting early the peak in predicted relative sea level is moved and overall predictions reduced close to the observed relative sea levels.

A series of block models demonstrated the importance of local ice directly over or next to a site of observed relative sea level. A small block of ice of approximately 0.2 m equivalent sea level can raise local predictions by 10 metres. The lesser importance of ice further away in the Ross Embayment was also demonstrated by placing a large block of ice of approximately 1.9 m equivalent sea level over Marie Byrd Land. This block predicts almost no change in the relative sea level in McMurdo Sound. Using this knowledge and the field observation constraints a model for the ice sheet in the Ross Embayment was constructed using blocks of ice. After many iterations a preferred model was selected that predicted well the observed relative sea levels at McMurdo Sound and Terra Nova Bay.

Finally, a full reconstruction for the Ross Embayment, Ross5, was developed as the preferred ice sheet model. Predictions for relative sea level at both Terra Nova Bay and McMurdo Sound closely match the observations. The predictions give the marine limit at 6,400 years BP for McMurdo Sound. This reconstruction adds 8.4 m equivalent sea level for the Ross Embayment area and the timing and ice volume agree with the Barbados far-field observations.

Chapter 6

Conclusions

6.1 Summary and conclusions

Observations of sea levels around the Earth indicate that Last Glacial Maximum equivalent sea levels were about 130 metres lower than the present day and that sea level rose rapidly towards present levels from about 18,000 to 7,000 years BP. This observed change establishes the volumes and rate of melting of the global ice sheets but does not establish where the melt-water came from. It is generally agreed that the Northern Hemisphere ice sheets did not contain enough ice to explain all of the observed sea level change and that there must have been an ice volume change in the Antarctic Ice Sheet since the Last Glacial Maximum. The amount of this change and how it was distributed, however, remain uncertain.

Where, when and how much ice was there in the Antarctic Ice Sheet since the Last Glacial Maximum are the questions addressed in this thesis. Specifically, what has been the evolution of the ice sheet in the Ross Embayment of Antarctica? The Ross Embayment area is important because it is one of the larger drainage basins of the Antarctic Ice Sheet.

The loading of ice sheets and the associated redistribution of global water on the Earth results in a spatially and temporally complex pattern of sea level change through the process of glacio-hydro-isostasy. With a knowledge of the rheology of the Earth and models of the ice sheets, the isostatic and eustatic changes in sea level can be predicted and compared with observed relative sea levels in order to refine the ice sheet models. This approach has been successfully used in other areas and is developed here with specific application to the Ross Embayment. Measurements of local sea level change are used to determine constraints on the part of the Antarctic Ice Sheet located in the Ross Embayment.

Observations of former sea levels in the Ross Embayment come from raised shorelines along isolated patches of ice-free coast. The evidence for the raised shorelines consists of raised beach ridges (both sand and boulder ridges), sea-ice cut bedrock

platforms, boulder pavements, and a delta deposit. To supplement existing information, shoreline evidence from localities in McMurdo Sound, Cape Ross and Cape Hallett was examined (Figure 1.1, 1.2, and 1.3). Three dating techniques were applied to obtain the timing of the relative sea level fluctuations — radiocarbon, optically stimulated luminescence and surface exposure dating. In Antarctica, all three methods have major limitations and one of the objectives of this thesis was to compare results of the methods as a guide for future work.

Radiocarbon dates were obtained from a raised delta deposit, a beach ridge, and from penguin nests on top of beach ridges. Ten samples provided ages between the present day and 5,840 calibrated years before the present and were combined with dates from Hall and Denton (1999) to form a relative sea level curve for McMurdo Sound (Figure 3.3).

Two samples dated using optically stimulated luminescence on a beach sand at Marble Point have late-Holocene ages. Despite some partially bleached grains giving large errors there were sufficient numbers of grains dated in this single grain method to be confident that the two samples were deposited during the Holocene. This is an important finding because it confirms the Holocene age of the radiocarbon samples and indicates that estimations of parameters in the dating method such as the reservoir correction are appropriate.

Surface exposure dating using the cosmogenic isotope chlorine-36 was tried on boulders, bedrock platforms, and boulder pavements. When compared with the radiocarbon and optically stimulated luminescence the ages obtained from this method were too old by several to many thousands of years. After assessing possible sources of error, I conclude that the bedrock samples appear too old because there was not sufficient erosion to remove the existing chlorine-36 from the rock. The boulder samples (glacial erratics either reworked into the beaches or ice rafted into place) also contained a record of an earlier exposure rather than being freshly exposed since the Last Glacial Maximum.

Two different corrections and a series of forward models have been used to constrain a possible prior-exposure history for the chlorine-36 ages. A constant offset correction is attractive because it implies a constant history for McMurdo Sound but in applying a best fit offset some ages become negative so this correction is not favoured. A non-constant offset implies an error in a parameter and this is hard to justify because any uncertainty in modelling parameters tend to make the ages older rather than younger. The forward models do illustrate that it is possible to suggest a consistent history for prior exposure and burial of samples. However, it is not possible to constrain the time of prior exposure (e.g. the Last Inter-glacial) without a second isotope such as beryllium-10 to indicate the length of burial time of the samples. At the time of dating, the ^{10}Be facility at the Australian National University accelerator mass spectrometer had not yet reached sufficient resolution to use this isotope as well.

Field observations indicate that sea levels since glacial retreat extended up to 33

metres above sea level at Cape Ross and lower to the south. Cape Hallett, the final field site, is much further north and was only able to provide a single point of sea level information (sea level was below 2.5 metres at 1,900 years before the present). Terra Nova Bay to the north of McMurdo Sound is the only other site in the Ross Embayment with an observed relative sea level curve. Published radiocarbon dating constrains this site from about 7,000 years to the present day with a marine limit of about 30 m.

The new observed relative sea level curve for McMurdo Sound provides the constraints that have been incorporated into the Ross Embayment ice sheet modelling. Predictions of relative sea level on the Scott Coast rely on several factors which have been discussed in turn — a rheological model for the Earth, a contribution of sea-level change from the Northern Hemisphere ice sheets (far-field effect), a contribution of Antarctic Ice Sheet ice from outside the Ross Embayment (intermediate-field) and the contributions from the change in the local ice cover.

A rheological model of the Earth is required for the glacio-hydro-isostatic modelling to determine the crustal rebound. While the rheological parameters for the Earth cannot be independently constrained for the mantle beneath Antarctica I have adopted a model based on rebound analysis from beneath the better constrained Northern Hemisphere ice sheets. The uncertainties from the Earth model are smaller than the errors arising from uncertainties in the ice sheet reconstructions (Figure 4.9). The Earth model used here is a three-layer laterally homogeneous model with a 65 km thick lithosphere, an upper mantle viscosity of 4×10^{20} Pa s, and a lower mantle viscosity of 1×10^{22} Pa s.

The ice sheets from the Last Glacial Maximum in the Northern Hemisphere contribute to the predicted relative sea level change in Antarctica mainly by changing the equivalent sea level and, to a lesser degree, by hydro-isostatic effects. The latter, in the absence of Antarctic ice sheet melting, introduces a small amplitude mid-Holocene highstand. Two models for the Last Glacial Maximum Northern Hemisphere ice sheets were investigated. The two models gave essentially the same prediction of relative sea level in the Holocene (maximum difference of 0.28 m — Figure 4.10) so the standard model was adopted (nhewice.new+fennice.new). The melting of the Northern Hemisphere ice sheets raised the relative sea levels on the Scott Coast above the present-day from 6,000 years before the present to the present day. Hence, less local ice is required in the Ross Embayment to produce the raised shorelines than would have been required if far-field melting was ignored.

The part of the Antarctic Ice Sheet outside the Ross Embayment has the glacio-hydro-isostatic effect of lowering the relative sea levels in McMurdo Sound because of mantle flow away from beneath the rest of Antarctica. If there was no change in the ice sheet in the Ross Embayment the area would lie in the broad peripheral bulge region of the distal Antarctic Ice Sheet. This distal Antarctic contribution at 6,000 years before the present ranges from -6.5 m to -1.5 m (Figure 4.14) according to the chosen ice

model.

Combining the Northern Hemisphere ice with that from the wider Antarctic Ice Sheet gives a maximum predicted relative sea level of +2 m to -4 m at 6,000 years before the present (Figure 4.15) depending on the choice of ice sheet models. When compared with the observed relative sea levels, this shows that there must have been additional ice in the Ross Embayment during the last glacial cycle. Sufficient extra local ice is required to produce a +18 metre to +24 metre relative-sea-level contribution to create the elevated shorelines up to the 20 metre marine limit observed in McMurdo Sound.

Three existing ice models were examined for the Ross Embayment and modifications were made to these to investigate ice volumes and melt timing of these models. The Stuiver et al. (1981) reconstruction significantly overpredicts relative sea levels at McMurdo Sound and Terra Nova Bay. If the ice thickness is uniformly scaled, a reduction to 27% of the original model is required so that the predictions match the observed values of relative sea level. This suggests that a model without ice streams for the Last Glacial Maximum and pre-Holocene in this part of Antarctica may not be valid.

The Huybrechts (1990) reconstruction, based on the assumption that the Antarctic Ice Sheet responds primarily to the rise in sea level from the melting of the Northern Hemisphere ice sheets causes a very high predicted relative sea level in Holocene time. In the Huybrechts (1990) reconstruction most of the melting of the Antarctic Ice Sheet occurs after 5,000 years BP. However, if melting occurs instead over a longer time interval from 10,000 years BP to the present day then the rate of relative sea level change is reduced and the peak relative sea level is lowered so that predicted relative sea levels fit the observations. While this shows that melt timing can have a large influence on predictions, the melt timing can also be constrained by considering far-field observations that record the volume and timing of melt water entering the oceans. The Huybrechts (1990) reconstruction, for example, has insufficient change in ice volume in the pre-Holocene to explain the difference between the observed global sea levels and the Northern Hemisphere contributions.

With the Nakada et al. (2000) reconstruction for the Antarctic Ice Sheet it has been demonstrated that small volumes of ice strategically located can accurately fit local relative sea levels. Further modelling using the Nakada et al. (2000) reconstruction as a base demonstrated that even a block (of size 400 x 400 x 0.4 km) containing only 0.2 metres equivalent sea level can raise the predicted local relative sea level by 10 m when placed directly over a site. It has also been demonstrated that a much larger volume (approximately 1.9 metres equivalent sea level) of ice can be placed in Marie Byrd Land (West Antarctica) at some distance from either McMurdo Sound or Terra Nova Bay and have almost no influence on predicted relative sea levels. Hence, where there are no observations of relative sea level it becomes very important to have other

field constraints such as trimlines indicating maximum ice heights.

With all of the above ice reconstructions it is possible to find modifications that produce Holocene ice volumes, location and melting such that agreement exists with the relative sea level observations from the mid-Holocene to the present day. Differentiating between such models, in the absence of a better distributed relative sea level data set, requires other observational data such as that from marine geology and glaciology.

Using the knowledge acquired from investigating existing models for the Antarctic Ice Sheet and field observations, a preliminary series of models have been developed that consist of blocks of ice distributed over the Ross Embayment. Iterations of this model yielded ice volumes that are within observed limits, are glaciologically realistic, and give a best-fitting model to the relative sea level observations at both McMurdo Sound and Terra Nova Bay. While such predictions could be repeated for each Earth model (not just the adopted ma4A Earth model) computing and time constraints limited the range of Earth models that could be tested. However, variations on the best fit model indicated that a thinner lithosphere (50 km instead of 65 km thick) predicts the relative sea level in McMurdo Sound and Terra Nova Bay even better than the standard Earth model, although it does not reach the observed marine limit at Cape Ross (33 metres above sea level).

The preferred ice sheet reconstruction for the Ross Embayment, the Ross5 model, is an amalgamation of all the outlined results. This model has the characteristics of being thinner over the mountain tops than the valleys, thicker in the interior of West Antarctica to match up with the Stuiver et al. (1981) reconstruction used for the distal Antarctic Ice Sheet, matching trimlines from glaciers and fitting the grounding line. Predictions of relative sea level change for McMurdo Sound are now in good agreement with observed values, including those at Cape Ross.

The Ross5 model (Figure 5.24) uses the fennice.new and nhewice.new models for the Northern Hemisphere ice sheets and the ma4A model for the Earth. This combination of ice sheets is most consistent with the more recent field evidence for the history of ice retreat and it gives global ice volumes that are in reasonable agreement with the far-field evidence as well as the Northern Hemisphere rebound analyses.

Because of uncertainties in the Earth model and the poor constraint on the early melting period, the Ross5 model is not necessarily the definitive answer but rather presents the best model found for the observations available for this thesis.

6.2 Discussion

Global positioning measurements of the present day crustal motion may soon impose further constraints on the ice sheet modelling. Predictions of the present-day relative sea level changes in the Ross Embayment from the model Ross5 are given in Figure 6.1. The relative sea level change on the Scott Coast is about 1.3 mm/year. Data currently

being collected requires a longer record (pers. comm. T. Wilson, Byrd Polar Research Center) to obtain a satisfactory signal and also requires an ability to distinguish the glacio-hydro-isostatic effects from any other crustal movements in the area. Figure 6.1 also indicates that the present day rebound from the ice sheet is not uniform over the Ross Embayment area and that a location in Northern Victoria Land would be a better site to seek measurement of the present day glacio-hydro-isostatic rebound signal. The glacial rebound signal over the area slightly east of the Transantarctic Mountains is very small so that the observations from around this region are likely to exhibit mostly a tectonic signature.

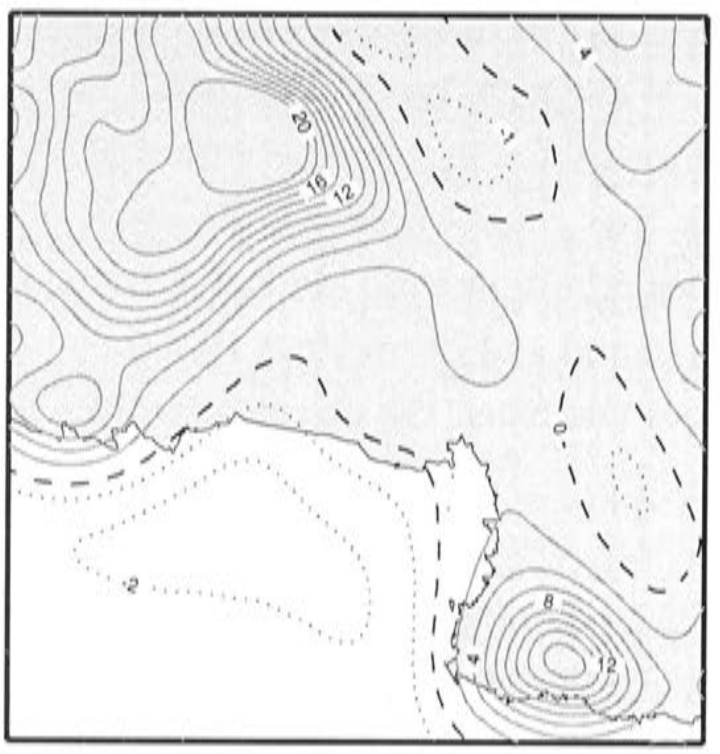

Figure 6.1: Present day relative sea level change in the Ross Embayment from the Ross5 model, giving some idea of the crustal rebound from this reconstruction. Contours are in mm/year and along the Scott Coast this is about 1.3 mm/year.

Far-field data and further constraints on the late-Pleistocene ice volumes in the Northern Hemisphere ice sheets would give a clearer idea of the volumes of ice required in Antarctica at the Last Glacial Maximum as well as of the timing of the southern ice sheet melting. Establishing palaeo-ice sheet elevations from nunataks close to the inland edge of the Transantarctic Mountains and in Marie Byrd Land would give valuable constraints on Last Glacial Maximum ice volumes. Stone et al. (2003) collected evidence of maximum ice sheet elevations from the coastal mountains of West Antarctica as well as dating the ice sheet retreat. More work of this nature in West Antarctica would provide worthy information for ice sheet modelling. Further marine grounding line evidence, especially from the central and eastern Ross Sea will allow this part of

the ice sheet to be better constrained and the ice sheet modelling to be improved.

Appendix A

Field Notes

This appendix is a precis of descriptive notes taken in the field from each site. They are placed in this thesis with the intention of being accessible for future workers who intend to visit these sites and would benefit from this knowledge which would not usually make it into published papers. Sites are described from south to north along the Scott Coast.

A.1 Commonwealth Stream Delta

This terrestrial delta is a very large, broad delta at the head of Explorers Cove. It is flat in slope and has only 9 m of relief over 320 m. The delta is dominantly medium sand with an occasional granodiorite cobble. The delta probably formed after some shore uplift from glacio-isostasy as there is no sign of any shell samples, despite the mollusc *Adamussium colbecki* being abundant in Explorers cove at present (Berkman 1994).

A.2 Cape Bernacchi

Beaches at Cape Bernacchi consist of 30+ cm boulders which are generally larger further up the beach and there is a higher concentration of boulders at the crests of the ridges. Frost wedges are developed on the beaches. The rock outcropping at Cape Bernacchi does not form into the sea ice eroded rock platforms seen further north. The marine limit is best defined by a change in slope to the moraine above.

A.3 South Stream

The present-day beach at South Stream is very flat and sandy with melt pools behind a low ridge. Ridges are not steep and consist of a wide (10 m) boulder zone of slightly more rounded stones, pebbles and sand. Ridges appear to decrease in height and grain size towards the stream and turn into hummocky ground with pits (30 cm deep). On

the south side of the stream the beaches are wide (40 m) with a rise of approximately 2.5 m to their crests and are composed of well rounded clasts. Further details of the delta at South Stream are in chapter 2 and also described in detail by (Webb 1997).

A.4 Marble Point

Marble Point possibly had a lagoonal type environment with a spit that formed joining from the mainland to the point at some stage in the mid-Holocene. Most of the beaches here are high energy with well-rounded boulder size material. The higher energy beaches face the north to north-east which is open to the sea and has a longer fetch. The beaches are well defined by about 30 cm of fine sand in the palaeo-swash zone. A pitted beach at Marble Point suggests rapid sedimentation and ice formation. On the surface of the beaches the amount of sand in general increases on the higher beach ridges which is a result of weathering, especially on the softer rocks like the marble and odd piece of granite. These form very rounded shapes and as individual crystals weather out they form a part of the sand. This can clearly be seen in the lee of marble boulders which have a coarse 5 to 7 mm white crystal tail which contrasts to the much browner sand.

Higher on Marble Point the ground has the beach/wave washed appearance of more rounded boulders — more like a pavement formation and less of the very random appearance of the glacial erratics covering the hill slopes around the area. It is not clear exactly where the marine limit is.

The lithology of the beaches are a representation of all the rock types in the area and contain marble, small amounts of Fe-rich granite, diorite (from dykes), volcanics, a very mafic intrusive, and gneiss.

Between Marble Point and Surko Stream the beaches have been disturbed with bulldozing. Much of the ground in the swales (in January) is very wet with prolific algae and moss development. Snow still lies in patches which in warmer weather ablates or melts quite rapidly. The active storm beach is extremely rubbly with no sand obviously present.

Below is a descriptive transect on the east side of the main raised beaches extending out to Marble Point across the beaches from south to north. The present sea ice is attached to the shore and probably does not break out. Beach is a well sorted sand with scattering of angular to very angular boulders approximately 10 cm in diameter.

The first indistinct beach ridge is approximately 30 to 50 m from the present shore on a gentle slope. Below this is poorly defined with the general sandy substrate and angular to subangular boulders averaging 10 to 20 cm in diameter.

The first distinct ridge is low angle with slight cusp formation (λ approximately 4 to 5 m). The beach surface is about 50:50 mix of sand and cobbles under a pavement of large crystals and sub-rounded to rounded cobbles with a size range 3 to 20

cm. Lithologies are dominantly granite, granodiorite, diorite and marble. Cobble size increases below the berm (about 10 cm below).

A swale (major) between this ridge and the 2nd major ridge is 20 to 30 m wide and contains marble bedrock. The swale is flat and snow covered except in patches which are sandy with a pebbly (1 to 2 cm) surface with odd larger cobbles (sub-angular to sub-rounded). There is an indistinct minor ridge in the middle of the swale.

Second distinct ridge has been modified by bulldozer action but has more boulders with sub-rounded to rounded clasts up to 30 to 40 cm in diameter with a larger percentage of bigger clasts than ridge 1. The ridge is much steeper and higher with a flat berm than the first. The clast lithologies as the same as before but contain a greater percentage of diorite. The pebble size is larger on the beach.

The second ridge slopes gently into a deep swale before climbing steeply onto a less well defined, yet still distinct, third beach ridge over a distance of about 8 m. This third ridge is variable over distance but has pavement like features, with a flat surface containing half buried stones. The lithology of the cobbles in the beach is the same as in ridge two. The surface of the beach is a coarse sand covered by pebbles a few mm to few cm in size. The ridge itself is quite flat with no real distinctive features and has a 2 to 3 m wide front face.

The swale between the third ridge and the next, pitted ridge is extremely wide and flat (approximately 60 m) very low, poorly developed ridges in a few places across the swale, especially towards the eastern edge of the area. The 'ridges' in the swales are like development seen in the lowest swale (described above) except with more dolerite clasts.

Ridge four is the high pitted beach described in Nichols (1968). The beach berm is high and rises steeply out of the swale. The cobbles on the beach range in size from a few cm up to approximately 20 cm in size and are sub-rounded to rounded (with rounded being dominant). The dominant lithologies are diorite and granodiorite with some marble, volcanics and granite. Weathering of the boulders and cobbles is much greater (chemical weathering) on this beach compared to the northern side (iron oxide stains on rock surfaces) of the headland.

Northern side: This side of the point appears to receive more physical and less chemical weathering. The surface is made up of an approximately 50:50 matrix of sand and boulders. There is a coarse sand on the surface which is covered by angular to sub-angular clasts from a few mm to 2 cm in size. The clast lithologies on the beaches are the same as the southern side. The average boulder size is 15 to 30 cm in diameter with the largest being approximately 50 cm in size.

There is a very wide (100 to 150 m) swale area between the top beach on the south side of the headland and the top beach on the northern side. The swale is predominantly flat with small rises and pavement like material with subangular clasts within a sandy matrix. The top beach ridge has a berm 4 to 5 m wide and drops about 2 m to the

front swale over a 3 to 4 m distance. Hence, it has a steep front face to it with only a slight back slope. The matrix is a sandy material with a covering of mainly 3 mm size crystals on top. The average cobble is subrounded and 5 to 15 cm (with the largest clast seen about 50 cm) in diameter. Boulders make up a reasonable proportion of the beach with a diorite and granodiorite mix of lithologies.

The swale in front contains a small, poorly defined ridge. It is made up of predominantly sandy to coarse sand to 4 mm pebble size material with larger cobbles to 30 cm. There is not much of a swale between this ridge and the next ridge down. In places along this beach westwards from Marble Point a number of smaller intervening beaches appear and disappear laterally along the beach.

Second major beach down is not as large as the top beach and is sandier. The berm has an approximately 0.5 m rise and is 2 to 3 m wide. The boulders on this beach are sub-rounded granodiorites, and diorite dominantly with some marble. The largest clast is only 30 cm with the main size range 10 to 15 cm. The beach has a sandy matrix with sub-angular (<1 cm) pebbles of a mixed lithology.

The next swale down towards the sea has an intervening ridge approximately 1 m down similar to the previous swale. There is a total drop of about 2 metres between the two berms of the ridges. The lower berm is very flat and (at the eastern end) wide. It has about 30% subrounded boulders predominantly granodiorite in lithology. There is a definite front to the berm with a drop of 1 to 2 m.

The front ridge is the active storm beach today. The berm has a height of 2.5 to 3 m. The ridge is predominantly bouldery with very little matrix and what matrix there is consists of sand with pebbles. The dominant lithology is granodiorite and diorite with some marble. The clasts are sub-angular to sub-rounded with larger clasts up to 90 cm. There is active cusp formation with a wavelength of 8 m wide and 4 m deep. The beach berm has two levels with an approximately 1 m drop in-between the levels. The higher berm has a greater percentage of larger clasts.

A.5 Kolich Point

The beach ridges at the point are high - the active beach storm berm is 4 to 5 m above sea level with a large, deep, water filled swale behind. There is cusp formation of a wavelength 10 to 15 m and 5 to 10 m deep and very little matrix. Boulders look like they are still being rounded with 'knock' marks from other boulders on the corners. The other raised beach berms are almost as high as the active berm with short, sandy swales. The dominant material is large (up to 1 to 2 m in diameter) diorite boulders that are well rounded. Rounding on boulders is greater than at Marble Point. The beaches rapidly become much lower towards the south because of a lower wave energy. North of the point the beaches become a small cliff with ridges at the base and beyond the cliffs is a flat beach area about 200 m wide with fluvial action. There is a clearly

defined marine limit with a change in the lithology to polymictic, and also by a change from mainly rounded rocks with sand to a moraine like angular fragments and varying sizes.

Figure A.1 shows a cross-section through a sandy beach to the south of Kolich Point and it is a typical example of a sandy Antarctic beach. There are two berms exposed in this example with the first berm displaying gravel storm overwash deposit. This consists of a gravel and small-boulder layer within the sandy beds. The slope up to the top of the berm shows layered sands with minor cross bedding flattening out to horizontal layered sands on top of the berm. A lack of any major crossbedding indicates a low energy environment. Dipping bedding occurs at the back of the beach area where the waves have washed over and deposited interbedded coarse, pebbly sand and medium grain size sandy beds. These trail off away from the berm top and are replaced by aeolian dunes dipping back towards the beach. The beds are crossbedded and contain a well sorted medium to coarse sand. These probably formed by wind action from behind the beach (estimated from looking at deflation tails off local boulders). There is evidence in one spot in this beach section of ice being incorporated into the beach. Below the top horizontally layered sands, is a patch of convoluted bedding which appears to be formed by the deformation of the sands in this area when ice melted (alternatively the deformation of a semi-plastic unit). Larger examples of ice in beaches are seen at Marble Point where pieces of ice have melted leaving large (2 to 3 m) pits which can be up to 2 metres deep in places.

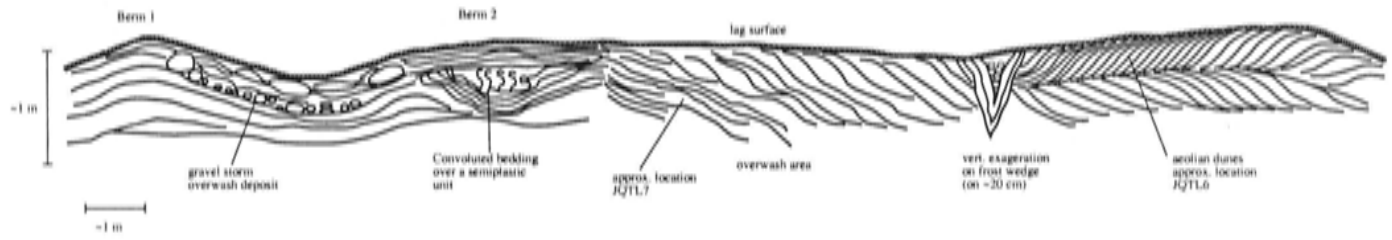

Figure A.1: Cross section through a sandy beach south of Kolich Point

A.6 Spike Cape

Spike Cape consists of a series of raised beaches (well developed) along the mainland with two low-lying tombolos connecting former islands. The two former islands have rocky beaches and rock platforms developed with cliffs on the seaward sides. The marine limit is a very well defined line with a change of monolithic to polylithic clasts that are angular and variable in clast size (very similar to Kolich Point). The marine limit shows up from a distance as a colour change to brown. The rock lithologies in this area range from granodiorite and diorite to gneisses and quartzite. The rock platforms around the two former islands are not well stepped (like Marble Point) and are are difficult to correlate to the beaches. On the mainland part of this area, by comparing

aerial photos from the 1960's to present day, ice extents there is evidence of the Wilson Piedmont Glacier having advanced over some of the raised beaches, and retreated again leaving the beaches undisturbed. There is evidence of ice push features on the beaches here as well as the typical pitting. The beaches to the north are altered by ponding in behind the ridges and overflow deposits.

High on the hill (on the mainland) there is a series of benches running parallel to the beaches, possibly cut by glacial action. One set of striations run along the benches. These are overprinted by another set of striations directed seaward. This area does not have any volcanic rocks in the moraine, whereas the two former islands do, suggesting that ice over the mainland was Wilson Piedmont Glacier ice and the Ross Sea drift covered the two former islands (more details are given in Webb (1997)).

A hole dug in the top beach at Spike Cape is described below:

3 to 4 m from the marine limit on a frost wedged fine gravelled deflation surface. The surface has boulders 1 to 10 cm in diameter of a mixed lithology. The deflation surface has fewer boulders than the beach ridges below.

0 to 160 mm: Deflation surface on top consisting of granodiorite and garnet gneiss pebbles up to 4 cm. Beneath is a fine to coarse unbedded sand. Coarser towards the top and gradually fining down. Bottom contact is abrupt but the grain size does not change. Material is brown in colour.

160 to 250 mm: Ripple laminated sands. Mid-sized well sorted sands which are interpreted as an overwash deposit. Occasional small pebble (few mm in size). Clasts are the same lithology as the surface. Ripples are of approximately 3 to 4 cm wavelength by 4 to 5 mm in height. Light brown to grey colour.

250 to 360 mm: A pebble layer which appears in parts of the hole to be rippled or at least layered with the sands above. Pebble layer is bedded on a fine (few mm) scale with granite/granodiorite pebbles from 1 to 2 mm up to 21 x 10 x 10 mm. The pebbles are poorly sorted and angular. Bedding is horizontal. Matrix supported with light brown to grey sand.

360 to 550 mm: Gradational contact on top into finer gravels. Permafrost layer begins at 370 mm. Difficult to see any bedding below this level. Gravels are fine 3 to 4 mm and well sorted with sand.

550 to 700 + mm: Frozen fine to medium sand. Appears massive. The contact to the above unit is wavey and abrupt with scours 2 cm x 5 cm.

A typical swale in this area is rocky with sub-rounded pebbles to boulders in a sandy matrix. The beach ridges have a wide, bouldery garnet-gneiss berm with boulders up to 0.5 m in size, typically 10 to 20 cm, with a sandy matrix. The berms and swales are about 20 m in width. All beaches are very similar but with varying average clast sizes and berm widths. The lowermost beach is fine gravel instead of sand.

A.7 Dunlop Island

Dunlop Island is a series of beach ridges, from lower energy on the south to higher energy on the northern side. On the north-eastern side the lower beaches are divided by small rocky headlands into a series of almost pocket like beaches. The rock outcrops are granodiorite to gneiss with dolerite dykes. On the northern point the material is almost shale like in the way it has fractured into sheets. All of the rock is extensively folded with dykes and the bedrock is eroded into platforms that correspond to the beaches. To the south the features are much flatter with berms that are difficult to distinguish in places. A boulder pavement is developed on the inland southern side and frost polygons are developed on the boulder pavement with a typical size 4 to 5 m wide with deep wide frost wedges (on the upper beaches these are about 0.5 m deep). The cobbles on the beaches are well rounded and well sorted. Ice push features are evident on all of the beaches. The permafrost layer is approximately 80 cm deep in late January.

A.8 Cape Roberts

Cape Roberts has superbly developed boulder pavements. They form very flat surfaces with interlocking boulders of approximately 40 cm in size. The bottom and sides of these boulders are rounded in the usual way but the tops are smoothed off (but still have rounded edges). No ice scours are present but also the surfaces are not a rough crystalline surface or polished. Some samples have a few centimetres of the rock broken off the surface which still leaves this a flat surface. Apart from the boulder pavements the Cape Roberts area has little beach development. The lower beaches are very rocky and the higher beaches have some fine gravels (no sand) as well as boulders. On the northern side the beaches have berms about 1 m high while on the southern side the ridges were steeper with higher berms. The higher ridges are much more developed than the lower ridges.

A.9 Cape Geology

The general Cape Geology area has very steep hills with very little foreshore area. The only real beaches are in the restricted area of Cape Geology and Botany Bay (SSSI 37). There are two definite ridges above the active beach there with the same height again to the marine limit. The marine limit is a change in colour from grey to brown. The beach south of the cape is very poorly developed with boulders of granite. The marine limit is not very distinct as it is on a steep slope with potential for boulders to roll down from above. Boulders below the marine limit are rounder than the moraine above. Below the top zone of 3 to 4 m the size range is gravel and boulders up to 1.5

m on average. In between the boulders there is a dominance of fist-sized well-rounded boulders.

A.10 Cape Ross

Cape Ross is a high, rocky headland with a slightly narrower tombolo to the mainland. The rock here is a coarse granite, with dolerite dykes. Close to the mainland are a series of well developed beach ridges. They are best developed on the northern side with well developed berms and swales in behind. Further down the hill on the northern side the ridge development stops before the snow cover (27 January). The upper beaches have some ice push features (mounds of boulders) preserved and in places has the appearance of a stone wall. The berms have boulders less than 1 m in size with many smaller boulders and swales are snow filled. There are some very large boulders on the northern side which must be ice rafted into place. The marine limit here is not visible as a snow tongue extends sideways around the hill at this height (rocks above are non-marine). On the southern side there is bedrock exposed from the snow cover. The rock forms poorly developed platforms dipping seawards (ice smoothed).

The fossil penguin rookery (see Baroni and Orombelli (1994)) consists of mounds of small stones in an otherwise flat but fairly rocky area. The mounds have a well developed soil (rich brown colour, only tiny fragments of rock, mainly crystals in between rocks) with some moss growth. The ridge the nests are on is a well developed rocky beach ridge with a definite slope, berm and long swale in behind. The nests appear to be mainly on the crest and just to each side of it. A typical spacing between nests is about 0.5 m.

A.11 Cape Bird

The marine limit is not clear at Cape Bird and is defined in most places by the talus slope from the hill behind. There are many outwash fans which cover the beach areas. There is no outcropping bedrock except high on the hills. To the north there are gravel beaches, which have extensive guano cover in the penguin colony. The best beach development is at Cape Bird B. At the point the beaches form a headland with an outwash fan on the southern side. The ridges are perpendicular to the coast at this point, and are made up of well rounded cobbles and gravels on the surface. The modern beach has well rounded, well sorted cobbles. Pits dug indicate the higher ridges are of a similar composition with mixed sand and gravels. Further south of Cape Bird B the beaches are poorly developed.

A.12 Cape Hallett

Seabee Hook at Cape Hallett is a flat lying gravel and sand spit lying on the northern side of the Daniell Peninsula which is interpreted as being formed by currents moving material northwards from the steep and, in places cliff like, edge to the peninsula. The beach is made up of gravels and boulders of volcanic lithology up to 0.5 m in size (dominant clast size 20 to 30 cm). The whole area has poor berm development - the only ones that look like true beach ridges are around the outside of the hook. The berms are changed or formed (the whole area is disturbed from the former station) into a series of elongated mounds with depressions in between.

Appendix B

Surface exposure sample details

B.1 ^{36}Cl Values and Blanks

Table C.1 gives the ^{36}Cl/Cl ratios for all the samples. Six blanks were run, one with each batch of samples. The following list is the measured values of the chlorine ratios from the AMS.

Each of the blanks corresponds to the following samples:

JQBlank15/7: samples cbc18/3, cbc18/4, crc1, crc2, crc5, ross12, ross14.

JQBlank10/7: samples ross17, crc8, ross15, crc11, crc3, crc6, dis9.

JQBlank18/5: samples dis12, cbc18/1, cbc18/5, dis4, cbc18/2.

JQBlankcrc4: samples crc4, crc1, crc9, crc12, dis4, ross13, ross16.

JQBlankac4071: samples ac4075, ac4075, ac4077, ac40715.

JQBlankac4076: samples ac4073, ac4076, ac4077, ac4079, ac40710, ac40712.

B.2 Potassium Analyses

Potassium contents were measured on the K-feldspar sample splits using an IL 443 Flame Photometer and the values of K_2O are listed in Table B.2.

B.3 Rock Composition

The Table B.3 on the following pages shows the values for the major elements. Where samples were close and had similar characteristics on bedrock samples the major and trace element data were determined for only one sample.

Sample	^{36}Cl/Cl x 10^{-15}	error	Sample	^{36}Cl/Cl x 10^{-15}	error
JQblank15/7	0.1	0.4	cbc18/1	32	2
JQblank10/7	0.2	0.3	cbc18/2	9	1
JQblank18/5	0.3	0.4	cbc18/3	32	2
JQblankcrc4	<0.1	-	cbc18/4	99	5
JQblank9/10	8	6	cbc18/5	124	16
JQblankac4076	0.35	0.35	ssc2	255	10
JQblankac4075	0.35	0.35	ross12	108	9
ac4071	74	4	ross13	315	15
ac4073	93	4	ross14	100	5
ac4075	188	8	ross15	118	6
ac4076	149	7	ross16	88	6
ac4077	76	7	ross17	95	5
ac4079	159	9	crc1	60	6
ac40710	163	7	crc2	93	5
ac40712	245	11	crc3	96	5
ac40715	354	16	crc4	54	3
dis1	163	11	crc5	57	4
dis4	94	4	crc6	59	4
dis6	56	5	crc8	130	7
dis9	43	3	crc9	141	5
dis10	80	5	crc11	144	7
dis12	58	3	crc12	128	6

Table B.1: Measured chlorine ratios

B.3.1 Trace Elements

Table B.4 gives details of the trace elements measured. Table B.5 is the values for the carbonate samples from Marble Point with the undissolved sediment (non-carbonate) split removed. Also accounts for a small split of solution removed during the sample processing.

B.4 Calculation values

Table B.6 gives the input values into the chlorine age calculation and the calculated results. The chlorine ratios, proportions of which elements stop the cosmogenic neutrons, the major absorber, production values, scaling and depth corrections, exposure age and the scaled exposure age for Antarctica are on this table.

Sample	% K_2O	% error	Sample	% K_2O	% error
cbc18/1	11.95	0.25	crc3	13.12	0.34
cbc18/2	12.74	0.29	crc4	13.40	0.29
cbc18/3	13.39	0.42	crc5	13.76	0.22
cbc18/4	13.15	0.62	crc6	12.91	0.22
cbc18/5	12.33	0.24	crc8	13.32	0.18
			crc9	13.02	0.12
ssc2	11.19	0.38	crc11	13.32	0.22
			crc12	13.10	0.15
dis1	13.13	0.20			
dis4	13.44	0.24	ross12	14.36	0.07
dis6	13.11	0.16	ross13	14.01	0.11
dis9	12.45	0.20	ross14	14.23	0.34
dis10	13.42	0.25	ross15	14.19	0.39
			ross16	14.29	0.27
crc1	13.09	0.13	ross 17	13.46	0.23
crc2	13.49	0.10			

Table B.2: % K_2O values measured.

Lab. No.	Field No.	Fe_2O_3	MnO	TiO_2	CaO	K_2O	S	P_2O_5	SiO_2	Al_2O_3	MgO	Na_2O	Fusion Loss	Total
jpq001a	cbc18/1	0.713	0.017	0.085	1.135	5.810	0.032	0.014	75.694	13.217	0.113	2.826		99.656
jqp002b	cbc18.2	1.553	0.037	0.177	1.810	4.507	0.006	0.060	73.194	14.657	0.285	3.739		100.025
jqp003b	cbc18/3	0.967	0.024	0.125	3.927	2.879	0.105	0.038	65.694	19.492	0.262	5.365		98.878
jqp004a	cbc18/4	0.670	0.017	0.103	3.928	2.683	0.085	0.034	66.003	19.777	0.274	5.692		99.266
jqp005a	cbc18.5	1.164	0.032	0.134	1.204	5.190	0.004	0.026	75.086	13.188	0.221	3.180		99.429
jqp006a	ssc2	1.192	0.032	0.080	0.984	4.700	0.013	0.028	74.528	13.480	0.102	4.233		99.372
jqp007a	ross12	1.719	0.038	0.267	1.909	5.139	0.008	0.134	73.293	13.701	0.408	2.876		99.492
jqp008b	ross13	2.062	0.050	0.314	3.171	3.785	0.011	0.424	70.775	14.860	0.588	3.509		99.549
jqp009a	ross14	2.979	0.081	0.431	3.161	3.481	0.006	0.418	70.389	14.137	0.969	3.328		99.380
jqp010a	ross15	2.119	0.046	0.338	3.298	3.089	0.008	0.331	70.354	15.256	0.754	3.889		99.482
jqp011a	ross16	1.803	0.043	0.278	2.649	4.173	0.007	0.285	72.329	14.264	0.622	3.188		99.641
jqp012a	ross17	1.593	0.055	0.205	1.636	6.358	0.014	0.164	70.190	15.074	0.667	2.958		98.914
jqp013a	ac4071	0.064	0.002	0.010	52.885	0.041	0.010	0.094	1.050	0.155	2.043	0.045	43.110	99.509
jqp013b	ac4071	0.049	0.001	0.008	52.876	0.038	0.000	0.082	1.066	0.153	2.024	0.033	43.110	99.440
jqp014a	ac4073	0.177	0.002	0.015	53.112	0.024	0.024	0.108	1.398	0.236	1.588	0.062	42.530	99.216
jqp014b	ac4073	0.101	0.002	0.013	53.164	0.027	0.009	0.113	1.425	0.243	1.583	0.051	42.530	99.261
jqp015a	ac4075	0.125	0.006	0.014	52.992	0.034	0.036	0.107	2.033	0.247	1.473	0.087	42.280	99.434
jqp015b	ac4075	0.110	0.005	0.016	53.023	0.034	0.020	0.090	1.975	0.247	1.451	0.092	42.280	99.343
jqp016a	ac4076	0.082	0.003	0.012	53.740	0.027	0.026	0.118	0.986	0.192	1.016	0.047	43.210	99.459
jqp016c	ac4076	0.027	-0.002	0.020	53.974	0.029	0.000	0.106	0.969	0.188	1.035	0.055	43.210	99.611
jqp017b	ac4077	0.135	0.004	0.023	52.419	0.030	0.017	0.082	1.325	0.165	2.045	0.035	43.030	99.310
jqp018b	ac4079	0.031	0.005	0.005	54.516	0.009	0.001	0.080	0.773	0.052	0.611	0.026	43.460	99.569

Table B.3: Table of Major element analyses for the surface exposure samples.

Lab. No.	Field No.	Fe_2O_3	MnO	TiO_2	CaO	K_2O	S	P_2O_5	SiO_2	Al_2O_3	MgO	Na_2O	Fusion Loss	Total
jqp019b	ac40710	0.069	0.010	0.007	53.356	0.021	0.000	0.072	1.209	0.180	1.188	0.048	43.560	99.720
jqp020a	ac40712	0.015	0.001	0.002	54.499	0.005	0.007	0.078	1.076	0.045	0.490	0.040	43.530	99.788
jqp020b	ac40712	0.009	0.002	0.006	54.411	0.005	0.000	0.069	1.080	0.045	0.469	0.016	43.530	99.642
jqp021b	ac40715	0.002	0.001	0.003	54.524	0.004	0.000	0.071	0.904	0.027	0.317	0.044	44.210	100.107
jqp022a	dis1	1.254	0.037	0.165	2.053	4.301	0.015	0.056	73.999	13.977	0.299	3.289		99.445
jqp023a	dis4	1.220	0.026	0.164	2.684	3.514	0.041	0.102	72.710	15.039	0.308	3.862		99.670
jqp024a	dis6	1.197	0.028	0.180	2.591	3.522	0.016	0.068	71.786	15.425	0.371	3.918		99.102
jqp025a	dis9	1.391	0.035	0.194	2.085	4.796	0.019	0.068	72.420	14.606	0.334	3.256		99.204
jqp026a	dis10	0.887	0.025	0.117	2.284	4.474	0.018	0.042	74.130	14.301	0.199	3.090		99.567
jqp027a	dis12	1.093	0.026	0.146	3.387	2.260	0.005	0.111	71.619	15.962	0.337	4.494		99.440
jqp028a	crc1	0.728	0.023	0.094	2.405	3.637	0.008	0.104	73.876	14.781	0.159	3.828		99.643
jqp029a	crc2	1.325	0.033	0.212	3.080	2.234	0.005	0.115	72.490	15.429	0.350	4.453		99.726
jqp030a	crc3	1.041	0.037	0.192	2.365	3.126	0.005	0.031	73.579	14.685	0.262	3.951		99.274
jqp031a	crc4	1.176	0.031	0.174	2.406	3.016	0.012	0.077	73.974	14.298	0.280	3.860		99.304
jqp032a	crc5	1.394	0.038	0.192	2.647	2.669	0.008	0.107	73.586	14.598	0.139	4.086		99.644
jqp033b	crc6	1.352	0.033	0.202	2.791	2.628	0.008	0.088	72.813	15.162	0.327	4.124		99.528
jqp034a	crc8	0.601	0.023	0.063	1.712	4.479	0.011	0.042	76.627	13.133	0.111	3.205		100.007
jqp035a	crc9	1.278	0.035	0.187	2.538	2.838	0.005	0.094	73.307	14.426	0.301	3.953		98.970
jqp036a	crc11	0.800	0.027	0.089	2.091	3.671	0.009	0.089	75.168	13.753	0.202	3.565		99.464
jqp037a	crc12	1.258	0.034	0.171	2.517	3.152	0.018	0.103	73.737	14.441	0.294	3.862		99.587

Sample	Li	Cr	Sm	Gd	Th	U
Blank30/10	0.743	1.058	0.278	0.002	0.11	0.002
Kilauea std	5.41	526	5.15	5.69	0.853	0.274
Kil. std ref.	4.8	471	5.21	5.59	0.853	0.274
% variation	11.3	10.5	1.16	1.7	6	1.5
ac4071	0.363	bkg	0.047	0.24	0.263	2.39
ac4073	0.525	bkg	0.119	0.307	0.601	4.06
ac4077	0.132	0.064	0.116	0.31	0.3	3.47
ac40710	0.728	0.067	0.058	0.226	0.255	1.79
ac40715	0.307	bkg	0.119	0.307	0.601	4.06
crc1	35	0.574	3.94	3.78	15	1.5
crc3	50	0.466	5.52	4.93	24	1.39
crc3-rep	44	0.59	5.7	5.44	25	2.2
crc3-bomb	45	0.267	4.93	5.17	21	1.81
crc6	54	0.526	1.99	2.17	5.98	1.05
crc8	24	0.602	2.83	2.7	19	3.64
crc11	30	0.602	6.13	5.3	24	2.48
cbc18/1	12	bkg	1.84	1.65	4.81	0.52
cbc18/2	34	0.214	4.98	4.87	28	1.85
cbc18/3	13	0.135	1.52	1.86	2.81	0.97
cbc18/4	23	0.067	2.32	2.38	8.84	1.56
cbc18/5	21	bkg	2.41	2.37	5.52	0.84
ssc2	20	0.87	6.97	6.84	16	2.43
ssc2-rep	20	1.35	6.36	6.4	16	2.14
ssc2-bomb	21	0.992	2.78	2.89	9.97	1.04
ross12	29	1.29	5.2	4.92	33	4.46
ross13	65	1.99	8.25	8.06	43	4.75
ross14	78	7.19	11	11	46	4.76
ross15	67	2.64	8	8	40	3.22
ross16	43	2.05	7.84	7.62	39	3.26
ross16-rep	53	2.66	7.36	7.3	35	3.08
ross16-bomb	42	1.95	3.84	3.82	23	2.06
ross17	39	7.53	7.52	7.46	40	5.67
dis4	29	1.03	1.93	2.13	6.18	2.59
dis10	24	0.76	3.23	3.25	13	1.64
dis12	29	1.31	2.56	2.9	11.5	11
dis12-rep	29	1.36	2.35	2.71	11	2.78
dis12-bomb	28	1.14	1.05	1.38	3.89	1.88

Table B.4: Analyses of selected rocks for trace elements. Values in ppm. Kilauea reproducibility errors: Li 11%, Cr 10% and Th 6%. Marble Li and Sm values are close to the blank and therefore may incorporate a 50% error. Cr values are affected by errors associated with low level concentrations with respect to the blank and also to reproducibility of Cr results between Kilauea std solutions. Reproducibility error is about 10%, total error may be 50%. bkg = background. Repeats and bombs (different preparation methods) are listed.

Sample	Weight for ^{36}Cl measurement (g)	CaO	CaO (WR)	MgO (WR)	FeO (WR)	CO_2 (WR)
ac4071	15.7303	53.56	52.52	2.02	0.06	43.45
ac4073	14.8734	53.97	52.34	1.57	0.18	42.89
ac4075	15.2767	54.15	51.99	1.45	0.12	42.45
ac4076	15.1131	54.74	53.74	1.02	0.08	43.34
ac4077	14.3702	53.46	51.57	2.01	0.13	42.75
ac4079	15.3118	55.29	54.46	0.60	0.03	43.41
ac40710	15.4289	54.54	53.66	1.19	0.07	43.46
ac40712	15.6375	55.43	54.15	0.49	0.01	43.04
ac40715	14.6424	55.65	54.79	0.32	0.00	43.35

Table B.5: Major element values (%) for the carbonate samples with the undissolved sediment (non-carbonate) removed. WR = whole rock.

Measurement	**cbc18/1**	**cbc18/2***	**cbc18/3**	**cbc18/4**	**cbc18/5**
Cl-36 atom/g	$1.36x10^5 \pm 9.85x10^3$	$2.429x10^4 \pm 3.34x10^3$	$2.228x10^5 \pm 1.42x10^4$	$3.41x10^5 \pm 1.78x10^4$	$4.262x1065 \pm 5.55x10^4$
Cl-36/Ca	—	—	—	—	—
Fraction stopped by:					
Cl-35	0.012 ± 0.001	0.001 ± 0.001	0.0247 ± 0.001	0.006 ± 0.000	0.009 ± 0.000
K-39(n,α)Cl-36	0.001 ± 0.000	0.001 ± 0.000	0.001 ± 0.000	0.001 ± 0.000	0.001 ± 0.000
Major elements	0.891	0.771	0.878	0.844	0.857
Trace elements	0.109	0.229	0.122	0.116	0.143
X-section (cm^2/g)	0.005 ± 0.000	0.006 ± 0.000	0.005 ± 0.000	0.005 ± 0.000	0.005 ± 0.000
Mean free path (cm^2/g)	203.5 ± 1.8	175.9 ± 1.4	216.3 ± 2.0	212.0 ± 1.9	196.2 ± 1.8
Major absorber	Potassium	Silicon	Silicon	Silicon	Potassium
Intrinsic prod'n (n/g/a)	3.196 ± 0.274	18.85 ± 1.72	3.785 ± 0.462	9.347 ± 0.859	4.154 ± 0.282
Production (atom/g/a):					
Cl-36 (atom/g)	$1.196x10^5 \pm 1.006x10^4$	$1.621x10^4 \pm 8.776x10^3$	$1.822x10^5 \pm 1.505x10^4$	$3.167x10^5 \pm 1.796x10^4$	$4.106x10^5 \pm 5.551x10^4$
Background Cl-36	$1.633x10^4 \pm 2.002x10^3$	$8.080x10^3 \pm 8.114x10^3$	$4.057x10^4 \pm 5.036x10^3$	$2.429x10^4 \pm 2.529x10^3$	$1.555x10^4 \pm 1.236x10^3$
Ca spallation	0.024 ± 0.004	0.023 ± 0.003	0.023 ± 0.003	0.022 ± 0.003	0.022x± 0.003
Ca (μ, α)	0.002 ± 0.001	0.002 ± 0.001	0.002 ± 0.001	0.002 ± 0.001	0.002 ± 0.001
K-spallation	17.74 ± 1.75	18.45 ± 1.82	19.42 ± 1.92	18.24 ± 1.8	17.03 ± 1.68
K(μ, α)	0.933 ± 0.093	0.971 ± 0.097	1.022 ± 0.102	0.960 ± 0.096	0.896 ± 0.090
Thermal n Cl-35	2.86 ± 0.335	0.282 ± 0.282	6.816 ± 0.554	1.811 ± 0.166	2.823 ± 0.246
Epithermal n Cl-35	0.431 ± 0.049	0.042 ± 0.042	0.875 ± 0.066	0.215 ± 0.019	0.340 ± 0.028
K-39(n,α)Cl-36	0.303 ± 0.024	0.328 ± 0.025	0.41 ± 0.032	0.433 ±0.034	0.406 ± 0.031
Total production	22.29 ± 1.79	20.09 ± 1.85	28.57 ± 2.00	21.68 ± 1.81	21.52 ± 1.7
Ratio muon/nucleon	0.061 ± 0.068	0.055 ± 0.074	0.069 ± 0.053	0.059 ± 0.069	0.062 ± 0.07
Altitude/lat. scaling:					
Spallation	1.001	1.001	1.001	1.001	1.001
Muons	1.001	1.001	1.001	1.001	1.001
Depth correction:					
Spallation	0.983	0.966	0.957	0.933	0.925
Thermal n	1.157	1.283	1.346	1.488	1.554
Epithermal n	1.022	1.041	1.044	1.059	1.074
Exposure age	5.401 ± 0.631	0.807 ± 0.444	6.427 ± 0.701	14.857 ± 1.53	19.513 ± 3.13
Scaled exposure age	4.380 ± 0.631	0.655 ± 0.444	5.212 ± 0.701	12.049 ± 1.53	15.826 ± 3.13

Measurement	**ssc2**	**ac4071**	**ac4073**	**ac4075***	**ac4076**
Cl-36 (atom/g)	$1.14x10^{6}\pm 6.72x10^{4}$	$1.450x10^{5}\pm 7.92717x10^{3}$	$2.016x10^{5}\pm 8.834x10^{3}$	$3.392x10^{5}\pm 3.508x10^{4}$	$2.942x10^{5}\pm 1.416x10^{4}$
Cl-36/Ca	—	$2.554x10^{-17}\pm 1.42x10^{18}$	$3.535x10^{-17}\pm 1.59x10^{-18}$	$5.962x10^{-17}\pm 6.19x10^{-18}$	$5.099x10^{-17}\pm 2.51x10^{-18}$
Fraction stopped by:					
Cl-35	0.019 ± 0.001	0.009 ± 0.000	0.008 ± 0.000	0.005 ± 0.002	0.006 ± 0.000
K-39(n,α)Cl-36	0.001 ± 0.000	—	—	—	—
Major elements	0.734	0.838	0.844	0.842	0.841
Trace elements	0.266	0.162	0.156	0.158	0.159
X-section (cm^2/g)	0.006 ± 0.000	0.003 ± 0.000	0.003 ± 0.000	0.003 ± 0.000	0.003 ± 0.000
Mean free path (cm^2/g)	170.2 ± 1.3	329.3 ± 3.2	312.1 ± 3.0	325.7 ± 4.3	326.4 ± 4.3
Major absorber	Silicon	Calcium	Calcium	Calcium	Calcium
Intrinsic prod'n (n/g/a)	12.93 ± 0.632	1.874 ± 0.253	2.763 ± 0.248	1.215 ± 0.099	1.17 ± 0.099
Production (atom/g/a):					
Cl-36 (atom/g)	$1.036x10^{6}\pm 6.767x10^{4}$	$1.374x10^{5}\pm 7.995x10^{3}$	$1.922x10^{5}\pm 8.876x10^{3}$	$3.363x10^{5}\pm 3.509x10^{4}$	$2.910x10^{5}\pm 1.416x10^{4}$
Background Cl-36	$1.041x10^{5}\pm 7.948x10^{3}$	$7.651x10^{3}\pm 1.040x10^{3}$	$9.371x10^{3}\pm 8.654x10^{2}$	$2.893x10^{3}\pm 9.935x10^{2}$	$3.234x10^{3}\pm 2.934x10^{2}$
Ca spallation	0.024 ± 0.003	17.69 ± 0.617	17.81 ± 0.621	17.9 ± 0.624	18.21 ± 0.635
Ca (μ,α)	0.002 ± 0.001	1.745 ± 0.349	1.749 ± 0.35	1.756 ± 0.351	1.792 ± 0.358
K-spallation	21.26 ± 2.1	—	—	—	—
K(μ,α)	1.115 ± 0.111	—	—	—	—
Thermal n Cl-35	5.413 ± 0.512	2.228 ± 0.193	1.927 ± 0.167	1.314 ± 0.456	1.448 ± 0.147
Epithermal n Cl-35	0.832 ± 0.077	0.322 ± 0.023	0.287 ± 0.021	0.193 ± 0.066	0.221 ± 0.017
K-39(n,α)Cl-36	0.366 ± 0.027	—	—	—	—
Total production	29.01 ± 2.16	21.99 ± 0.735	21.77 ± 0.732	21.16 ± 0.852	21.67 ± 0.744
Ratio muon/nucleon	0.065 ± 0.052	0.114 ± 0.019	0.112 ± 0.019	0.108 ± 0.02	0.109 ± 0.02
Altitude/lat. scaling:					
Spallation	1.008	1.001	1.009	1.011	1.006
Muons	1.004	1.001	1.004	1.005	1.003
Depth correction:					
Spallation	0.967	0.959	0.959	0.959	0.967
Thermal n	1.272	1.393	1.396	1.390	1.325
Epithermal n	1.039	1.027	1.029	1.027	1.023
Exposure age	37.27 ± 3.86	6.294 ± 0.425	8.921 ± 0.515	16.19 ± 1.84	13.64 ± 0.825
Scaled exposure age	30.227 ± 3.86	5.105 ± 0.425	7.235 ± 0.515	13.131 ± 1.84	11.062 ± 0.825

Measurement	**ac4077***	**ac4079**	**ac40710**	**ac40712***	**ac40715***
Cl-36 (atom/g)	$1.430\text{x}10^5 \pm 1.849\text{x}10^4$	$2.535\text{x}10^5 \pm 1.455\text{x}10^4$	$2.721\text{x}10^5 \pm 1.182\text{x}10^4$	$4.535\text{x}10^5 \pm 4.647\text{x}10^4$	$6.369\text{x}10^5 \pm 6.660\text{x}10^4$
Cl-36/Ca	$2.54\text{x}10^{-17} \pm 3.29\text{x}10^{-18}$	$4.331\text{x}10^{-17} \pm 2.52\text{x}10^{-18}$	$4.75\text{x}10^{-17} \pm 2.12\text{x}10^{-18}$	$7.751\text{x}10^{-17} \pm 7.96\text{x}10^{-18}$	$1.088\text{x}10^{-16} \pm 1.14\text{x}10^{-17}$
Fraction stopped by:					
Cl-35	0.006 ± 0.002	0.002 ± 0.000	0.003 ± 0.000	0.005 ± 0.002	0.006 ± 0.002
K-39(n,α)Cl-36	—	—	—	—	—
Major elements	0.834	0.842	0.841	0.841	0.845
Trace elements	0.164	0.158	0.159	0.159	0.156
X-section (cm^2/g)	0.003 ± 0.000	0.003 ± 0.000	0.003 ± 0.000	0.003 ± 0.000	0.003 ± 0.000
Mean free path (cm^2/g)	328.4 ± 3.1	324.4 ± 4.3	327.6 ± 4.3	326.3 ± 4.3	328.4 ± 2.8
Major absorber	Calcium	Calcium	Calcium	Calcium	Calcium
Intrinsic prod'n (n/g/a)	2.378 ± 0.25	1.155 ± 0.098	1.186 ± 0.099	1.127 ± 0.963	0.720 ± 0.048
Production (atom/g/a):					
Cl-36 (atom/g)	$1.372\text{x}10^5 \pm 1.859\text{x}10^4$	$2.522\text{x}10^5 \pm 1.455\text{x}10^4$	$2.704\text{x}10^5 \pm 1.182\text{x}10^4$	$4.509\text{x}10^5 \pm 4.638\text{x}10^4$	$6.352\text{x}10^5 \pm 6.660\text{x}10^4$
Background Cl-36	$5.709\text{x}10^3 \pm 2.000\text{x}10^3$	$1.323\text{x}10^3 \pm 1.189\ \text{x}10^2$	$1.758\text{x}10^3 \pm 1.538\text{x}10^2$	$2.689\text{x}10^3 \pm 9.260\text{x}10^2$	$1.728\text{x}10^3 \pm 5.874\text{x}10^2$
Ca spallation	16.62 ± 0.58	18.84 ± 0.657	18.49 ± 0.645	18.72 ± 0.653	18.88 ± 0.658
Ca (μ, α)	1.637 ± 0.328	1.851 ± 0.37	1.812 ± 0.363	1.834 ± 0.367	1.842 ± 0.638
K-spallation	—	—	—	—	—
K(μ, α)	—	—	—	—	—
Thermal n Cl-35	1.37 ± 0.471	0.536 ± 0.054	0.691 ± 0.069	1.19 ± 0.413	1.204 ± 0.413
Epithermal n Cl-35	0.184 ± 0.063	0.091 ± 0.007	0.116 ± 0.008	0.191 ± 0.065	0.191 ± 0.065
K-39(n,α)Cl-36	—	—	—	—	—
Total production	19.82 ± 0.818	21.32 ± 0.756	21.11 ± 0.743	21.93 ± 0.858	22.12 ± 0.863
Ratio muon/nucleon	0.109 ± 0.02	0.102 ± 0.02	0.103 ± 0.02	0.106 ± 0.02	0.106 ± 0.02
Altitude/lat. scaling:					
Spallation	1.004	1.009	1.013	1.013	1.022
Muons	1.002	1.004	0.116	1.006	1.010
Depth correction:					
Spallation	0.943	0.983	0.983	0.975	0.975
Thermal n	1.513	1.175	1.177	1.253	1.255
Epithermal n	1.033	1.013	1.013	1.018	1.018
Exposure age	6.982 ± 0.997	11.99 ± 0.824	13.0 ± 0.741	21.06 ± 2.37	29.71 ± 3.44
Scaled exposure age	5.663 ± 0.997	9.724 ± 0.824	10.543 ± 0.741	17.080 ± 2.37	24.096 ± 3.44

Measurement	**dis1**	**dis4**	**dis6***	**dis9**	**dis10**
Cl-36 (atom/g)	$4.77x10^5 \pm 3.67x10^4$	$3.145x10^5 \pm 1.353x10^4$	$1.304x10^5 \pm 1.87x10^4$	$1.998x10^5 \pm 1.41x10^4$	$2.409x10^5 \pm 2.24x10^4$
Cl-36/Ca	—	—	—	—	—
Fraction stopped by:					
Cl-35	0.012 ± 0.001	0.008 ± 0.000	0.008 ± 0.001	0.013 ± 0.000	0.013 ± 0.001
K-39(n,α)Cl-36	0.001 ± 0.000	0.001 ± 0.000	0.001 ± 0.000	0.001 ± 0.000	0.001 ± 0.000
Major elements	0.855	0.851	0.817	0.827	0.820
Trace elements	0.146	0.150	0.183	0.173	0.181
X-section (cm^2/g)	0.005 ± 0.000	0.005 ± 0.000	0.005 ± 0.000	0.005 ± 0.000	0.005 ± 0.000
Mean free path (cm^2/g)	202.4 ± 1.8	208.0 ± 1.8	199.7 ± 1.7	188.7 ± 1.5	196.9 ± 1.7
Major absorber	Silicon	Silicon	Silicon	Potassium	Silicon
Intrinsic prod'n (n/g/a)	7.314 ± 0.361	7.774 ± 0.31	10.27 ± 1.77	9.592 ± 1.64	9.378 ± 1.6
Production (atom/g/a):					
Cl-36 (atom/g)	$4.396x10^5 \pm 3.683x10^4$	$2.871x10^5 \pm 1.355x10^4$	$9.539x10^4 \pm 2.026x10^4$	$1.473x10^5 \pm 1.673x10^4$	$1.895x10^5 \pm 2.445x10^4$
Background Cl-36	$3.740x10^4 \pm 2.573x10^3$	$2.740x10^4 \pm 1.140x10^3$	$3.496x10^4 \pm 7.823x10^3$	$5.249x10^4 \pm 9.039x10^3$	$5.137x10^4 \pm 9.834x10^3$
Ca spallation	0.024 ± 0.004	0.021 ± 0.003	0.0217 ± 0.003	0.021 ± 0.003	0.023 ± 0.003
Ca (μ, α)	0.002 ± 0.001	0.002 ± 0.000	0.002 ± 0.001	0.002 ± 0.001	0.002 ± 0.001
K-spallation	19.69 ± 1.94	17.83 ± 1.76	17.73 ± 1.75	17.11 ± 1.69	19.42 ± 1.92
K(μ, α)	1.029 ± 0.103	0.938 ± 0.938	0.931 ± 0.093	0.900 ± 0.09	1.021 ± 0.102
Thermal n Cl-35	3.1 ± 0.282	2.952 ± 0.232	2.778 ± 0.451	3.218 ± 0.251	3.626 ± 0.418
Epitherm Cl-35	0.445 ± 0.039	0.307 ± 0.022	0.308 ± 0.049	0.465 ± 0.035	0.489 ± 0.055
K-39(n,α)Cl-36	0.359 ± 0.028	0.521 ± 0.041	0.475 ± 0.037	0.316 ± 0.025	0.389 ± 0.030
Total production	24.65 ± 1.97	22.57 ± 1.78	22.25 ± 1.81	22.03 ± 1.71	24.98 ± 1.97
Ratio muon/nucleon	0.061 ± 0.061	0.062 ± 0.067	0.062 ± 0.068	0.063 ± 0.068	0.063 ± 0.06
Altitude/lat. scaling:					
Spallation	1.013	1.001	1.006	1.001	1.002
Muons	1.006	1.001	1.003	1.001	1.001
Depth correction:					
Spallation	0.974	0.885	0.901	0.966	0.957
Thermal n	1.226	1.756	1.680	1.284	1.343
Epithermal n	1.031	1.089	1.083	1.040	1.045
Exposure age	18.212 ± 2.15	12.912 ± 1.2	4.309 ± 0.985	6.739 ± 0.934	7.656 ± 1.17
Scaled exposure age	14.770 ± 2.15	10.472 ± 1.2	3.495 ± 0.985	5.463 ± 0.934	6.209 ± 1.17

Measurement	**dis12***	**crc1**	**crc2**	**crc3**	**crc4**
Cl-36 (atom/g)	$2.439x10^5 \pm 1.61x10^4$	$1.863x10^5 \pm 1.87x10^4$	$3.991x10^5 \pm 2.32x10^4$	$4.5x10^5 \pm 2.71x10^4$	$2.215x10^5 \pm 1.54x10^4$
Cl-36/Ca	—	—	—	—	—
Fraction stopped by:					
Cl-35	0.008 ± 0.001	0.002 ± 0.000	0.009 ± 0.001	0.012 ± 0.001	0.007 ± 0.001
K-39 (n,α)Cl-36	0.001 ± 0.000	0.001 ± 0.000	0.001 ± 0.000	0.001 ± 0.000	0.001 ± 0.000
Major elements	0.819	0.784	0.780	0.732	0.732
Trace elements	0.182	0.216	0.220	0.268	0.268
X-section (cm^2/g)	0.005 ± 0.000	0.005 ± 0.000	0.005 ± 0.000	0.005 ± 0.000	0.005 ± 0.000
Mean free path (cm^2/g)	214.1 ± 1.9	196.8 ± 1.7	200.9 ± 1.7	184.2 ± 1.8	183.7 ± 1.4
Major absorber	Silicon	Silicon	Silicon	Silicon	Silicon
Intrinsic prod'n (n/g/a)	11.84 ± 1.86	10.96 ± 1.73	11.66 ± 0.329	16.99 ± 2.35	16.87 ± 0.316
Production (atom/g/a):					
Cl-36 (atom/g)	$2.006x10^5 \pm 1.856x10^4$	$1.782x10^5 \pm 1.873x10^4$	$3.539x10^5 \pm 2.344x10^4$	$3.596x10^5 \pm 3.044x10^4$	$1.687x10^5 \pm 1.717x10^4$
Background Cl-36	$4.323x10^4 \pm 9.200x10^3$	$8.103x10^3 \pm 1.231x10^3$	$4.523x10^4 \pm 3.374x10^3$	$9.043x10^4 \pm 1.383x10^4$	$5.284x10^4 \pm 7.265x10^3$
Ca spallation	0.024 ± 0.003	0.023 ± 0.003	0.024 ± 0.004	0.024 ± 0.003	0.024 ± 0.003
Ca (μ, α)	0.002 ± 0.000	0.002 ± 0.001	0.002 ± 0.001	0.002 ± 0.001	0.002 ± 0.001
K-spallation	19.49 ± 1.92	19.04 ± 1.88	20.15 ± 1.99	19.26 ± 1.9	19.83 ± 1.96
K(μ, α)	1.026 ± 0.103	1.002 ± 0.1	1.056 ± 0.106	1.009 ± 0.101	1.039 ± 0.104
Thermal n Cl-35	2.253 ± 0.367	0.493 ± 0.040	2.36 ± 0.243	3.664 ± 0.372	2.071 ± 0.335
Epithermal Cl-35	0.298 ± 0.048	0.066 ± 0.005	0.337 ± 0.034	0.512 ± 0.050	0.300 ± 0.048
K-39(n,α)Cl-36	0.391 ± 0.031	0.382 ± 0.030	0.367 ± 0.028	0.370 ± 0.029	0.362 ± 0.027
Total production	23.49 ± 1.96	21.01 ± 1.88	24.29 ± 2.01	24.84 ± 1.94	23.63 ± 1.99
Ratio muon/nucleon	0.060 ± 0.064	0.055 ± 0.071	0.059 ± 0.062	0.062 ± 0.061	0.059 ± 0.064
Altitude/lat. scaling:					
Spallation	1.001	1.001	1.009	1.009	1.009
Muons	1.001	1.001	1.004	1.004	1.004
Depth correction:					
Spallation	0.966	0.957	0.974	0.957	0.966
Thermal n	1.293	1.344	1.228	1.340	1.285
Epithermal n	1.036	1.013	1.029	1.044	1.037
Exposure age	8.627 ± 1.09	8.568 ± 1.2	14.817 ± 1.6	14.734 ± 1.73	7.199 ± 0.959
Scaled exposure age	6.997 ± 1.09	6.949 ± 1.2	12.017 ± 1.6	11.950 ± 1.73	5.839 ± 0.959

Measurement	**crc5***	**crc6**	**crc8**	**crc9**	**crc11**
Cl-36 (atom/g)	$2.147x10^5 \pm 1.8x10^4$	$2.458x10^5 \pm 1.71x10^4$	$5.348x10^5 \pm 4.65x10^4$	$5.946x10^5 \pm 3.2x10^4$	$5.233x10^5 \pm 2.58x10^4$
Cl-36/Ca	—	—	—	—	—
Fraction stopped by: Cl-35	0.008 ± 0.001	0.007 ± 0.000	0.009 ± 0.002	0.008 ± 0.001	0.005 ± 0.000
K-39(n,α)Cl-36	0.001 ± 0.000	0.001 ± 0.000	0.001 ± 0.000	0.001 ± 0.000	0.001 ± 0.000
Major elements	0.818	0.817	0.834	0.829	0.740
Trace elements	0.182	0.183	0.166	0.171	0.260
X-section (cm^2/g)	0.005 ± 0.000	0.005 ± 0.000	0.005 ± 0.000	0.005 ± 0.000	0.005 ± 0.000
Mean free path (cm^2/g)	207.2 ± 1.8	207.5 ± 2.2	204.5 ± 1.9	210.5 ± 1.9	186.7 ± 1.6
Major absorber	Silicon	Silicon	Silicon	Silicon	Silicon
Intrinsic prod'n (n/g/a)	5.193 ± 0.312	5.26 ± 0.316	15.42 ± 0.29	16.74 ± 0.315	16.95 ± 0.304
Production (atom/g/a):					
Cl-36 (atom/g)	$1.964x10^5 \pm 1.820x10^4$	$2.298x10^5 \pm 1.171x10^4$	$4.732x10^5 \pm 4.821x10^4$	$5.345x10^5 \pm 3.315x10^4$	$4.838x10^5 \pm 2.581x10^4$
Background Cl-36	$1.835x10^4 \pm 2.849x10^3$	$1.606x10^4 \pm 1.301x10^3$	$6.166x10^4 \pm 1.294x10^4$	$6.010x10^4 \pm 8.676x10^3$	$3.949x10^4 \pm 1.323x10^3$
Ca spallation	0.022 ± 0.003	0.023 ± 0.003	0.024 ± 0.004	0.023 ± 0.003	0.023 ± 0.003
Ca (μ, α)	0.002 ± 0.001	0.002 ± 0.001	0.002 ± 0.001	0.002 ± 0.001	0.002 ± 0.001
K-spallation	18.94 ± 1.87	18.25 ± 1.8	20.03 ± 1.98	18.35 ± 1.81	19.15 ± 1.89
K(μ, α)	0.992 ± 0.099	0.956 ± 0.096	1.05 ± 0.105	0.959 ± 0.096	1.001 ± 0.1
Thermal n Cl-35	2.837 ± 0.462	1.993 ± 0.194	2.406 ± 0.529	2.726 ± 0.444	1.767 ± 0.144
Epithermal n Cl-35	0.31 ± 0.045	0.257 ± 0.023	0.341 ± 0.074	0.309 ± 0.050	0.225 ± 0.017
K-39(n,α)Cl-36	0.510 ± 0.040	0.382 ± 0.031	0.368 ± 0.029	0.463 ± 0.036	0.420 ± 0.032
Total production	23.61 ± 1.93	21.87 ± 1.81	24.22 ± 2.05	22.83 ± 1.87	22.59 ± 1.9
Ratio muon/nucleon	0.061 ± 0.064	0.059 ± 0.069	0.0560 ± 0.062	0.061 ± 0.066	0.058 ± 0.066
Altitude/lat. scaling:					
Spallation	1.009	1.009	1.009	1.013	1.013
Muons	1.004	1.004	1.004	1.006	1.006
Depth correction:					
Spallation	0.901	0.957	0.974	0.917	0.933
Thermal n	1.650	1.361	1.228	1.565	1.478
Epithermal n	1.074	1.045	1.030	1.065	1.060
Exposure age	8.398 ± 1.05	10.636 ± 1.2	19.988 ± 2.71	24.065 ± 2.54	21.968 ± 2.24
Scaled exposure age	6.811 ± 1.05	8.626 ± 1.2	16.211 ± 2.71	19.517 ± 2.54	17.817 ± 2.24

Measurement	**crc12**	**ross12**	**ross13**	**ross14***	**ross15**
Cl-36 (atom/g)	$5.589 \times 10^5 \pm 2.76 \times 10^4$	$4.068 \times 10^5 \pm 3.51 \times 10^4$	$1.14 \times 10^6 \pm 5.79 \times 10^4$	$4.052 \times 10^5 \pm 2.65 \times 10^4$	$7.358 \times 10^5 \pm 1.56 \times 10^5$
Cl-36/Ca	—	—	—	—	—
Fraction stopped by:					
Cl-35	0.012 ± 0.000	0.006 ± 0.000	0.006 ± 0.000	0.005 ± 0.001	0.021 ± 0.007
K-39(n,α)Cl-36	0.001 ± 0.000	0.001 ± 0.000	0.001 ± 0.000	0.001 ± 0.000	0.001 ± 0.000
Major elements	0.742	0.778	0.673	0.619	0.667
Trace elements	0.258	0.222	0.327	0.381	0.333
X-section (cm^2/g)	0.005 ± 0.000	0.006 ± 0.000	0.007 ± 0.000	0.007 ± 0.000	0.006 ± 0.000
Mean free path (cm^2/g)	185.3 ± 1.5	172.2 ± 1.3	153.8 ± 1.0	137.0 ± 0.8	156.9 ± 1.0
Major absorber	Silicon	Potassium	Gadolinium	Gadolinium	Gadolinium
Intrinsic prod'n (n/g/a)	17.62 ± 0.315	23.64 ± 1.56	31.53 ± 1.79	32.48 ± 2.04	28.59 ± 1.77
Production (atom/g/a):					
Cl-36 (atom/g)	$4.697 \times 10^5 \pm 2.781 \times 10^4$	$3.412 \times 10^5 \pm 3.574 \times 10^4$	$1.063 \times 10^6 \pm 5.822 \times 10^4$	$3.293 \times 10^5 \pm 2.904 \times 10^4$	$4.805 \times 10^5 \pm 1.807 \times 10^5$
Background Cl-36	$8.920 \times 10^4 \pm 3.560 \times 10^3$	$6.562 \times 10^4 \pm 6.532 \times 10^3$	$7.708 \times 10^4 \pm 6.197 \times 10^3$	$7.590 \times 10^4 \pm 1.185 \times 10^4$	$2.553 \times 10^5 \pm 9.068 \times 10^4$
Ca spallation	0.219 ± 0.003	0.023 ± 0.003	0.024 ± 0.004	0.024 ± 0.004	0.024 ± 0.004
Ca (μ, α)	0.002 ± 0.001	0.002 ± 0.001	0.002 ± 0.001	0.002 ± 0.001	0.002 ± 0.001
K-spallation	17.84 ± 1.76	20.61 ± 2.03	21.02 ± 2.07	21.26 ± 2.1	21.57 ± 2.13
K(μ, α)	0.933 ± 0.093	1.066 ± 0.107	1.088 ± 0.109	1.1 ± 0.11	1.116 ± 0.112
Thermal n Cl-35	4.515 ± 0.376	2.366 ± 0.249	1.841 ± 0.17	1.739 ± 0.278	6.413 ± 2.29
Epithermal n Cl-35	0.507 ± 0.041	0.304 ± 0.031	0.291 ± 0.027	0.307 ± 0.049	1.032 ± 0.369
K-39(n,α)Cl-36	0.482 ± 0.036	0.469 ± 0.035	0.361 ± 0.026	0.323 ± 0.023	0.358 ± 0.026
Total production	24.3 ± 1.8	24.84 ± 2.05	24.63 ± 2.08	24.75 ± 2.12	30.52 ± 3.15
Ratio muon/nucleon	0.065 ± 0.062	0.059 ± 0.06	0.057 ± 0.061	0.057 ± 0.061	0.0659 ± 0.05
Altitude/lat. scaling:					
Spallation	1.013	1.032	1.032	1.032	1.032
Muons	1.006	1.015	1.015	1.015	1.015
Depth correction:					
Spallation	0.885	0.916	0.957	0.966	0.966
Thermal n	1.732	1.582	1.328	1.270	1.280
Epithermal n	1.089	1.083	1.049	1.043	1.040
Exposure age	19.773 ± 1.92	13.954 ± 1.89	45.441 ± 4.83	13.51 ± 1.69	16.037 ± 6.37
Scaled exposure age	16.036 ± 1.92	11.317 ± 1.89	36.854 ± 4.83	10.957 ± 1.69	13.006 ± 6.37

Measurement	**ross16***	**ross17**
Cl-36 (atom/g)	$3.253 \times 10^5 \pm 2.68 \times 10^4$	$4.163 \times 10^5 \pm 3.54 \times 10^4$
Cl-36/Ca	—	—
Fraction stopped by:		
Cl-35	0.006 ± 0.001	0.009 ± 0.001
K-39(n,α)Cl-36	0.001 ± 0.000	0.001 ± 0.000
Major elements	0.696	0.722
Trace elements	0.304	0.278
X-section (cm^2/g)	0.006 ± 0.000	0.007 ± 0.000
Mean free path (cm^2/g)	159.8 ± 1.1	150.6 ± 1.0
Major absorber	Silicon	Potassium
Intrinsic prod'n (n/g/a)	24.77 ± 1.63	30.3 ± 1.64
Production (atom/g/a):		
Cl-36 (atom/g)	$2.578 \times 10^5 \pm 2.881 \times 10^4$	$2.999 \times 10^5 \pm 4.074 \times 10^4$
Background Cl-36	$6.751 \times 10^4 \pm 1.063 \times 10^4$	$1.164 \times 10^5 \pm 2.015 \times 10^4$
Ca spallation	0.024 ± 0.004	0.023 ± 0.003
Ca (μ, α)	0.002 ± 0.001	0.002 ± 0.001
K-spallation	21.28 ± 2.1	19.17 ± 1.89
K(μ, α)	1.105 ± 0.111	0.993 ± 0.099
Thermal n Cl-35	2.009 ± 0.323	3.364 ± 0.605
Epithermal n Cl-35	0.310 ± 0.050	0.481 ± 0.086
K-39(n,α)Cl-36	0.375 ± 0.028	0.395 ± 0.029
Total production	25.11 ± 2.13	24.43 ± 1.99
Ratio muon/nucleon	0.058 ± 0.06	0.061 ± 0.062
Altitude/lat. scaling:		
Spallation	1.026	1.031
Muons	1.011	1.014
Depth correction:		
Spallation	0.957	0.916
Thermal n	1.331	1.555
Epithermal n	1.048	1.087
Exposure age	10.39 ± 1.48	12.45 ± 2.0
Scaled exposure age	8.427 ± 1.48	10.097 ± 2.0

Table B.6: Measurement values and production rates for all the samples. Samples with stars are estimates of the chlorine values only. Values of 70 ± 10 ppm were used for all except cbc18/2 (80±10 ppm). Varying the chlorine contents for these samples does not make a significant difference to the exposure age - the results will not change. The scaled exposure age includes the correction for the low atmospheric air pressure over the Antarctic continent and this is the final age.

Appendix C

List of Samples

Below is a table of samples and their locations. This data is also contained within the appropriate chapters for each but is here as a total list for reference. Details such as errors on the heights are in the chapter associated with the dating method (usually up to ±1 m). Longitude and latitiude are for the outcrops or beach ridges from which the samples are taken rather than each sample.

Sample	Location	Height (m a.s.l.)	Longitude	Latitude
C-14				
ANUA9517	South Stream	7.4	163° 44' 17" E	77° 27' 10" S
ANUA9523	South Stream	7.4	163° 44' 17" E	77° 27' 10" S
ANUA9519	South Stream	7.6	163° 44' 17" E	77° 27' 10" S
ANUA6093	South Stream	12.6	163° 44' 17" E	77° 27' 10" S
ANUA6904	South Stream	8.4	163° 44' 17" E	77° 27' 10" S
ANUA6901	Marble Point	14.2	163° 48' E	77° 26.1' S
ANUA9329	Cape Hallett	2.5	170° 12' 41" E	72° 19' 12.3" S
ANUA9431	Cape Bird	3.7	166° 54.05' E	77° 6.28' S
ANUA10023	Cape Bird	5.4	166° 54.05' E	77° 6.28' S
ANUA10024	Cape Bird	4.7	166° 54.05' E	77° 6.28' S
OSL				
JQTL1	Marble Point	19	163° 48' E	77° 26.1' S
JQTL5	Marble Point	15	163° 48' E	77° 26.1' S

continued...

Sample	Location	Height (m a.s.l.)	Longitude	Latitude
Cl-36				
cbc18/1	Cape Bernacchi	1.2	163° 49.6' E	77° 29.0' S
cbc18/2	Cape Bernacchi	3.2	163° 49.6' E	77° 29.0' S
cbc18/3	Cape Bernacchi	5.1	163° 49.6' E	77° 29.0' S
cbc18/4	Cape Bernacchi	7.0	163° 49.6' E	77° 29.0' S
cbc18/5	Cape Bernacchi	8.2	163° 49.6' E	77° 29.0' S
ssc2	South Stream	8.6	163° 44' 17" E	77° 27' 10" S
ac4071	Arnold Cove	1.1	163° 44' 1"E	77° 25' 10" S
ac4073	Arnold Cove	4.7	163° 44' 1"E	77° 25' 10" S
ac4075	Arnold Cove	10.7	163° 44' 1"E	77° 25' 10" S
ac4076	Arnold Cove	11.2	163° 44' 1"E	77° 25' 10" S
ac4077	Arnold Cove	4.5	163° 44' 1"E	77° 25' 10" S
ac4079	Arnold Cove	9.2	163° 44' 1"E	77° 25' 10" S
ac40710	Arnold Cove	13.9	163° 44' 1"E	77° 25' 10" S
ac40712	Arnold Cove	16.5	163° 44' 1"E	77° 25' 10" S
ac40715	Arnold Cove	22.3	163° 44' 1"E	77° 25' 10" S
dis1	Dunlop Island	13.0	163° 31' 3" E	77° 14' 10" S
dis4	Dunlop Island	12.4	163° 31' 3" E	77° 14' 10" S
dis6	Dunlop Island	6.2	163° 31' 3" E	77° 14' 10" S
dis9	Dunlop Island	3.5	163° 31' 3" E	77° 14' 10" S
dis10	Dunlop Island	2.5	163° 31' 3" E	77° 14' 10" S
dis12	Dunlop Island	9.4	163° 31' 3" E	77° 14' 10" S
crc1	Cape Roberts	2.5	163° 10.8' E	77° 14.59' S
crc2	Cape Roberts	2.7	163° 10.8' E	77° 14.59' S
crc3	Cape Roberts	3.3	163° 10.8' E	77° 14.59' S
crc4	Cape Roberts	4.9	163° 10.8' E	77° 14.59' S
crc5	Cape Roberts	7.0	163° 10.8' E	77° 14.59' S
crc6	Cape Roberts	7.1	163° 10.8' E	77° 14.59' S
crc8	Cape Roberts	11.9	163° 10.8' E	77° 14.59' S
crc9	Cape Roberts	12.3	163° 10.8' E	77° 14.59' S
crc11	Cape Roberts	14.1	163° 10.8' E	77° 14.59' S
crc12	Cape Roberts	14.1	163° 10.8' E	77° 14.59' S
ross12	Cape Ross	26.7	163° 0' E	76° 44.73' S
ross13	Cape Ross	30.2	163° 0' E	76° 44.73' S
ross14	Cape Ross	31.7	163° 0' E	76° 44.73' S
ross15	Cape Ross	27.4	163° 0' E	76° 44.73' S
ross16	Cape Ross	23.3	163° 0' E	76° 44.73' S
ross17	Cape Ross	28.4	163° 0' E	76° 44.73' S

Table C.1: Sample locations and heights. Locations are for the group of samples and heights are metres above mean sea level and have errors up to ± 1 m (see specific tables or graphs in chapters for individual errors).

Bibliography

Adamiec, G. and M. J. Aitken (1998). Dose-rate conversion factors: update. *Ancient TL 16*, 37–50.

Anderson, J. B., S. S. Shipp, L. R. Bartek, and D. E. Reid (1992). Evidence for a grounded ice sheet on the Ross Sea continental shelf during the late Pleistocene and preliminary paleodrainage reconstruction. *Antarctic Research Series 57*, 39–62.

Anderson, J. B., S. S. Shipp, A. L. Lowe, J. Smith Wellner, and A. B. Mosola (2002). The Antarctic Ice Sheet during the Last Glacial Maximum and its subsequent retreat history: a review. *Quaternary Science Reviews 21*, 49–70.

Andrews, J. T., E. W. Domack, W. L. Cunningham, A. Leventer, K. J. Licht, A. J. T. Jull, D. J. DeMaster, and A. E. Jennings (1999). Problems and possible solutions concerning radiocarbon dating of surface marine sediments, Ross Sea, Antarctica. *Quaternary Research 52*(2), 206–216.

Andrews, J. T., H. Erlenkeuser, K. Tedesco, A. E. Aksu, and A. J. T. Jull (1994). Late Quaternary (Stage 2 and 3) Meltwater and Heinrich Events, Northwest Labrador Sea. *Quaternary Research 41*, 26 – 34.

Baroni, C. and G. Orombelli (1991). Holocene raised beaches at Terra Nova Bay, Victoria Land, Antarctica. *Quaternary Research 36*, 157–177.

Baroni, C. and G. Orombelli (1994). Abandoned penguin rookeries as Holocene paleoclimatic indicators in Antarctica. *Geology 22*, 23–26.

Bentley, M. J. (1999). Volume of Antarctic ice at the Last Glacial Maximum, and its impact on global sea level change. *Quaternary Science Reviews 18*, 1569–1595.

Bentley, M. J. and J. B. Anderson (1998). Glacial and marine geological evidence for the ice sheet configuration in the Weddell Sea Antarctic Peninsula region during the Last Glacial Maximum. *Antarctic Science 10*(3), 309–325.

Berkman, P. A. (1994). Geochemical signatures of meltwater in mollusc shells from Antarctic coastal areas during the Holocene. *Memoirs of National Institute of Polar Research Special Issue 50*, 11–33.

Berkman, P. A. and S. L. Forman (1996). Pre-bomb radiocarbon and the reservoir correction for calcareous marine species in the Southern Ocean. *Geophysical Research Letters 23*(4), 363 – 366.

Berkman, P. A., A. J. T, S. Bjork, E. Colhoun, S. D. Emslie, I. D. Goodwin, B. L. Hall, C. P. Hart, H. K, I. A, I. O, J. Lopez-Martinez, W. B. Lyons, M. C. G. Mabin, P. Quilty, M. Taviani, and Y. Yoshida (1998). Circum-Antarctic coastal environmental shifts during the Late Quaternary reflected by emerged marine deposits. *Antarctic Science 10*, 345–362.

Boulton, G. S., P. Dongelmans, and M. Punkari, M an dBroadgate (2001). Paleoglaciology of an ice sheet through a glacial cycle: the European ice sheet through the Weichselian. *Quaternary Science Reviews 20*(4), 591 – 625.

Brook, E. J., M. D. Kurz, J. R. P. Ackert, G. M. Raisbeck, and F. Yiou (1995). Cosmogenic nuclide exposure ages and glacial history of late Quaternary Ross Sea drift in McMurdo Sound, Antarctica. *Earth and Planetary Science Letters 131*, 41–56.

Cerling, T. E. and H. Craig (1994). Geomorphology and in-situ cosmogenic isotopes. *Annual Reviews Earth Planetary Science 22*, 273–317.

Chappell, J. and H. Polach (1991). Post-glacial sea-level rise from a coral record at Huon Peninsula, Papua New Guinea. *Nature 349*, 147–149.

Cofaigh, C. O. (1999). Holocene emergence and shoreline delevelling, southern Eureka Sound, High Arctic Canda. *Geographie Physique et Quaternaire 53*(2), 235–247.

Conway, H., B. L. Hall, G. H. Denton, A. M. Gades, and E. D. Waddington (1999). Past and future grounding-line retreat of the West Antarctic Ice Sheet. *Science 286*, 280 – 286.

David, T. W. E. and H. E. Priestley (1914). Glaciology, physiography, statigraphy and tectonic geology of South Victoria Land: British Antarctic Expedition, 1907 - 1909, reports on scientific investigations. *Geology 1*, 319.

Dell, R. K. (1990). Antarctic mollusca. *Royal Society of New Zealand Bulletin 27*, 265–273.

Denton, G. H., J. G. Brockheim, S. C. Wilson, J. E. Leide, and B. G. Anderson (1989). Late Quaternary ice-surface fluctuations of Beardmore Glacier, Transantarctic Mountains. *Quaternary Research 31*, 183–209.

Denton, G. H., J. G. Brockheim, S. C. Wilson, and M. Stuiver (1989). Late Wisconsin and Early Holocene Glacial History, Inner Ross Embayment, Antarctica. *Quaternary Research 31*, 151 – 182.

Denton, G. H. and T. J. Hughes (2000). Reconstruction of the Ross ice drainage

system, Antarctica, at the Last Glacial Maximum. *Geografiska Annaler 82A*(2-3), 143–166.

Domack, E. W., M. Taviani, and A. Rodriguez (1999). Recent sediment remoulding on a deep shelf, Ross Sea: Implications for radiocarbon dating of Antarctic marine sediments. *Quaternary Science Reviews 18*, 1445 – 1451.

Drewry, D. J. (1979). Late Wisconsin reconstructions for the Ross Sea region, Antarctica. *Journal of Glaciology 24*(90), 231 – 244.

Dyke, A. S. and W. R. Peltier (2000). Forms, response times and variability of relative sea-level curves, glaciated North America. *Geomorphology 32*, 315–333.

Evans, J. M., J. O. Stone, L. K. Fifield, and R. G. Cresswell (1997). Cosmogenic chlorine-36 production in K-feldspar. *Nuclear Instruments and Methods in Physics Research B 123*, 334–340.

Fairbanks, R. G. (1989). A 17,000-year glacio-eustatic sea level record: influence of glacial melting rates on the Younger Dryas event and deep-ocean circulation. *Nature 342*, 637–642.

Farrell, W. E. and J. A. Clark (1976). On postglacial sealevel. *Geophysics Journal 46*, 79 – 116.

Forman, S. L., O. Ingolfsson, V. Gataullin, W. F. Manley, and H. Lokrantz (1999). Late Quaternary stratigraphy of western Yamal Peninsula, Russia: New constraints on the configuration of the Eurasian ice sheet. *Geology 27*(9), 807–810.

Gordon, J. E. and D. D. Harkness (1992). Magnitude and geographic variation of the radiocarbon content in Antarctic marine life: Implications for reservoir corrections in radiocarbon dating. *Quaternary Science Reviews 11*, 697–708.

Gregory, M. R., R. M. Kirk, and M. C. G. Mabin (1984). Shore types of Victoria Land, Ross Dependency, Antarctica. *New Zealand Antarctic Record 5*(3), 23–40.

Gunn, B. M. and G. Warren (1962). Geology of Victoria Land between the Mawson and Mulock Glaciers, Antarctica. *New Zealand Geological Survey Bulletin 71*, 1–143.

Hall, B. L. and G. H. Denton (1999). New relative sea-level curves for the southern Scott Coast, Antarctica: Evidence for Holocene deglaciation of the western Ross Sea. *Journal of Quaternary Science 14*(7), 641+.

Hall, B. L. and G. H. Denton (2000a). Extent and chronology of the Ross Sea and the Wilson Piedmont glacier along the Scott Coast at the Last Glacial Maximum. *Geografiska Annaler 82A*, 337–363.

Hall, B. L. and G. H. Denton (2000b). Radiocarbon chronology of Ross Sea drift, Eastern Taylor valley, Antarctica: Evidence for a grounded ice sheet in the Ross Sea at the Last Glacial Maximum. *Geografiska Annaler 82A*, 305–336.

Harrington, H. J. and I. C. McKellar (1958). A radiocarbon date for penguin colonization of Cape Hallett, Antarctica. *New Zealand Journal of Geology and Geophysics 1*(3), 571–576.

Heine, J. C. and T. W. Speir (1989). Ornithogenic soils of Cape Bird Adèlie penguin rookeries, Antarctica. *Polar Biology 10*, 89–99.

Higham, T. (1994). Radiocarbon dating New Zealand prehistory with Moa eggshell: some preliminary results. *Quaternary Science Reviews 13*, 163–169.

Huybrechts, P. (1990). A 3-D model for the Antarctic ice sheet: a sensitivity study on the glacial-interglacial contrast. *Climate Dynamics 5*, 79–92.

Johnston, P. (1993). The effect of spatially non-uniform water loads on prediction of sea-level change. *Geophysical Journal International 114*, 615–634.

Johnston, P. and K. Lambeck (1999). Postglacial rebound and sea level contributions to changes in the geoid and the Earth's roataion axis. *Geophysical Journal International 136*, 537–558.

Jouzel, J., G. Raisebeck, J. P. Benoist, F. Yiou, C. Lorius, D. Raynaud, J. R. Petit, N. I. Barkov, Y. S. Korotkevitch, and V. M. Kotlyakov (1989). A comparison of deep Antarctic ice cores and their applicaitons for climate between 65,000 and 15,000 years ago. *Quaternary Research 31*, 135–150.

Karl, H. A. (1989). High resolution seismic-relection interpretaions of some sediment deposits, Antarctic continental margin. *Marine Geology 85*, 205 – 233.

Kaufmann, G. and K. Lambeck (1997). Implications of Late Pleistocene glaciation of the Tibetan Plateau for present-day uplift rates and graivity anomalies. *Quaternary Research 48*(3), 267–279.

Kellogg, T. B., T. Hughes, and D. E. Kellogg (1996). Late Pleistocene interactions of East and West Antarctic ice-flow regimes: Evidence from the McMurdo Ice Shelf. *Journal of Glaciology 42*(142), 486–500.

Kellogg, T. B., D. E. Kellogg, and M. Stuiver (1990). Late Quaternary history of the southwestern Ross Sea: evidence from debris bands on the McMurdo Ic Shelf, Antarctica. *Antarctic Research Series 50*, 25–56.

Kirk, R. M. (1970). Beach observations at Cape Royds, Ross Island, McMurdo Sound, Antarctica, 1965 - 66. Geography Dept, University of Canterbury, New Zealand.

Kirk, R. M. (1990). Raised beaches, late Quaternary sea levels and deglacial sequences on the Victoria Land Coast, Ross Sea, Antarctica. In D. Gilleson and S. Fitzsimons (Eds.), *Proceedings of a meeting held in the Department of Geography and Oceanography, Australian Defence Force Academy, Canberra.*

Lambeck, K. (1995). Constraints on the Late Weichselian ice sheet over the Barents Sea from observations of raised shorelines. *Quaternary Science Reviews 14*, 1–16.

Lambeck, K., P. Johnston, C. Smither, and M. Nakada (1996). Glacial rebound of the British Isles - III. Constraints on mantle viscosity. *Geophysical Journal International 125*, 340–354.

Lambeck, K., A. Purcell, J. Johnston, M. Nakada, and Y. Yokoyama (2003). Water-load definition in the glacio-hydro-isostatic sea-level equation. *Quaternary Science Reviews 22*, 309–318.

Lambeck, K., C. Smither, and P. Johnston (1998). Sea-level change, glacial rebound and mantle viscosity for Northern Europe. *Geophysical Journal International 134*, 102–144.

Lambeck, K., Y. Yokoyama, P. Johnston, and A. Purcell (2000). Global ice volumes at the Last Glacial Maximum and early Lateglacial. *Earth and Planetary Science Letters 181*(4), 513–527.

Le Masurier, W. E. (1990). *Volcanoes of the Antarctic Plate and Southern Oceans*, Volume 48 of *Antarctic Research Series*, pp. 487. American Geophysical Union, Washington DC.

Licht, K. J. and J. T. Andrews (1997). Diamictons of the east-central Ross Sea continental shelf: implications for ice sheet extent during the Last Glacial Maximum (LGM). In *Symposium on Antarctica and Global Change: interactions and impacts*. Antarctic CRC.

Licht, K. J., A. E. Jennings, J. T. Andrews, and K. M. Williams (1996). Chronology of late Wisconsin ice retreat from the western Ross Sea, Antarctica. *Geology 24*(3), 223–226.

Long, A., R. B. Hendershott, and P. S. Martin (1983). Radiocarbon dating of fossil eggshell. *Radiocarbon 25*(2), 533–539.

Mabin, M. C. G. (1986). The Ross Sea section of the Antarctic Ice Sheet at 18,000 yr B.P.: evidence from Holocene sea-level changes along the Victoria Land Coast. *South African Journal of Science 82*, 506–508.

Murray, A. S., J. M. Olley, and G. G. Ciatcheon (1995). Measurement of equivalent doses in quartz from contemporary water-lain sediments using optically stimulted luminescence. *Quaternary Science Reviews 14*, 365–371.

Murray, A. S. and R. G. Roberts (1998). Measurement of the equivalent dose in quartz using a regenerative-dose single-aliquot protocol. *Radiation Measurements 29*, 503–515.

Murray, A. S. and A. G. Wintle (2000). Luminescence dating of quartz using an improved single-aliquot regenerative-dose protocol. *Radiation Measurements 32*, 57–73.

Nakada, M., R. Kimura, K. Moriwaki, H. Miura, and H. Maemoku (2000). Late Pleistocene and Holocene melting history of the Antarctic Ice Sheet derived from sea-level variations. *Marine Geology 167*(1-2), 85–103.

Nakada, M. and K. Lambeck (1987). Glacial rebound and relative sea-level variations: A new appraisal. *Geophysical Journal of the Royal Astronomical Society 90*, 171 – 224.

Nakada, M. and K. Lambeck (1988). The melting history of the late Pleistocene Antarctic Ice Sheet. *Nature 333*, 36–40.

Nichols, R. L. (1968). Coastal geomorphology, McMurdo Sound, Antarctica. *Journal of Glaciology 7*(51), 449–478.

Noller, J. S., J. M. Sowers, and W. R. Lettis (2000). *Quaternary Geochronology: Methods and Applications*, Chapter Cosmogenic nuclide buildup in surficial materials, pp. 61– 76. American Geophysical Union.

Orombelli, G., C. Baroni, and G. Denton (1991). Late Cenozoic glacial history of the Terra Nova Bay region, Northern Victoria Land, Antarctica. *Geogr. Fis. Dinam. Quat. 3*, 139–163.

Orombelli, G. and G. H. Denton (1990). Late Cenozoic glacial history of the Terra Nova Bay region, Northern Victoria Land, Antarctica. *Antarctic Journal 25*(5), 51–52.

Peltier, W. R. (1998). Postglacial variations in the level of the sea: implications for climate dyanmics and solid-earth geophysics. *Reviews of Geophysics 36*(4), 603–689.

Peltier, W. R. and J. T. Andrews (1976). Glacial-isostatic adjustment - 1. The forward problem. *Geophysical Journal of the Royal Astrological Society 46*, 605–646.

Petit, J. R., J. Jouzel, D. Raynaud, N. I. Barkov, J. M. Marnola, I. Basile, M. Bender, J. Chappellaz, M. Davis, G. Delaygue, M. Delmotte, V. M. Kotlyakov, M. Legrand, V. Y. Lipenkov, C. Lorius, L. Pépin, C. Ritz, E. Saltzman, and M. Stievenard (1999). Climate and atmospheric history of the past 420,000 years from the Vostok ice core, Antarctica. *Nature 399*, 429–436.

Prescott, J. R. and J. T. Hutton (1994). Cosmic ray contributions to dose-rates for luminescence and ESR dating: large depths and long-term time variations. *Radiation Measurements 23*(2/3), 497–500.

Questiaux, D. G. (1990). Optical dating of loess: comparisons between different grain size fractions for infrared and green excitation wavelengths. *Nuclear Tracks and Radiation Measurements 18*(1/2), 133–139.

Sawagaki, T. and K. Hirakawa (1999). Melting of the Antarctic Ice Sheet during the

last glacial period:- terrestrial evidence from Lutzow Holm Bay. In *8th international symposium on Antarctic Earth Sciences.*

Sejrup, H. P., E. Larsen, J. Landvik, K. E. L, H. Haflidason, and A. Nesje (2000). Quaternary glaciations in southern fennoscandia: evidence from southwestern Norway and the northern North Sea region. *Quaternary Science Reviews 19*(7), 667–685.

Shackleton, N. J. (1987). Oxygen isotopes, ice volume and sea level. *Quaternary Science Reviews 6*, 183–190.

Shipp, S., J. Anderson, and E. Domack (1999). Late Pleistocene-Holocene retreat of the West Antarctic ice-sheet system in the Ross Sea: Part 1 - geophysical results. *Geological Society of America Bulletin 111*(10), 1486–1516.

Spooner, N. A., J. M. Olley, D. G. Questiaux, and X. Y. Chen (2000). Optical dating of an aeolian deposit on the Murrumbidgee floodplain. *Quaternary Science Reviews (Quaternary Geochronology) 20*(5-9), 835–840.

Stirling, C. H. (1996). *High-precision U-series dating of corals from Western Australia: Implications for Last Interglacial sea-levels.* Ph. D. thesis, The Australian National University.

Stockton, W. L. (1984). The biology and ecology of the epifaunal scallop Adamussium colbecki on the west side of McMurdo Sound, Antarctica. *Marine Biology 78*, 171–178.

Stone, J. O. (2000). Air pressure and cosmogenic isotope production. *Journal of Geophysical Research 105*(B10), 23753–23759.

Stone, J. O., G. L. Allan, L. K. Fifield, and R. G. Cresswell (1996). Comogenic chlorine - 36 from calcium spallation. *Geochemica et Cosmochimica Acta 60*(4), 679–692.

Stone, J. O., G. A. Balco, D. E. Sugden, M. W. Caffee, L. C. Sass, S. G. Cowdery, and C. Siddoway (2003). Holocene deglaciation of Marie Byrd Land, West Antartica. *Science 299*(5603), 99–102.

Stone, J. O., K. Lambeck, L. K. Fifield, J. M. Evans, and R. G. Cresswell (1996). A lateglacial age for the Main Rock Platform, Western Scotland. *Geology 24*(8), 707–710.

Stone, J. O. H., J. A. Peterson, L. K. Fifield, and R. G. Cresswell (1997). Cosmogenic chlorine-36 exposure ages for two basalt flows in the newer volcanics province, Western Victoria. *Proceedings of the Royal Society of Victoria 109*(2), 121–131.

Stuiver, M., G. H. Denton, T. J. Hughes, and J. L. Fastook (1981). History of the marine ice sheet in West Antarctica during the last glaciation: A working

hypothesis. In G. H. Denton and T. J. Hughes (Eds.), *The Last Great Ice Sheets*, pp. 319–436. John Wiley and Sons, New York.

Stuiver, M. and H. A. Polach (1977). Reporting of C-14 data. *Radiocarbon 19*(3), 355–363.

Stuiver, M. and P. J. Reimer (1993). Extended C-14 database and revised CALIB radiocarbon calibration program. *Radiocarbon 35*, 215–230.

Stuiver, M., P. J. Reimer, E. Bard, J. W. Beck, G. S. Burr, K. A. Hughen, B. Kromer, G. McCormac, J. van der Plicht, and M. Spurk (1998). INTCAL98 radiocarbon age calibration, 24,000 - 0 cal BP. *Radiocarbon 40*(3), 1041–1083.

Svendsen, J. I., V. I. Astakhov, D. Y. Bolshiyanov, I. Demidov, J. A. Dowdeswell, V. Gataullin, C. Hjort, H. W. Hubberten, L. E, J. Mangerud, M. Melles, P. Moller, M. Saarnisto, and M. J. Siegert (1999). Maximum extent of the Eurasian ice sheets in the Barents and Kara Sea region during the Weichselian. *Boreas 28*, 234–242.

Tushingham, A. M. and W. R. Peltier (1991). Ice-3G: a new global model of Late Pleistocene deglaciation based upon geophysical predictions of post-glacial relative sea level change. *Journal of Geophysical Research 96*(B3), 4497–4523.

Webb, P. G. (1997). Late Pleistocene / Holocene glacial history of the Scott Coast, western McMurdo Sound. Honours thesis, Victoria University of Wellington.

Yokoyama, Y. (1999). *Sea-level change in Australasia and the Radiocarbon timescale calibration during the last 50,000 years*. Ph. D. thesis, Australian National University.

Zwartz, D. P. (1995). *The recent history of the Antarctic Ice Sheet: Constraints from sea level change*. Ph. D. thesis, The Australian National University.